Jairo Rúa Pazos

Optimisation of flexible operation of natural gas combined cycles with post-combustion CO_2 capture

Jairo Rúa Pazos

Doctoral thesis

Doctoral theses at NTNU, 2021:184

NTNU
Norwegian University of
Science and Technology
Thesis for the degree of
Philosophiae Doctor
Faculty of Engineering
Department of Energy and Process Engineering

NTNU
Norwegian University of
Science and Technology

NTNU
Norwegian University of
Science and Technology

NTNU

Jairo Rúa Pazos

Optimisation of flexible operation of natural gas combined cycles with post-combustion CO$_2$ capture

Thesis for the degree of Philosophiae Doctor

Trondheim, May 2021

Norwegian University of Science and Technology
Faculty of Engineering
Department of Energy and Process Engineering

◘ NTNU
Norwegian University of
Science and Technology

NTNU
Norwegian University of Science and Technology

Thesis for the degree of Philosophiae Doctor

Faculty of Engineering
Department of Energy and Process Engineering

PRINTED IN
NORWAY
NO - 1598

NORDIC SWAN ECOLABEL

Printed matter
2041 0731

Dedicated to my parents and sister.

Preface

This thesis is submitted in partial fulfilment of the requirements for the degree of philosophiae doctor (Ph.D.) at the Norwegian University of Science and Technology (NTNU). The research described herein was carried out at the Department of Energy and Process Engineering at the Faculty of Engineering, with Associate Professor Lars Olof Nord as main supervisor. Professor Magne Hillestad from Department of Chemical Engineering at NTNU was co-supervisor. The research was funded by the Department of Energy and Process Engineering at NTNU.

Abstract

Anthropogenic greenhouse gas emissions have continuously grown since the Industrial Revolution. Global warming is the result of increasing concentrations of these gases in the atmosphere, which create imbalances between inflow and outflow radiation that lead to the increase of the mean temperature of the planet. There is scientific consensus on that the prolonged temperature rise of oceans and land has altered the climate and jeopardised the biosphere. Temperature increase above $1.5°C$ with respect to pre-industrial levels is likely to produce deep changes in natural ecosystems, alter biodiversity, and threaten human health and security. Therefore, current mitigation policies aim at reducing the overall emissions of greenhouse gases to restrain this temperature rise.

Decarbonisation of the power sector will play a fundamental role in the abatement of global warming as it is the largest CO_2 emitter and electrification of other industries is becoming an essential approach to reduce their greenhouse gas emissions. Deployment of intermittent renewable energy sources, mainly wind and solar, has concentrated most of the efforts to reduce the emissions associated with the power sector. However, a broader portfolio of technologies is necessary to meet the increasing power demand whilst ensuring safe and sustainable power generation. In this context, flexibility is and will be the cornerstone of a reliable and efficient electric market. Thermal power plants integrated with carbon capture and storage (CCS) systems can deliver low-carbon electricity at a large scale and balance the differences between power demand and supply originated by the increasing share of renewable sources. Thus, these power generation systems are expected to be one of the foundations of the power sector.

This thesis is a summary of a set of scientific contributions that aimed at optimising the flexible operation of thermal power plants integrated with absorption-based post-combustion CO_2 capture plants. These included the analysis of the dominant dynamic of this type of power generation systems, the identification of the main bottlenecks hindering their flexible operation and transient performance, and the development of different methodologies that allowed overcoming these restrictions and ensuring safe yet efficient dynamic operation.

Thermal power plants and post-combustion CO_2 capture systems exhibit distinct dynamic behaviour because their dominant dynamics occur in different time scales. Flexible operation requires understanding the main factors dictating the

dynamic performance of each plant and how their integration affects power generation. A qualitative analysis discussed the components and processes governing the dynamic behaviour of thermal power and capture plants, both individually and integrated, whereas dynamic simulations demonstrated the almost negligible effect of the capture plant in the power generation capacity of natural gas combined cycles. This indicated that carbon capture does not limit the dispatchable nature of this type of thermal power plants and highlighted the suitability of thermal power with CCS to balance power markets with large shares of intermittent renewable energy sources.

Thermal and mechanical stresses, however, do limit the ramping capacity of thermal power plants. Thick-walled equipment experiences large temperature gradients during flexible operation that generate high peaks of stress in the material and might ultimately lead to deformations and failure. This thesis presents a methodology to operate thermal power plants based on model predictive control that incorporates the calculation of stress in critical components. This control strategy computes optimal power generation ramps that result in the fastest possible operation with stress levels within allowable limits.

Stress monitoring can avoid the instant failure of critical components by reducing the maximum peaks of stress. Nevertheless, regular operation of thermal power plants induces damage in the equipment even with safe levels of stress. Flexible operation increases this deterioration and reduces the lifetime operation of the power plant due to the more frequent and pronounced thermal gradients and their associated stress variations. Scheduling can consider these factors to determine operation profiles for thermal power plants that maximise revenue while reducing the deterioration of the equipment and considering the inherent uncertainty associated with intermittent power generation from renewable energy sources. This approach is proposed in a method that formulates the scheduling of thermal power plants as a scenario-tree stochastic optimisation problem where the damage of the equipment is a constraint.

Optimisation-based control strategies also enhance the transient performance of thermal power plants integrated with post-combustion CO_2 capture. Model predictive control can consider the different dynamic behaviour of both plants and compute optimal control actions according to their dominant dynamics. A control strategy based on offset-free model predictive control is proposed to reinforce the flexible power dispatch of thermal power plants and to stabilise the the main process variables of integrated systems. Dynamic simulations demonstrated the effectiveness of this control strategy to balance drastic changes on power demand, keep specified capture ratios, and reduce the deviations achieved in the main process performance variables of these power systems.

Acknowledgements

This thesis would not have been possible without the confidence and support of my main supervisor Lars O. Nord. I deeply appreciate the freedom you gave to take decisions, learn independently and make mistakes. You encouraged me to think differently and consider distinct perspectives while giving me the confidence of knowing you had my back. This is a philosophy I will always cherish and bring with me, both in my professional and personal life.

My gratitude to my co-supervisor Magne Hillestad, whose kindness and wise words taught me how to approach challenges in a different manner. I appreciate your closeness and that your door was always open for me. I would also like to thank Mai Bui and Niall Mac Dowell for hosting me at Imperial College London. Working together with you and sharing so many moments and interesting conversations with your group broadened my mind and allowed me to grow as a researcher. I also thank Johannes Jäschke for his willingness to collaborate with me and the enriching discussions. Special mention to Rubén Mocholí Montañés for providing me the models that laid the foundation of this thesis and for setting high standards that pushed me to give my best.

This Ph.D. has been an unique academic experience, but it has also been an exceptional opportunity to discover the beautiful Norway and share fantastic moments with people from different cultures. I thank all my friends and colleagues in Trondheim for each moment spent with me, including the days at Moholt, the ski and training sessions, the group dinners and the coffee breaks. It was these tiny details what made me feel part of this international community.

I would like to thank to Raquel, Anxo, María, Alexis, María, Rubén, Michi and Borja for the ski days, tasty dinners and great memories. In your company I was closer to home. A big thank you to David, for the happiness you irradiate and your uniqueness. I hope we can repeat some of those late nights with interesting and endless conversations.

To my good, old friends back home. It feels our friendship does not age and we never took different paths. Knowing that everything will be the same when I return home brings me nostalgia, comfort and joy. I am thankful and proud of calling you friends, and I truly hope our relationship stays the same for years to come.

A warm thank you to my partners in crime, Roberto and Giorgia. Sharing this experience was special. Throughout these years we struggled, procrastinated, laughed and succeeded. But, the most important part is, we did it together. Your company and support has been invaluable to me.

My heart-felt gratitude to Marta, the most important person during these three years. My companion during this journey. Despite being the person that suffered the most the ups and downs of this Ph.D., I always knew I had you by my side. Thank you for helping me to put aside my worries, for the enjoyable ski days, the lovely dinners, the beautiful summer trips, and for all the silly, fun moments you had to put up with almost every day. I will always treasure these unforgettable memories.

Agradecimientos a mi padrino. Aunque no tengamos un contacto tan continuo, siento que nuestra relación es tan cercana cómo siempre. Gracias por todo el apoyo a lo largo de los años.

A mis abuelos. Se que emigrar fue duro, pero estoy seguro de que ver irse a un nieto aun lo es más. Siento generaros la angustia y preocucapión de la distancia y os agradezco que, a pesar de ello, me animeis a seguir mi camino. Si hay alguien a quien nunca podré devolver todo el afecto y el apoyo recibido es a vosotros. Gracias.

Me gustaría también pedir disculpas a mi hermana, por no haber podido estar más cerca de ti apoyándote en momentos difíciles y compartiendo ocasiones alegres. No poder vernos con más frecuencia ha sido la parte más complicada de toda esta experiencia. Te agradezco profundamente tu compresión, tu apoyo, tu ánimo y tu cariño. Espero que nuestra relación nunca cambie.

Por último, mi más sentido agradecimiento a mis padres, por todos los sacrificios que habéis tenido que sufrir para darme una educación. Gracias por demostrarme el valor del trabajo y el esfuerzo, por confiar en mí, por animarme siempre a mejorar, y por el apoyo y cariño incondicional. Gran parte de lo que consigo os lo debo a vosotros.

<div align="right">

Jairo Rúa Pazos
9 May 2021, Oslo

</div>

Contents

List of Figures

List of Tables

Nomenclature

Latin symbols

$\hat{\widetilde{A}}$	State estimation	–
$\widetilde{A}$	Delta-input state matrix	–
A	State matrix	–
A_a	Augmented state matrix	–
A_eq	Linear equality constraint matrix	–
A_ineq	Linear inequality constraint matrix	–
a	Coefficients simplified models	–
$\widetilde{B}$	Delta-input input matrix	–
B	Input matrix	–
B_a	Augmented input matrix	–
B_d	Disturbance input matrix	–
B_eq	Linear equality constraint vector	–
B_ineq	Linear inequality constraint vector	–
b	Coefficients simplified models	–
$\widetilde{C}$	Delta-input output matrix	–
C	Output matrix	–
c	Centre validity function	–
C_a	Augmented output matrix	–
C_d	Disturbance output matrix	–

c_{eq}	Nonlinear equality constraint	–
c_{ineq}	Nonlinear inequality constraint	–
C_{m}	Specific heat capacity	J/kg K
Δu	Delta-input control vector	–
δu	Delta-input control action	–
D	Damage	–
d	Disturbance vector	–
E	Young's modulus	MPa
F	MIMO delta-input penalty vector	–
f	Delta-input penalty vector	–
$f(z)$	Nonlinear objective function	–
F_r	Centrifugal force	N/m^3
G	MIMO delta-input inequality matrix	–
g	Delta-input inequality matrix	–
H	Delta-input matrix output equation	–
h	Convection coefficient	W/m^2 K
I	Identity matrix	–
J	Objective function	–
K	Observer gain matrix	–
K_f	Kalman filter	–
k_{m}	Heat conduction coefficient	W/m K
l	Cost function	–
M	Number local ARX models	–
m	Number operation points	–
M_{unc}	Number uncertainty realisations	–
N	Time horizon	–

N_r	Robust time horizon	–
n_u	Order ARX input	
n_y	Order ARX output	
n_f	Experimental cycles before fatigue failure	–
n_oper	Operation cycles at specific strain amplitude and mean strain	–
n_r	Number of ranges	–
P	MIMO delta-input inequality vector	–
p	Delta-input inequality vector	–
Pr	Price electricity	Euro/MWh
Q	Weight matrix	–
Q_p	Process noise covariance	–
R	Penalty vector	–
r	Radius	m
R^2	Coefficient of determination	–
R_m	Measurement noise covariance	–
S	Scenarios	–
T	Temperature deviation from design	°C
t	Time	s
t_exp	Experimental operation time at specific stress and temperature	s
t_oper	Operation time at specific stress and temperature	s
u	Manipulated variable	–
u_d	Displacement	–
w	Width validity function	–
y	Predicted variable, output vector	–
Z	Estimator covariance matrix	–
z	Optimisation variables	–

Greek symbols

α	Thermal diffusivity	1/K
α^*	Thermal expansion coefficient	m^2/s
$\Delta\varepsilon$	Strain amplitude	–
$\Delta\varepsilon_\mathrm{e}$	Elastic strain amplitude	–
$\Delta\varepsilon_\mathrm{p}$	Plastic strain amplitude	–
Γ	Delta-input weight matrix	–
γ	Local operating point	–
λ	Weights objective function	–
ω	Rotational speed	rad/s
ω_i	Scenario weight	–
Φ	MIMO delta-input weight matrix	–
Ψ	Unit lower triangular matrix	–
ψ	Local validity function	–
ρ	Density	$\mathrm{kg/m}^3$
σ^2	Covariance	–
σ'_f	Tensile strength coefficient	MPa
σ_r	Radial stress	MPa
σ_z	Longitudinal stress	MPa
σ_effl	Linearised von Mises effective stress	MPa
σ_eff	von Mises effective stress	MPa
σ_θ	Axial stress	MPa
υ	Poisson's coefficient	–
ε	Stochastic error	–
ε'_f	Ductility coefficient	–
ε_r	Radial strain	–

ε_z	Longitudinal strain	–
$\varepsilon_{\mathrm{effl}}$	Linearised von Mises effective strain	–
$\varepsilon_{\mathrm{eff}}$	von Mises effective strain	–
ε_θ	Axial strain	–

Subscripts

0	Initial conditions
creep	Creep damage
drum	Drum
d	Disturbance
fatigue	Fatigue damage
i	Inner
o	Outer
pow	Power
ramp	Ramping rate
ref	Reference trajectory
turb	Turbine
u	Inputs
wall	Wall
x	States

Superscripts

b	Elastic fitting parameter
c	Plastic fitting parameter
-	Previous estimation
low	Lower bound
up	Upper bound

Acronyms

ARX	Autorregressive model with exogeneous variable
BECCS	Bio-energy carbon capture and storage
BPP	Biomass power plant
CCS	Carbon capture and storage
CPP	Coal power plant
FEM	Finite element method
GISS	Goddard Institute for Space Studies
GT	Gas turbine
GWP	Global warming potential
HP	High pressure
HPT	High-pressure turbine
HRSG	Heat-recovery steam generator
IP	Intermediate pressure
IPT	Intermediate-pressure turbine
LHV	Lower heating value
LMN	Local model network
LP	Low pressure
LPT	Low-pressure turbine
MEA	Monoethanolamine
MIMO	Multi-input multi-output
MMt	Million metric tons
MPC	Model predictive control
NGCC	Natural gas combined cycle
NLP	Nonlinear programming
PCC	Post-combustion carbon capture

PV   Photovoltaic

QP   Quadratic programming

RH   Reheater

SH   Superheater

SISO   Single-input single-output

Chapter 1

Introduction

This thesis analyses the dynamic behaviour of thermal power plants integrated with CO_2 capture and investigates different methodologies to enhance their flexible operation. The objectives and proposed methodologies do not correspond to an unique field of study, but to a blend of disciplines, including process and mechanical engineering, control and optimisation. This introductory chapter presents the background that motivates the development of the studies included herein and the main contributions achieved by combining these distinct fields. It also includes a brief description of the structure of the contents, and a summary of the publications derived from this Ph.D. thesis.

1.1 Background and motivation

Global warming mitigation is one of the greatest challenges in the twenty-first century. The prolonged greenhouse gas emissions from human activities have lead to a temperature rise that threatens to change natural ecosystems and climate behaviour (IPCC, 2014). There exist different approaches to combat global warming, including mitigation and palliative policies. To date, global warming mitigation has concentrated most of the efforts to limit the average temperature increase of the planet, being the reduction of greenhouse gas emissions the cornerstone of this endeavour (IPCC, 2018).

The power sector is the largest contributor to the global CO_2 emissions because of its historical reliance on fossil fuels (IEA, 2019; IPCC, 2014). Thus, its decarbonisation can produce significant progress towards the mitigation of global warming. Furthermore, developing a sustainable power sector can ease the reduction of greenhouse emissions from other economic sectors, since electrification is one of the main approaches to limit the global temperature rise (IEA, 2019).

Renewable energy sources are consistently gaining prominence in the power sector, extensively increasing the deployment of large infrastructures and their contribution to the overall power generation mix (IEA, 2019). Power generation

from intermittent renewable energy sources, mainly wind and solar, can reduce the CO_2 emissions associated with the power sector at the expense of increasing the variability of power supply. Energy storage is considered as a promising technology that can balance sudden changes in renewable power generation, but its application in a growing electricity market in the short- and mid-term is highly limited by its cost-effectiveness, technology maturity and commercial availability at large scale (IEA, 2014). Nevertheless, renewable power represents only one element of the portfolio of technologies that will be required to deliver a technically feasible and financially viable energy system.

In this context, thermal power generation with carbon capture and storage is understood to play a uniquely important role, providing significant value through flexible operation (Boot-Handford et al., 2014; IPCC, 2005). This refers to the capacity of this type of energy systems to rapidly change their operating conditions and balance large mismatches between power supply and demand. Thus, there are several criteria that power generation systems must meet in order to deliver flexible operation, including steep ramp rates, fast start-ups and shut-downs, high off-design efficiency, broad operation ranges, low minimum compliant loads, and the ability to frequently cycle among different operating points in a fast, safe and yet efficient manner.

Thermal power plants can balance the variability renewable energy sources introduce in the electric grid because of their capacity to provide large changes of power within minutes, while carbon capture and storage reduces notably the emissions associated with their operation. Therefore, it is of vital importance that carbon capture technology can operate synergistically with intermittent renewable power sources, and consequently ensuring that CCS does not inhibit the flexible and dispatchable nature of thermal power plants. However, there is scarce knowledge and experience on the flexible operation of capture systems and the effect they have on thermal power plants during transient operation (Bui et al., 2014, 2018b). Consequently, there is need of understanding the processes that govern the dynamic behaviour of these low-carbon power generation systems, identifying the bottlenecks that hinder their flexible operation, and developing methodologies and control strategies that enhance their capacity to balance the power grid with reduced emissions. Chapter 2 provides a more thorough description of the current energy scenario and discusses more extensively the requirements of future power systems and the role thermal power plants with CCS might have.

1.2 Objectives

Flexible operation of thermal power plants integrated with carbon capture and storage is the main objective of this Ph.D. thesis. The achievement of this goal would allow to notably reduce the emissions associate with the power sector, balance the electric grid more efficiently and in a reliable manner, support the

deployment of renewable energy sources, and enhance the decarbonisation of other sectors through electrification. However, this objective is too generic and big to be addressed directly. Therefore, the approach in this Ph.D. thesis was to decompose it into smaller and simpler objectives that can be managed individually. These are:

1. Understanding the dynamic behaviour of thermal power plants and CO_2 capture, the processes that govern their transient operation, and identify the main bottlenecks limiting their flexible and faster performance.

2. Developing methodologies and control strategies that overcome these limitations and enhance the flexible operation of thermal power plants integrated with carbon capture and storage.

3. Address the additional issues that arise from the flexible operation this type of power systems and propose solutions to mitigate their effect.

1.3 Contributions

This thesis presents a series of analysis, methodologies and control approaches to enhance the flexible operation of thermal power systems with and without CO_2 capture. The main contributions are:

1. Qualitative analysis of dominant dynamics and processes governing the transient performance of thermal power plants and CO_2 capture systems.

2. Understanding the effect of integrating CO_2 capture plants with thermal power plants on the capacity to dispatch flexible power and balance the electric grid.

3. Development of a control methodology that considers the stress in critical equipment of thermal power plants and limits its maximum level.

4. Comparison of linear and nonlinear formulations for optimal control of thermal power plants with stress monitoring.

5. Identification and construction of data-based linear surrogate models to predict nonlinear dynamic behaviour in thermal power plants and CO_2 capture systems.

6. Development of a scheduling method to maximise the revenue of flexible thermal power plants, enhance their lifetime utilisation, and consider the uncertainty associated with power generation from intermittent renewable energy sources.

7. Evaluation of model predictive control methodologies for optimal and flexible operation of thermal power plants integrated with CO_2 capture.

These methodologies and control strategies were formulated in a generic manner with the objective of easing their implementation in a broad range of power plants and scenarios. There are many situations where these approaches can lead to notable advances, including start-ups and shut-downs, that were not tested, and there are even more refinements that might improve the proposed control and scheduling approaches. The author hopes this work contributes to the academic community and to the transition towards a better and more sustainable power system.

1.4   Thesis structure

This thesis comprises six chapters that present the motivation and analysis included in five journal papers. Chapter 2 describes the energy scenario since the Industrial Revolution, presents the main available evidence supporting global warming, and briefly discusses the main approaches to mitigate its effects. This is the foundation to discuss the fundamental purpose of the power sector in future energy systems and the role flexible thermal power plants and CCS can have. Then, each chapter refers to an unique paper, except Chapter 4 that describes the content of two journal publications. These chapters are self-contained and should be possible to read them independently. Nevertheless, the structure follows a logical order, rather than chronological, to ease the understanding of the reader, motivate topics covered in upcoming chapters, and describe methods or approaches needed in future sections.

Chapter 3 analyses qualitatively the transient behaviour of both thermal power plants and post-combustion capture systems, discusses the dominant dynamics that govern their operation, identifies the main bottlenecks inhibiting better flexible performance, and includes the results that demonstrate how the integration of both plants has an almost negligible impact on the power generation of the thermal power plant. Chapter 4 addresses one of the most important bottlenecks of thermal power plants identified in the previous chapter, the thermal and mechanical stresses in the equipment of the steam cycle, and presents a methodology to control the power plant and limit the stress within safety levels. This chapter describes two formulations to ease the implementation of this control methodology with stress monitoring. Chapter 5 considers a longer time scale of operation of thermal power plants and includes a scheduling method to include the uncertainty on power demand generated by large shares of renewable power generation and enhance the integration, profit and lifetime utilisation of flexible thermal power plants with and without CO_2 capture. Chapter 6 discusses a model predictive control strategy to stabilise and optimise the transient performance of a natural gas combined cycle with post-combustion CO_2 capture, and presents an algorithm to achieve optimal reference tracking in this type of energy systems. Finally, Chapter 7 summarises the main contributions of this Ph.D. thesis and dis-

cusses possible future research paths to continue enhancing the flexible operation of thermal power plants integrated with carbon capture and storage.

1.5 Publications and scientific dissemination

The work during these three years of Ph.D. has resulted in five journal papers, four conference papers, and a six-month research stay at Imperial College London.

1.5.1 Journal articles

Rúa, J., Bui, M., Nord, L. O., and Mac Dowell, N. Does CCS reduce power generation flexibility? A dynamic study of combined cycles with post-combustion CO_2 capture. *International Journal of Greenhouse Gas Control*, 95:102984, 2020. (Chapter 3)

Rúa, J., Agromayor, R., Hillestad, M., and Nord, L. O. Optimal dynamic operation of natural gas combined cycles accounting for stresses in thick-walled components. *Applied Thermal Engineering*, 170:114858, 2020. (Chapter 4)

Rúa, J. and Nord, L. O. Optimal control of flexible natural gas combined cycles with stress monitoring: Linear vs nonlinear model predictive control. *Applied Energy*, 265:114820, 2020. (Chapter 4)

Rúa, J., Verheyleweghen, A., Jäschke, J., and Nord, L. O. Optimal scheduling of flexible thermal power plants with lifetime enhancement under uncertainty. *Applied Thermal Engineering*, 191:116794, 2021. (Chapter 5)

Rúa, J., Hillestad, M., and Nord, L. O. Model predictive control for combined cycles integrated with CO_2 capture plants. *Computers & Chemical Engineering*, 146:107217, 2021. (Chapter 6)

1.5.2 Conference articles

Rúa, J., Montañés, R.M. and Riboldi, L., Nord, L.O. Dynamic Modeling and Simulation of an Offshore Combined Heat and Power (CHP) Plant. In *Proceedings of the 58th Conference on Simulation and Modelling (SIMS 58), 25-27 September 2017, Reykjavik, Iceland*, pages 241-250. Linköping University Electronic Press, 2017.

Agromayor, R., Rúa, J. and Kristoffersen, R. Simulation of Starting and Stopping Vortices of an Airfoil. In *Proceedings of the 58th Conference on Simulation and Modelling (SIMS 58), 25-27 September 2017, Reykjavik, Iceland*, pages 66-75. Linköping University Electronic Press, 2017.

Rúa, J. and Nord, L. O. Exergy Analysis for Combined Heat and Power (CHP) Plants. In *Proceedings of The 59th Conference on Simulation and Modelling (SIMS 59), 26-28 September 2018, Oslo Metropolitan University, Norway*, pages 1–8. Linköping University Electronic Press, 2018.

Rúa, J. and Nord, L. O. Stress Monitoring During Optimal Dynamic Operation of a Natural Gas Combined Cycle: Linear Vs Nonlinear Formulation. In *International Conference on Applied Energy, 12-15 August 2019, Västerås, Sweden.* Energy Proceedings, 2019.

Chapter 2

Energy context

The Industrial Revolution marks a major turning point in history, shaping modern societies and natural ecosystems. During the period between 1760 and 1840, factories transitioned from traditional production methods based on elementary tools and manual labour to mechanised processes where machines and steam power were the main driving forces. Industrialisation originated population and economic growths, increased the standard of living of western societies, and changed the structure of many industries and processes. However, the Industrial Revolution also set the beginning of a harmful period where the continuous temperature rise of oceans and land has altered the climate and jeopardised the biosphere.

2.1 Global warming

Since the end of the Industrial Revolution, the atmospheric concentration of carbon dioxide, methane, nitrous oxides, and other greenhouse gases has increased until levels not reached before. High concentration of these gases produces imbalances in the radiation entering and leaving the atmosphere and, consequently, a net energy increase that translates into global warming. Fig. 2.1 represents the global average atmospheric concentration of CO_2 and the average land-sea temperature anomaly since the end of the Industrial Revolution. Measurements of temperature anomaly by two independent institutions, Goddard Institute for Space Studies (GISS) and Met Office Hadley Centre, show reasonable agreement and correlate with the increasing CO_2 concentration measured in the atmosphere. Natural drivers may describe the variability in temperature anomalies before the second half of the 20th century, but temperature data in the last decades cannot be explained without considering anthropogenic forcings (Canty et al., 2013; IPCC, 2014; Knutson et al., 2016, 2017).

Analysis of the data from the Vostok ice core extracted in Antarctica supports the hypothesis that global warming is the result of human activity (Petit et al., 1999). This project provides further evidence of the historic correlation existing
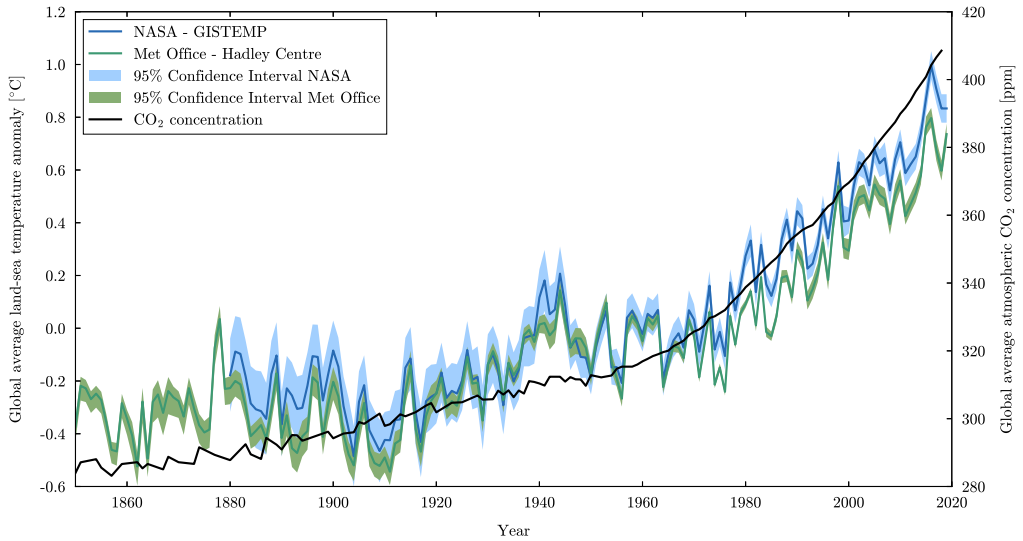
Figure 2.1: Global average land-sea temperature anomaly and atmospheric CO_2 concentration since the end of the industrial revolution. Data obtained from Morice et al. (2012), Bereiter et al. (2015), Lenssen et al. (2019), GISTEMP Team (2020).
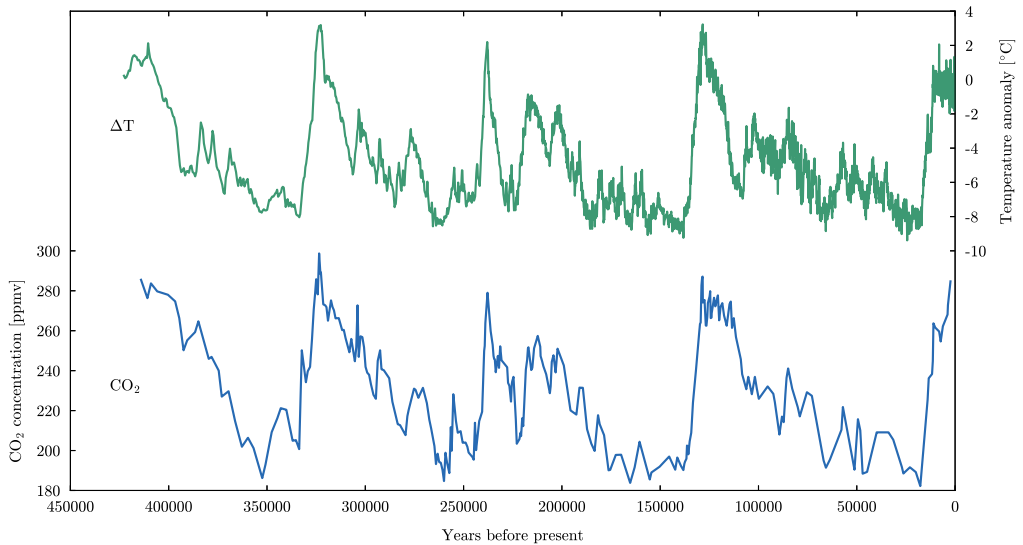
Figure 2.2: Atmospheric CO_2 concentration and temperature difference with respect to the mean recent time value (i.e. corresponding departure from -438‰ mean deuterium value) obtained from Vostok ice core data (Petit et al., 1999).

between CO_2 concentration and average global temperature millennia before human influence on climate, as shown in Fig. 2.2. Thus, the impossibility to explain current global temperature with solely natural drivers, the historic relationship between CO_2 concentration and average global temperature, and the increase in recent decades of anthropogenic greenhouse gas emissions and global temperature, indicate that the human factor is the main responsible of global warming (IPCC, 2014).

Carbon dioxide has the largest impact on the overall temperature rise among the many gases that contribute to the greenhouse gas effect (IPCC, 2014). This occurs despite it has the lowest global warming potential (GWP), as the large CO_2 emissions compared to other greenhouse gases offset the difference in GWP (IPCC, 2014). Therefore, most of the efforts to mitigate climate change have concentrated on reducing the overall CO_2 emissions.

Current mitigation strategies aim at limiting to 1.5 °C the temperature increase with respect to pre-industrial levels in 2050, instead of the previous, less-ambitious goal of 2 °C (IPCC, 2018). This temperature difference would reduce risks related to health, livelihood, food and water supply, and human security; lower most adaptation needs to mitigate climate change, which would benefit the more threatened countries with less resources; and contain the effects on climate, biodiversity and natural ecosystems (IPCC, 2018).

Mitigation policies defined under the Paris Agreement (UNFCCC, 2015) are not sufficient to limit the temperature increase below 1.5 °C (IPCC, 2018). There are, however, different pathways and several portfolios of measures that may limit global warming to 1.5 °C with no or limited overshoot, but these alternatives need to stay within a total carbon budget of 770-420 $GtCO_2$ emissions with uncertainties of ± 1000 $GtCO_2$ (IPCC, 2018, Summary for Policymakers, p. 14). Reduction of energy and resource intensity, decarbonisation, and carbon dioxide removal are the three types of measures that might achieve this objective. Their contribution varies depending on the pathway and technology portfolio considered, but all scenarios require profound and fast transitions in all sectors to limit the temperature rise below 1.5 °C and mitigate the effects of global warming (IPCC, 2018). Furthermore, energy demand is expected to increase in future years (IEA, 2019). Thus, this transition needs to address the dual challenge of mitigating climate change while meeting the increasing energy demand.

Deployment of clean energy technologies and utilisation of low-carbon sources might fulfil both objectives, but large investments and rapid changes across all sectors will be necessary to reach a sustainable energy system. Fig. 2.3 represents the energy consumption by source between 1949 and 2019. Nuclear and renewable energy sources have progressively increased their contribution to the overall energy consumption in this period. Nevertheless, they still represent a small share albeit recent efforts on expanding the total installed capacity of renewable technologies. Fossil fuels have historically been the main energy sources of the global energy system, with their contribution growing over decades because of the increase in
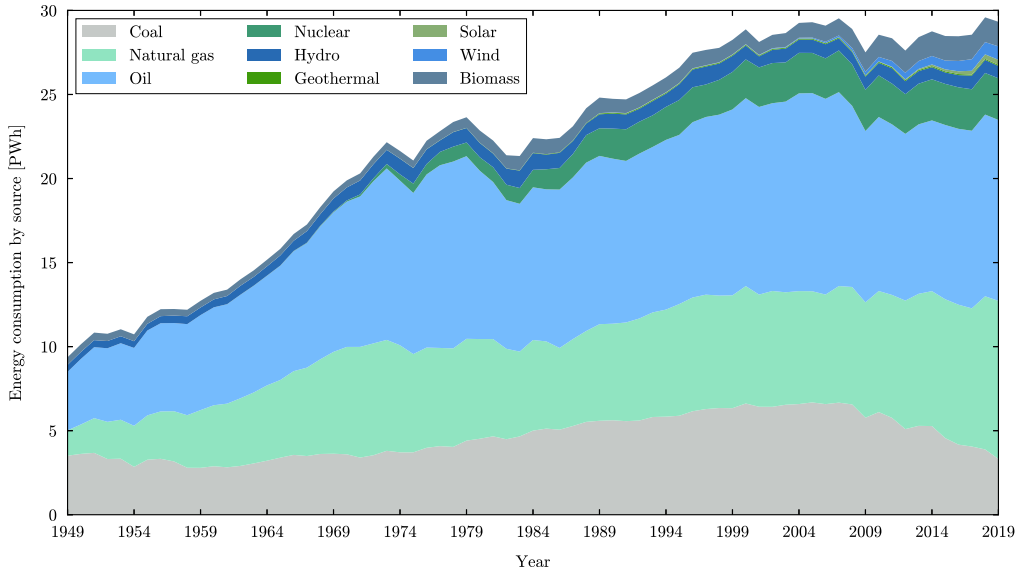
Figure 2.3: Global primary energy consumption by source between 1949 and 2019. Source: U.S. Energy Information Administration (2020).
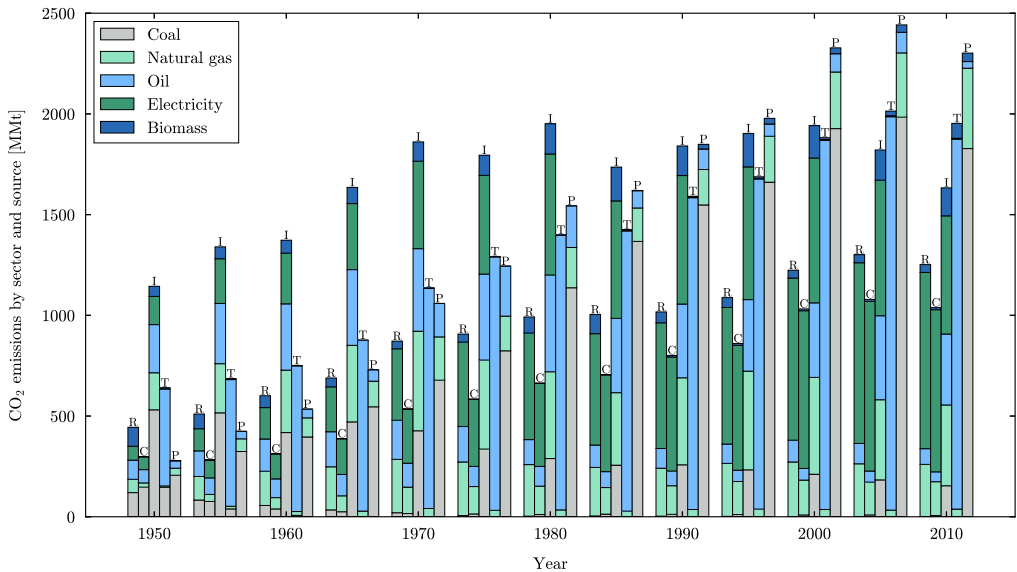
Figure 2.4: Global CO_2 emissions in million metric tons (MMt) by sector and source between 1950 and 2010. The sectors are: Residential (R), Commercial (C), Industry (I), Transport (T), and Power (P). Source: U.S. Energy Information Administration (2020).

energy demand. CO_2 emissions have risen accordingly, although a plateau might have been reached in the last two decades (see Fig. 2.4). The stabilisation of CO_2 emissions despite the increasing energy demand and reliance on fossil fuels is the result of past environmental measures such as fuel switching from coal to low-carbon energy sources, mainly natural gas, and the utilisation of clean technologies. This proves the effectiveness of the transition towards a sustainable energy system and points out the urgent need to accelerate deeper changes that allow meeting the 1.5 °C goal.

The effects of the current transition towards a sustainable energy system are also observable in the CO_2 emissions and energy consumption of different sectors, represented respectively in Figs. 2.4 and 2.5. Energy consumption from the residential, commercial and industrial sectors has slowly increased over time, whereas the transport and power sectors have experienced more pronounced growths and are responsible for the overall rise in energy demand.

Electrification of different processes, industries and technologies is the main contributor to the rapid energy consumption increase in the power sector. This trend is expected to continue as it eases the decarbonisation of other sectors where there are fewer alternatives to reduce greenhouse gas emissions (IEA, 2019). Therefore, the power sector will require profound changes in order to meet a continuously increasing demand whilst reducing CO_2 emissions. This goal has been partially achieved in the last decades since the increase of CO_2 emissions associated to the power sector is not as acute as of its energy consumption (see Figs. 2.4
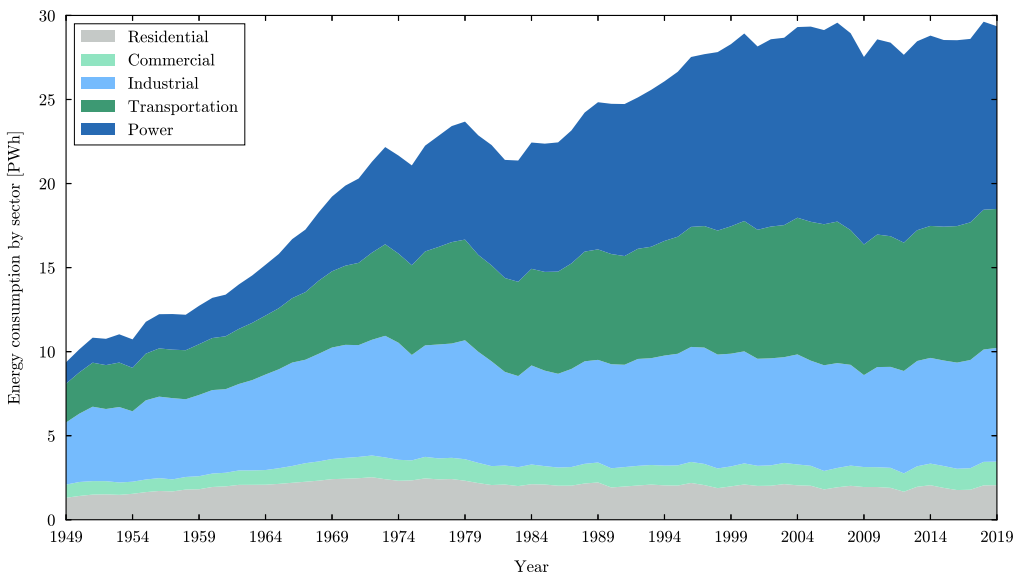
Figure 2.5: Global primary energy consumption by sector between 1949 and 2019. Source: U.S. Energy Information Administration (2020).

and 2.5). Nevertheless, the decarbonisation of the power sector will require further measures, prompt action and technological advancement (Heuberger et al., 2017, 2018).

2.2   Power sector: past, present and future

Historic reliance on fossil fuels and increasing demand of power due to the continuous electrification of other sectors make power generation the largest source of CO_2 emissions (see Fig. 2.4). Fig. 2.6 illustrates the contribution of different sources to the total net electricity generation since 1949. Traditional thermal power plants have been the foundation of current power sector as they are the largest contributors. Coal-fired units were the main drivers in the past because of the well-established technology and the low prices of the fuel. However, as a result of the transition towards low-carbon technology, power plants based on burning natural gas have increased their share in recent years at expense of reducing the power generation of the more polluting and less efficient coal power plants.

Nuclear plants have been the largest power generation source among the technologies that can deliver electricity without greenhouse emissions. The role of this energy source in the future is, however, uncertain. Whilst the recent accident in Fukushima (Japan, 2011) and the memories from the nuclear disaster in Chernobyl (Ukraine, 1986) turned part of the public opinion against this technology and some countries have started phasing out their nuclear power plants, energy
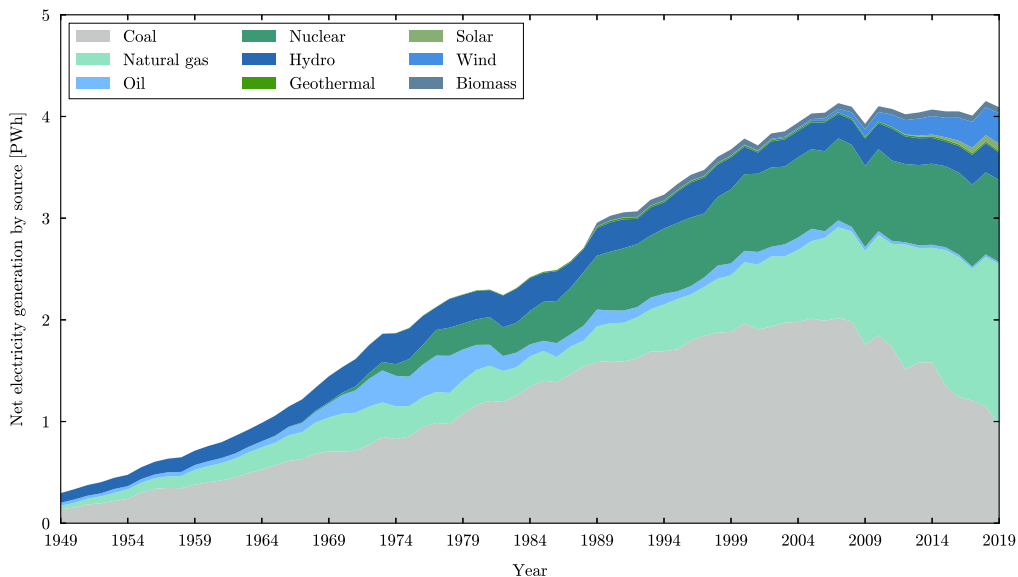
Figure 2.6: Global net electricity generation by source between 1949 and 2019. Source: U.S. Energy Information Administration (2020).

planning studies suggest nuclear power as one of the main drivers to reach the target of limiting global warming to 1.5 °C respect to pre-industrial levels (Eser et al., 2017; Heuberger et al., 2017; IEA, 2019). Thus, nuclear power generation may be considered as one of the contributors in the future power sector.

The contribution of renewable energy sources to the power generation mix was traditionally based on hydropower plants and biomass. Efforts in recent years have concentrated in the deployment of onshore and offshore wind generators, and photovoltaic (PV) and thermal solar systems (IEA, 2019). Installed power generation capacity of these renewable energy sources will continue to grow, gaining progressive relevance within the power sector (IEA, 2019). This affects specially offshore wind and PV solar plants owing to their large installation potential, growing experience, and reduction of costs (Eser et al., 2017; IEA, 2019). Hydropower is expected to contribute with 15% of the total power demand, a share similar to recent years (IEA, 2019). Biomass may also play an important role in the decarbonisation of the power sector since it can deliver carbon-neutral electricity, or even negative emissions if combined with carbon capture and storage in a technology known as BECCS (bio-energy CCS) (Bui et al., 2017; Fajardy and Mac Dowell, 2017; IPCC, 2018), but its efficacy at large scale is yet to be demonstrated (Bui et al., 2018a). Furthermore, biomass is an energy source that can reduce the CO_2 emissions of different sectors, including fuel-switching in different industries, use of biofuels in the residential and transport sectors, and biomass for heating in the residential, commercial and industrial sectors. This broad range of applicability might limit the utilisation of biomass in the power sector and hence its contribution to the delivery of low-carbon electricity.

Wind and solar power concentrate most of the efforts to decarbonise the production of electricity, but these technologies also add uncertainty and reliability issues associated with their intermittent power generation. Mismatches between demand and supply can hence originate from this intermittent power generation. Moreover, the increasing reliance on the power sector and growing share of energy from wind and solar sources will intensify this problem.

Future energy systems need to address this issue and develop mechanisms to compensate the volatility associated with power generation from renewable energy sources. Flexible dispatch of power refers to the capacity of power systems to modify the power supply and balance the variability in the demand, and is considered the cornerstone of an efficient, reliable and sustainable power sector (IEA, 2019). Energy storage, interconnection between power systems, demand management, curtailment, power conversion and rapid operation changes of different power plants are the main procedures to balance power generation and demand (Kondziella and Bruckner, 2016; Lund et al., 2015). These mechanisms are necessary to achieve a flexible power system, but their applicability differs in the time scale and amount of power that needs balancing.

Rapid changes in power generation from renewable energy sources can momentarily alter the frequency and voltage of the power grid, whose control occurs

in the short time scale, i.e. within milliseconds and seconds. There are different electronic devices specifically installed in the power grid, e.g. supercapacitors, to regulate these parameters. However, power suppliers also contribute to the stabilisation of both frequency and voltage (Carrasco et al., 2006). Traditionally, thermal power plants have modified the rotational speed of their turbines. In future power systems with several flexible power dispatch mechanisms, energy storage technologies with immediate response, e.g. electric batteries, and wind turbines supplying active and reactive power will also contribute to the regulation in the short time scale (Carrasco et al., 2006; Divya and Østergaard, 2009). Therefore, the new power generation technologies will complement existing power plants and provide power operators with more options to ensure adequate frequency and voltage control.

Mismatches between power supply and demand occur in longer time scales, i.e. in the order of seconds and minutes. This type of imbalance is arguably the most complex issue related to volatility of wind and solar power. Thus, most procedures and technologies to achieve flexible power generation focus on this problem.

Energy storage with batteries can balance small power mismatches in the grid for short periods of time but cannot provide or absorb significant amounts of power for long periods because of their limited capacity (Dunn et al., 2011). Moreover, their cost-effectiveness, technology maturity and commercial availability at large scale restrict the deployment of this technology (Chen et al., 2009; IEA, 2014). In contrast, thermal energy storage has larger capacity and can balance the grid for longer periods of time (Farid et al., 2004). Thermal solar power is the main application of this type of energy storage. This limits the effect of this technology on the overall reserve capacity of the power grid since the contribution of thermal solar power to the total electricity generation is small. Pumped-hydro storage is the most mature technology and has the largest capacity of all energy storage alternatives. The main drawbacks are its reliance on surplus of clean electricity in energy systems with limited power from renewable energy sources and increasing demand, and the need of adequate geographical conditions, which constraints its installation to countries with suitable orography (Lund et al., 2015). Nevertheless, the growing installed capacity predicted for the future of solar, and specially wind, power will benefit pumped-hydro storage. Conversion of excess power to gas or hydrogen is another energy storage approach that will profit from the increasing renewable energy capacity, although it is currently limited by the shortage of power from sustainable energy sources and the lack of production facilities and distribution networks (Lund et al., 2015). Demand management can complement these energy storage technologies as it provides mechanisms to smooth peak and valley demands and achieve a more stable power system (Lund et al., 2015).

Grid interconnections ease the balance of power demand and supply by offsetting a fraction of this difference to other power systems (Lund et al., 2015). This is specially important for small energy systems where flexible power dispatch

is more difficult because of the more limited mechanisms available (Huber et al., 2014). While this approach allows sharing the balancing problem among different power systems, it does not solve completely this issue since the power supply still needs to meet the demand.

Overall, the technologies and mechanisms discussed so far that are able to dispatch flexible power cannot address independently and simultaneously the main two issues associated with intermittent power generation from renewable energy sources: balancing large variations of power generation within short periods of time. Some of these technologies can currently offer fast response for limited power balance, or large power capacity for short periods of time. Other balancing mechanisms show potential to contribute to flexible future energy systems, but they still require further research, development, and investment in infrastructure. Thermal power plants can address both issues (Alobaid et al., 2017; Hentschel et al., 2016).

2.3 Flexible thermal power generation and CCS

Thermal power plants will play a fundamental role balancing supply and demand in future energy systems. This type of power plants possess large energy capacity, i.e. can deliver substantial power generation changes by modifying their operating conditions, and are able to ramp up and down, start up and shut down in short periods of time (Hentschel et al., 2016). Consequently, they can absorb the high volatility from renewable power generators.

Base-load operation was the main power generation mode in the past. Thermal power plants operated at nominal conditions most of the time with few start ups and shut downs, which lead to efficient and profitable power generation. Deployment of renewable energy technologies and its associated variability will require a change in the design and operation of thermal power plants (Lise et al., 2013; Oswald et al., 2008). As a result, these units will cycle more frequently and with steeper ramps, and will be exposed to more start ups and shut downs (Eser et al., 2017; Gonzalez-Salazar et al., 2018; Huber et al., 2014; Lew et al., 2012; Oswald et al., 2008). Steady-state operation at off-design conditions will be also more common. This will require to modify the design of thermal power plants to achieve higher efficiencies at different part loads (Riboldi and Nord, 2018).

Minimun load, start-up time and maximum load gradient are normally the three criteria that assess the operational flexibility of thermal power plants (Alobaid et al., 2017). Minimum load refers to the lowest possible power output that guarantees stable stable combustion and $CO - NO_x$ levels in compliance with emission regulations. Gas turbines limit natural gas combined cycles to 40-50% of the nominal load, although this level is expected to decrease to 20% with sequential-combustion designs; whereas biomass and coal-fired power plants can operate at 20% of nominal conditions (Alobaid et al., 2017). Having a low minimum load

allows thermal power plants to act as spinning reserves, avoid excessively frequent start ups and shut downs, and balance more rapidly the variation in renewable power generation.

Start up, shut down and ramping time depend on both design of the power plant and the control strategy implemented. The design of flexible thermal power plants is a trade-off among efficiency at nominal and off-design conditions, and adequate transient performance. It determines size and geometry of steam generators in the steam cycle, and hence its heat capacitance, dynamic behaviour, and time to start up and ramp up and down (see Chapter 3). However, the design does not completely determine the transient performance of thermal power plants. Suitable control strategies can reduce the time required to start up, shut down and cycling between operating loads. Moreover, these control procedures may be adapted over time according to the needs of every individual power plant, in contrast to its design, which can only be modified under major remodelling work. Therefore, the analysis of the dynamic behaviour and different control strategies for flexible thermal power plants will be fundamental in the transition towards a sustainable power sector.

Thermal power plants are the main responsible for the CO_2 emissions throughout history but, at the same time, they are expected to be one of the pillars during the decarbonisation of the power sector. A natural question might arise at this point: How can these two statements hold, if they are contradicting each other? The key to deliver low-carbon electricity and provide flexible thermal power generation is carbon capture and storage (CCS).

Carbon capture and storage groups all technologies that can remove CO_2 emissions from fixed-point sources and transport them to locations where can be safely stored and isolated from the atmosphere (IPCC, 2005). Post-combustion, pre-combustion and oxy-combustion are the fundamental methods to capture CO_2 emissions that otherwise would be emitted to the environment (Boot-Handford et al., 2014; Bui et al., 2018a; IPCC, 2005; MacDowell et al., 2010). Fig. 2.7 summarises the main characteristics of these three CO_2 capture systems.

Integration of thermal power plants with any of these CCS technologies enables flexible power generation with low or null CO_2 emissions. Therefore, this type of systems can balance the intermittent power generation from renewable energy sources while reducing, or removing, the greenhouse emissions of the power sector (Alie et al., 2009; Brouwer et al., 2015; Montañés et al., 2016). Moreover, CCS could also deliver negative emissions if combined with biomass power plants (Bui et al., 2017, 2018a; Fajardy and Mac Dowell, 2017).

Bio-energy CCS is considered essential to accomplish the target of limiting the temperature increase 1.5 °C respect to pre-industrial levels (Daggash and Mac Dowell, 2019; IPCC, 2018), but it is still at development stages (Bui et al., 2018a). Rapid action is, however, necessary to do not exceed the available carbon budget and meet the 1.5 °C goal. Delay in the deployment of renewable and low-carbon technologies would impede energy system decarbonisation, and lead to
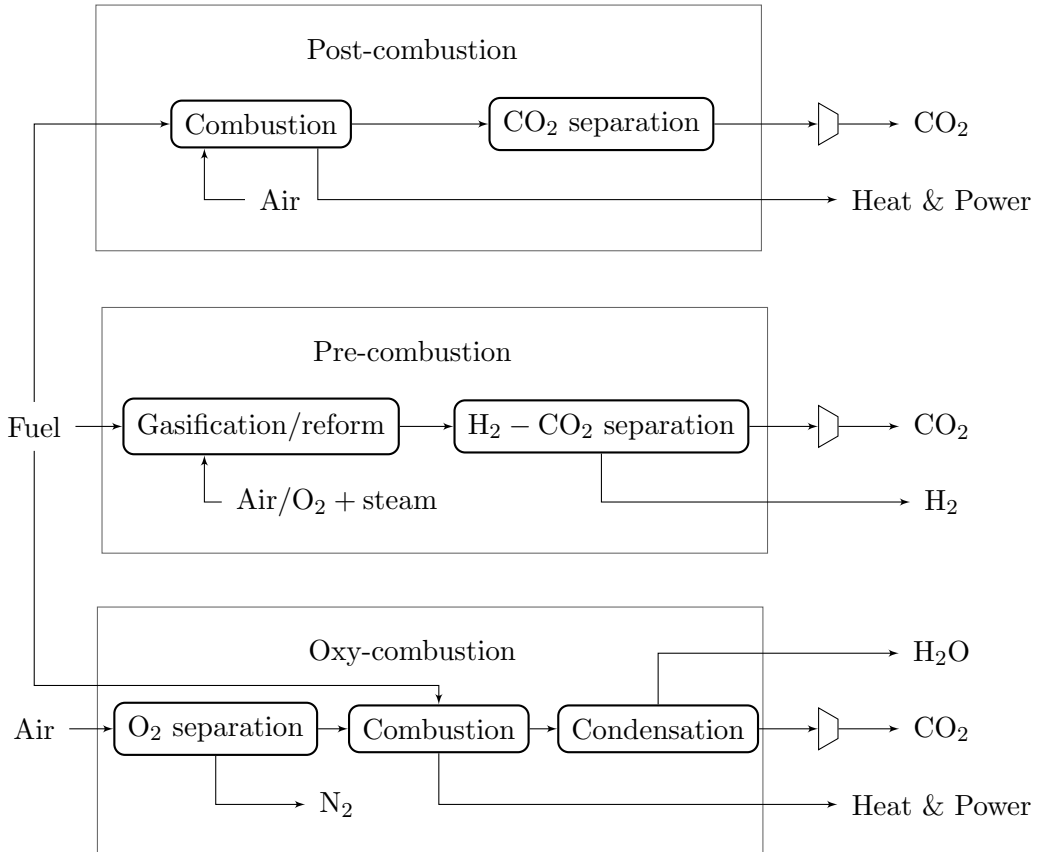
Figure 2.7: Schematic representation of CO_2 capture systems for power generation.

capacity over-sizing and higher costs (Heuberger et al., 2018). Thus, the utilisation of available low-carbon technologies seems the most efficient and cost-effective approach to decarbonise the power sector.

Post-combustion CO_2 capture is arguably the most mature CCS technology and the most likely to be deployed at large scale (Bui et al., 2018a; IPCC, 2005). This type of capture plants can be easily integrated with thermal power plants and can remove close to all carbon emissions. Nevertheless, the expansion of post-combustion CO_2 capture in future power sectors with large installed capacity of renewable energy requires deep understanding of the dynamic behaviour of this CCS system and the coupling effects when integrated with thermal power plants (Alie et al., 2009; Montañés et al., 2016).

Despite there are already two full-scale coal-fired power plants integrated with post-combustion CO_2 capture and several pilot plants functioning (Bui et al., 2018a), transient operation of these energy systems has not been extensively studied. Dynamic modelling and simulation remains the main tool to gain insight into the dynamics of flexible thermal power with CCS (Bui et al., 2014, 2018b). There-

fore, developing further knowledge and experience into the dynamic behaviour could help improve the accuracy and robustness of dynamic process control and scheduling during flexible operation, plant start-up and shut-down. This could ultimately accelerate the deployment and utilisation of flexible thermal power plants integrated with post-combustion CO_2 capture.

Chapter 3

Dynamic behaviour of thermal power plants and CO$_2$ capture systems

Flexible operation of thermal power plants integrated with post-combustion CO$_2$ capture requires frequent and rapid cycling between different loads, and more start ups and shut downs. This performance expands the time these energy systems operate in transient conditions and entails adequate procedures and control strategies for different operation modes. Understanding the intrinsic dynamic behaviour of thermal power plants, post-combustion CO$_2$ capture units, and integrated systems is essential for the development of such strategies and the identification of bottlenecks that inhibit better transient performance. Furthermore, coupling of power and capture plants might affect power generation during dynamic operation. It is hence fundamental to ascertain whether power control strategies are needed to compensate the effects of system integration. This chapter is based on Rúa et al. (2020b) and describes the dynamic behaviour of thermal power generation and CO$_2$ capture individually, and the combined transient performance of the integrated system.

3.1 Thermal power plants

Heavy-duty thermal power plants are the main complement to post-combustion CO$_2$ capture within the power sector since this technology is more cost-effective with large-emission sources (IPCC, 2005). Large-scale coal and biomass power plants (CPP and BPP, respectively) operate under the same principle. Combustion of the fuel provides the energy to produce pressurised, superheated steam that generates power through its expansion in a steam turbine of several stages. Supercritical coal-fired power plants use once-through steam generators, whereas subcritical coal-fired and biomass plants have several sections at lower and higher

pressures (Alobaid et al., 2017). These plants also include reheating and preheating of steam and water, as it increases the efficiency of the steam cycle (Alobaid et al., 2017).

Similarly, natural gas combined cycles (NGCCs) consist of a steam cycle where steam expanded in a multi-stage turbine generates electrical power. Reheating is also part of contemporary configurations owing to its efficiency increase. However, steam cycles in modern NGCCs have three pressure levels to minimise the temperature difference, and hence exergy destruction, between the exhaust gas of the gas turbine and the working fluid in the steam cycle (Alobaid et al., 2017; Bolland, 1991; Kehlhofer et al., 2009). One main difference between NGCCs and CPPs/BPPs is the gas turbine. This component generates most of the power in NGCCs while its exhaust gases are the energy source to produce steam in the bottoming cycle. Because of the increasing efficiency of modern, heavy-duty gas turbines, NGCCs can reach overall efficiencies of up to 64% with respect to the lower heating value (LHV) of the fuel. In contrast, CPPs and BPPs have nominal efficiencies around 45% due to their exclusive reliance on the steam cycle to generate power (Hentschel et al., 2016).

Gas turbines also change the transient behaviour of NGCCs compared to other thermal power plants with power generation exclusively from the steam cycle. Turbomachinery components, i.e. pumps, compressors, turbines, and electric motors, can change their operating point within seconds. Thus, they introduce negligible dynamics in the overall behaviour of thermal power plants. Gas turbines exhibit this transient performance, albeit combustion stability and damage in the first stage of turbine blades limit the maximum ramps (Kehlhofer et al., 2009). Modern, heavy-duty gas turbines can deliver up to 17.5%/min ramps. NGCCs inherit this ramping capacity from gas turbines and can hence provide steep power ramps within seconds. This enhances the utilisation of NGCCs as flexible power plants to balance power demand and supply.

Steam generators are, on the contrary, the main limitation of large-scale thermal power plants during transient operation (Alobaid et al., 2017; Kehlhofer et al., 2009). These power systems require substantial amounts of energy to produce pressurised, superheated steam and hence electricity. Heat transfer between energy source and steam cycle occurs at small temperature differences to minimise exergy destruction, which results in large heat transfer areas. Consequently, steam generators are bulky equipment with large mass of metal. The heat capacitance of this type of components allows the storage of large amounts of energy. This produces a delay between the change of conditions in the energy source side and the water/steam counterpart, and slows down the transient operation of the overall thermal power plant.

Steam turbines generate all the power in CPPs and BPPs. Therefore, for a given nominal power output, these plants need larger mass flow rates of steam than NGCCs. This requirement leads to bigger and bulkier steam generators in CPPs and BPPs, and thus to slower transient operation. Moreover, gas turbines account

for most of the power output in NGCCs, which enhances the rapid dynamic behaviour and balancing capability of this type of thermal power plant (Alobaid et al., 2017; Kehlhofer et al., 2009). Fig. 3.1 shows a generic dynamic behaviour of different thermal power plants of similar nominal power output and illustrates their different transient performance and minimum load.

There exist different approaches to enhance the rapid transient operation of large-scale thermal power plants. Valves at the inlet of steam turbines can control power generation, although this approach should be avoided to reduce the overall energy losses in the steam cycle and maximise efficiency. Faster changes in the gas turbine load in NGCCs and the fuel consumption in CPPs and BPPs can also lead to rapid dynamic behaviour. However, drastic operation changes in the steam generator can increase the thermal and mechanical stresses in thick-walled components and damage the equipment. This phenomena is one of the main bottlenecks inhibiting faster dynamic behaviour in thermal power plants, and needs to be considered during transient operation (see Chapter 4). Adequate scheduling may also deliver flexible thermal power generation, since it allows to anticipate variations on power demand and plan the change of operation according to the dynamic behaviour of each thermal power plant (see Chapter 5).
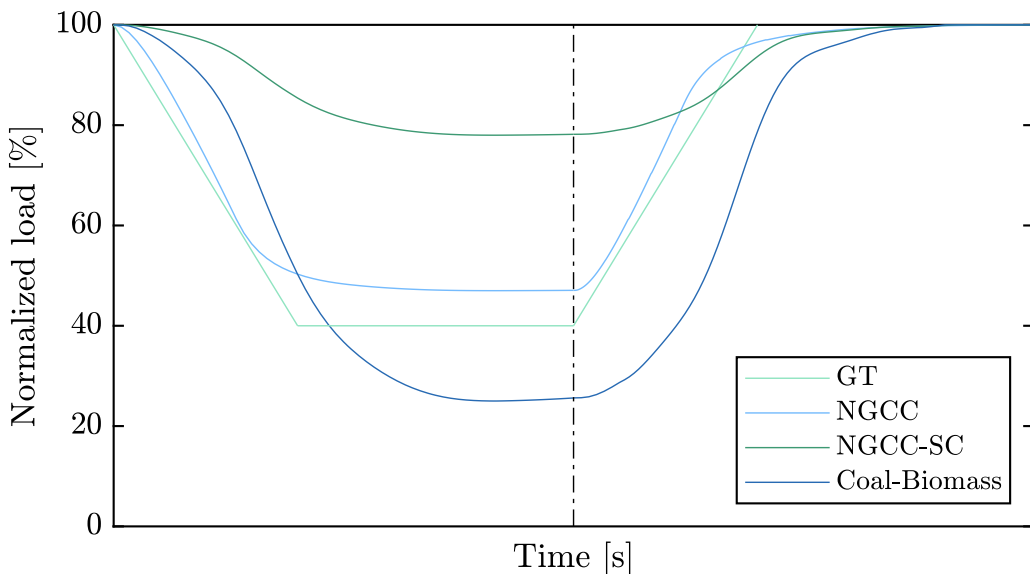
Figure 3.1: Generic dynamic behaviour of different thermal power plants of similar size. Maximum and minimum loads and power generation shares depend on power plant design. The vertical line indicates increasing load dynamic behaviour. The nomenclature is as follows. GT: gas turbine, NGCC: natural gas combined cycle, SC: steam cycle.

3.2 Post-combustion capture plants

Post-combustion capture plants remove CO_2 from flue gases of thermal power plants. There are several chemical methods to separate CO_2 from the exhaust gas, being absorption the most mature approach (Bui et al., 2018a; IPCC, 2005). This type of carbon capture comprises two unit operations: absorption and desorption (or regeneration) (MacDowell et al., 2010).

Absorption CO_2 capture uses a liquid solvent, normally a solution of water and monoethanolamine (MEA), to remove CO_2 from the main stream of gases. Carbon removal occurs inside a packed absorber column where lean, liquid solvent and exhaust gas flow in a counter-current configuration to enhance the absorption of CO_2. In this context, lean indicates low mole fraction of CO_2 in the liquid solvent, whereas rich refers to high mole fractions. The low-carbon exhaust gas is released at the top of the column into the atmosphere, whereas the liquid solvent rich in CO_2 circulates to the desorption section from the bottom of the absorber.

Regeneration of rich solvent includes three elementary units: desorber column, reboiler and condenser. In this second packed column, the desorption process between the rich-loading solvent and a vapour stream removes the excess CO_2 from the solvent, which leaves the column at the bottom and enters the reboiler. This unit provides heat to the liquid in order to break the chemical bonds formed during the absorption process and generate the vapour stream that flows upwards in the desorber and enters the condenser at the top. The purpose of this component is to isolate the CO_2 for future compression and transport, and to produce a liquid reflux that recirculates back to the desorber column.

Capture plants with this configuration also include auxiliary equipment to improve the efficiency of the process, ease the control of the plant during transient operation, and overcome pressure losses. Some of these components are blowers, pumps, compressors, valves, heat exchangers and storage tanks. This equipment behaves differently during transient operation. Therefore, the overall dynamic behaviour of the capture plant depends on the individual contributions of the different components.

Blowers, compressors and pumps, i.e. the rotating equipment, do not introduce any dynamic disturbance during transient operation since these components have almost negligible dynamics. They can modify their operation within seconds and hence are the fastest equipment in post-combustion capture plants. Similarly, piping and heat exchangers do not introduce any dynamic behaviour during the transient of the capture plant, although they are responsible for long delays because of the circulating time in this equipment (Flø et al., 2016; Montañés et al., 2018). Large vessels such as absorber and desorber sumps, storage tanks or reboiler hotwells introduce significant inertia, which buffers and smooths the overall dynamic behaviour of the capture plant (Flø et al., 2016; Montañés et al., 2018). Liquid hold-up in the absorber and desorber columns has a similiar effect, smoothing possible variations along both components. However, their contribu-

tion to the overall dynamics of the capture plant is significantly smaller because of the reduced amount of stored liquid in the packing material. Therefore, the dynamic behaviour of post-combustion capture plants is not governed by the mass balance but by the total volume of solvent, the volumetric capacity of the plant, and the solvent circulation time.

Exhaust gas and steam are the two main inputs of absorption-based capture plants. Thus, transient operation of these plants results from changes in the conditions of any of these flows, i.e. mass flow rate, temperature, pressure or composition. From a control perspective, variations in the exhaust gas are considered as disturbances, whereas the steam conditions are normally regarded as manipulated variables.

Changes in the exhaust gas flow rate during open-loop operation illustrate the small effect of mass balance compared to storage volume in the dynamic behaviour of capture plants. This type of variations principally affects the absorber column. Different conditions in the exhaust gas modify the amount of CO_2 in the packing material and alter the absorption process. As a result, there is a change of energy released in this exothermic reaction, which leads to shifts in the temperature profile along the absorber and offsets in CO_2 capture rate (Bui et al., 2016; Kvamsdal and Rochelle, 2008; Montañés et al., 2018; Tait et al., 2016). Chemical and thermal inertia dominate these variations since the stabilization time of both absorber temperature profile and CO_2 capture rate are larger than the rise time of flue gas flow rate (Montañés et al., 2018). However, these changes in the absorption section do not propagate significantly throughout the capture plant for moderate disturbances in the exhaust gas and constant mass flow rates of solvent, which shows the smoothing effect of large volumes of solvent (Bui et al., 2016, 2018b; Flø et al., 2016; Lawal et al., 2010; Montañés et al., 2017a, 2018). Nevertheless, sufficiently large changes in the exhaust gas conditions should overcome this buffering capacity and propagate to the desorption section.

Modifications of the steam flow conditions also affect the dynamic behaviour of CO_2 capture plants. These changes alter the temperature in the reboiler, and consequently the vapour stream state and operating conditions in the desorber, which ultimately lead to different lean loading in the solvent leaving the column (Bui et al., 2020; Flø et al., 2016; Garðarsdóttir et al., 2015; Lawal et al., 2010; Montañés et al., 2017a). Notable deviations in lean loading might propagate to the absorption section, affecting the absorption capacity of the solvent and the energy released in these chemical reactions, which shift the temperature profile in the absorber column and the CO_2 capture rate (Bui et al., 2016; Flø et al., 2016; Lawal et al., 2010; Montañés et al., 2017a, 2018). If these operation changes also affect the rich loading of the solvent leaving the absorber, the conditions in the desorber can further change because of the different stripping conditions of the solvent entering the desorption section. This results in a continuous feedback between both sections of the capture plant that lead to slow dynamic behaviour and long stabilisation time. Similarly, small variations in the lean loading may be

buffered by the large volumes of solvent along the capture plant.

Overall, the slow transient performance of post-combustion capture plants is a combination of individual factors. Transport delay introduced by heat exchangers and piping, long residence time because of large solvent vessels, and total volume of solvent stored or held-up in the capture plant are arguably the main contributions to the long stabilisation time and slow dynamics observed in CO_2 capture plants. These factors enhance the interaction between the absorbtion and desorption columns. Modifications in the exhaust gas or steam conditions drive the transient operation of capture plants, whereas the absorber and desorber define the dynamic behaviour that propagates throughout the capture plants and feedback each other with continuous operation changes. During this process, large storage tanks, sumps and hotwells buffer and smooth these dynamics, whilst piping and heat exchangers introduce delays. This set of individual contributions shapes the dynamic behaviour of CO_2 capture plants.

3.3 Thermal power plants integrated with CO_2 capture plants

Integration of thermal power plants with CO_2 capture requires different level of structural and operational modifications in both systems depending on the approach. There are essentially two ways to integrate power and capture plants. The simplest form is an "end of pipe" solution. It connects the exhaust gas of the thermal capture plant to the CO_2 capture process, where a external supply source produces the energy required in solvent regeneration. This alternative does not impose any operational limitation and efficiency penalty in the thermal power plant, but it presents the challenge of mitigating the emissions associated with the external energy source. The second approach considers steam extraction from the power plant as energy source for the regeneration of solvent in the capture plant. This method removes the necessity to mitigate the additional emissions related to solvent regeneration, although it affects the operation of the power plant and involves minor structural adjustments. Despite these drawbacks, this second option is normally preferred.

There are different process configurations to integrate thermal power and CO_2 capture plants (Botero et al., 2009; Jonshagen et al., 2012; Jordal et al., 2012; Lucquiaud et al., 2009; Mac Dowell and Shah, 2014). Steam extraction from the crossover between the intermediate- and low- pressure (IP-LP) sections of the steam turbine is the most preferred option (Garðarsdóttir et al., 2017; Lawal et al., 2012; Montañés et al., 2017b). This configuration reduces the net power output of thermal power plants but avoids using external energy sources and additional mechanisms to mitigate their CO_2 emissions. Furthermore, pressurised water from different sections of the steam generator or the condenser can be extracted to control the temperature of the steam fed into the reboiler (Fernandez et al.,

2016; Garðarsdóttir et al., 2017; Montañés et al., 2017b). Fig. 3.2 represents a process diagram of a natural gas combined cycle integrated with a post-combustion capture plant where steam extraction occurs at the IP-LP crossover and spray cooling with pressurised water controls its temperature.

The steam requirement of CO$_2$ capture plants is smaller than the steam available in thermal power plants at different operation points (Jordal et al., 2012; Rezazadeh et al., 2015). Therefore, steam extraction from the steam cycle is not a constraint during transient operation of the integrated system. The dynamics of this process are almost negligible, since valves normally regulate the amount of extracted steam and can move from fully open to close within seconds. Consequently, steam extraction can affect the dynamic behaviour of both power and
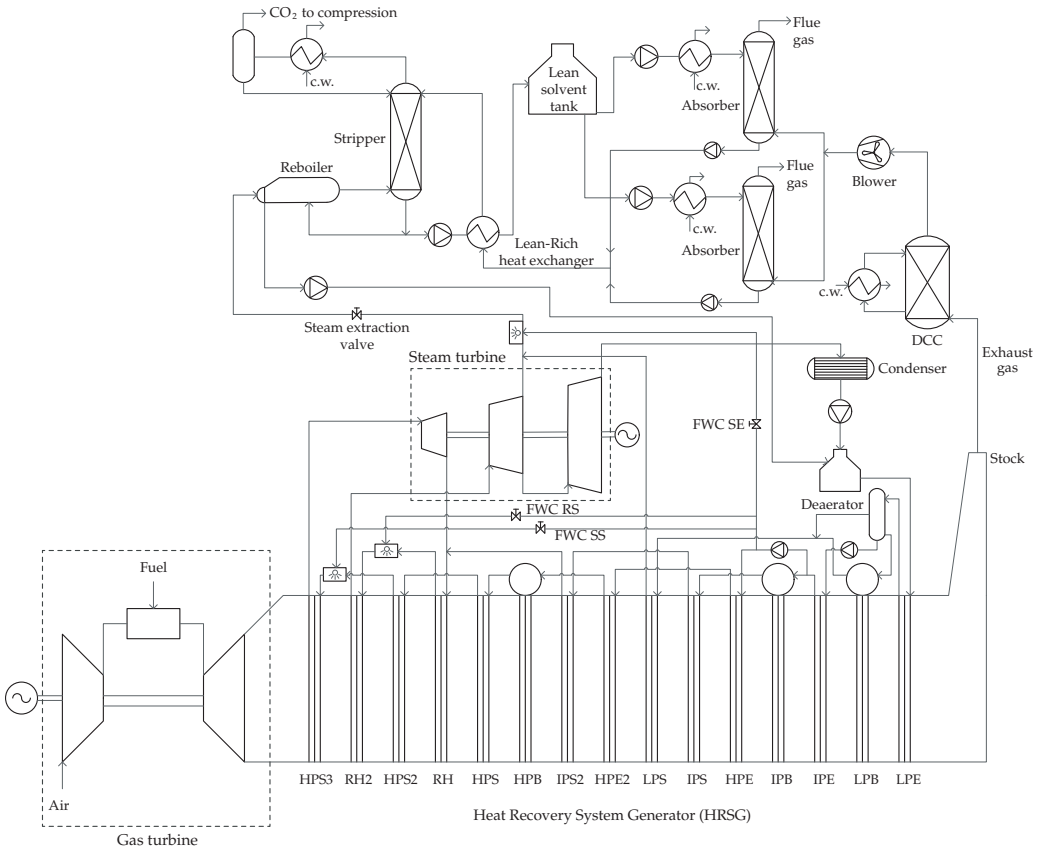
Figure 3.2: Process diagram of a natural gas combined cycle integrated with a post-combustion capture plant. Steam extraction occurs at the crossover between the intermediate- and low- pressure steam turbines. Spray cooling with pressurised water regulates the temperature of the steam. The nomenclature is as follows. E: economiser, B: boiler, S: super-heater, R: reheater, P: pressure, L: low, I: intermediate, H:high, FWC: feed-water cooling, RS: reheated steam, SS: superheated steam, SE: steam extraction, DCC: direct contact cooler, c.w.: cooling water.

capture plants.

Different time scales govern the dynamic behaviour of integrated systems. Heat capacitance in the steam generator limits the transient operation of thermal power plants, whose stabilisation time is in the order of minutes, whereas the large volume of solvent, transport delays and long residence times prolong the dynamic operation of CO_2 capture plants, needing hours to completely stabilise (Garðarsdóttir et al., 2017; Lawal et al., 2012; Montañés et al., 2017b). System integration must consider the distinctive dynamic behaviour of thermal power and capture plants, and address the process interactions that may arise associated with this difference during transient operation.

Power demand defines the operation of thermal power plants. This determines the exhaust gas conditions, i.e. mass flow rate, temperature, and CO_2 concentration, and thus the performance of post-combustion capture plants. Changes in the exhaust gas are disturbances to the capture plant, since they cannot be controlled and depend exclusively on the power demand and generation. Control strategies usually modify the amount of steam fed into the reboiler to remove the offset of key process variables and balance the alterations introduced by varying power demand in the capture plant (Salvinder et al., 2019; Wu et al., 2020). There are several more control actions used to stabilise CO_2 capture plants, but steam extraction is the unique one that interacts with the power plant.

Steam extraction changes in long time scales, i.e. in the time scale dictated by the slow dynamics of capture plants, lead to longer stabilisation times and small fluctuations in power generation from the low-pressure section of the steam turbine (Garðarsdóttir et al., 2017; Lawal et al., 2010; Montañés et al., 2017b). This interaction is not significant for thermal power plants, since their faster dynamics stabilise the net power generation within minutes and the small variations in steam extraction in longer time scales do not influence the overall power output (Garðarsdóttir et al., 2017; Lawal et al., 2010; Montañés et al., 2017b). However, steam extraction in the short time scale, i.e. within the dominant dynamics of thermal power plants, might affect power generation because of the interaction with the transient performance in the steam cycle. Flexible operation of thermal power plants integrated with CO_2 capture systems must consider this issue and study the possible dynamic interaction between power generation and steam extraction in the short time scale.

3.4 Power generation flexibility

Steam extraction in the short time scale affects power generation during transient operation of thermal power plant. This interaction might limit the balancing capacity of these energy systems. To study the dynamic interaction between power generation and steam extraction, a modern NGCC integrated with liquid-absorption CO_2 capture was excited with high-frequency signals. Integration be-

tween the thermal power and capture plants occurred at the IP-LP crossover of the steam turbine. Therefore, the excitation signals were superimposed in the steam extraction valve. This allowed the identification of possible dynamic interactions between both plants and tested whether CO_2 capture affects notably the power generation capacity of the NGCC.

This study used a physics-based dynamic model of a 615 MW NGCC with triple pressure steam cycle and reheating integrated with a 30 wt% MEA-based post-combustion capture process. Fig. 3.2 represents the process diagram of this model. Details about the design, dynamic modelling and validation are presented in the work by Montañés et al. (2017b). The signal superimposed in the steam extraction valve was a damping sine with an offset of 0.69, amplitude of 0.29, and natural and damping frequencies of 0.01 and 0.001 Hz, respectively. A signal with these characteristics ensures that variations in the steam extraction occur faster than the dominant dynamics of the NGCC, despite highly oscillating valve movements do not occur in practice during open-loop operation. Nevertheless, this analysis provides insight into the transient effects of variations in steam extraction on power generation.

Both thermal power and capture plant had only regulatory controllers to guarantee stable operation. This included the stabilisation of steam temperature at the steam turbine inlet, pressures in the deaerator and the low-pressure drum, and inventory control throughout the integrated system. However, the solvent mass flow rate remained constant at nominal conditions, which allowed the variation of the CO_2 capture ratio and the temperature in the reboiler.

The implementation of an excitation signal in the steam extraction valve during a change of load in the gas turbine from 100% to 70% highlighted the interaction between power generation in the NGCC and steam extraction from the capture process. Fig. 3.3 illustrates the effect of varying steam extraction on the net power output and the different steam turbine sections during transient operation of the NGCC. Steam extraction had negligible influence on the high-pressure section of the steam cycle, and hence in the power generation from the high-pressure steam turbine (Fig. 3.3b). In contrast, steam extraction had the largest effect on the low-pressure section of the steam turbine because of the continuous variation on the available mass flow rate (Fig. 3.3d). Power generation from the intermediate-pressure section also fluctuated considerably as a result of the changes of intermediate pressure originated by the varying mass flow rate of steam and sliding-pressure operation of the steam cycle (Fig. 3.3c), although the effect of steam extraction was more pronounced in the low-pressure steam turbine.

Overall, the net power output of the NGCC was almost not affected by the varying power generation from the intermediate- and low-pressure sections of the steam turbine (Fig. 3.3a). This behaviour originates from a dual contribution: the contrary performance of the IP and LP steam turbines and the distinct shares of the gas and steam turbine in the net power output of the NGCC. Figs. 3.3c and 3.3d show how steam extraction had an opposite effect on the power generation

from the intermediate- and low-pressure sections of the steam turbine, which balanced the net power output produced by these two sections. Fig. 3.4 represents the power generation share produced by the gas turbine and each of the sections of the steam turbine at different operation loads. The gas turbine produces most of the power output of the NGCC at both nominal and part-load, whereas the intermediate- and low-pressure steam turbines have smaller contributions. Thus, small variations in these power generation shares lead to almost negligible variations in the overall power generation of the NGCC. High-frequency oscillations in steam extraction do not have a notable effect on total power generation and, consequently, the NGCC can produce power independently of the capture process.
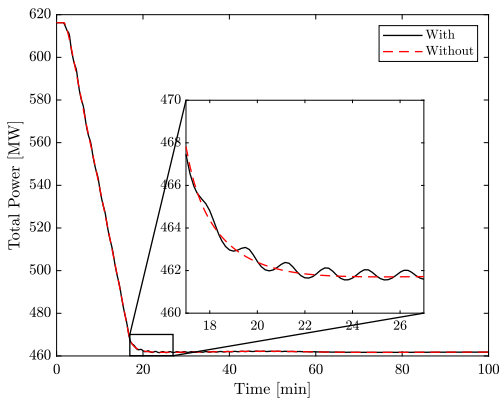
(a) Total power generation of the natural gas combined cycle.
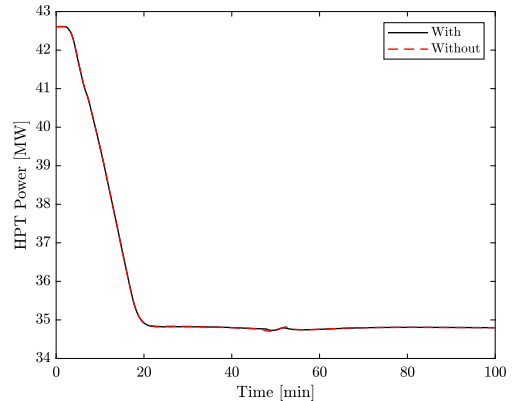
(b) Power generation of the high-pressure steam turbine.
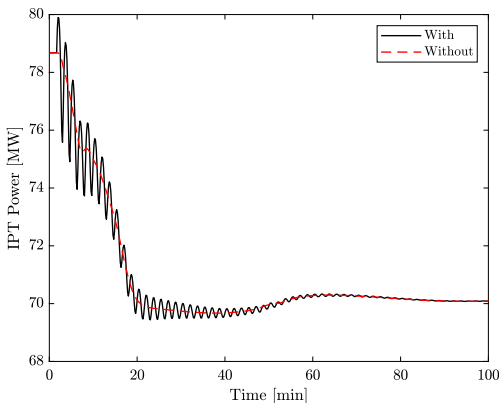
(c) Power generation of the intermediate-pressure steam turbine.
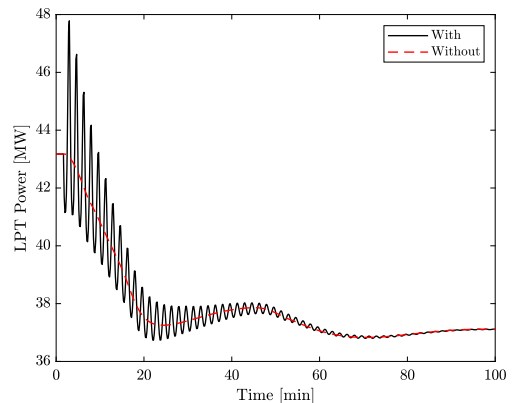
(d) Power generation of the low-pressure steam turbine.

Figure 3.3: Power generation during a gas turbine load change from 100% to 70% with and without fast dynamic fluctuations in the steam extraction valve.

The exhaust gas conditions and steam availability dictate the transient per-
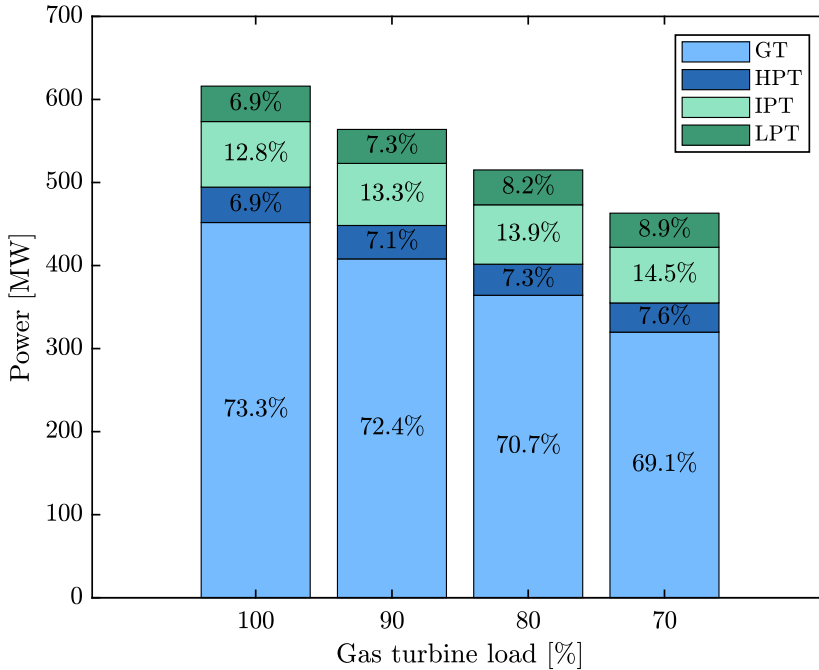
Figure 3.4: Power distribution of the natural gas combined cycle with CCS at different gas turbine loads. Nomenclature: gas turbine(GT), high-pressure steam turbine (HPT), intermediate-pressusre steam turbine (IPT), low-pressure steam turbine (LPT).

formance of post-combustion capture plants. Fig. 3.5 represents the dynamic behaviour of key process variables in the CO_2 capture plant during a load change in the NGCC. Two different dynamics occur simultaneously in these parameters and hence in the capture plant.

Load changes in the gas turbine lead to mass flow rate variations of the exhaust gas that drive the long-term transient operation of the capture plant. Less steam is available in the steam cycle of the power plant because of the decrease of gas turbine load. As a result, there is a reduction of steam extraction for a given opening of the steam extraction valve. Fig. 3.5c shows the drastic drop of steam mass flow rate in the reboiler that follows the load reduction in the gas turbine, and the long stabilisation period arising from the slow dynamics of the capture plant. The reboiler temperature followed similar variations as a consequence of this steam mass flow rate reduction (Fig. 3.5d), which, in turn, affected the lean loading of the solvent at the outlet of the desorber column (Fig. 3.5b) and the capture ratio (Fig. 3.5a). This dynamic behaviour originates from heat capacitance of the reboiler, which creates a delay between the changes in the mass flow rate of the extracted steam and the temperature in the reboiler. Similarly, the residence time within the desorber and the chemical and thermal inertia in the packing material lead to smoother changes in the lean loading of the solvent in the long time

scale. In contrast, the capture ratio experienced fast and drastic variations since modifications in the exhaust gas conditions affect directly the absorber column and thus this process variable. Variations in the lean loading of the solvent also contribute to the transient behaviour of the capture ratio, although its effect is delayed by the long circulation time and large volumes of solvent.

Fast dynamic fluctuation in the steam extraction and the process variables of the capture plant aroused from the high-frequency signal superimposed on the opening of the extraction valve. However, these variations did not disrupt the transient behaviour of the plant as the main process variables followed the same trajectory as in the scenario without fluctuations (Fig. 3.5). This dynamic behaviour highlights that steam availability in the power plant has a more pronounced effect on the dynamic response of the capture plant than the fast dynam-

(a) CO_2 capture ratio.

(b) Lean solvent CO_2 concentration.

(c) Steam mass flow rate.

(d) Reboiler temperature.
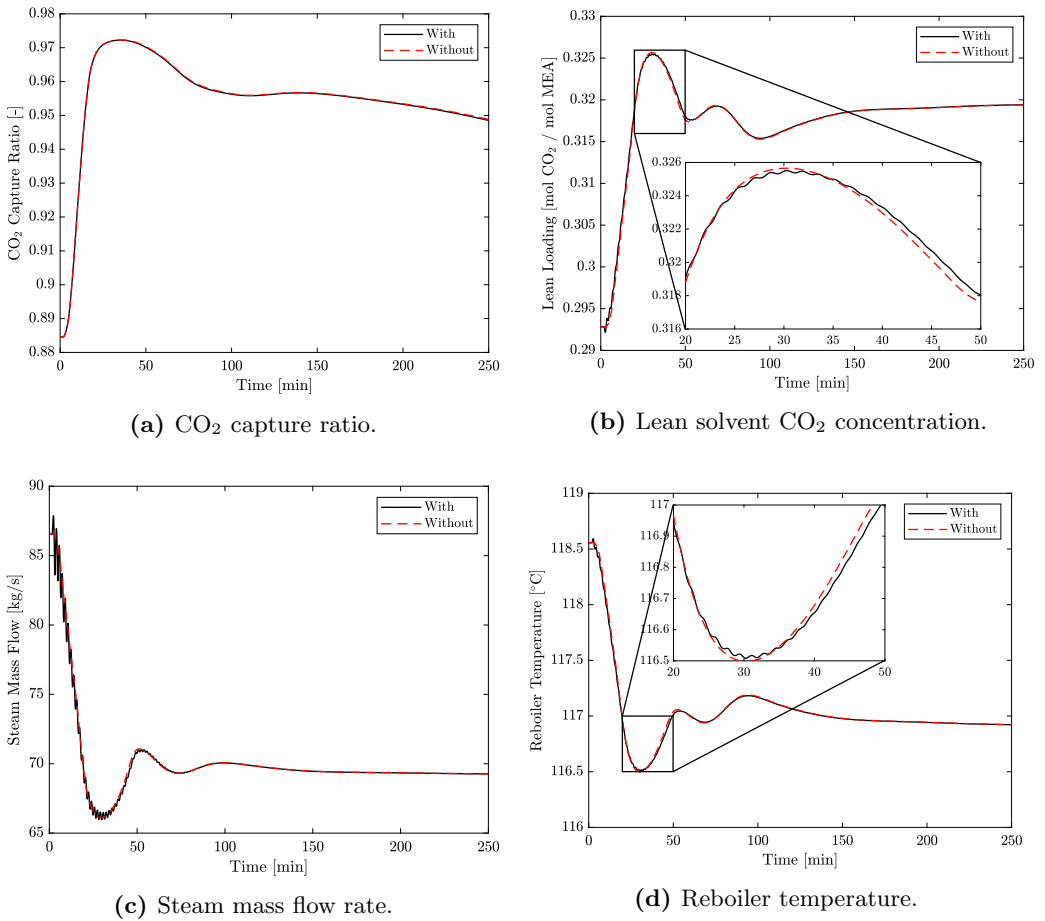
Figure 3.5: Dynamic behaviour of key process variables in the post-combustion capture plant during a gas turbine load change from 100% to 70% with and without fast dynamic fluctuations in the steam extraction valve.

ics of the steam extraction valve. Furthermore, the high-frequency fluctuations in steam extraction become smoother throughout the capture plant. Because of these variations being so rapid, there is insufficient time to affect the heat transfer in the reboiler and thus affect its temperature, the lean loading of the solvent at the outlet of the desorber column, and the capture ratio in the absorption section. Fig. 3.5 illustrates the smoothing effect of the high-frequency variations.

Chapter 4

Flexible operation with stress monitoring

Future power generation systems will require faster cycling and more frequent start ups and shut downs of thermal power plants to balance the intermittent power generation from renewable energy sources. Chapter 3 described the dynamic behaviour of distinct thermal power plants and identified the main bottlenecks inhibiting better transient performance of these systems. Thermal and mechanical stresses are one of the main limitations during changes in load, as it restrains the maximum power generation ramps this type of power plants can achieve.

A model predictive control (MPC) strategy is proposed to overcome the limitations imposed by thermal and mechanical stresses and enhance flexible operation of thermal power plants. This methodology models the stresses arising in thick-walled components, e.g. high-pressure steam drums and steam turbine rotors, and includes them in the dynamic optimisation problem of the MPC controller as inequality constraints. This ensures that the changes of load are optimal without exceeding the maximum allowable stresses in critical equipment.

This chapter describes this MPC strategy and is based on Rúa and Nord (2020); Rúa et al. (2020a). It follows a building-block approach, where modelling of stresses and simplified models of the power plant are firstly presented. Subsequently, the description of the dynamic optimisation program details how these models are included in the MPC strategy. Both linear and nonlinear formulations are considered. Finally, a case study illustrates the effectiveness of the proposed methodology.

4.1 Thermal and mechanical stresses

Equipment with thick walls presents the largest stresses in thermal power plants. This includes high-pressure steam drums, rotors of the steam turbines, casings,

blades, piping and tubes in superheating and reheating sections of steam generators (Viswanathan, 1989; Viswanathan and Stringer, 2000). These components operate at high temperature and pressure, which lead to large mechanical stresses and temperature gradients that originate thermal stresses (Kim et al., 2000). Furthermore, the rotating equipment presents centrifugal forces that contribute to the effect of mechanical stresses (Can Gülen and Kim, 2014). Adequate control strategies with stress monitoring must consider these different sources of stress and combine them in a common framework.

High-pressure steam drums and rotors in the first-stage of steam turbines are sensitive equipment to thermal and mechanical stress. Stress modelling of these two components simplifies because of their geometry, which eases their implementation in MPC strategies. Steam drums may be approximated by cylinders where plane strain applies, whereas rotors posses disk shapes with plane stress (Timoshenko and Goodier, 1951).

Thermal stresses depend on temperature gradients (Kim et al., 2000; Timoshenko and Goodier, 1951). Computation of these gradients requires to know the temperature distribution along the wall of the equipment. Because of the geometry of drums and rotors, temperature can be assumed to exclusively vary in the radial direction. The one-dimensional heat equation in cylindrical coordinates, Eq. 4.1, provides hence the temperature distribution in these components.

$$\frac{1}{r}\frac{\partial}{\partial r}\left(r\frac{\partial T}{\partial r}\right) = \frac{1}{\alpha}\frac{\partial T}{\partial t} \tag{4.1}$$

Here, T refers to the temperature difference respect to the design temperature of the equipment, r is a generic radius, and α is the thermal diffusivity of the material.

An implicit Crank-Nicolson method was used to discretise Eq. 4.1. This allowed including and solving the heat equation during each iteration of the dynamic optimisation problem in the MPC strategy. Evaporative steam convection was the boundary condition in the inner wall of the steam drum, whereas natural convection with air at ambient temperature, i.e. 25 °C, determined the heat losses of the outer wall. Similarly, forced convection with superheated, pressurised steam was the boundary condition in the outer wall of the rotor, whilst a von Neumann condition set to zero the variation of the temperature at the centre of the disk. The implementation of these boundary conditions in the discretised heat equation is described in Rúa et al. (2020a) and the supplementary material included therein.

4.1.1 Plane strain

Plane strain applies to geometries where the longitudinal direction is notably larger than any of the other two directions and implies that the longitudinal strain is zero (Timoshenko and Goodier, 1951). To develop an expression for

the thermal and mechanical stresses arising in a steam drum, consider the linear momentum equation in cylindrical coordinates assuming variations only in the radial direction:

$$\frac{d\sigma_r}{dt} + \frac{1}{r}(\sigma_r - \sigma_\theta) + F_r = 0 \tag{4.2}$$

the strain-displacement relations:

$$\varepsilon_r = \frac{du_d}{dr} \tag{4.3a}$$

$$\varepsilon_\theta = \frac{u_d}{r} \tag{4.3b}$$

and the constitutive relations between stress and strain (Timoshenko and Goodier, 1951):

$$\varepsilon_r - \alpha^* T = \frac{1}{E}\left[\sigma_r - \upsilon\left(\sigma_\theta + \sigma_z\right)\right] \tag{4.4a}$$

$$\varepsilon_\theta - \alpha^* T = \frac{1}{E}\left[\sigma_\theta - \upsilon\left(\sigma_r + \sigma_z\right)\right] \tag{4.4b}$$

$$\varepsilon_z - \alpha^* T = \frac{1}{E}\left[\sigma_z - \upsilon\left(\sigma_\theta + \sigma_r\right)\right] \tag{4.4c}$$

where σ and ε indicate stress and strain, respectively, in the radial, r, axial, θ, and longitudinal, z, directions; F_r is the centrifugal force, E Young's modulus, υ Poisson's coefficient, and α^* the thermal expansion coefficient. The strain in the longitudinal direction, ε_z, is zero because of the plane strain assumption.

Combine Eqs. 4.2, 4.3, and 4.4 to obtain an ordinary differential equation relating displacement, temperature gradient and centrifugal forces:

$$\frac{d^2 u_d}{dr^2} + \frac{1}{r}\frac{du_d}{dr} - \frac{u_d}{r^2} = \frac{(1+\upsilon)}{(1-\upsilon)}\alpha^* \frac{dT}{dr} - \frac{(1-2\upsilon)(1+\upsilon)}{(1-\upsilon)}\rho\omega^2 r \tag{4.5}$$

with u being the displacement, and the centrifugal force defined as $F_r = \rho\omega^2 r$.

Expressions for the stress components are found by inserting Eq. 4.3 into Eq. 4.4:

$$\sigma_r = \frac{E\upsilon}{(1-2\upsilon)(1+\upsilon)}\left[\frac{1-\upsilon}{\upsilon}\frac{du_d}{dr} + \frac{u_d}{r}\right] - \frac{E\alpha^*}{1-2\upsilon}T \tag{4.6a}$$

$$\sigma_\theta = \frac{E\upsilon}{(1-2\upsilon)(1+\upsilon)}\left[\frac{du_d}{dr} + \frac{1-\upsilon}{\upsilon}\frac{u_d}{r}\right] - \frac{E\alpha^*}{1-2\upsilon}T \tag{4.6b}$$

$$\sigma_z = \frac{E\upsilon}{(1-2\upsilon)(1+\upsilon)}\left[\frac{du_d}{dr} + \frac{u_d}{r}\right] - \frac{E\alpha^*}{1-2\upsilon}T \tag{4.6c}$$

Mechanical stresses generated by inner and outer pressure in the steam drum enter Eq. 4.6 as boundary conditions:

$$\sigma_r = p_i \qquad \text{for} \quad r = r_i$$

$$\sigma_r = p_o \qquad \text{for} \quad r = r_o$$

Integration routines can solve simultaneously Eqs. 4.5 and 4.6. These equations may be also discretised and combined with the temperature distribution to obtain a linear system of equations that can be easily included in linear dynamic optimisation problems. This approach is described in Rúa et al. (2020a). Moreover, Eq. 4.5 can be analytically integrated and combined with Eq. 4.6 to obtain a third method to compute the thermal and mechanical stresses. This approach is presented in Rúa and Nord (2020) and leads to:

$$
\sigma_r = \left(1 - \frac{r_i^2}{r^2}\right) \frac{E\,\alpha^*}{(1+v)(1-2v)} \int_{r_i}^{r_o} rT\,\mathrm{d}r - \frac{E\,\alpha^*}{(1-v)} \int_{r_i}^{r} rT\,\mathrm{d}r - p_i
$$
$$
+ \left[\frac{r_o^2\,r_i^2}{(r_o^2 - r_i^2)\,r^2} - \frac{r_o^2}{(r_o^2 - r_i^2)}\right](p_o - p_i)
$$
(4.8a)

$$
\sigma_\theta = \left(1 + \frac{r_i^2}{r^2}\right) \frac{E\,\alpha^*}{(1-v)(r_o^2 - r_i^2)} \int_{r_i}^{r_o} rT\,\mathrm{d}r + \frac{E\,\alpha^*}{1-v} \left(\frac{1}{r^2} \int_{r_i}^{r} rT\,\mathrm{d}r - T\right)
$$
$$
+ \left[\frac{r_o^2\,r_i^2}{(r_o^2 - r_i^2)\,r^2} + \frac{r_o^2}{(r_o^2 - r_i^2)}\right](p_i - p_o) - p_i
$$
(4.8b)

$$
\sigma_z = \frac{2\,v\,E\,\alpha^*}{(r_o^2 - r_i^2)(1-v)} \int_{r_i}^{r_o} rT\,\mathrm{d}r - \frac{E\,\alpha^*}{1-v} T + p_i \left(\frac{2\,v\,r_o^2}{r_o^2 - r_i^2} - 2v\right)
$$
$$
- p_o \frac{2\,v\,r_o^2}{r_o^2 - r_i^2}
$$
(4.8c)

There are two possible approaches to solve Eq. 4.8. Numerical integration can compute the different stress components, although this approach leads to nonlinear solutions. In contrast, the integrals in Eq. 4.8 can be discretised using the trapezoidal rule, which allows writing the stress components as a linear system of equations.

4.1.2   Plane stress

In contrast to plan strain, plane stress applies to geometries where the longitudinal direction is negligible compared to the radial and axial directions, and indicates that the longitudinal stress is zero (Timoshenko and Goodier, 1951).

The development of expressions for the stresses in the other two directions also requires the linear momentum equation in radial direction, Eq. 4.2, and the strain-displacement relations in Eq. 4.3. The constitutive relations between stress and strain with the plane stress assumption reduce to:

$$\sigma_r = \frac{E}{1 - v^2} \left[\varepsilon_r + v\,\varepsilon_\theta - (1 + v)\,\alpha^* T \right] \tag{4.9a}$$

$$\sigma_\theta = \frac{E}{1 - v^2} \left[\varepsilon_\theta + v\,\varepsilon_r - (1 + v)\,\alpha^* T \right] \tag{4.9b}$$

Combine Eqs. 4.2, 4.3, and 4.9 to obtain an ordinary differential equation relating displacement, temperature gradient and centrifugal forces under the assumption of plane stress:

$$\frac{\mathrm{d}^2 u_\mathrm{d}}{\mathrm{d}r^2} + \frac{1}{r}\frac{\mathrm{d}u_\mathrm{d}}{\mathrm{d}r} - \frac{u_\mathrm{d}}{r^2} = (1 + v)\,\alpha^* \frac{\mathrm{d}T}{\mathrm{d}r} - \frac{1 - v^2}{E}\rho\omega^2 r \tag{4.10}$$

Insert 4.3 into 4.9 to obtain expressions for the stress components:

$$\sigma_r = \frac{E}{1 - v^2} \left[\frac{\mathrm{d}u_\mathrm{d}}{\mathrm{d}r} + v\frac{u_\mathrm{d}}{r} - (1 + v)\,\alpha^* T \right] \tag{4.11a}$$

$$\sigma_\theta = \frac{E}{1 - v^2} \left[v\frac{\mathrm{d}u_\mathrm{d}}{\mathrm{d}r} + \frac{u_\mathrm{d}}{r} - (1 + v)\,\alpha^* T \right] \tag{4.11b}$$

Mechanical stress due to pressure also enters these expressions as boundary conditions. However, two approaches might be available to model mechanical stress in the rotor in the first-stage of the high-pressure steam turbine. If the shaft where the rotor lies is hollow, the boundary conditions are:

$$\sigma_r = p_\mathrm{i} \qquad \text{for} \quad r = r_\mathrm{i}$$

$$\sigma_r = p_\mathrm{o} \qquad \text{for} \quad r = r_\mathrm{o}$$

whereas, if the shaft is solid and rigid, these boundary conditions become:

$$u_\mathrm{d}(r) = 0 \qquad \text{for} \quad r = r_\mathrm{i}$$

$$\sigma_r = p_\mathrm{o} \qquad \text{for} \quad r = r_\mathrm{o}$$

Similarly to the plane strain case, integration routines can solve Eqs. 4.1, 4.10 and 4.11 to obtain the temperature distribution, displacement and stress components in the rotor. These equations can also be discretised and combined into a linear system that allows their direct solution. This approach is detailed in (Rúa et al., 2020a). Further analytical development is also possible by combining and

integrating Eqs. 4.10, 4.11. This removes the displacement from the computation of the stresses and leads to the expressions (Rúa and Nord, 2020):

$$
\begin{aligned}
\sigma_r = {} & \left[1 + v + \frac{(1-v)\, r_\mathrm{i}^2}{r^2} \right] \frac{r_\mathrm{o}^2}{(1+v)\, r_\mathrm{o}^2 + (1-v)\, r_\mathrm{i}^2} \left(\frac{E\,\alpha}{r_\mathrm{o}^2} \int_{r_\mathrm{i}}^{r_\mathrm{o}} rT\, \mathrm{d}r - p_\mathrm{o} \right) \\
& - \frac{E\,\alpha}{r^2} \int_{r_\mathrm{i}}^{r} rT\, \mathrm{d}r + \frac{\rho\,\omega^2\, r_\mathrm{o}^2\, (1+v)}{8\left[(1+v)\, r_\mathrm{o}^2 + (1-v)\, r_\mathrm{i}^2 \right]} \left[r_\mathrm{o}^2\, (3+v) - r_\mathrm{i}^2\, (1+v) \right] \\
& + \frac{\rho\,\omega^2\, r_\mathrm{o}^2\, r_\mathrm{i}^2\, (1-v)}{8\, r^2 \left[(1+v)\, r_\mathrm{o}^2 + (1-v)\, r_\mathrm{i}^2 \right]} \left[r_\mathrm{o}^2\, (3+v) - r_\mathrm{i}^2\, (1+v) \right] \\
& + \frac{\rho\,\omega^2}{8} \left[(1+v)\, r_\mathrm{i}^2 - (3+v)\, r^2 \right]
\end{aligned}
\tag{4.14a}
$$

$$
\begin{aligned}
\sigma_\theta = {} & \left[1 + v - \frac{(1-v)\, r_\mathrm{i}^2}{r^2} \right] \frac{r_\mathrm{o}^2}{(1+v)\, r_\mathrm{o}^2 + (1-v)\, r_\mathrm{i}^2} \left(\frac{E\,\alpha}{r_\mathrm{o}^2} \int_{r_\mathrm{i}}^{r_\mathrm{o}} rT\, \mathrm{d}r - p_\mathrm{o} \right) \\
& + E\,\alpha \left(\frac{1}{r^2} \int_{r_\mathrm{i}}^{r_\mathrm{o}} rT\, \mathrm{d}r - T \right) + \frac{\rho\,\omega^2}{8} \left[(1+v)\, r_\mathrm{i}^2 - (1+3v)\, r^2 \right] \\
& + \frac{\rho\,\omega^2\, r_\mathrm{o}^2\, r_\mathrm{i}^2\, (1-v)}{8\, r^2 \left[(1+v)\, r_\mathrm{o}^2 + (1-v)\, r_\mathrm{i}^2 \right]} \left[r_\mathrm{i}^2 (1+v) - r_\mathrm{o}^2 (3+v) \right] \\
& + \frac{\rho\,\omega^2\, r_\mathrm{o}^2\, (1+v)}{8\left[(1+v)\, r_\mathrm{o}^2 + (1-v)\, r_\mathrm{i}^2 \right]} \left[r_\mathrm{o}^2 (3+v) - r_\mathrm{i}^2 (1+v) \right]
\end{aligned}
\tag{4.14b}
$$

Applying the trapezoidal rule to Eq. 4.14 allows expressing these equations as a linear system, which may be combined with Eq. 4.1 to compute the temperature distribution and stress components directly (Rúa and Nord, 2020).

4.1.3   Effective stress

Stresses in different directions are not suitable to evaluate the overall state of materials and impose constraints in optimisation-based procedures. The von Mises equivalent, or effective, stress defined in Eq. 4.15 is a scalar measure of the overall effective stress that predicts the yielding of materials under complex loading. Therefore, it is an appropriate parameter to implement constraints related to material deformation and damage.

$$
\sigma_\mathrm{eff}^2 = \sigma_r^2 + \sigma_\theta^2 + \sigma_z^2 - (\sigma_r\, \sigma_\theta + \sigma_\theta\, \sigma_z + \sigma_z\, \sigma_r)
\tag{4.15}
$$

Linear MPC requires linear equality and inequality constraints. Eq. 4.15 was hence linearised to include a scalar measure of the overall stress in the linear formulation of the MPC strategy. Eq. 4.16 represents this first-order Taylor approximation:

$$
\sigma_\mathrm{effl}^2 = \sigma_\mathrm{effl,0}^2 + \nabla \sigma_\mathrm{effl,0}^2 \Delta\sigma + \mathcal{O}(\Delta x^2)
\tag{4.16}
$$

Simulations with finite element methods (FEMs) validated the effectiveness of the different stress models to predict the mechanical, thermal and von Mises stress under the assumptions of plane strain and stress. Fig. 4.1 presents validation results for both high-pressure steam drum and rotor following two approaches: 1) computing simultaneously temperature distribution, displacement and stresses in different directions with Eqs. 4.6 and 4.11; and 2) computing temperature distribution and stress components with Eqs. 4.8 and 4.14.
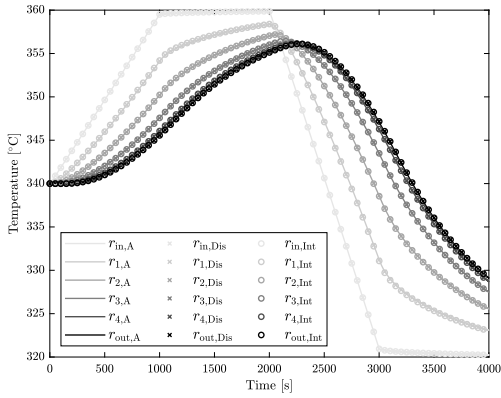
(a) Temperature of the drum along six equidistant radii.
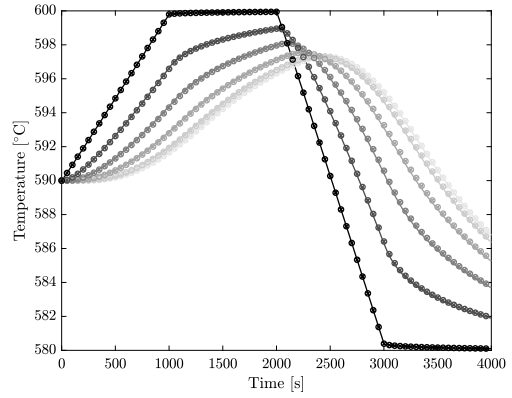
(b) Temperature of the rotor along six equidistant radii.
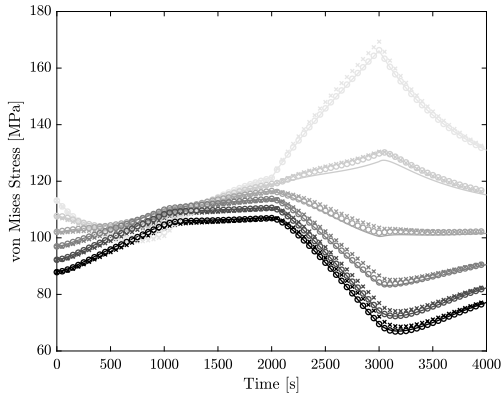
(c) von Mises stress in the drum along six equidistant radii.
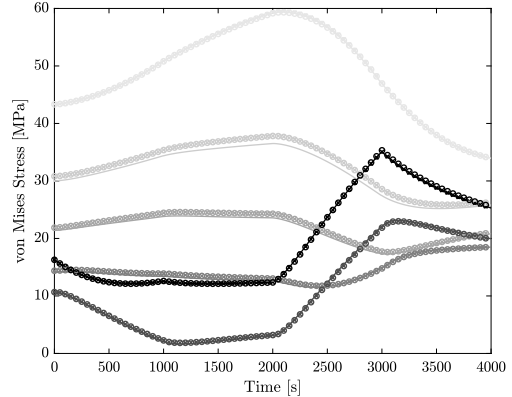
(d) von Mises stress in the rotor along six equidistant radii.

Figure 4.1: Validation results of the stress models for the two proposed approaches. A refers to the results obtained in ANSYS, Dis refers to the modelling approach based on computing the displacement, and Int to the approach based on applying the trapezoidal rule to the integrals in Eqs. 4.8 and 4.14.

4.2 System identification

Model predictive control requires the periodic solution of dynamic optimisation problems. The frequency of these solutions depends on the dynamic behaviour of the controlled system and the computational cost of the optimisation problem. Good control strategies must anticipate the dominant dynamics and determine suitable control actions that stabilise the system. Large-scale NGCCs have dominant dynamics within a few hundred seconds, which limits the time spam to solve the dynamic optimisation problem to approximately a minute or less (Peng et al., 2001; Prasad et al., 1998). This inhibits the utilisation of high-fidelity dynamic models in MPC strategies since this type of models needs longer computational times for a single simulation. Therefore, simplified models able to predict the performance of these dynamic systems with reduced computational cost were required.

System identification refers to the process of constructing dynamic data-based models (Ljung, 1987). Simulations of the high-fidelity dynamic model at different operation points, i.e. distinct gas turbine loads, provided the data to obtain simplified models. These simulations were in closed-loop with random Gaussian signals (RGS) superimposed simultaneously in the set-points of the controllers as this approach leads to richer data and hence better identification (Forssell and Ljung, 1999; Gevers, 2005; Gevers and Ljung, 1986; Gevers et al., 2006; Mišković et al., 2008).

Auto-regressive models with exogeneous variables (ARXs) were fitted to the different sets of data. Eq. 4.17 represents the general structure of this type of model:

$$y(t) + a_1\, y(t-1) + \cdots + a_{n_y}\, y(t-n_y) = b_1\, u(t-1) + \cdots + b_{n_u}\, u(t-n_u) + \varepsilon(t) \quad (4.17)$$

where n_y and n_u are the number of past outputs and inputs, and $\varepsilon(t)$ is white-noise.

ARX models cannot predict the behaviour of nonlinear systems over a broad operation range because of their linearity. However, several local ARX models were developed at different operation range and combined into a local model network (LMN) (Johansen and Foss, 1993). Fig. 4.2 illustrates the structure of a local model network composed of several ARX models. A Gaussian validity function determined the contribution of every local ARX model to overall output of the local model network. Eq. 4.18 defines the form of the this validity function:

$$\xi_i(\gamma) = \frac{exp\Big(-\frac{1}{2}\Big[(\gamma - c_i)/w_i\Big]^2\Big)}{\sum_{k=1}^{M} exp\Big(-\frac{1}{2}\Big[(\gamma - c_i)/w_i\Big]^2\Big)} \quad (4.18)$$

with c_i and w_i setting, respectively, the centres and widths of the local interpola-
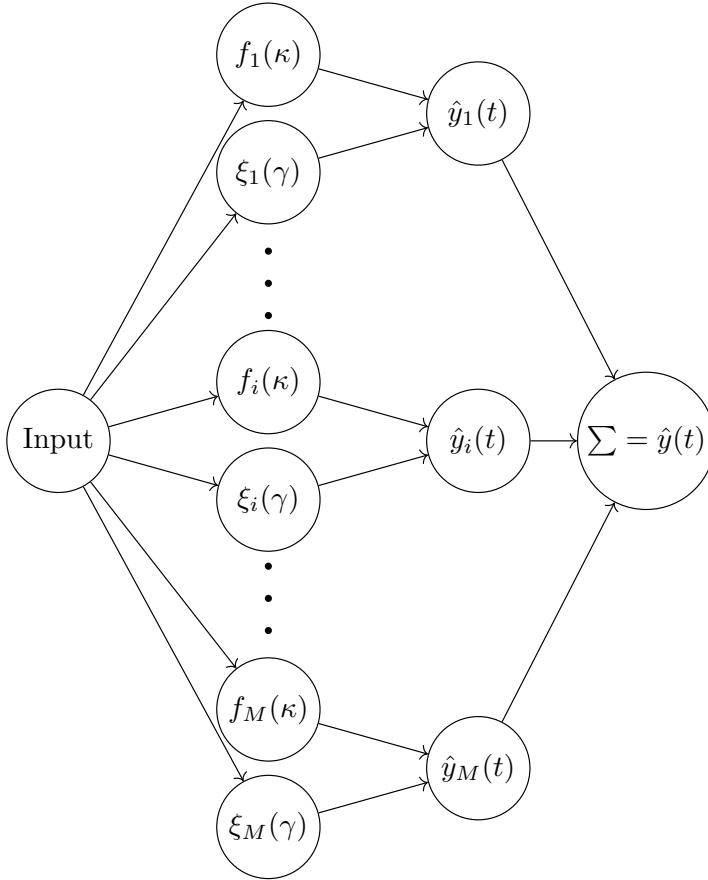
Figure 4.2: Structure of a local model network.

tion functions; whereas Eq. 4.19 determines the output of the LMN:

$$\hat{y}(t) = \sum_{k=1}^{M} f_i(\kappa) \; \xi_i(\gamma) \tag{4.19}$$

where M is the number of local models, $f_i(\kappa)$ is the evaluation of the each ARX model under the conditions defined by κ, ξ is the local validity function associated to each ARX model, and γ is the parameter defining the current operating point, i.e. the current GT load.

There are different approaches to identify the parameters of the different ARX local models (Johansen and Foss, 1993):

1. Select the centres and widths based on the knowledge of the system and compute the ARX model parameters based on existing methods as prediction error, maximum likelihood or least squares.

2. Calculate the ARX model parameters based on existing methods and then optimise the value of the validity function variables in order to minimise the global prediction error.

3. Select the validity function variables based on experience and then compute the parameters of the ARX models with the objective of minimising the global prediction error.

4. Compute simultaneously the validity function variables and the model parameters with a multi-variable nonlinear optimisation whose objective function is the global prediction error.

Fitting methods that consider all local models simultaneously, i.e. minimise the global error of the LMN, lead to better identification than approaches that treat the ARX models individually. In contrast, optimising the parameters of the validity does not improve significantly the prediction (Johansen and Foss, 1993; Prasad et al., 1998). Therefore, the parameters of the different local ARX models integrating the LMN were fitted with a least-squares method that minimised the global error while keeping the centres and widths of the validity function constant.

Identification of the local ARX parameters improves with suitable pre-processing of the data. Thus, the nominal values of each variable was substrated from the original data. Therefore, the LMN computes the deviation of the different process variables from their set-point or nominal value. This approach also eases the formulation of the dynamic optimisation problem embedded in the MPC strategy.

4.3   Model predictive control

Model predictive control is a suitable strategy for stress monitoring because it allows computing the effective stress arising in the equipment and imposing constraints that limit the maximum level it can achieve. Stress modelling depends on the geometry of the equipment and might lead to nonlinear models. Therefore, both linear and nonlinear formulations of the dynamic optimisation problem included in the proposed MPC strategy are presented. Section 4.3.1 describes the linear MPC formulation and how to include in the optimisation problem the models from Sections 4.1 and 4.2, whereas Section 4.3.2 details the nonlinear MPC strategy. Section 4.3.3 compares the computational cost of both formulations, since this is one of the main limitations associated with optimisation-based control strategies.

4.3.1   Linear formulation

Linear model predictive control relies on the periodic solution of a quadratic programming (QP) problem. The mathematical formulation of this optimisation

problem is:

$$\min_{z \in \mathbb{R}^n} \; f(z) = \frac{1}{2} \, z^T Q \, z + d \, z \tag{4.20a}$$

subject to

$$A_{\text{eq}} \, z = B_{\text{eq}} \tag{4.20b}$$

$$A_{\text{ineq}} \, z \leq B_{\text{ineq}} \tag{4.20c}$$

$$z^{\text{low}} \leq z \leq z^{\text{up}} \tag{4.20d}$$

with

$$Q \succcurlyeq 0 \tag{4.20e}$$

Vector z represents the optimisation variables in the QP problem. These include the responses and manipulated variables of the simplified models, i.e. y and u in Eq. 4.17, and the temperature, displacement, and stress models included in the linear system of equations described in Section 4.1. The degrees of freedom are the manipulated variables u, which affect the behaviour of the simplified models and hence determine the boundary conditions of the equipment where stress is monitored.

Eq. 4.20b is the linear equality constraint of the optimisation problem. It includes all the simplified and stress models, and ensures that they are satisfied independently of the changes in the degrees of freedom. The inequality constraints are Eqs. 4.20c and 4.20d. The latter includes lower and upper bounds for all optimisation variables and thus limits the maximum effective stress in the equipment, whereas Eq. 4.20c adds extra inequality constraints such as maximum ramping of the gas turbine. Eqs. 4.20a is the objective function, which aims at minimising the deviation of different process variables from their set-points. The weighting matrix Q and vector d in Eqs. 4.20a determine the control priority, i.e. the variables that require tighter control, and balance the different orders of magnitude that might exist among the optimisation variables.

This optimisation problem is repeated over time, with a period fixed by the sampling time at which measurements from the power plant are taken. The result of this computation is a set of control sequences of all manipulated variables. The first control action is implemented in the actual power plant. The length of these sequences is a trade-off between computational cost and performance prediction. Longer control sequences, i.e. larger time horizons, lead to better predictions of the transient performance of the system, but increase the number of optimisation variables and degrees of freedom and hence the computational cost. Therefore, the selection of adequate sampling times and time horizons depends on the knowledge of the dynamic behaviour of the system and the time available for computing the optimal sequence of control actions.

4.3.2   Nonlinear formulation

Nonlinear model predictive control solves a nonlinear programming (NLP) problem every sampling time to compute the control action implemented in a system. The mathematical formulation of an NLP problem is:

$$\min_{z \in \mathbb{R}^n} \; f(z) \tag{4.21a}$$

subject to

$$c_{\mathrm{eq}}(z) = 0 \tag{4.21b}$$

$$c_{\mathrm{ineq}}(z) \leq 0 \tag{4.21c}$$

$$A_{\mathrm{eq}} \; z = B_{\mathrm{eq}} \tag{4.21d}$$

$$A_{\mathrm{ineq}} \; z \leq B_{\mathrm{ineq}} \tag{4.21e}$$

$$z^{\mathrm{low}} \leq z \leq z^{\mathrm{up}} \tag{4.21f}$$

Variable z represents the vector of optimisation variables with lower and upper bounds defined in Eq. 4.21f. The nonlinear equality and inequality constraints are, respectively, c_{eq} and c_{ineq} in Eqs. 4.21b and 4.21c. The linear counterpart of these constraints are Eqs. 4.21d and 4.21e, and have the same structure as those in the QP problem. The objective function $f(z)$ defined in Eq. 4.21a can be any linear or nonlinear function.

In this formulation, the simplified and stress models can be either linear or nonlinear constraints depending on their structure. This adds modelling flexibility and ensures that the physics of the system and the monitored stresses are always met regardless of the linearity of the models.

4.3.3   Computational time analysis

Computational performance can restrict the implementation of MPC strategies. Dynamic optimisations must be carried out within the sampling time available to guarantee the implementation of new control actions with sufficient frequency and before taking new measurements. Thus, the evaluation of computational cost is fundamental during the selection of suitable optimisation-based control strategies.

Linear and nonlinear MPC strategies differ on the dynamic optimisation problem they solve, which leads to different computational times. To compare the performance of linear and nonlinear formulations of the same MPC strategy, the same simplified models and linear system of equations describing the stresses were implemented in the nonlinear optimisation problem. Therefore, the simplified models enter as a linear equality constraint in Eq. 4.21d and the constraint in the gas turbine load ramp as a linear inequality constraint in Eq. 4.21e. In the NLP problem, the von Mises equivalent stress defined in Eq. 4.15 is used instead of the linearised version defined in Eq. 4.16 and implemented in the QP problem.

This model represents a nonlinear constraint in the nonlinear dynamic optimisation problem. Table 4.1 summarises the computational time of a single dynamic optimisation with a time horizon of 30 for each formulation and stress modelling approach, i.e. computing the displacement or using the integral expressions, relative to the fastest optimisation.

Table 4.1: Relative computational time for both MPC formulations and stress modelling approaches. Dis refers to the stress model based on the displacement calculation and Int to the integral stress model.

Formulation	Linear		Nonlinear	
Stress Model	Dis	Int	Dis	Int
Relative Time	1.88	1	41.02	27.19

Despite the utilisation of the same simplified and stress models, the QP problem shows superior computational performance compared to the NLP formulation. This occurs because of the suitable numerical properties that QP problems possess. In this type of formulations, the calculation of gradients is analytical and its convexity leads to global solutions. In contrast, NLP problems require the numerical computation of gradients through finite differences and only local solutions can be guaranteed. Calculating these gradients numerically supposes a large penalty in the computational performance, which leads to longer computational times. There exist several approaches to improve the calculation of gradients, e.g. automatic differentiation or complex step methods, but these require further analytical development, cannot generally equate the computational performance of QP problems, and still lead to local solutions (Nocedal and Wright, 2006).

Better computational performance enables linear MPC strategies to expand the time horizon to capture more dynamics, reduce the sampling time or include stress monitoring in more pieces of equipment, which translates into superior control and safer operation. Therefore, nonlinear formulations should be avoided whenever is possible to formulate the control problem linearly. However, linear modelling is not always possible without excessive loss of accuracy.

Stress modelling also affects the computational performance of the proposed MPC strategy, although its effect is not as pronounced as the formulation approach of the dynamic optimisation problem. Models based on the integral definitions of the stress components, Eqs. 4.8 and 4.14, lead to slightly faster results than those obtained from the model additionally computing the displacement, Eqs. 4.5, 4.6, 4.10 and 4.11. The computational improvement originates from the reduction on optimisation variables, since the displacement is not calculated in the integral stress models. This improvement offsets the drawback of having denser matrices in the linear system of equations that arise from Eqs. 4.8 and 4.14. Less sparsity indicates that the matrix of the linear system of equations modelling the stress has more information, and hence this modelling approach needs less spatial and

temporal discretizations to achieve the same accuracy. This factor further reduces the number of optimisation variables in the optimisation problem where the integral models are used, which enhances its computational performance. Overall, the difference in computational time is small between these modelling approaches, so both are deemed suitable for MPC strategies with stress monitoring.

4.4 Stress monitoring during dynamic operation

Dynamic simulations where a modern NGCC needed to balance a reduction of 165 MW on power demand tested the effectiveness of the proposed MPC strategy with stress monitoring. Two scenarios demonstrated the capability to compute the optimal control actions whilst limiting the stress in the high pressure steam drum and steam turbine rotor to allowable levels. The first scenario considered yield stress limits provided by material specifications, whereas the second case reduced the value to evaluate whether the MPC strategy could simultaneously compute optimal control inputs and limit the stress development. Table 4.2 includes the physical and mechanical properties considered for the drum and rotor disk (Viswanathan and Bakker, 2001a). Since the maximum allowable stress presented in Table 4.2 was not reached with a realistic value during the considered scenario, a reduced value of the yield stress of 125 MPa was used to demonstrate the capability of the control methodology to predict the stress and adapt the operation of the power plant. Table 4.3 summarises the lower and upper bounds imposed in the different optimisation variables during the dynamic simulations.

Constraints on the effective stress in different equipment can modify the overall operation of thermal power plants. These changes originate from the need to reduce the temperature gradients in critical components and hence limit the thermal stresses that arise because of operation changes. Fig. 4.3 illustrates the effect of different stress constraints on the mechanical power generated by the NGCC and the variation on gas turbine load to balance the changes in power demand. The MPC strategy lead to drastic changes in the gas turbine load when the maximum allowable stress was high, prioritising in this way the balance between power demand and supply. The ramping capability was exclusively limited by the constraint in the gas turbine ramps provided by the manufacturer, which was 15%/min in both scenarios. Furthermore, the MPC strategy lead to an undershoot

Table 4.2: Physical and mechanical properties of the materials considered for the high pressure drum and rotor disk. The materials for the drum and rotor are, respectively, SA-515 Grade 70 and X18CrMnMoNbVN12.

Component	ρ [kg/m^3]	C_{m} [J/kgK]	k_m [W/mK]	α^* [m^2/s]	α [$1/K$]	E [GPa]	υ [$-$]	h_{o} [W/m^2K]	h_{i} [W/m^2K]	Yield [MPa]
Drum	7850	434	47	1.38e-05	1.36e-5	178	0.3	5000	0.065	190
Rotor	7700	460	29	8.19e-06	1.25e-5	127	0.292	4000	-	69

Table 4.3: Lower and upper bounds of the optimisation variables.

	LMN			Drum			Rotor	
Lower	Variable	Upper	Lower	Variable	Upper	Lower	Variable	Upper
400	$\dot{W}$	615.867	$-\infty$	T_{wall}	∞	$-\infty$	T_{wall}	∞
-10	T_{SH}	15	-0.001	u_{d}	0.001	-0.001	u_{d}	0.001
-10	T_{RH}	15	$-\infty$	σ_r	∞	$-\infty$	σ_r	∞
$-\infty$	p_{turb}	∞	$-\infty$	σ_θ	∞	$-\infty$	σ_θ	∞
$-\infty$	T_{drum}	∞	$-\infty$	σ_z	∞	0	σ_{effl}	69
$-\infty$	p_{drum}	∞	0	σ_{effl}	190/125			
60	u_1	100						
-0.01655	u_2	0.97345						
-0.06882	u_3	0.92188						

of the gas turbine load to compensate for the slow transient performance of the steam cycle. Therefore, the fast dynamics of the gas turbine dictated the flexible and fast operation of the NGCC. This highlights the usefulness of optimisation-based control strategies, since models describing the dominant dynamics of each component can be included, which allows the improvement of the control inputs.

In contrast, lower constraints on the effective stress limited the ramping capacity of the NGCC (Fig. 4.3). This occured because these constraints became active before those limiting the ramp of the gas turbine. Fig. 4.4 shows the effective stress arising in the high pressure steam drum and rotor disk during the transient operation of the NGCC. With low limits in the equivalent stress, the MPC strategy reduced the rate of decrease in the gas turbine load to achieve smoother temperature gradients in the high pressure drum to avoid exceeding the
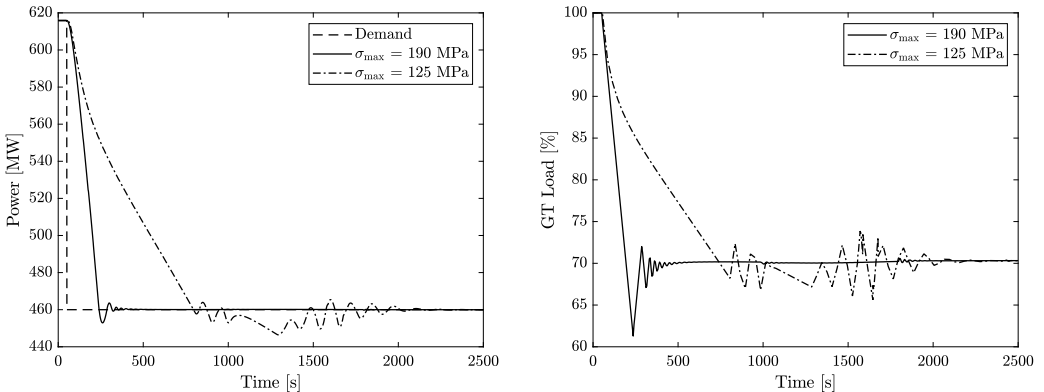
(a) Mechanical power generation with different stress constraints in the drum.

(b) Gas turbine load profile with different stress constraints in the drum.

Figure 4.3: Effect of stress constraints on power generation and gas turbine load.

maximum allowable stress. Therefore, the dominant dynamics of the steam cycle governed the transient operation of the NGCC instead the fast operation of the gas turbine. The low stress limits required the reduction of temperature gradients in the HRSG, a process dictated by the thermal capacitance of the equipment. As a result, the overall dynamic behaviour was slower and required longer stabilisation time.

Furthermore, Fig. 4.4 compares the stress estimated during the optimisation in the MPC strategy and the exact stress computed a posteriori with the true temperature and pressure profiles in the equipment. The equivalent stress predicted by the MPC strategy during transient operation of the thermal power plant captured the overall tendency of stress development since the trajectory of both true and predicted stress is similar. Nevertheless, the prediction of the MPC strategy anticipated the dynamic behaviour of the stress arising in the equipment, specially in the steam drum. The lack of detailed data of the temperature distribution in the different components of the high-fidelity NGCC model might explain this behaviour. This forces the MPC controller to estimate the initial temperature along the walls of the equipment at each sampling time and provide this information to the dynamic optimisation problem. Stress prediction during the control of the NGCC operation would improve if the detailed dynamic model of the NGCC provided the actual temperature distribution.

Stress constraints also affected the temperature control of superheated and reheated steam. Furthermore, Fig. 4.5 compares the dynamic behaviour of these temperatures for high and low constraints on the equivalent stress of the high
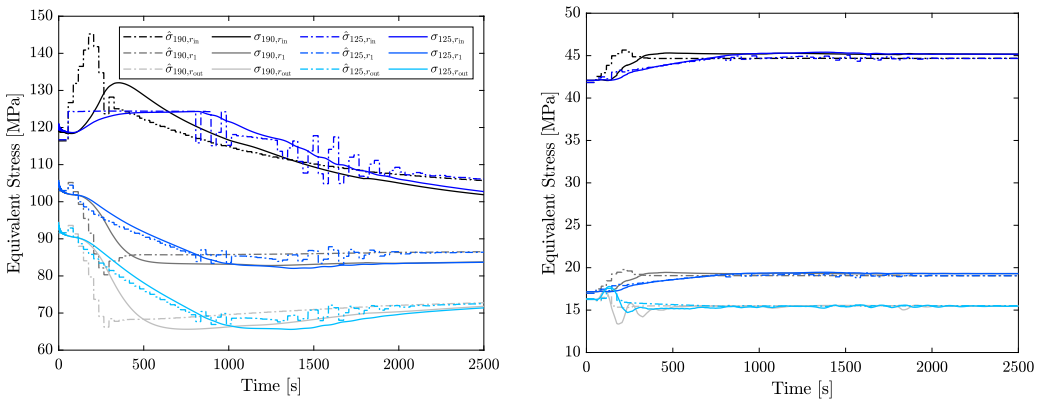
(a) Equivalent stress in the high pressure steam drum along three equidistant radii.

(b) Equivalent stress in the high pressure rotor disk along three equidistant radii.

Figure 4.4: Effect of stress constraints on the effective stress arising in different components during transient operation of the NGCC. Dashed lines indicate the values estimated during the transient performance and solid lines refer to posterior calculations of the effective stress using the computed gas turbine profile and stress models with more discretizations.

pressure steam drum. Lower stress limits lead to slower ramps in the gas turbine and more progressive changes in the steam cycle. Consequently, the variations in the superheated and reheated steam temperature followed also this progressive evolution and eased the stabilisation of these two process variables. Moreover, the slower transient performance in the steam cycle lead to smaller offset in these temperatures. Nevertheless, the proposed MPC strategy can rapidly limit the steam temperature variation without exceeding the temperature limitations in both test cases.
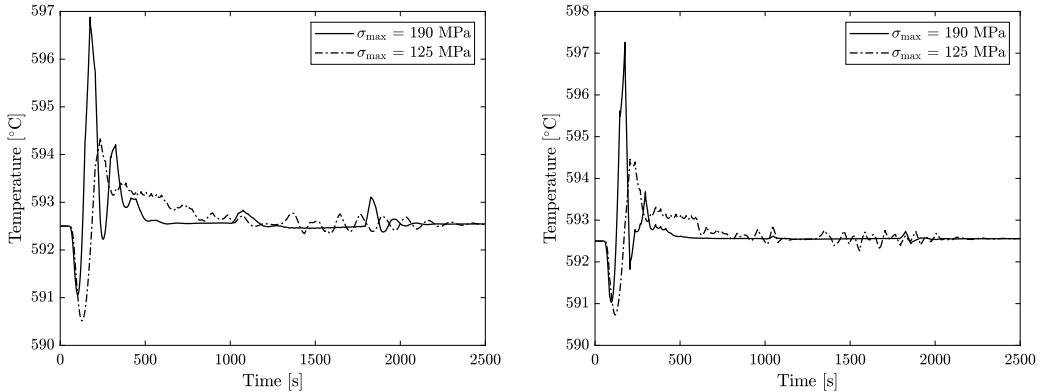
(a) Superheated steam temperature with different stress constraints in the drum.

(b) Reheated steam temperature with different stress constraints in the drum.

Figure 4.5: Effect of stress constraints on the superheated and reheated steam temperature.

This case study demonstrated the effectiveness of model predictive control strategies with stress monitoring to enhance the flexible operation of thermal power plants whilst limiting the maximum stress arising in critical equipment. This control strategy considers the distinct dynamic behaviour of the different components and respects both operational and material constraints. Thus, when the stress constraints were high, the MPC controller undershooted the gas turbine load to overcome the slow response of the steam cycle and balance faster the power demand. On the contrary, the proposed MPC strategy slows down the changes in gas turbine load if there are tighter limits on the maximum allowable stress of the equipment.

Chapter 5

Scheduling under uncertainty with lifetime enhancement

Thermal and mechanical stresses are one of the main limitations for flexible operation of thermal power plants. The combination of these individual contributions can lead to excessively high effective stress values that result in deformation of the equipment. Chapter 4 presented a methodology to compute optimal power ramps while limiting the maximum value of the stress arising in thick-walled components. However, regular operation induces damage in the equipment of thermal power plants that reduces their lifetime even if these control strategies keep the stress levels within safe limits (Viswanathan, 1989; Viswanathan and Stringer, 2000).

Creep and fatigue are arguably the main damage mechanisms that initiate and grow cracks in highly loaded components of thermal power plants, ultimately leading to lack of reliability and failures due to fractures or large deformations (Can Gülen and Kim, 2014; Viswanathan, 1989; Viswanathan and Stringer, 2000). Creep is the damage associated with prolonged operation at specific temperature and stress levels, which can result in deformations in the short term, and crack growth and cavitation in the long term (Viswanathan and Bakker, 2001a,b; Viswanathan and Stringer, 2000). Fatigue is the progressive and persistent structural damage originating from cyclic loading in the material (Suresh, 1998; Viswanathan, 1989; Viswanathan and Stringer, 2000). There exist two main types of fatigue depending on the frequency of the loads acting on the equipment: low- and high-cycle fatigue. The former affects the components of thermal power plants that operate at high temperature and pressure, e.g. headers, superheater and reheater tubes, steam turbine rotors; whereas high-cycle fatigue affects the equipment that experiences vibration, e.g. turbomachinery components (Mukhopadhyay et al., 1998; Viswanathan, 1989; Viswanathan and Stringer, 2000). Additional damage phenomena that can affect the residual lifetime operation of thermal power plants are corrosion, embrittlement, oxidation,

pitting and erosion (Viswanathan, 1989). Nevertheless, degradation of the equipment in thermal power plants is normally a combination of different phenomena (Barella et al., 2011; Das et al., 2003; Paterson and Wilson, 2002; Wang et al., 2012).

Flexible operation of thermal power plants enhances the damage associated with the two main degradation mechanisms because of the larger and more frequent temperature gradients (Benato et al., 2014, 2015, 2016). The control strategies described in Chapter 4 limit the maximum effective stress in the short-time scale and inhibit the instant deformation of the equipment owing to momentary peaks of stress. However, damage control and the associated improvement on operational lifetime in critical equipment befalls in longer time scales (i.e. days, weeks and months), or once the failure has already occurred. Scheduling accounts for the daily and weekly variations of power demand and generation. Therefore, damage control can be integrated during the scheduling of flexible thermal power plants to enhance their lifetime utilisation. Scheduling of daily and weekly operation of flexible thermal power plants in power markets with large shares of renewable energy confronts three main challenges:

1. Determine an optimal power generation profile that balances the intermittent power generation from renewable energy sources.

2. Consider the uncertainty associated with renewable power generation.

3. Enhance the lifetime of critical equipment in the thermal power plant by limiting the damage during daily operation.

Modern scheduling methods rely on optimisation-based approaches where uncertainty might be included (Nosratabadi et al., 2017; Pandžić et al., 2013; Saber and Venayagamoorthy, 2011). However, damage analysis occurs normally after the fault happens. Thus, there exist a decoupling between power generation scheduling of thermal power plants and deterioration control in critical equipment. This chapter is based on Rúa et al. (2021b) and presents a method to optimally schedule power generation from thermal power plants that considers the uncertainty associated with renewable energy sources and limits the deterioration of specific components to enhance their lifetime utilisation. Section 5.1 describes the proposed method and presents different deterioration models that might include the case of a natural gas combined cycle. Section 5.2 details the mathematical formulation of the scheduling methodology, including how to account for uncertainty in power generation from renewable energy sources and include constraints on the maximum damage in the equipment. A case study analysed in Section 5.3 illustrates the application of the proposed methodology to the scheduling of a day-ahead power generation profile for a natural gas combined cycle. Finally, Section 5.4 discusses the importance of adequate selection of design temperatures in the equipment.

5.1 Method

The economic viability of thermal power plants in power markets dominated by the large deployment of renewable energy sources depends on their capacity to deliver flexible power and balance the electric grid (Eser et al., 2017; Gonzalez-Salazar et al., 2018). Scheduling considers the ramping ability of thermal power plants to determine their operation profile according to the power demand and supply from other energy sources, e.g. wind and solar. Flexible operation leads, however, to large temperature gradients and more frequent cycling that accelerate the deterioration of thermal power plants (Can Gülen and Kim, 2014; Kim et al., 2000). Therefore, scheduling methods must consider the damage associated with flexible operation to compute optimal power generation profiles that balance the grid, are economically viable for the power plant operator, and enhance the lifetime utilisation of the power plant. Moreover, the uncertainty associated to power generation from renewable sources affects the power demand, and plays hence a fundamental role during the scheduling process. Fig. 5.1 presents the proposed method to optimally schedule the power generation of thermal power plants under uncertainty with enhancement of their lifetime.

This method relies on formulating the scheduling of power generation from thermal power plants as a stochastic optimisation problem. Deregulated power markets offer one-day ahead estimations of power demand. This allows power plant operators to offer selling prices for specific shares of the total power generation throughout the day. Thus, the boundary conditions of the optimisation problem are the estimation of power demand, its associated uncertainty, and the selling price of electricity. The case study in Section 5.3 does not include uncertainty on the selling price, but the scheduling method can include it similarly to the uncertainty associated with power demand. These boundary conditions define a stochastic optimisation problem that aims at maximising the revenue obtained by the plant operator while it limits the damage originated in the equipment by the computed operation profile. Therefore, the damage in specific components is a constraint within the optimisation problem. This method also offers the possibility of including the damage in the objective function together with a penalty term, although finding a trade-off between the weights of the revenue and deterioration in the objective function might not be easy and possibly case-dependant. In contrast, determining a value for the constraint that sets the maximum allowable damage in a specific component attends to the properties of the material and the scheduled maintenance, which are both known by plant operators.

Damage calculation is a sequential procedure where the optimal power generation profile considered at each iteration during the optimisation is the boundary condition of a dynamic simulation that recreates the behaviour of an actual thermal power plant. This simulation provides data to compute the stresses and strains in the equipment of interest throughout the operation period. Damage is subsequently computed by considering these stresses and strains and the adequate
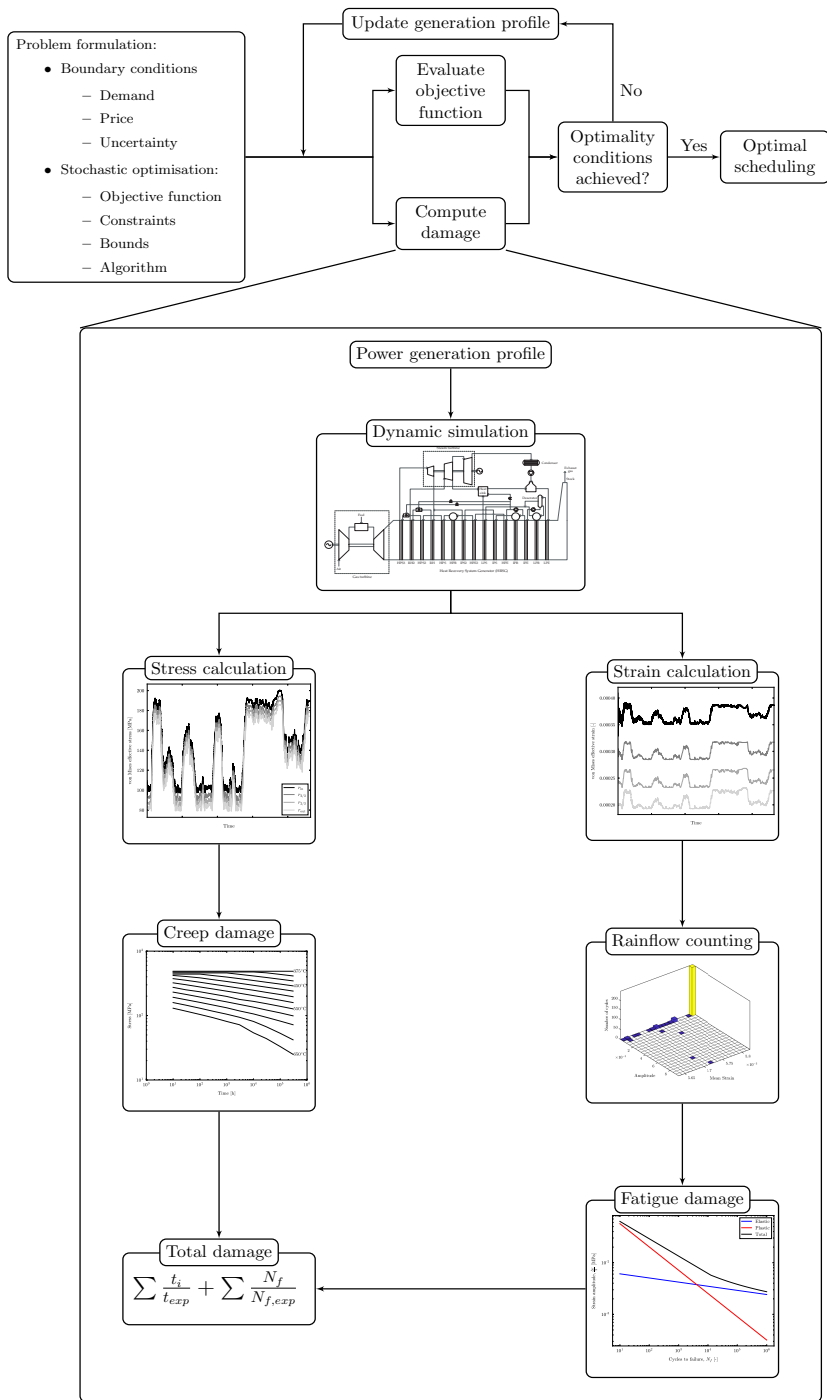
Figure 5.1: Method to optimally schedule the power generation profile of thermal power plants with lifetime enhancement under uncertainty.

experimental data for the material of the equipment. The total deterioration owing to the different damage mechanisms is the result of a linear summation rule. Fig. 5.1 presents this procedure to obtain the damage generated by different mechanisms from the operation profile of a thermal power plant.

Estimation of the damage generated by a given operation profile requires different steps and involves several models. Section 5.1.1 describes the dynamic model of the natural gas combined cycle considered in the case study, and the simplified models used during the optimisation that replicate its behaviour. Section 5.1.2 presents different methods to model the damage that arises in the equipment.

5.1.1 Dynamic modelling of a natural gas combined cycle

The proposed method for scheduling thermal power plants requires a model that replicates the behaviour of these power generation systems to compute the deterioration in their equipment. The case study used to prove the effectiveness of this method in Section 5.3 considers a triple-pressure NGCC with reheating. Fig. 3.2 represents the process diagram of this thermal power plant, while Section 3.4 describes the dynamic modelling approach followed to develop a model that behaves as an actual thermal power plant.

Methodologies relying on optimisation-based procedures cannot use high-fidelity models since their computational cost inhibits their utilisation. Simplified models that capture the behaviour of the high-fidelity counterparts must be used instead. System identification is a suitable approach to develop simple dynamic models, as discussed in Section 3.2. However, scheduling captures the long-term operation of thermal power plants and does not require detail representation of the fast dynamics of thermal power plants. Quasi-steady state models are thus sufficient to model the behaviour of actual power systems without excessive loss of accuracy. Consequently, the development of these models reduces to standard regression procedures.

Temperatures and pressures in the equipment of interest are normally the thermodynamic variables estimated by simplified models, as they are the boundary conditions of the stress models that allow the computation of creep and fatigue, which are the two main mechanisms inducing damage in this type of power plants. This method eases the implementation of other deterioration mechanisms such as hot corrosion, which would only require the development of simplified models to estimate the composition of the flue gas and its deposition in specific components. In addition, a simplified model for predicting the power generation of the thermal power plant is also needed.

There are many pieces of equipment in a thermal power plant that deteriorate from frequent cycling and severe temperature gradients (Viswanathan, 1989; Viswanathan and Stringer, 2000). The tubes in the superheating section of the heat-recovery steam generator (HRSG) face both challenges during regular operation and are hence considered to prove the effectiveness of the proposed method in

the case study in Section 5.3. Creep is a major issue for this type of components because of the high temperature of the steam and exhaust gas, and the drastic operation changes originated from frequent ramping, start-ups and shut-downs.

The estimation of creep damage in this components requires knowledge of the inner and outer temperatures, and the pressure of the steam. The pressure of the exhaust gas may be approximated to atmospheric pressure without loss of accuracy. The quasi-steady state behaviour of these variables exhibits a direct relation with the gas turbine load. Thus, linear polynomials with the structure presented in Eq. 5.1 lead to adequate estimations.

$$x = a + b\,u \tag{5.1}$$

Here, x represents the predicted variables, i.e. mechanical power generation, and inner and outer pressure and temperature in the superheated tubes; u is the manipulated variable, which is the gas turbine load as it dictates the operation profile of the NGCC, and parameters a and b are fitted to the high-fidelity model for each variable. Table 5.1 summarises the fitting parameters of each variable and presents the coefficient of determination R^2 that measures the agreement between the high-fidelity and simplified models. Fig. 5.2 presents a comparison between the high-fidelity and simplified models for the considered temperatures and pressure. The high values of the coefficient of determination R^2 demonstrate these models based on Eq. 5.1 can predict the quasi-steady state performance of the process variables of interest with high accuracy albeit their simplicity. Therefore, they are suitable to replace the high-fidelity models in the stochastic optimisation.

Table 5.1: Fitting parameters of the simplified models and coefficient of determination R^2.

x	Power	Inner pressure	Inner temperature	Outer temperature
a	90	6.48	377.17	768.57
b	5.25	0.08	1.83	-1.45
$R^2[\%]$	99.95	99.88	95.58	93.43

5.1.2   Damage estimation methods

There are many damage mechanisms that contribute to the deterioration of the equipment in thermal power plants (Viswanathan, 1989). Creep and low cycle fatigue are arguably the ones mostly related to flexible operation. These damage phenomena depend on the stress and strain levels. Therefore, these variables must be calculated before estimating the degradation in the power plant. Section 4.1 describes two different approaches to compute stresses and strains under the assumptions of plane stress and strain.

(a) Steam pressure. **(b)** Steam temperature. **(c)** Exhaust gas temperature.
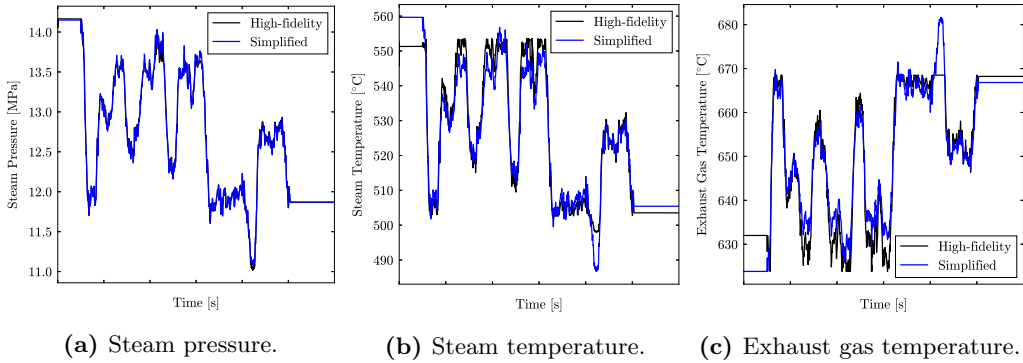
Figure 5.2: Comparison between the prediction of the high-fidelity and simplified models.

Experimental data and charts are the foundation of damage calculations (Suresh, 1998; Viswanathan, 1989). There are many procedures to obtain this data for different degradation mechanisms. Fig. 5.3 represents the charts normally used to estimate the creep damage. This type of experimental data relates the stress level and the temperature at which occurs with the maximum operating time that a material can hold before failure (Viswanathan, 1989).
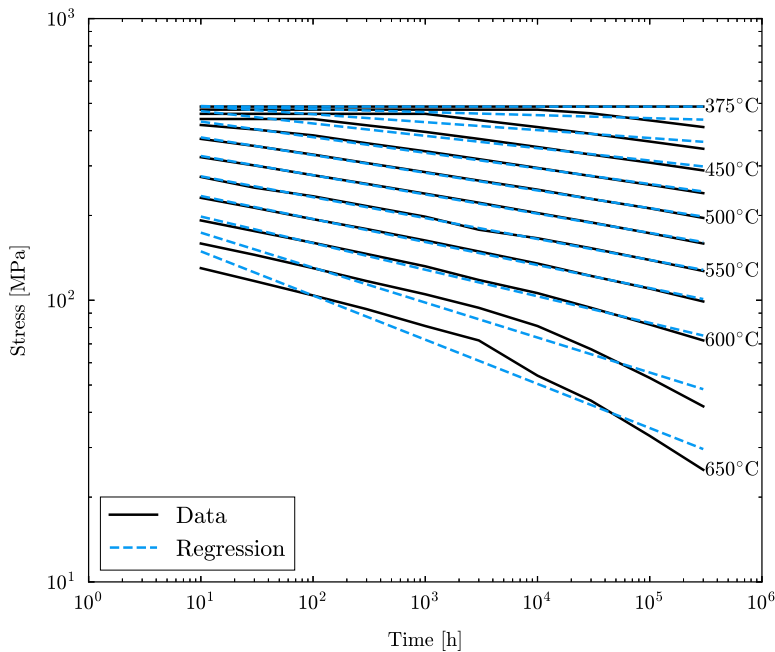
Figure 5.3: Diagram with experimental data to estimate the creep damage. The black lines represent the data obtained experimentally whereas the blue lines are linear regression models used during the optimisation.

The damage induced by creep in the equipment of the thermal power plant is the summation of the ratios between the actual time that a component operates at specific temperature and stress levels and the time before failure at those conditions, which obtained from the charts. Mathematically, the definition of creep damage is:

$$D_{\text{creep}} = \sum_{i=1}^{m} \frac{t_{\text{oper}}}{t_{\text{exp}}} \tag{5.2}$$

where t_{oper} is the time that a component of the power plant operates at a specific temperature and stress level, t_{exp} is the maximum operational time obtained experimentally at those levels, and m is the number of operation points considered.

Charts to estimate the maximum operation time before failure are a composition of many discrete points obtained from experiments. Therefore, obtaining the maximum operational time given a pair of stress-temperature values requires a two-dimensional interpolation. This type of calculations is not suitable for optimisation-based approaches since it may lead to convergence issues owing to points lying outside the data range during the iteration process. To avoid this numerical issue, linear models of the experimental data were developed by standard least-squares to have continuous models that ease the convergence of the optimisation. Fig. 5.3 compares the experimental data and the creep data estimation by these regression models.

Fatigue is the damage associated with cycling loading in any component during regular operation (Suresh, 1998). The calculation of this deterioration mechanism also relies on experimental data. Damage owing to high-cycle fatigue correlates with the stress cycles, whereas low-cycle fatigue is related with the strain (Schijve, 2003; Suresh, 1998). Therefore, the estimation of the damage originated by fatigue needs the stress and strain profiles throughout the operation of thermal power plants. These profiles are the result of complex multi-axial loading. However, the experimental data obtained in a lab originate from uni-axial loading test in uniform samples. To utilise this data in the calculation of fatigue damage under multi-axial loading, the stress and strain profiles must be standardised, i.e. the variable spectrum within the stress and strain profiles is transformed into uniform loading profiles. Rainflow counting is a procedure that extracts the hysteris cycles from the loading spectrum and generates uniform loading cycles from non-uniform stress and strain profiles (Downing and Socie, 1982; Marsh et al., 2016; Matsuishi and Endo, 1968; Sunder et al., 1984; Suresh, 1998). This results in a set of amplitudes and mean stress, or strain, ranges with an associated number of cycles (see Fig. 5.1 - Rainflow counting).

Similarly to the creep damage calculation, the damage due to fatigue is the ratio between the number of cycles at a given amplitude and the maximum number of cycles at that amplitude before failure. Eq. 5.3 represents this computation, known as the linear cumulative damage hypothesis formulated by Miner-Pålmgren

(Fatemi and Yang, 1998; Miner, 1945; Schijve, 2003):

$$D_{\text{fatigue}} = \sum_{i=1}^{n_r} \frac{n_{\text{oper}}}{n_{\text{f}}} \qquad (5.3)$$

where n_{oper} is the number of operation cycles for a given strain amplitude and mean strain, n_r is the number of the different considered ranges, and n_{oper} is the experimental data for the maximum number of cycles before failure. This experimental data is normally represented by the Coffin-Manson equation (Schijve, 2003; Suresh, 1998):

$$\frac{\Delta\varepsilon}{2} = \frac{\Delta\varepsilon_{\text{e}}}{2} + \frac{\Delta\varepsilon_{\text{p}}}{2} = \frac{\sigma_f'}{E} \left(2\,n_{\text{f}}\right)^b + \varepsilon_f' \left(2\,n_{\text{f}}\right)^c \qquad (5.4)$$

with σ_f' and ε_f' being, respectively, the tensile strength and ductility coefficient scaled to fit the experimental data, and b and c are fitting parameters. The elastic contribution to the overall strain amplitude is $\Delta\varepsilon_{\text{e}}/2$, whereas $\Delta\varepsilon_{\text{p}}/2$ is the plastic component. Fig. 5.4 illustrates the experimental fatigue data fitted to the Coffin-Manson equation.
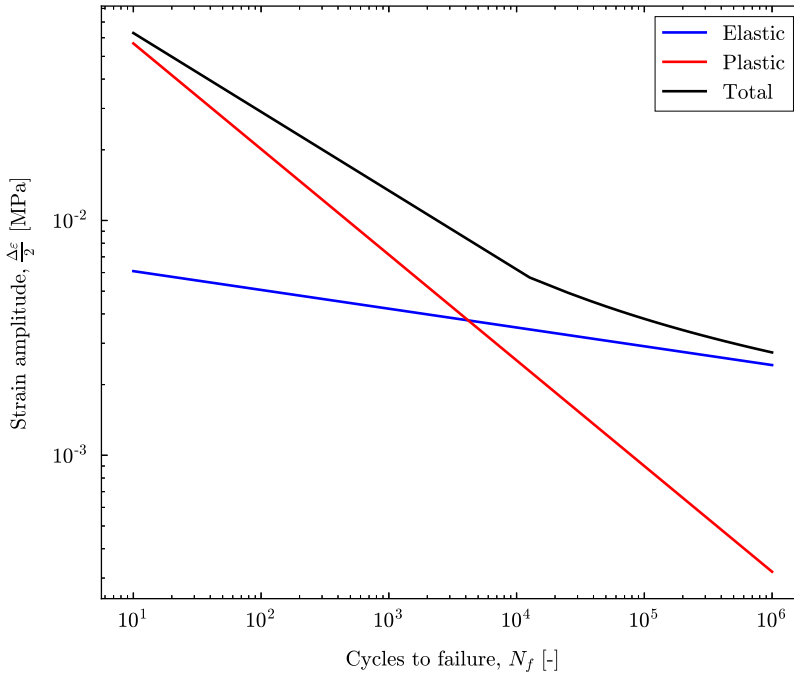
Figure 5.4: Diagram with experimental data to estimate the fatigue damage. The black line represents the maximum experimental number of cycles to failure given that a strain amplitude is a combination of elastic and plastic effects.

The overall damage originating from the simultaneous deterioration from different phenomena is the summation of the individual contributions:

$$D = D_{\text{creep}} + D_{\text{fatigue}} \tag{5.5}$$

5.2   Stochastic optimisation

Intermittent power generation from renewable energy sources adds variability to the electric grid. Scheduling of power generation from thermal power plants becomes hence more complex since they need to balance these fluctuations whilst being profitable and durable. To consider the intrinsic variability of energy systems with large deployment of renewable sources and expand the lifetime operation of balancing power plants, the proposed scheduling method determines the power generation profile of flexible thermal units through a scenario-based multistage optimisation with constraints imposed on the maximum damage. This approach defines the scheduling problem as a stochastic optimisation problem with deterioration constraints.

Scenario-based multistage optimisation models uncertainty as discrete realisations of a probability density function. It considers the different possible combinations of these realisations, and integrates them in an optimisation framework that aims at finding the optimal solution of all possible uncertain scenarios (Lucia et al., 2013). This formulation is suitable for scheduling problems because it can consider only specific variations on power demand that represent the entire uncertainty associated with intermittent energy sources. Moreover, optimisation-based approaches can include both equality and inequality constraints, which allows limiting the maximum damage on the equipment of power plants and enhance their lifetime utilisation. Fig. 5.5 represents schematically a scenario-based multistage optimisation. Given a known initial operation point, x_0, this approach uses a scenario-tree to expand M different uncertainty realisations, d, over a robust time horizon N_{r}, i.e. the period of time until uncertainty is branched. These realisations represent possible power demands that the thermal power plant must balance by modifying its manipulated variable, u, which is the gas turbine load in NGCCs and the fuel input in coal and biomass power plants, to produce the adequate amount of power.

The selection of the number of uncertainty realisations, M_{unc}, and the length of the robust time horizon, N_{r}, is a trade-off between covering more uncertainty and computational cost. The size of scenario-based multistage optimisation problems grows exponentially with these parameters, as shown by Eq. 5.6. Therefore, it is not possible to infinitely increase the number of uncertainty realisation and robust horizon to cover all possible scenarios.

$$S = M_{\text{unc}}^{N_{\text{r}}} \tag{5.6}$$
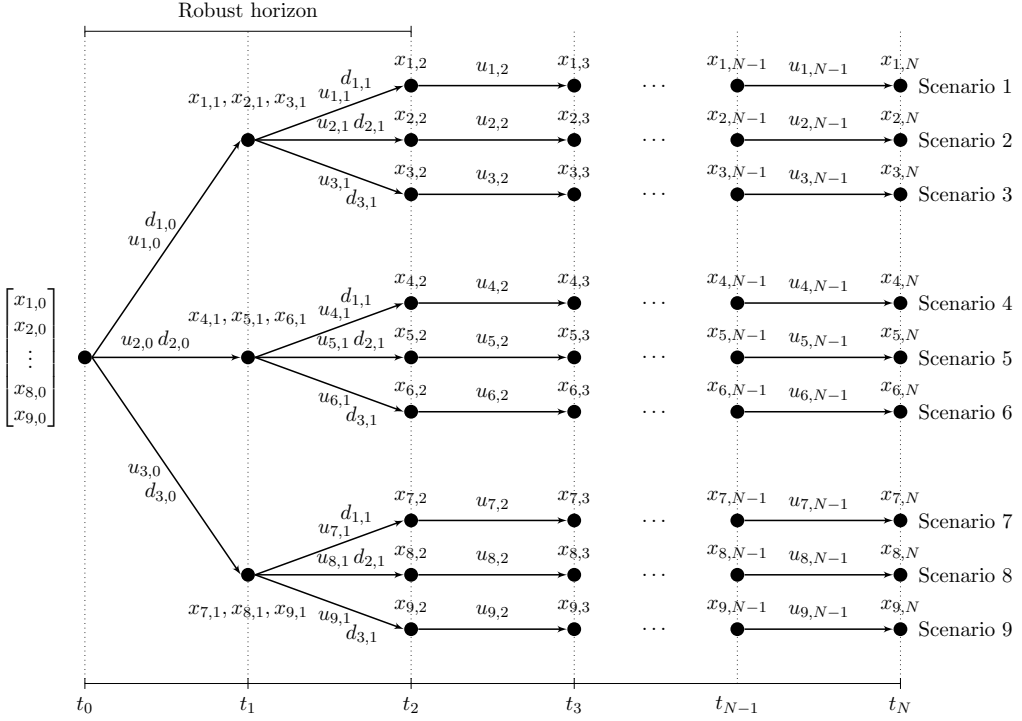
Figure 5.5: Schematic representation of a scenario-tree with $M_r = 3$ uncertainty realisations and a robust time horizon $N_r = 2$.

A solution to the scalability issue associated with scenario-based optimisation is to re-solve the optimisation problem continuously with updated information, e.g. every two hours. This means that it is not necessary to branch the scenario tree until the end of the prediction horizon. Instead, its expansion might be stopped after a short robust horizon that includes variability in the near future, and from this moment on consider the uncertainty unchanging. This simplification significantly reduces the computational cost (see Eq. 5.6), and is possible because information about the far future does not need to be accurately represented at the time when the decision is made, because the decisions will be refined in the next optimisation, when the scheduling problem is solved again with new information.

The mathematical formulation of the scheduling problem as a scenario-tree optimisation problem is:

$$\min_{x_{i,j}, u_{i,j}} \sum_{i=1}^{S} \omega_i \sum_{j=0}^{N-1} \ell(x_{i,j}, u_{i,j}, Pr_j) \tag{5.7a}$$

subject to

$$x_{i,0} = x_{\text{init}} \qquad\qquad \forall i \in \mathcal{S} \qquad\qquad (5.7b)$$

$$x_{i,j} = f(x_{i,j}, u_{i,j}, d_{i,j}) \qquad\qquad \forall i \in \mathcal{S}, \forall j \in \mathcal{N} \qquad (5.7c)$$

$$c_{\text{ineq}}(x_{i,j}, u_{i,j}) \leq D_{\text{max}} \qquad\qquad \forall i \in \mathcal{S}, \forall j \in \mathcal{N} \qquad (5.7d)$$

$$(x_{i,j}, u_{i,j})^{\text{low}} \leq (x_{i,j}, u_{i,j}) \leq (x_{i,j}, u_{i,j})^{\text{up}} \quad \forall i \in \mathcal{S}, \forall j \in \mathcal{N} \qquad (5.7e)$$

$$\sum_{i=1}^{S} E_i^* \, u_i = 0 \qquad\qquad \forall i \in \mathcal{S} \qquad\qquad (5.7f)$$

where the subscripts $(\cdot)_{i,j}$ refer to the ith scenario at the jth sample time, $\mathcal{S}$ is the set of scenarios $\mathcal{S} := \{1, \ldots, S\}$, and $\mathcal{N}$ denotes the set of indices j defining the sampling time such $\mathcal{N} := \{1, \ldots, N\}$.

The cost function in Eq. 5.7a is a weighted average of the individual cost functions of each scenario, where ω_i is the coefficient that determines the weight of each scenario. Since scheduling problems aim at maximising the operating profit, the cost function is defined as:

$$\ell(x_{i,j}, \, u_{i,j}, \, Pr_j) = - x_{i,j}^{\text{T}} \, Pr_j \qquad\qquad (5.8)$$

with Pr_j representing the price of the generated power and $x_{i,j}$ the scheduled power generation, which is a vector including the discrete sequence of operation points that define the quasi-steady state net power production of the NGCC throughout each scenario.

Eq. 5.7c represents the equality constraints of the stochastic optimisation problem. It includes the simplified models for power generation, inner pressure and temperature, and outer temperature in Eq. 5.1 and Table 5.1, and ensures that the solution to the scheduling problem satisfies the behaviour of the considered thermal power plant. These simplified models, and thus Eq. 5.7c, only guarantee that the solution satisfies the quasi-steady state performance of the power plant. This opposes to the original model predictive control application where the equality constraints predict future dynamic behaviour of the system (Lucia et al., 2013).

The inequality constraint in Eq. 5.7d defines the maximum allowable damage in every piece of equipment considered in the thermal power plant, D_{max}. Therefore, this inequality constraint compares the result from the procedure in Fig. 5.1 to compute the damage in different components by distinct mechanisms with the maximum damage determined by plants operators. Eq. 5.7e represents the remaining inequality constraints of the optimisation problem, which are the lower and upper bounds of the computed thermodynamic variables in the equipment x, i.e. temperatures, pressures and power; and the manipulated variable u. Eq. 5.7b sets the initial conditions of the power plant, which are common for all scenarios.

Scenario-tree optimisations include the uncertainty in the process by the continuous branching of different scenarios. This approach considers a broader range

of operating conditions, but it also imposes extra restrictions during the optimisation. As the disturbances associated with the uncertainty cannot be predicted, the control inputs must not anticipate them and the power plant states x in every node must be equal. This implies that the control inputs leading to a node within the robust horizon are equal for the different scenarios branching from that node (Krishnamoorthy et al., 2016, 2018; Lucia et al., 2013; Thombre et al., 2020). These restrictions are the non-anticipativity constraints, and are enforced in the optimisation problem by Eq. 5.7f, where $u_i = [u_{i,0}, u_{i,1}, u_{i,2}, \ldots, u_{i,N-1}] \in \mathbb{R}^N$.

5.3 Scheduling of a natural gas combined cycle

A case study demonstrates the effectiveness of the proposed method to schedule the power generation of a flexible NGCC while limiting the creep damage in the tubes of its superheater. Fig. 5.6 represents the power demand profile estimated by the grid operator and scaled down to the power generation range of the actual power plant. This demand curve is a coarser simplification of the actual profile since scheduling aims at defining overall power generation profiles and NGCCs can respond within seconds to small, unscheduled variations in power demand (Alobaid et al., 2017; Kehlhofer et al., 2009). In addition, Fig. 5.6 includes the representation of two different uncertainty profiles to illustrate how this scheduling method can accommodate any type of variability. This case study considered $\pm 5\%$ constant uncertainty in the estimated power demand, i.e. the grey area in Fig. 5.6.
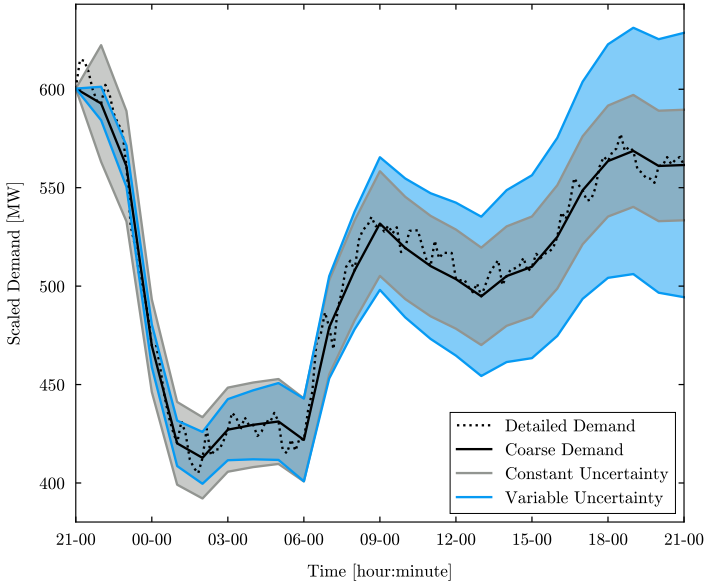
Figure 5.6: Demand profile estimated in day-ahead markets with a coarse simplification and intervals for constant and increasing uncertainty.

This case study also considered time and robust horizons of 24 and 2 hours, respectively, with a sampling time of 1 hour; whereas 3 uncertainty realisations were considered, leading to a total of 9 scenarios that were equally weighted, i.e. $\omega_i = 1/9$. Consequently, Fig. 5.5 represents this stochastic problem for the considered realisations and robust time horizon. Fig. 5.7 illustrates the price curve of the electricity considered in this case study.
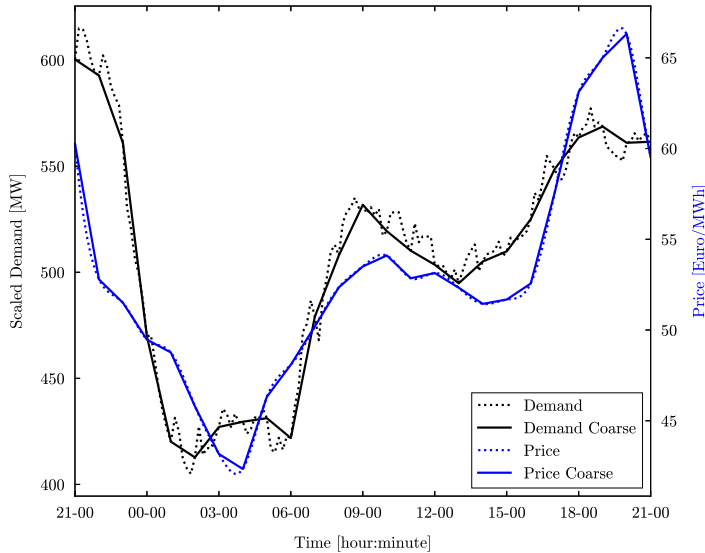
Figure 5.7: Demand profile estimated in day-ahead markets with a coarse simplification and deterministic electricity prices.

The stochastic optimisation problem was solved using a sequential least-squares quadratic programming (SLSQP) algorithm (Kraft, 1988, 1994) included in the nonlinear optimisation package NLOPT (Johnson, 2020). Creep was the only damage mechanisms considered in the tubes of the superheater since this is the main deterioration phenomena in this type of component (Viswanathan, 1989; Viswanathan and Stringer, 2000). T91 was the material considered for these tubes as this is a martensitic steel for high temperature applications. Table 5.2 details the main physical and mechanical properties of this material (Spigarelli et al., 1999). This case study also assumed that the design temperature of these tubes was 510 °C.

Table 5.2: Physical and mechanical properties of T91 martensitic steel.

ρ [kg/m^3]	C_m[J/kgK]	k_m[W/mK]	α^*[m^2/s]	α[1/K]	E[MPa]	v[−]	h_o[W/m^{2}K]	h_i[W/m^{2}K]
7750	770	33	5.53e-05	1.3e-5	180000	0.3	2000	400

The scheduling problem was firstly solved *without* a constraint in the damage to obtain a set of results that maximised the profit and served as a benchmark. Subsequently, the stochastic optimisation problem was resolved with a maximum total damage $D_{\max} = 0.00017$. This value was lower than that obtained in the unconstrained optimisation[1], and thus the scheduling method needed to address this challenge.

The nomenclature referring to the different scenarios in the stochastic optimisation problem follows the sequence of uncertainty realisations, where H, M and L indicate the high (105%), medium (100%) and low (95%) values of the power demand estimated by the grid operator. Thus, a pair of letters defines each scenario since the robust time horizon considered in this work is 2. The first letter refers to the uncertainty realisation in the first sampling time and the second letter indicates the next one. For instance, the pair HL refers to the scenario where the scheduled power considers the highest demand in the first sampling time, and the lowest in the second. Moreover, the letter X is used to indicate all uncertainty realisations (e.g. XH refers to all scenarios where the second uncertainty realisation represents the higher demand profile, independently of the first realisation).

Fig. 5.8 compares the accumulated damage in the tubes of the superheater resulting from the two power generation profiles computed with and without damage constraint. The proposed scheduling method did not exceed the maximum allowable damage and satisfied the inequality constraint in Eq. 5.7d. This constraint was active in the HH scenario, which becomes the bottleneck that inhibits more power generation from the NGCC. This limitation on the HH scenario also affected the HM and HL scenarios. This coupling occured because of the non-anticipativity constraints in Eq. 5.7f, which enforced the set of scenarios HX to coincide in the first uncertainty realisation, i.e. in the first sampling time of the robust horizon. This generated that the HL scenario changed when the constraint in the damage is imposed, albeit it had not reached this limit in the unconstrained case. This illustrates the effects of combining in a stochastic optimisation problem the damage limitation of the equipment with the uncertainty in the estimated power demand.

Imposing constraints on the maximum allowable damage affects the net power generation profile and thus the total revenue of the NGCC. Fig. 5.9 compares the revenue obtained at each scenario in the constrained and unconstrained scheduling problems. Revenue in the MX and LX scenarios remained equal because these did not exceed the maximum allowable damage in the unconstrained optimisation and reached hence the same optimal solution in the constrained case. However, the damage and non-anticipativity constraints modified the power generation profiles in the HX scenarios, which resulted in a reduction of the total power production (see Figs. 5.10a and 5.10b). This decrease was negligible compared to

---

[1]In this context, unconstrained refers to the case where there was no limitation on the maximum damage. However, the optimisation problem still included the remaining equality and inequality constraints.
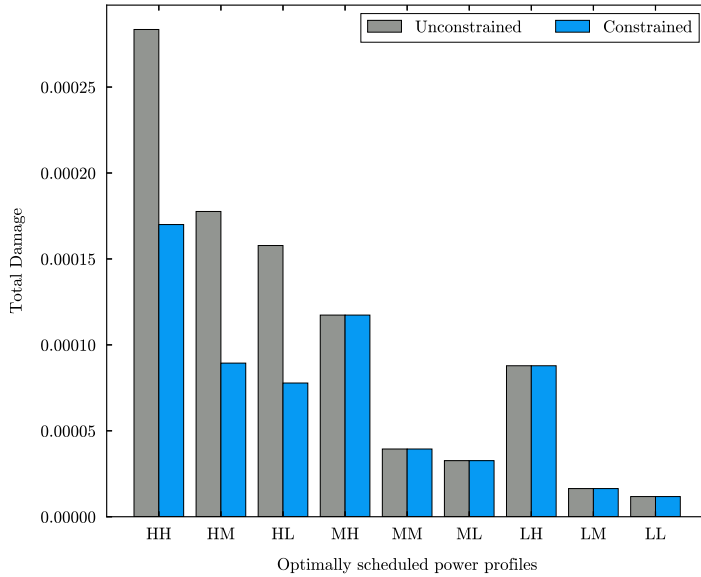
Figure 5.8: Total creep damage in the tubes of the superheater for the different scenarios considered in the stochastic optimisation. H, M and L indicate the high (105%), medium (100%) and low (95%) values of the power demand. A pair of letters defines two uncertainty realisations and hence the trajectory of each scenario.
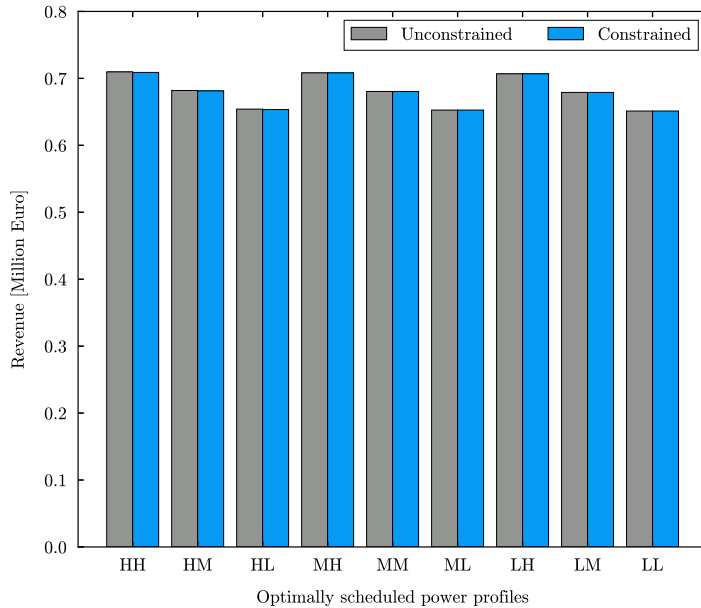
Figure 5.9: Revenue for the different scenarios considered in the stochastic optimisation with and without damage constraints. H, M and L indicate the high (105%), medium (100%) and low (95%) values of the power demand. A pair of letters defines two uncertainty realisations and hence the trajectory of each scenario.

the total power generation of the NGCC within a day and occurred mostly in a period of mid-range prices. Therefore, the reduction of the revenue in the HX scenarios (0.11% in the HH scenario) is insignificant with respect to the damage abatement. This trade-off demonstrates the advantage of the proposed scheduling method. The formulation of the scheduling problem as a stochastic optimisation with damage constraints allows to modify power generation profiles where it leads to significant reductions on the deterioration of the equipment while affecting minimally the overall revenue of the power plant. This approach is specially relevant for damage mechanisms that concentrate at specific periods of time such as creep. The main disadvantage of this method is the sub-optimal results obtained in some scenarios, e.g. HL, as a consequence of the non-anticipativity constraints. Nevertheless, this penalty might be mitigated by updating and resolving the scheduling problem more frequently.

Fig. 5.10 presents the main process variables relevant for scheduling of thermal power plants for different scenarios after optimising the power generation profile with and without damage constraints. There are the scheduled power, the maximum wall temperature, the highest von Mises stress and the creep damage in the tubes of the superheater. Figs. 5.10a and 5.10b show the change in the power generation profile of the HX scenarios that originated from the constraints on the accumulated damage. These changes lead to different operating conditions in the NGCC, including lower temperatures in the wall of the tubes in the superheated, Figs. 5.10c and 5.10d, and smaller values of effective stress, Figs. 5.10e and 5.10f, which resulted in less deterioration due to creep, Figs. 5.10g and 5.10h. This analysis shows that small modifications in the power generation profile of the NGCC significantly reduced the maximum value of creep damage. Such behaviour stems from the effect of a combined reduction of wall temperature and effective stress on the overall creep damage (see Fig. 5.3), and proves the effectiveness of including damage control methods in the scheduling process.

5.4   Effect of design temperature on creep damage

Temperature and stress determine the damage in the equipment originated by creep. The operating conditions of thermal power plants define the wall temperature in different pieces of equipment, so it is a boundary condition during the deterioration process. In contrast, the thermal component of the overall effective stress depends on the temperature distribution along the wall and the design temperature of the equipment as described in Section 4.1. Both boundary conditions and thermal properties of the material define the temperature gradient in the wall, whereas the design temperature is a design choice. This selection refers to the temperature where the component is free of stress and fixes the relative value from where stress arises. Therefore, it has a critical impact on the damage of thermal power plants during regular operation. Fig. 5.11 shows the effect of

(a) Power without damage constraints.

(b) Power with damage constraints.

(c) Maximum wall temperature without damage constraints.

(d) Maximum wall temperature with damage constraints.

(e) Maximum von Mises stress without damage constraints.

(f) Maximum von Mises stress with damage constraints.

(g) Total damage without damage constraints.

(h) Total damage with damage constraints.

Figure 5.10: Optimal scheduling of a flexible NGCC with and without damage limitation under uncertainty.

the design temperature on the shape and magnitude of von Mises stress of the superheater tubes in the unconstrained HH scenario. The wall temperature and stress profiles show opposite behaviour when the design temperature is higher than the maximum temperature in the wall (see, e.g., the lines for 590 °C and 570 °C in Fig. 5.11). However, both wall temperature and von Mises stress follow the same trajectory when the wall temperature is above the design temperature lines for (510 °C and 490 °C in Fig. 5.11). Consequently, when the design temperature switches between being higher or lower than the wall temperature because of changes in the operating conditions, the profile over time of the von Mises effective stress is a combination of both trajectories (lines for 550 °C and 530 °C in Fig. 5.11).
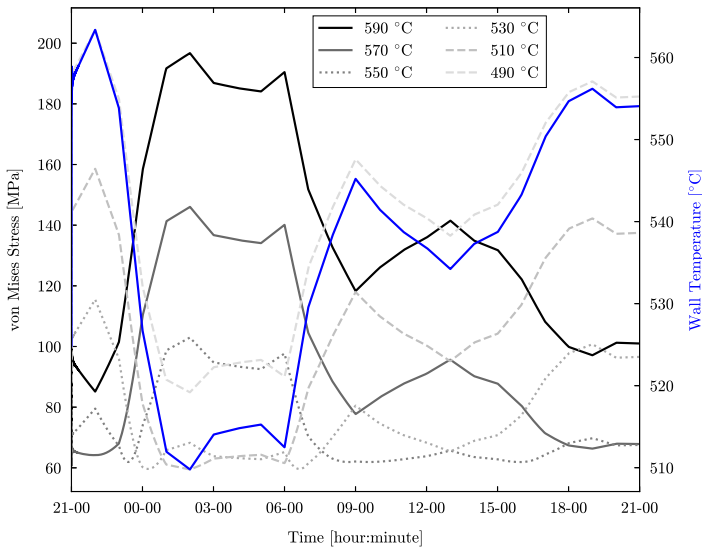
Figure 5.11: Effective stress in the unconstrained HH scenario for different design temperatures. The maximum wall temperature for this scenario is included for shape comparison.

The inverse tendency between wall temperature and effective stress indicate that the power generation profile that maximises the revenue also minimises the damage when the design temperature is always higher than the wall temperature and if there exists direct relation between power generation and wall temperature, i.e. more power leads to higher wall temperatures. This condition is key to understand the effect of design temperature on damage. If the design temperature of the equipment is above the peak of the wall temperature, e.g. lines for 590 °C and 570 °C in Fig. 5.11, and this condition holds, a reduction in power generation leads to lower wall temperature and hence to larger temperature difference with the design temperature and more thermal stress. In this case, the increased on effective stress overcomes the reduction of wall temperature, leading to higher

damage due to creep. Therefore, the optimal solution is the upper bound of power generation, a limit where the creep damage cannot be further reduced. On the contrary, the proposed methodology can find an operating profile that reduces the damage compared to the upper bound of the power generation if there is not a direct relation between power generation and wall temperature.

Creep damage depends on the effective stress and the temperature of the material at which occurs. The design temperature affects these two factors simultaneously. Fig. 5.11 illustrates the different peak levels of stress for different design temperatures and how this maximum value switches among different times. Therefore, the adequate selection of design temperature can notably reduce the total creep damage because of this combined effect. Table 5.3 compares the maximum effective stress value, the associated wall temperature at the instant it occurs and the accumulated damage, for three different scenarios and a broad range of design temperatures. These results demonstrate the trade-off existing between wall temperature and effective stress, since the lowest accumulated damage at each scenario occurred at the lowest combination of both variables, and not at the smallest value of the maximum stress. Design temperatures closer to the highest wall temperature cause the maximum stress at the lowest wall temperatures because of the larger temperature difference (e.g. rows for design temperatures in the range 570 – 550 °C in Table 5.3), whilst design temperatures similar to the mean of the wall temperature reduce the overall temperature difference throughout the operation of the power plant but have the peak of stress at higher wall temperatures (rows 550 – 520 °C in Table 5.3). Consequently, a balance between maximum stress and wall temperature is necessary to reduce the creep damage and enhance the lifetime utilisation of thermal power plants.

Table 5.3: Effect of design temperature on the maximum effective stress, wall temperature at which occurs and total damage for different scenarios. Data for the HH scenario may be compared with Fig. 5.11.

T_{design} [°C]	HH			MM			LL		
	$\sigma_{\text{eff,max}}$ [MPa]	T_{wall} [°C]	Damage	$\sigma_{\text{eff,max}}$ [MPa]	T_{wall} [°C]	Damage	$\sigma_{\text{eff,max}}$ [MPa]	T_{wall} [°C]	Damage
590	196.75	509.77	$7.08\ 10^{-5}$	210.39	503.92	$1.09\ 10^{-4}$	224.13	498.07	$1.6\ 10^{-4}$
570	146.09	509.77	$5.44\ 10^{-7}$	159.19	503.92	$9.95\ 10^{-7}$	172.50	498.07	$1.74\ 10^{-6}$
560	123.98	509.77	$4.54\ 10^{-8}$	136.61	503.92	$8.12\ 10^{-8}$	149.57	498.07	$1.55\ 10^{-7}$
550	102.96	509.77	$3.39\ 10^{-8}$	114.82	503.92	$8.34\ 10^{-9}$	127.22	498.07	$1.14\ 10^{-8}$
540	96.12	563.34	$3.38\ 10^{-7}$	94.38	503.92	$3.10\ 10^{-8}$	105.84	498.07	$9.21\ 10^{-9}$
530	115.53	563.34	$3.84\ 10^{-6}$	104.35	554.72	$3.85\ 10^{-7}$	104.23	554.65	$1.09\ 10^{-7}$
520	136.57	563.34	$3.68\ 10^{-5}$	124.14	554.72	$4.34\ 10^{-6}$	124.02	554.65	$1.26\ 10^{-6}$
510	158.60	563.34	$2.84\ 10^{-4}$	144.92	554.72	$3.94\ 10^{-5}$	144.79	554.65	$1.17\ 10^{-5}$
500	181.32	563.34	$1.77\ 10^{-3}$	168.60	562.40	$2.86\ 10^{-4}$	168.40	562.32	$8.74\ 10^{-5}$
490	204.46	563.34	$9.22\ 10^{-3}$	192.95	562.40	$1.70\ 10^{-3}$	192.74	562.32	$5.30\ 10^{-4}$

Chapter 6

Model predictive control for combined cycles with CO_2 capture

Flexible operation of thermal power plants requires the development of new design methodologies, control strategies and scheduling approaches. There are several bottlenecks that limit the cycling capacity of this type of power systems. Chapter 4 described a control strategy to consider the stress arising in the equipment of thermal power plants and optimise their dynamic operation, whereas Chapter 5 presented a scheduling method to enhance their lifetime utilisation and maximise the revenue in power markets dominated by the uncertainty of renewable energy sources. However, modern energy systems require a profound reduction of CO_2 emissions from thermal power plants in addition to improved flexible operation to balance the grid.

Carbon capture and storage is a technology that complements traditional power systems to deliver low-carbon electricity (IPCC, 2005). There exist many different methods to reduce the CO_2 emissions associated with thermal power generation, being post-combustion capture with liquid solvents the most mature technology with two full-scale coal power plants already in operation (Bui et al., 2018a). Nevertheless, the integration between post-combustion capture systems and thermal power plants might create performance issues during transient operation associated with the coupling of both systems. The deployment of this technology in power markets with large shares of renewable energy requires that system integration does not limit the intrinsic flexibility of thermal power plants and control strategies to regulate the transient operation of both capture and power plants.

Chapter 3 qualitatively discussed the dynamic behaviour of this type of energy systems and demonstrated that integration of CCS with thermal power plants has almost negligible influence on the flexibility of power generation. This chapter is

based on Rúa et al. (2021a) and describes a model predictive control strategy to optimise the dynamic operation of the integrated systems. Section 6.1 describes the dynamic model of a modern NGCC used to replicate the behaviour of an actual power plant and the simplified models developed and included in the MPC strategy. Section 6.2 presents the model predictive control strategy, its mathematical formulation and discusses how to achieve offset-free tracking in the presence of disturbances. A case study where the integrated system needs to balance a decrease in power demand demonstrates the fast control without offset achieved by the proposed MPC strategy in Section 6.3.

6.1 Dynamic modelling of NGCC-PCC systems

A dynamic high-fidelity model of a triple-pressure natural gas combined cycle with reheating integrated with a full-scale post-combustion CO_2 capture plant was used to replicate the operation of an actual power generation system. Section 3.4 described the main characteristic of this NGCC-PCC model and detailed the modelling approach followed to capture its dynamic behaviour. Fig. 3.2 represents the process diagram of this thermal power plant integrated with the capture system.

Model predictive control consists on the periodic solution of a dynamic optimisation problem to compute the control actions imposed on a system. The high computational cost of large high-fidelity models inhibits their utilisation on optimisation-based control strategies. Consequently, this type of control methodologies use instead simplified models that replicate the behaviour of the main process variables of these systems. The development of these simplified models followed the same approach described in Section 4.2, where data generated by imposing simultaneous RGS signals on the controllers of the dynamic model allowed the identification of the local ARX models integrating a local model network capable of predicting nonlinear behaviour. The process variables identified in the NGCC-PCC system were the net power generation of the NGCC, the superheating and reheating temperatures in the steam cycle, the capture ratio of the PCC plant and the reboiler temperature. A polynomial model described the behaviour of power generation because of the linear relationship between this variable and the gas turbine load. Table 6.1 details the coupling between controlled and manipulated variables and shows the prediction accuracy of the local model network for each input-output pair measured by the coefficient of determination R^2. The low R^2 of the superheating and reheating temperature originate from the nature of the validation data. The RGS signals superimposed on the controllers fluctuated faster than the dominant dynamics of the steam cycle, which lead to drastic and fast changes in the controlled and manipulated variables. This created a challenging set of data to predict that allowed testing whether the local model network could predict large and frequent fluctuations. In contrast, the PCC data does

not show this behaviour because of the slower dominant dynamics of the capture plant and its buffering effect, mainly through solvent vessels and liquid hold-ups (Rúa et al., 2020b). This transient performance results in smoother and slower variations easier to predict that lead to higher R^2 values.

Table 6.1: Input-output pairs with model order and coefficient of determination.

Plant	Input-output pair		Order		Nominal		R^2[%]
	Controlled variable (y)	Manipulated variable (u)	n_y	n_u	n_y	n_u	
	Power generation	Gas turbine load					99.95
NGCC	Superheated steam temperature	Opening attemperator valve 1	2	2	592.7 °C	0.02655	69.59
	Reheated steam temperature	Opening attemperator valve 2	2	2	592.5 °C	0.07882	74.37
PCC	Capture rate	Mass flow lean solvent	1	1	90 %	614	98.40
	Reboiler temperature	Opening steam extraction valve	1	1	119.22 °C	0.69	99.09

ARX models are suitable for system identification procedures because the computation of their coefficients becomes a simple least-square problem or a convex optimisation, whereas other structures may involve more complex, possibly non-convex, identification problems (Huusom et al., 2010). However, for analysis purposes, state-space forms of ARX models are preferred. The realisation in observable form of the ARX model in Eq. 4.17 is (Chen, 2013):

$$x_{k+1} = A\,x_k + B\,u_k \qquad (6.1a)$$
$$y_k = C\,x_k \qquad (6.1b)$$

with

$$A = \begin{bmatrix} -a_1 & 1 & 0 & \cdots & 0 \\ -a_2 & 0 & 1 & \cdots & 0 \\ \vdots & \vdots & \vdots & \ddots & \vdots \\ -a_{n_y-1} & 0 & 0 & \cdots & 1 \\ -a_{n_y} & 0 & 0 & \cdots & 0 \end{bmatrix} \quad B = \begin{bmatrix} 0 \\ \vdots \\ b_1 \\ \vdots \\ b_{n_u} \end{bmatrix} \quad C = [1\,0\,\ldots\,0]$$

where B has $n_y - n_u$ zeros, and $x \in \mathbb{R}^{n_y}$, $u, y \in \mathbb{R}$, $A \in \mathbb{R}^{n_y \times n_y}$, $B \in \mathbb{R}^{n_y \times 1}$, and $C \in \mathbb{R}^{1 \times n_y}$. This realisation is valid when the ARX model leads to proper rational transfer functions, i.e. $n_y \geq n_u$. The stochastic error term in Eq. 4.17 is not included because of the deterministic data used during system identification.

6.2 Model predictive control formulation

The main objectives of thermal power plants with CO_2 capture are the generation of power to meet the demand and the capture of sufficient CO_2 to reach the established target of reduction of emissions. In power markets with large contributions of intermittent renewable energy sources, these goals require efficient transient performance of thermal power plants integrated with PCC systems and the tight control of key process variables.

   Model predictive control for reference tracking is a suitable control strategy that can address both issues. This approach formulates an optimisation problem whose goal is to minimise the deviation of key process variables from their set-points (Rawlings et al., 2017). However, this MPC formulation does not ensure offset-free control because of possible plant-model mismatches and disturbances affecting the actual system. Therefore, the reference tracking formulation is combined with methods to achieve offset-free control (Borrelli and Morari, 2007).

   Process and measurement disturbances also affect the performance of the control strategy because of differences between the actual states of the system and the initial conditions used in the optimisation problem. Thus, this MPC strategy includes a Kalman filter to update the state estimations and correct possible mismatches between the predictions of the responses by the simplified models and the measurements from the NGCC-PCC system (Kalman, 1960). Fig. 6.1 shows a diagram of the MPC strategy. This section presents the different blocks integrating this control strategy and their mathematical formulation. Section 6.2.1 discusses reference tracking and offset-free MPC, and describes the formulation of this optimisation problem, whereas Section 6.2.2 builds up on this and defines a simpler dynamic optimisation problem, called delta-input formulation, that only depends on the manipulated variables. Section 6.2.3 describes the estimator that predicts the states on the actual NGCC-PCC systems.

6.2.1   Reference tracking and offset-free MPC

Reference tracking with MPC strategies consist on the solution of a dynamic optimisation problem that minimises the difference between outputs of a system and reference trajectories. The general formulation of linear MPC problems for reference tracking is:

$$\min_{x,u} \ \sum_{k=0}^{N-1} \frac{1}{2} ||Q\left(y_k - y_{\text{ref}}\right)|| + ||R\left(u_k - u_{k-1}\right)|| \tag{6.2a}$$

subject to

$$x_{k+1} = A\,x_k + B\,u_k \tag{6.2b}$$

$$y_k = C\,x_k \tag{6.2c}$$

$$y^{\text{low}} \leq y_k \leq y^{\text{up}} \tag{6.2d}$$

$$u^{\text{low}} \leq u_k \leq u^{\text{up}} \tag{6.2e}$$

 where $||\cdot||$ represents the two-norm that leads to a quadratic programming (QP) optimisation problem. Eq. 6.2b and 6.2c ensure that the state-space realisation of the identified ARX models is satisfied. Eqs. 6.2d and 6.2e limit the minimum and maximum values of the controlled and manipulated variables, respectively. The objective function in Eq. 6.2a minimises the difference between controlled
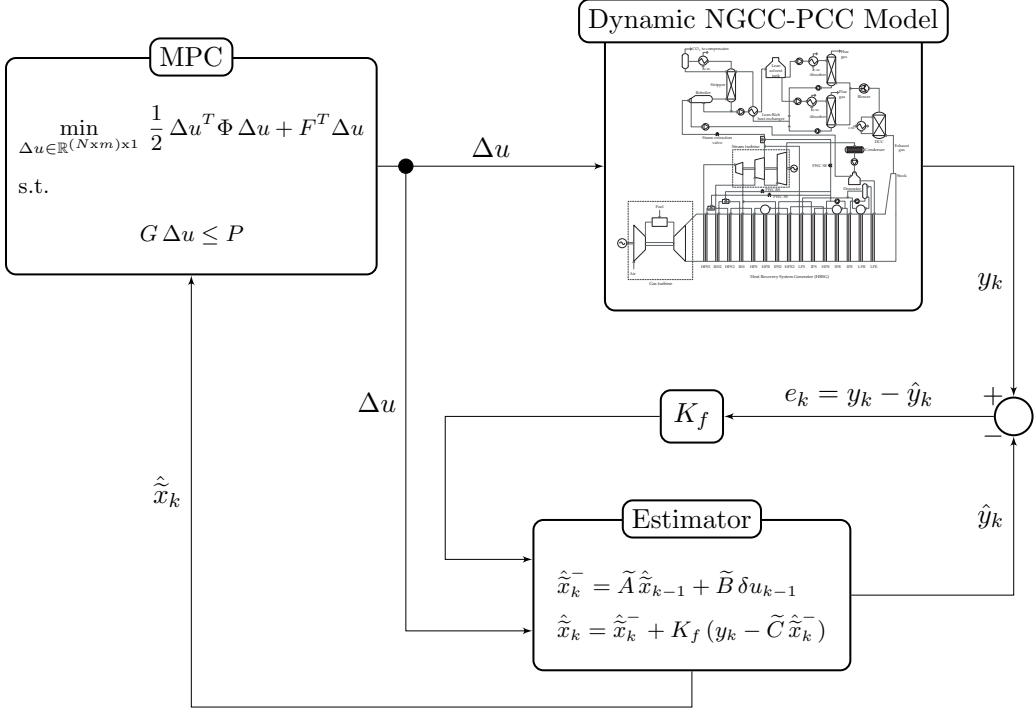
Figure 6.1: Diagram of the proposed MPC strategy with a Kalman filter. Expressions within the diagram are developed throughout Section 6.2, while the dynamic model of the NGCC-PCC system is described in Section 3.4.

variables and their references y_{ref}, and imposes a penalty in excessive utilisation of control inputs.

This formulation does not guarantee offset-free control because of possible mismatches between plant and model, and the presence of disturbances. This issue might be overcome by augmenting the models embedded in the MPC strategy, i.e. Eq. 6.1, with disturbance models that act as integrators and remove the tracking error (Pannocchia, 2015; Pannocchia and Rawlings, 2003; Rawlings et al., 2017). The augmented state-space model is:

$$x_{\mathrm{a},k+1} = A_{\mathrm{a}}\, x_{\mathrm{a},k} + B_{\mathrm{a}}\, u_k \qquad (6.3\mathrm{a})$$

$$y_k = C_{\mathrm{a}}\, x_{\mathrm{a},k} \qquad (6.3\mathrm{b})$$

with:

$$\begin{bmatrix} x_{k+1} \\ d_{k+1} \end{bmatrix} = \begin{bmatrix} A & B_{\mathrm{d}} \\ 0 & I \end{bmatrix} \begin{bmatrix} x_k \\ d_k \end{bmatrix} + \begin{bmatrix} B \\ 0 \end{bmatrix} u_k$$

$$y_k = \begin{bmatrix} C & C_{\mathrm{d}} \end{bmatrix} \begin{bmatrix} x_k \\ d_k \end{bmatrix}$$

75

This formulation achieves offset-free control if the model is stabilisable, the pair (A, C) is observable, the number of disturbances n_d is equal to the number of outputs:

$$n_d = p = 1$$

and the following condition holds (Borrelli and Morari, 2007; Pannocchia, 2015; Pannocchia and Rawlings, 2003; Rawlings et al., 2017):

$$\text{rank} \begin{bmatrix} A - I & B_d \\ C & C_d \end{bmatrix} = n_y + n_d$$

This condition is satisfied if the pair (A, C) is observable, as the disturbance matrices $B_d \in \mathbb{R}^{n_y \times n_d}$ and $C_d \in \mathbb{R}^{1 \times n_d}$ can be chosen freely. The state-space model is, however, in observable form. Thus, the pair (A, C) is always observable. This indicates that offset-free control reduces to the adequate selection of the disturbance model B_d and C_d.

The MPC formulation for the augmented system is:

$$\min_{x,u} \sum_{k=0}^{N-1} \frac{1}{2} ||Q (y_k - y_{\text{ref}})|| + ||R (u_k - u_{k-1})|| \tag{6.4a}$$

subject to

$$x_{a,k+1} = A_a \, x_{a,k} + B_a \, u_k \tag{6.4b}$$

$$y_k = C_a \, x_{a,k} \tag{6.4c}$$

$$y^{\text{low}} \leq y_k \leq y^{\text{up}} \tag{6.4d}$$

$$u^{\text{low}} \leq u_k \leq u^{\text{up}} \tag{6.4e}$$

6.2.2 Delta-input formulation

The reference tracking problem augmented with a disturbance model in Eq. 6.4 already leads to optimal control actions that remove the tracking error. Nevertheless, delta-input formulations are more suited to this type of control problems since they penalise directly the rate of change of the manipulated variables (Borrelli and Morari, 2007). Furthermore, it reduces the number of optimisation variables and the computational cost of the dynamic optimisation. Section 6.2.2.1 describes the delta-input formulation of the MPC problem in Eq. 6.4, whereas Section 6.2.2.2 discusses how several state-space models can be merged into a common MPC problem.

6.2.2.1 Delta-input formulation for SISO systems

Define the delta-input control action that determines the rate of change of a manipulated variable:

$$\delta u_k := u_k - u_{k-1} \tag{6.5}$$

and augment the state-space equation in Eq. 6.3 with this new state and control input:

$$\widetilde{x}_{k+1} = \widetilde{A}\,\widetilde{x}_k + \widetilde{B}\,\delta u_k \tag{6.6a}$$

$$y_k = \widetilde{C}\,\widetilde{x}_k \tag{6.6b}$$

which is expressed:

$$\begin{bmatrix} x_{a,k+1} \\ u_k \end{bmatrix} = \begin{bmatrix} A_a & B_a \\ 0 & I \end{bmatrix} \begin{bmatrix} x_{a,k} \\ u_{k-1} \end{bmatrix} + \begin{bmatrix} B_a \\ I \end{bmatrix} \delta u_k$$

$$y_k = [C_a \quad 0] \begin{bmatrix} x_{a,k} \\ u_{k-1} \end{bmatrix}$$

Define the vectors of controlled and manipulated variables over a time horizon N:

$$\delta u_k = [\delta u_0 \ \delta u_1 \ \ldots \ \delta u_{N-1}]^T$$

$$y = [y_1 \ y_2 \ \ldots \ y_N]^T$$

and eliminate the states in Eq. 6.6. The output equation, over the time horizon N, becomes:

$$y = H\delta u + A_0 \widetilde{x}_0 \tag{6.7}$$

with

$$H = \begin{bmatrix} H_1 & 0 & \cdots & \cdots & 0 \\ H_2 & H_1 & 0 & \cdots & 0 \\ \vdots & \ddots & \ddots & \ddots & \vdots \\ \vdots & & H_2 & H_1 & 0 \\ H_N & \cdots & \cdots & H_2 & H_1 \end{bmatrix} \quad A_0 = \begin{bmatrix} \widetilde{C}\,\widetilde{A} \\ \widetilde{C}\,\widetilde{A}^2 \\ \widetilde{C}\,\widetilde{A}^3 \\ \vdots \\ \widetilde{C}\,\widetilde{A}^N \end{bmatrix}$$

where

$$H_i = \widetilde{C}\,\widetilde{A}^{i-1}\,\widetilde{B} \qquad i \in \{1, 2, \ldots, N\}$$

$$\widetilde{x}_0 = \widetilde{x}[0]$$

Inserting this reduced output equation, Eq. 6.7, and the definition of the delta control input in Eq. 6.5, into Eq. 6.4d and Eq. 6.4e, the inequality constraints of the standard MPC formulation become:

$$\begin{bmatrix} -H \\ H \\ -\Psi \\ \Psi \end{bmatrix} \delta u \leq \begin{bmatrix} -(y^{\text{low}} - A_0\,\widetilde{x}_0) \\ y^{\text{up}} - A_0\,\widetilde{x}_0 \\ -(u^{\text{low}} - u_{-1}) \\ u^{\text{up}} - u_{-1} \end{bmatrix} \tag{6.8}$$

77

where Ψ is an unit lower triangular matrix:

$$
\Psi = \begin{bmatrix}
1 & 0 & \cdots & \cdots & 0 \\
1 & 1 & \ddots & & \vdots \\
\vdots & \ddots & \ddots & \ddots & \vdots \\
\vdots & & \ddots & 1 & 0 \\
1 & \cdots & \cdots & 1 & 1
\end{bmatrix}
$$

Following the same approach, the objective function Eq. 6.4a becomes:

$$
\begin{aligned}
J &= \frac{1}{2}\left(||Q(y - y_{\text{ref}})|| + ||R\delta u||\right) = \\
&= \frac{1}{2}\left(||Q(H\delta u + A_0\widetilde{x}_0 - y_{\text{ref}})|| + ||R\delta u||\right) = \\
&= \frac{1}{2}\Big[\delta u^T(H^T Q H + R)\delta u + \\
&\quad + 2(A_0\widetilde{x}_0 - y_{\text{ref}})Q H \delta u + \\
&\quad + (A_0\widetilde{x}_0 - y_{\text{ref}})^T Q(A_0\widetilde{x}_0 - y_{\text{ref}})\Big]
\end{aligned}
\tag{6.9}
$$

where the last term may be dropped since is constant.

Therefore, the MPC strategy can be expressed as the QP problem:

$$
\min_{\delta u \in \mathbb{R}^N} \ \frac{1}{2}\delta u^T \Gamma \, \delta u + f^T \delta u
\tag{6.10a}
$$

subject to

$$
g\,\delta u \leq p
\tag{6.10b}
$$

with the matrix and vector in Eq. 6.10b defined in Eq. 6.8, and:

$$
\Gamma = H^T Q H + R
$$
$$
f = (A_0\widetilde{x}_0 - y_{\text{ref}})Q H
$$

6.2.2.2 Delta-input formulation for MIMO systems

This section extends the delta-input formulation to the case where there are several controlled and manipulated variables. Consider m single-input single-output (SISO) models with manipulated variables defined as delta-input control actions and grouped in a vector as:

$$
\Delta u := [\delta u_1 \ \delta u_2 \ \ldots \ \delta u_m]^T
\tag{6.11}
$$

where each component is a sequence of control actions over a time horizon N for a given manipulated variable:

$$
\delta u_j = [\delta u_{j,1} \ \ldots \ \delta u_{j,N}]^T \quad j \in \{1, \ldots, m\}
$$

The MPC delta-input formulation can be extended as:

$$\min_{\Delta u \in \mathbb{R}^{(N \times m) \times 1}} \frac{1}{2} \Delta u^T \Phi \, \Delta u + F^T \Delta u \tag{6.12a}$$

subject to

$$G\Delta u \leq P \tag{6.12b}$$

where

$$\Phi = \begin{bmatrix} \Gamma_1 & 0 & \cdots & 0 \\ 0 & \Gamma_2 & \ddots & \vdots \\ \vdots & \ddots & \ddots & 0 \\ 0 & \cdots & 0 & \Gamma_m \end{bmatrix} \quad F = \begin{bmatrix} f_1 \\ f_2 \\ \vdots \\ f_m \end{bmatrix}$$

$$G = \begin{bmatrix} g_1 & 0 & \cdots & 0 \\ 0 & g_2 & \ddots & \vdots \\ \vdots & \ddots & \ddots & 0 \\ 0 & \cdots & 0 & g_m \end{bmatrix} \quad P = \begin{bmatrix} p_1 \\ p_2 \\ \vdots \\ p_m \end{bmatrix}$$

6.2.3   Estimator

Measurements of process variables normally differ from the states in the actual power plant. This difference originates from process and measurement noise and might lead to the computation of suboptimal control actions. State observers consider the uncertainty associated with the measurements and the process to estimate the real state of the system, which becomes the initial conditions in the optimisation problem (see Fig. 6.1). For the considered NGCC-PCC system, state estimation includes the augmented system in Eq. 6.6, i.e. the main process variables computed with the simplified models, the disturbances, and the new state that originates from the definition of the delta-input control action.

The estimator computes the augmented state at each discrete time k as a combination of the current, or a priori, state prediction and a correction based on the measured output y_k:

$$\hat{\widetilde{x}}_k = \widetilde{A}\,\hat{\widetilde{x}}_{k-1} + \widetilde{B}\,\delta u_{k-1} + K\,(y_k - \widetilde{C}\,(\widetilde{A}\,\hat{\widetilde{x}}_{k-1} + \widetilde{B}\,\delta u_{k-1})) \tag{6.13}$$

where $\hat{\ }$ indicates estimated variables, and $K \in \mathbb{R}^{(n_y+1+n_d) \times p}$ is the observer gain:

$$K := \begin{bmatrix} K_x \\ K_d \\ K_u \end{bmatrix}$$

in which K_x, K_d, K_u are the observer gains for the states, disturbances and control input, respectively.

There are several approaches to choose the observer gain K. Observer stability is the only requirement constraining its selection, i.e. the eigenvalues of the system $(\widetilde{A} - K\widetilde{C}\widetilde{A})$ must lie inside the unit circle. Pole placement routines compute observer gain matrices that fix the eigenvalues of a matrix pair in specific coordinates and make the estimator stable (see, e.g. (Pannocchia, 2015)). Nevertheless, Kalman filters are arguably the most widely used observer gain matrices (Kalman, 1960). Calculation of the Kalman filter matrix gain is a two-step process. First, the a priori state $\hat{\widetilde{x}}_{k-1}^{-}$ and covariance matrix P_k^{-} are computed from previous estimations:

$$\hat{\widetilde{x}}_k^{-} = \widetilde{A}\,\hat{\widetilde{x}}_{k-1} + \widetilde{B}\,\delta u_{k-1} \tag{6.14a}$$

$$P_k^{-} = \widetilde{A}\,P_{k-1}\,\widetilde{A}^T + Q_{\mathrm{p}} \tag{6.14b}$$

with Q_{p} representing the covariance of the process noise $w \in \mathcal{N}(0, Q_{\mathrm{p}})$. Then, these a priori estimates are updated based on current measurements:

$$K_f = \frac{P_k^{-}\,\widetilde{C}^T}{\widetilde{C}\,P_k^{-}\widetilde{C}^T + R_{\mathrm{m}}} \tag{6.14c}$$

$$\hat{\widetilde{x}}_k = \hat{\widetilde{x}}_k^{-} + K_f\,(y_k - \widetilde{C}\,\hat{\widetilde{x}}_k^{-}) \tag{6.14d}$$

$$P_k = (I - K_f\,\widetilde{C})\,P_k^{-} \tag{6.14e}$$

where R_{m} is the covariance associated to the measurement noise $v \in \mathcal{N}(0, R_{\mathrm{m}})$, and K_f is the Kalman filter used to estimate the current state $\hat{\widetilde{x}}_k$ and the covariance matrix P_k required at the next sampling time.

6.3 Dynamic operation of integrated systems

Natural gas combined cycles with CO_2 capture are expected to balance the grid within minutes. A case study where a NGCC integreted with a PCC plant needs to balance a drastic change in power demand demonstrates the effectiveness of the proposed MPC strategy to stabilise both plants with minimal deviations of the main process variables from their set-points. During this dynamic simulation, the sampling time was 30 seconds whereas the time horizon within the dynamic optimisation covered 600 seconds, i.e. $N = 20$. These parameters ensured the capture of the dominant dynamics of the NGCC, which are the fastest dynamics of the NGCC-PCC system (see Chapter 3). Table 6.2 includes the bounds for the controlled and manipulated variables considered during the dynamic simulations. Furthermore, the maximum ramp rate of the gas turbine was limited to 15%/min according to the standards suggested by manufacturers. Table 6.3 summarises the matrices and vectors to create the augmented models, the estimator based on the Kalman filter, and the weights in the objective function for each input-output pair.

Table 6.2: Lower and upper bounds of the controlled and manipulated variables.

Variable	Lower	Upper
Power [MW]	450	615
Gas turbine load [%]	60	100
Superheating temperature [°C]	587.7	597.7
Attemperator valve 1 [-]	0.01	1
Reheating temperature [°C]	587.5	597.5
Attemperator valve 2 [-]	0.01	1
Capture ratio [-]	0.85	0.95
Mass flow lean solvent [kg/s]	300	800
Reboiler temperature [°C]	115.22	120.22
Steam extraction valve [-]	0.01	1

Table 6.3: Matrices and vectors defining the disturbance (B_d, C_d) and noise (Q_p, R_m) models; and weights for controlled variables (λ_Q) and penalties in movement of manipulated variables (λ_R).

Variable	B_d	C_d	Q_p	R_m	λ_Q	λ_R
Power	-	-	-	-	1	1
Superheating temperature	$\begin{bmatrix} 0 \\ 0 \\ 0.01 \end{bmatrix}$	0	I_{4x4}	0.01	10	0.01
Reheating temperature	$\begin{bmatrix} 0 \\ 0 \\ 0.01 \end{bmatrix}$	0	I_{4x4}	0.01	10	0.01
Capture ratio	$\begin{bmatrix} 0.1 \\ 0.1 \end{bmatrix}$	0	I_{3x3}	0.1	50000	0.001
Reboiler temperature	$\begin{bmatrix} 0.01 \\ 0.01 \end{bmatrix}$	0	I_{3x3}	0.1	100	10

Transient operation of the NGCC-PCC system aroused from a step change reduction in the power demand that forced the power plant to reduce its load. This operation change modified the exhaust gas and steam cycle conditions, which, in turn, disturbed the post-combustion CO_2 capture plant. Fig. 6.2 shows key process variables in the NGCC-PCC system during dynamic operation and demonstrates the effectiveness of the proposed MPC strategy to achieve optimal offset-free control.

The NGCC stabilised first because of its faster dominant dynamics. Balancing of the power demand occurred within 90 seconds owing to the negligible dynamics of the gas turbine and albeit the constraint on its maximum ramp rate, which was
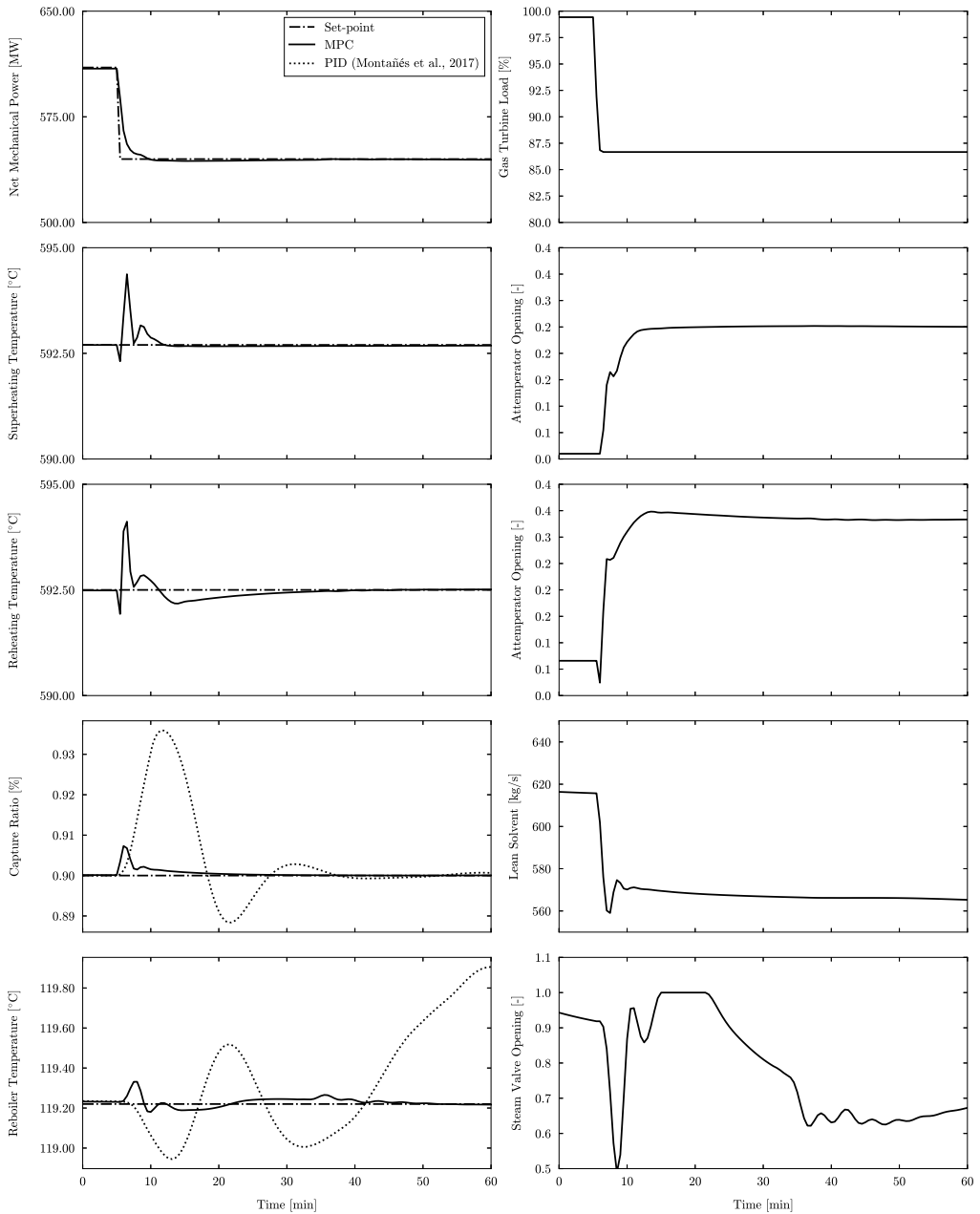
Figure 6.2: Dynamic behaviour of process variables from the NGCC-PCC system with the proposed MPC strategy during a power demand reduction of 70 MW.

active during the first instants of transient operation. The gas turbine compensates the slower dynamic performance of the steam cycle since the heat capacitance of the HRSG prolongs its stabilisation time. Temperature control of the super-

heated and reheated steam shows this behaviour as they required more time to return to their set-points. Nevertheless, the deviation of these variables was less than 2°C while the stabilisation time was 10 minutes, which is less than the values obtained with traditional PID controllers (Montañés et al., 2017b; Prasad et al., 1998; Rúa et al., 2020a). The tight control on the temperature of the hot sections of the steam cycle is fundamental to ensure safe operation and avoid damaging this equipment due to high temperatures. This resulted in aggressive changes in the opening of both attemperator valves.

Post-combustion CO_2 capture plants exhibit longer transient performance because of their slower dominant dynamics, which are governed by large vessels of solvent, transports delays, and liquid hold-ups (see Chapter 3). Fig. 6.2 illustrates this behaviour, especially in the stabilisation time of the reboiler temperature, which needed 45 minutes to reach its set-point. However, the proposed MPC strategy removed the offset of the capture ratio in a similar time than variables in the steam cycle, equating the transient performance of this variable with those of the power plant. Furthermore, the control of the capture ratio occurred with minimal deviation from its set-point and without fluctuations. This smooth behaviour originates from the utilisation of optimisation-based strategies, whose prediction capability leads to better and faster performance during reference tracking. Traditional PIDs can also achieve offset-free control of different process variables in NGCC-PCC systems, although they lead to larger deviations from the set-point and require longer stabilisation time (Montañés et al., 2017b).

The reboiler temperature required more time to stabilise around its set-point and occurred with more fluctuations. This dynamic behaviour resulted from the interaction between the absorber and desorber sections in the capture plant. Changes in the mass flow rate of lean solvent to control the capture ratio modify the operation of the desorption column, which leads to different rich and lean loading in the solvent and force the adjustment of the heat input to maintain a stable temperature in the reboiler. Different lean loading at the outlet of the desorber influences the absorption process and hence requires further modifications of its manipulated variable. Whilst changes of mass flow rate of lean solvent lead to rapid control of the capture ratio, the continuous interaction, transport delay and large liquid hold-ups between both absorption and desorption sections lead to slow stabilisation of the reboiler temperature. Moreover, the heat capacitance of the reboiler contributes to the long transient performance of the desorption process. Despite these slow dominant dynamics, the proposed MPC strategy achieved offset-free control of the reboiler temperature within 45 minutes with deviations below 0.15°C respect to the set-point. This is a significant improvement if compared with PID controllers, which produce longer stabilisation time with larger offsets (Montañés et al., 2017b). Furthermore, the reduction of the maximum deviation allows increasing the nominal operating temperature of the reboiler without reaching levels where solvent degration occurs, leading to an improvement of the stripping efficiency and a potential reduction in steam extraction.

This case study did not include any tuning procedure to enhance the performance of the MPC strategy. However, adequate tuning of the weights in the objective function, the noise models in the estimator and the disturbance models in the augmented system could improve the dynamic behaviour of the NGCC-PCC system.

Chapter 7

Conclusions and future research

Flexible operation of thermal power plants integrated with CO_2 capture requires understanding the dynamic behaviour of both systems, the identification of the main bottlenecks inhibiting faster operation, and the development of adequate procedures and control strategies that allow overcoming these limitations. This thesis presents a set of scientific contributions that aim at enhancing the flexible and safe operation of this type of power generation systems. Section 7.1 summarises the main findings achieved in this Ph.D. thesis, whereas Section 7.2 discusses future research paths to keep developing solutions that improve the current performance of thermal power generation with carbon capture and storage.

7.1   Conclusions

Thermal power plants and post-combustion CO_2 capture exhibit distinct transient behaviour because their dominant dynamics occur in different timescales. Heat capacitance of steam generators is the main limitation of thermal power plant. This type of equipment absorbs large amounts of energy owing to their enormous mass of metal, which slows down the heat transfer between the energy source and the working fluid, generates large temperature gradients and thermal stresses, and leads to delayed changes of operation. In contrast, post-combustion CO_2 capture plants have several limiting factors that contribute to the overall slow dynamic behaviour observed in pilot test campaigns and dynamic simulations. Varying boundary conditions drive the transient operation of these capture systems whereas the continuous interaction between the absorption and desorption sections prolong their stabilisation time. This coupling includes the change of operating conditions within the absorption and desorption columns, the transport delay introduced by heat exchangers and piping, and the long residence time resulting from the large volume of solvent stored in vessels and held-up through-

out the capture plant. This long stabilisation time of capture plants also affects thermal power plants when these two systems are integrated, which leads to small oscillations in the mass flow rate of steam extracted from the IP-LP crossover in the steam turbine. However, dynamic simulations of a natural gas combined cycle integrated with a post-combustion capture plant demonstrated that rapid oscillations in steam extraction do not alter the overall power output of the power plant and proved that CCS does not inhibit the flexible and dispatchable nature of thermal power plants.

Thermal and mechanical stresses are one of the main limitations during cycling operation of thermal power plants. Control strategies based on model predictive control with stress monitoring can compute optimal control actions that do not exceed the maximum allowable stress levels defined by the operator. Both linear and nonlinear formulations of these control strategy are available, so different stress and power plant models can be included. However, linear formulations proved to be computationally superior because of their more suitable numerical properties and convexity. Dynamic simulations with drastic changes of power demand and different stress limits showed that this control methodology can adjust the transient behaviour of natural gas combined cycles to guarantee operating conditions that do not exceed the stress limits. Moreover, these dynamic studies also illustrated how this optimisation-based methodology with stress monitoring under- and over-shoots the gas turbine load when there is not risk of exceeding the maximum stress levels to compensate the slow transient performance of the steam cycle. Therefore, the increase of ramping rates of gas turbines and the stress limits of the material in critical equipment can enhance the flexible operation of natural gas combined cycles.

Scheduling can also improve the flexible operation of thermal power plants in electric markets dominated by intermittent renewable energy sources. Regular operation deteriorates equipment subjected to high pressures and temperatures. Cycling and more frequent start-ups and shut-downs expedite this process. The scheduling method proposed in this thesis relies on the formulation of the scheduling problem as a stochastic optimisation. It aims at computing optimal power generation profiles while accounting for the variability associated with renewable power generation and limiting the maximum damage in specific components of thermal power plants. The scheduling of a natural gas combined cycle in a power market with high variability in power demand demonstrated how this scheduling method can restrain the deterioration of the equipment with almost negligible loss of economic profit. Furthermore, this analysis highlighted the important role of the design temperature of the equipment in the lifetime utilisation of the thermal power plant. Its selection determines the stress and strain levels and, consequently, can limit the cycling capabilities and lifetime operation of specific components.

Control strategies that consider the integration of thermal power plants with CO_2 capture systems can also improve their dynamic behaviour. Model predictive control considers the distinct transient performance of these power generation

systems to compute control actions that lead to optimal operation of both power and capture plants. This approach results in smaller deviations of key process variables from their set-point and shorter stabilisation times, which allows increasing the efficiency of different processes by operating these systems closer to their constraints.

Overall, the contributions of this Ph.D. thesis might be summarised as:

Optimisation-based methodologies can enhance the flexible operation of thermal power plants with CO_2 capture by computing optimal control actions and power generation profiles that limit the maximum stress in the system, lead to faster and tighter reference tracking of key process variables, and expand the plants lifetime without reducing, or even increasing, the economic profit.

7.2 Future research

Start-up procedures for post-combustion CO_2 capture plants is the biggest question yet to answer in the field of carbon capture. Despite there is not sufficient experience on actual operation of CCS systems and power generation with CO_2 capture, dynamic simulations and pilot plant test campaigns have allowed understanding the steady-state and dynamic behaviour of these energy systems during cycling operation. However, there is not knowledge on how to start-up a post-combustion capture plant *alone*, the time needed to reach steady-state operation, and the design of control strategies. Thus, there are several research questions that need answers within the topic of start-up of post-combustion capture plants:

- Which is the sequence of processes that lead to safer and faster start-up?

- Is supplementary firing needed? If so, how can the supplementary emissions be offset? Does supplementary firing impose higher capture rates?

- Can the start-up sequences of thermal power and capture plants be combined to avoid supplementary firing? Does this integration limit the intrinsic flexible operation of thermal power plants?

- Can the start-up sequence of CO_2 capture plants be combined with industrial processes?

- How is the design of control structures for start-up sequences?

- Is it necessary to switch between different control designs in the transition from start-up to regular operation? If so, how?

Uncertainty will also play a major role in the deployment and operation of CCS systems. Scheduling and control strategies must consider the uncertainty associated with industrial processes and power generation systems to enhance the

performance of CCS systems. Furthermore, it is necessary to develop refined statistical models that can predict the variability in power prices, power demand and cost of CO_2 emissions. This type of analysis will also affect the effect of different carbon policies on the economic viability of CCS, as considering uncertainty can create a competitive edge in cap and trade schemes.

Natural gas combined cycles are arguably one of the masterpieces of mechanical engineering. Improvements in this field are limited, and progress is only achieved by gradual minor modifications. The application of the proposed control strategy with stress monitoring to start-ups and shut-downs can however improve the actual sequences and reduce the time required to reach steady-state operation. Exhaust gas recirculation is probably the largest modification that can be implemented in modern natural gas combined cycles. This technology can lead to higher concentrations of CO_2 in the exhaust gas of this type of thermal power plants and notably improve the efficiency of the capture process. Therefore, the development of exhaust gas recirculation processes and understanding its effect on the gas turbine is a key research path within the field of power generation of natural gas combined cycles with CO_2 capture.

Bibliography

Alie, C., Douglas, P. L., and Davison, J. On the operability of power plants with CO_2 capture and storage. *Energy Procedia*, 1(1):1521–1526, 2009.

Alobaid, F., Mertens, N., Starkloff, R., Lanz, T., Heinze, C., and Epple, B. Progress in dynamic simulation of thermal power plants. *Progress in energy and combustion science*, 59:79–162, 2017.

Barella, S., Bellogini, M., Boniardi, M., and Cincera, S. Failure analysis of a steam turbine rotor. *Engineering Failure Analysis*, 18(6):1511–1519, 2011.

Benato, A., Stoppato, A., and Bracco, S. Combined cycle power plants: A comparison between two different dynamic models to evaluate transient behaviour and residual life. *Energy conversion and management*, 87:1269–1280, 2014.

Benato, A., Stoppato, A., and Mirandola, A. Dynamic behaviour analysis of a three pressure level heat recovery steam generator during transient operation. *Energy*, 90:1595–1605, 2015.

Benato, A., Bracco, S., Stoppato, A., and Mirandola, A. Dynamic simulation of combined cycle power plant cycling in the electricity market. *Energy conversion and management*, 107:76–85, 2016.

Bereiter, B., Eggleston, S., Schmitt, J., Nehrbass-Ahles, C., Stocker, T. F., Fischer, H., Kipfstuhl, S., and Chappellaz, J. Revision of the EPICA Dome C CO_2 record from 800 to 600 kyr before present. *Geophysical Research Letters*, 42(2):542–549, 2015.

Bolland, O. A comparative evaluation of advanced combined cycle alternatives. *Journal of Engineering for Gas Turbines and Power*, 113:190–197, 1991.

Boot-Handford, M. E., Abanades, J. C., Anthony, E. J., Blunt, M. J., Brandani, S., Mac Dowell, N., Fernández, J. R., Ferrari, M.-C., Gross, R., Hallett, J. P., et al. Carbon capture and storage update. *Energy & Environmental Science*, 7 (1):130–189, 2014.

Borrelli, F. and Morari, M. Offset free model predictive control. In *2007 46th IEEE Conference on Decision and Control*, pages 1245–1250. IEEE, 2007.

Botero, C., Finkenrath, M., Bartlett, M., Chu, R., Choi, G., and Chinn, D. Redesign, optimization, and economic evaluation of a natural gas combined cycle with the best integrated technology CO_2 capture. *Energy Procedia*, 1(1): 3835–3842, 2009.

Brouwer, A. S., van den Broek, M., Seebregts, A., and Faaij, A. Operational flexibility and economics of power plants in future low-carbon power systems. *Applied Energy*, 156:107–128, 2015.

Bui, M., Gunawan, I., Verheyen, V., Feron, P., Meuleman, E., and Adeloju, S. Dynamic modelling and optimisation of flexible operation in post-combustion CO_2 capture plants—A review. *Computers & Chemical Engineering*, 61:245–265, 2014.

Bui, M., Gunawan, I., Verheyen, V., Feron, P., and Meuleman, E. Flexible operation of CSIRO's post-combustion CO_2 capture pilot plant at the AGL Loy Yang power station. *International Journal of Greenhouse Gas Control*, 48:188–203, 2016.

Bui, M., Fajardy, M., and Mac Dowell, N. Bio-Energy with CCS (BECCS) performance evaluation: Efficiency enhancement and emissions reduction. *Applied energy*, 195:289–302, 2017.

Bui, M., Adjiman, C. S., Bardow, A., Anthony, E. J., Boston, A., Brown, S., Fennell, P. S., Fuss, S., Galindo, A., Hackett, L. A., et al. Carbon capture and storage (CCS): the way forward. *Energy & Environmental Science*, 11(5): 1062–1176, 2018a.

Bui, M., Tait, P., Lucquiaud, M., and Mac Dowell, N. Dynamic operation and modelling of amine-based CO_2 capture at pilot scale. *International Journal of Greenhouse Gas Control*, 79:134–153, 2018b.

Bui, M., Flø, N. E., de Cazenove, T., and Mac Dowell, N. Demonstrating flexible operation of the Technology Centre Mongstad (TCM) CO_2 capture plant. *International Journal of Greenhouse Gas Control*, 93:102879, 2020.

Can Gülen, S. and Kim, K. Gas turbine combined cycle dynamic simulation: a physics based simple approach. *Journal of engineering for gas turbines and power*, 136(1), 2014.

Canty, T., Mascioli, N., Smarte, M., and Salawitch, R. An empirical model of global climate-Part 1: A critical evaluation of volcanic cooling. *Atmospheric Chemistry and Physics*, 13(8):3997, 2013.

Carrasco, J. M., Franquelo, L. G., Bialasiewicz, J. T., Galván, E., PortilloGuisado, R. C., Prats, M. M., León, J. I., and Moreno-Alfonso, N. Power-electronic

systems for the grid integration of renewable energy sources: A survey. *IEEE Transactions on industrial electronics*, 53(4):1002–1016, 2006.

Chen, B. *Linear Systems Theory and Design*. Oxford University Press, 2013.

Chen, H., Cong, T. N., Yang, W., Tan, C., Li, Y., and Ding, Y. Progress in electrical energy storage system: A critical review. *Progress in natural science*, 19(3):291–312, 2009.

Daggash, H. A. and Mac Dowell, N. The implications of delivering the UK's Paris Agreement commitments on the power sector. *International Journal of Greenhouse Gas Control*, 85:174–181, 2019.

Das, G., Chowdhury, S. G., Ray, A. K., Das, S. K., and Bhattacharya, D. K. Turbine blade failure in a thermal power plant. *Engineering failure analysis*, 10 (1):85–91, 2003.

Divya, K. and Østergaard, J. Battery energy storage technology for power systems—An overview. *Electric power systems research*, 79(4):511–520, 2009.

Downing, S. D. and Socie, D. F. Simple rainflow counting algorithms. *International journal of fatigue*, 4(1):31–40, 1982.

Dunn, B., Kamath, H., and Tarascon, J.-M. Electrical energy storage for the grid: a battery of choices. *Science*, 334(6058):928–935, 2011.

Eser, P., Chokani, N., and Abhari, R. S. Operational and financial performance of fossil fuel power plants within a high renewable energy mix. *Journal of the Global Power and Propulsion Society*, 1:16–27, 2017.

Fajardy, M. and Mac Dowell, N. Can BECCS deliver sustainable and resource efficient negative emissions? *Energy & Environmental Science*, 10(6):1389–1426, 2017.

Farid, M. M., Khudhair, A. M., Razack, S. A. K., and Al-Hallaj, S. A review on phase change energy storage: materials and applications. *Energy conversion and management*, 45(9-10):1597–1615, 2004.

Fatemi, A. and Yang, L. Cumulative fatigue damage and life prediction theories: a survey of the state of the art for homogeneous materials. *International journal of fatigue*, 20(1):9–34, 1998.

Fernandez, E. S., del Rio, M. S., Chalmers, H., Khakharia, P., Goetheer, E. L., Gibbins, J., and Lucquiaud, M. Operational flexibility options in power plants with integrated post-combustion capture. *International Journal of Greenhouse Gas Control*, 48:275–289, 2016.

Flø, N. E., Kvamsdal, H. M., Hillestad, M., and Mejdell, T. Dominating dynamics of the post-combustion CO_2 absorption process. *Computers & Chemical Engineering*, 86:171–183, 2016.

Forssell, U. and Ljung, L. Closed-loop identification revisited. *Automatica*, 35(7): 1215–1241, 1999.

Garðarsdóttir, S. Ó., Normann, F., Andersson, K., Prölß, K., Emilsdóttir, S., and Johnsson, F. Post-combustion CO_2 capture applied to a state-of-the-art coal-fired power plant—The influence of dynamic process conditions. *International Journal of Greenhouse Gas Control*, 33:51–62, 2015.

Garðarsdóttir, S. Ó., Montañés, R. M., Normann, F., Nord, L. O., and Johnsson, F. Effects of CO_2-absorption control strategies on the dynamic performance of a supercritical pulverized-coal-fired power plant. *Industrial & Engineering Chemistry Research*, 56(15):4415–4430, 2017.

Gevers, M. Identification for Control: From the Early Achievements to the Revival of Experiment Design. *European journal of control*, 11:1–18, 2005.

Gevers, M. and Ljung, L. Optimal experiment designs with respect to the intended model application. *Automatica*, 22(5):543–554, 1986.

Gevers, M., Mišković, L., Bonvin, D., and Karimi, A. Identification of multi-input systems: variance analysis and input design issues. *Automatica*, 42(4):559–572, 2006.

GISTEMP Team. GISS Surface Temperature Analysis (GISTEMP), version 4, 2020. NASA Goddard Institute for Space Studies. Data set accessed 2020-07-17 at `data.giss.nasa.gov/gistemp/`.

Gonzalez-Salazar, M. A., Kirsten, T., and Prchlik, L. Review of the operational flexibility and emissions of gas-and coal-fired power plants in a future with growing renewables. *Renewable and Sustainable Energy Reviews*, 82:1497–1513, 2018.

Hentschel, J., Spliethoff, H., et al. A parametric approach for the valuation of power plant flexibility options. *Energy Reports*, 2:40–47, 2016.

Heuberger, C. F., Rubin, E. S., Staffell, I., Shah, N., and Mac Dowell, N. Power capacity expansion planning considering endogenous technology cost learning. *Applied Energy*, 204:831–845, 2017.

Heuberger, C. F., Staffell, I., Shah, N., and Mac Dowell, N. Impact of myopic decision-making and disruptive events in power systems planning. *Nature Energy*, 3(8):634–640, 2018.

Huber, M., Dimkova, D., and Hamacher, T. Integration of wind and solar power in europe: Assessment of flexibility requirements. *Energy*, 69:236–246, 2014.

Huusom, J. K., Poulsen, N. K., Jørgensen, S. B., and Jørgensen, J. B. Tuning of methods for offset free MPC based on ARX model representations. In *Proceedings of the 2010 American Control Conference*, pages 2355–2360. IEEE, 2010.

IEA. Technology Roadmap, Energy storage. `https://www.iea.org/publications/freepublications/publication/TechnologyRoadmapEnergystorage.pdf`, 2014.

IEA. World Energy Outlook 2019. IEA, Paris, 2019. `https://www.iea.org/reports/world-energy-outlook-2019/`.

IPCC. IPCC Special Report on Carbon Dioxide Capture and Storage. Prepared by Working Group III of the Intergovernmental Panel on Climate Change [Metz, B., O. Davidson, H. C. de Coninck, M. Loos, and L. A. Meyer (eds.)]. Cambridge University Press, Cambridge, United Kingdom and New York, NY, USA, 2005.

IPCC. Climate Change 2014: Synthesis Report. Contribution of Working Groups I, II and III to the Fifth Assessment Report of the Intergovernmental Panel on Climate Change [Core Writing Team, R.K. Pachauri and L.A. Meyer (eds.)], IPCC, Geneva, Switzerland, 2014.

IPCC. Summary for Policymakers. In: Global warming of 1.5°C. An IPCC Special Report on the impacts of global warming of 1.5°C above pre-industrial levels and related global greenhouse gas emission pathways, in the context of strengthening the global response to the threat of climate change, sustainable development, and efforts to eradicate poverty. [V. Masson-Delmotte, P. Zhai, H. O. Pörtner, D. Roberts, J. Skea, P. R. Shukla, A. Pirani, W. Moufouma-Okia, C. Péan, R. Pidcock, S. Connors, J. B. R. Matthews, Y. Chen, X. Zhou, M. I. Gomis, E. Lonnoy, T. Maycock, M. Tignor, T. Waterfield (eds.)]. World Meteorological Organization, Geneva, Switzerland, 2018.

Johansen, T. A. and Foss, B. Constructing NARMAX models using ARMAX models. *International Journal of Control*, 58(5):1125–1153, 1993.

Johnson, S. G. The NLopt nonlinear-optimization package. `http://github.com/stevengj/nlopt`, 2020.

Jonshagen, K., Sammak, M., and Genrup, M. Postcombustion CO_2 capture for combined cycles utilizing hot-water absorbent regeneration. *Journal of Engineering for Gas Turbines and Power*, 134(1), 2012.

Jordal, K., Ystad, P. A. M., Anantharaman, R., Chikukwa, A., and Bolland, O. Design-point and part-load considerations for natural gas combined cycle plants with post combustion capture. *International Journal of Greenhouse Gas Control*, 11:271–282, 2012.

Kalman, R. E. A new approach to linear filtering and prediction problems. *Journal of Basic Engineering*, pages 35–45, 1960.

Kehlhofer, R., Hannemann, F., Rukes, B., and Stirnimann, F. *Combined-Cycle Gas & Steam Turbine Power Plants.* Pennwell Books, 2009.

Kim, T., Lee, D., and Ro, S. Analysis of thermal stress evolution in the steam drum during start-up of a heat recovery steam generator. *Applied Thermal Engineering*, 20(11):977–992, 2000.

Knutson, T., Zhang, R., and Horowitz, L. W. Prospects for a prolonged slowdown in global warming in the early 21st century. *Nature communications*, 7(1):1–12, 2016.

Knutson, T., Kossin, J. P., Mears, C., Perlwitz, J., and Wehner, M. F. Detection and attribution of climate change. In: Climate Science Special Report: Fourth National Climate Assessment, Volume I. [Wuebbles, D.J., D.W. Fahey, K.A. Hibbard, D.J. Dokken, B.C. Stewart, and T.K. Maycock (eds.)]. U.S. Global Change Research Program, Washington, DC, USA, 2017.

Kondziella, H. and Bruckner, T. Flexibility requirements of renewable energy based electricity systems–a review of research results and methodologies. *Renewable and Sustainable Energy Reviews*, 53:10–22, 2016.

Kraft, D. A software package for sequential quadratic programming. *Forschungsbericht- Deutsche Forschungs- und Versuchsanstalt fur Luft- und Raumfahrt*, 1988.

Kraft, D. Algorithm 733: TOMP–Fortran modules for optimal control calculations. *ACM Transactions on Mathematical Software (TOMS)*, 20(3):262–281, 1994.

Krishnamoorthy, D., Foss, B., and Skogestad, S. Real-time optimization under uncertainty applied to a gas lifted well network. *Processes*, 4(4):52, 2016.

Krishnamoorthy, D., Foss, B., and Skogestad, S. A distributed algorithm for scenario-based model predictive control using primal decomposition. *IFAC-PapersOnLine*, 51(18):351–356, 2018.

Kvamsdal, H. M. and Rochelle, G. T. Effects of the temperature bulge in CO_2 absorption from flue gas by aqueous monoethanolamine. *Industrial & Engineering Chemistry Research*, 47(3):867–875, 2008.

Lawal, A., Wang, M., Stephenson, P., Koumpouras, G., and Yeung, H. Dynamic modelling and analysis of post-combustion CO_2 chemical absorption process for coal-fired power plants. *Fuel*, 89(10):2791–2801, 2010.

Lawal, A., Wang, M., Stephenson, P., and Obi, O. Demonstrating full-scale post-combustion CO_2 capture for coal-fired power plants through dynamic modelling and simulation. *Fuel*, 101:115–128, 2012.

Lenssen, N. J., Schmidt, G. A., Hansen, J. E., Menne, M. J., Persin, A., Ruedy, R., and Zyss, D. Improvements in the GISTEMP uncertainty model. *Journal of Geophysical Research: Atmospheres*, 124(12):6307–6326, 2019.

Lew, D., Brinkman, G., Kumar, N., Besuner, P., Agan, D., and Lefton, S. Impacts of wind and solar on fossil-fueled generators. Technical report, National Renewable Energy Lab.(NREL), Golden, CO (United States), 2012.

Lise, W., van der Laan, J., Nieuwenhout, F., and Rademaekers, K. Assessment of the required share for a stable EU electricity supply until 2050. *Energy Policy*, 59:904–913, 2013.

Ljung, L. *System identification: theory for the user*. Prentice-hall, 1987.

Lucia, S., Finkler, T., and Engell, S. Multi-stage nonlinear model predictive control applied to a semi-batch polymerization reactor under uncertainty. *Journal of Process Control*, 23(9):1306–1319, 2013.

Lucquiaud, M., Chalmers, H., and Gibbins, J. Capture-ready supercritical coal-fired power plants and flexible post-combustion CO_2 capture. *Energy Procedia*, 1(1):1411–1418, 2009.

Lund, P. D., Lindgren, J., Mikkola, J., and Salpakari, J. Review of energy system flexibility measures to enable high levels of variable renewable electricity. *Renewable and Sustainable Energy Reviews*, 45:785–807, 2015.

Mac Dowell, N. and Shah, N. Dynamic modelling and analysis of a coal-fired power plant integrated with a novel split-flow configuration post-combustion CO_2 capture process. *International Journal of Greenhouse Gas Control*, 27: 103–119, 2014.

MacDowell, N., Florin, N., Buchard, A., Hallett, J., Galindo, A., Jackson, G., Adjiman, C. S., Williams, C. K., Shah, N., and Fennell, P. An overview of CO_2 capture technologies. *Energy & Environmental Science*, 3(11):1645–1669, 2010.

Marsh, G., Wignall, C., Thies, P. R., Barltrop, N., Incecik, A., Venugopal, V., and Johanning, L. Review and application of Rainflow residue processing techniques for accurate fatigue damage estimation. *International Journal of Fatigue*, 82: 757–765, 2016.

Matsuishi, M. and Endo, T. Fatigue of metals subjected to varying stress. *Japan Society of Mechanical Engineers, Fukuoka, Japan*, 68(2):37–40, 1968.

Miner, M. Cumulative damage in fatigue. *Journal of Applied Mechanics*, 12: A159–A164, 1945.

Mišković, L., Karimi, A., Bonvin, D., and Gevers, M. Closed-loop identification of multivariable systems: With or without excitation of all references? *Automatica*, 44(8):2048–2056, 2008.

Montañés, R. M., Korpås, M., Nord, L. O., and Jaehnert, S. Identifying operational requirements for flexible ccs power plant in future energy systems. *Energy Procedia*, 86(22.10):1016, 2016.

Montañés, R. M., Flø, N. E., and Nord, L. O. Dynamic process model validation and control of the amine plant at CO_2 Technology Centre Mongstad. *Energies*, 10(10):1527, 2017a.

Montañés, R. M., GarÐarsdóttir, S. Ó., Normann, F., Johnsson, F., and Nord, L. O. Demonstrating load-change transient performance of a commercial-scale natural gas combined cycle power plant with post-combustion CO_2 capture. *International Journal of Greenhouse Gas Control*, 63:158–174, 2017b.

Montañés, R. M., Flø, N. E., and Nord, L. O. Experimental results of transient testing at the amine plant at Technology Centre Mongstad: Open-loop responses and performance of decentralized control structures for load changes. *International Journal of Greenhouse Gas Control*, 73:42–59, 2018.

Morice, C. P., Kennedy, J. J., Rayner, N. A., and Jones, P. D. Quantifying uncertainties in global and regional temperature change using an ensemble of observational estimates: The HadCRUT4 data set. *Journal of Geophysical Research: Atmospheres*, 117(D8), 2012.

Mukhopadhyay, N., Chowdhury, S. G., Das, G., Chattoraj, I., Das, S., and Bhattacharya, D. An investigation of the failure of low pressure steam turbine blades. *Engineering failure analysis*, 5(3):181–193, 1998.

Nocedal, J. and Wright, S. *Numerical optimization*. Springer Science & Business Media, 2006.

Nosratabadi, S. M., Hooshmand, R.-A., and Gholipour, E. A comprehensive review on microgrid and virtual power plant concepts employed for distributed energy resources scheduling in power systems. *Renewable and Sustainable Energy Reviews*, 67:341–363, 2017.

Oswald, J., Raine, M., and Ashraf-Ball, H. Will British weather provide reliable electricity? *Energy Policy*, 36(8):3212–3225, 2008.

Pandžić, H., Kuzle, I., and Capuder, T. Virtual power plant mid-term dispatch optimization. *Applied Energy*, 101:134–141, 2013.

Pannocchia, G. Offset-free tracking MPC: A tutorial review and comparison of different formulations. In *2015 European control conference (ECC)*, pages 527–532. IEEE, 2015.

Pannocchia, G. and Rawlings, J. B. Disturbance models for offset-free model-predictive control. *AIChE journal*, 49(2):426–437, 2003.

Paterson, I. and Wilson, J. Use of damage monitoring systems for component life optimisation in power plant. *International journal of pressure vessels and piping*, 79(8-10):541–547, 2002.

Peng, H., Ozaki, T., Toyoda, Y., and Oda, K. Exponential ARX model-based long-range predictive control strategy for power plants. *Control Engineering Practice*, 9(12):1353–1360, 2001.

Petit, J.-R., Jouzel, J., Raynaud, D., Barkov, N. I., Barnola, J.-M., Basile, I., Bender, M., Chappellaz, J., Davis, M., Delaygue, G., et al. Climate and atmospheric history of the past 420,000 years from the Vostok ice core, Antarctica. *Nature*, 399(6735):429, 1999.

Prasad, G., Swidenbank, E., and Hogg, B. A local model networks based multivariable long-range predictive control strategy for thermal power plants. *Automatica*, 34(10):1185–1204, 1998.

Rawlings, J. B., Mayne, D. Q., and Diehl, M. *Model predictive control: theory, computation, and design*, volume 2. Nob Hill Publishing Madison, WI, 2017.

Rezazadeh, F., Gale, W. F., Hughes, K. J., and Pourkashanian, M. Performance viability of a natural gas fired combined cycle power plant integrated with post-combustion CO_2 capture at part-load and temporary non-capture operations. *International Journal of Greenhouse Gas Control*, 39:397–406, 2015.

Riboldi, L. and Nord, L. O. Optimal design of flexible power cycles through Kriging-based surrogate models. In *Turbo Expo: Power for Land, Sea, and Air*, volume 51043, page V003T08A002. American Society of Mechanical Engineers, 2018.

Rúa, J. and Nord, L. O. Optimal control of flexible natural gas combined cycles with stress monitoring: Linear vs nonlinear model predictive control. *Applied Energy*, 265:114820, 2020.

Rúa, J., Agromayor, R., Hillestad, M., and Nord, L. O. Optimal dynamic operation of natural gas combined cycles accounting for stresses in thick-walled components. *Applied Thermal Engineering*, 170:114858, 2020a.

Rúa, J., Bui, M., Nord, L. O., and Mac Dowell, N. Does CCS reduce power generation flexibility? A dynamic study of combined cycles with post-combustion CO_2 capture. *International Journal of Greenhouse Gas Control*, 95:102984, 2020b.

Rúa, J., Hillestad, M., and Nord, L. O. Model predictive control for combined cycles integrated with CO_2 capture plants. *Computers & Chemical Engineering*, 146:107217, 2021a.

Rúa, J., Verheyleweghen, A., Jäschke, J., and Nord, L. O. Optimal scheduling of flexible thermal power plants with lifetime enhancement under uncertainty. *Applied Thermal Engineering*, 191:116794, 2021b.

Saber, A. Y. and Venayagamoorthy, G. K. Resource scheduling under uncertainty in a smart grid with renewables and plug-in vehicles. *IEEE systems journal*, 6 (1):103–109, 2011.

Salvinder, K., Zabiri, H., Taqvi, S. A., Ramasamy, M., Isa, F., Rozali, N., Suleman, H., Maulud, A., and Shariff, A. An overview on control strategies for CO_2 capture using absorption/stripping system. *Chemical Engineering Research and Design*, 147:319–337, 2019.

Schijve, J. Fatigue of structures and materials in the 20th century and the state of the art. *International journal of fatigue*, 25(8):679–702, 2003.

Spigarelli, S., Cerri, E., Bianchi, P., and Evangelista, E. Interpretation of creep behaviour of a 9Cr–Mo–Nb–V–N (T91) steel using threshold stress concept. *Materials science and technology*, 15(12):1433–1440, 1999.

Sunder, R., Seetharam, S., and Bhaskaran, T. Cycle counting for fatigue crack growth analysis. *International Journal of Fatigue*, 6(3):147–156, 1984.

Suresh, S. *Fatigue of materials*. Cambridge University Press, 1998.

Tait, P., Buschle, B., Ausner, I., Valluri, P., Wehrli, M., and Lucquiaud, M. A pilot-scale study of dynamic response scenarios for the flexible operation of post-combustion CO_2 capture. *International Journal of Greenhouse Gas Control*, 48: 216–233, 2016.

Thombre, M., Mdoe, Z., and Jäschke, J. Data-Driven Robust Optimal Operation of Thermal Energy Storage in Industrial Clusters. *Processes*, 8(2):194, 2020.

Timoshenko, S. and Goodier, J. N. *Theory of Elasticity*. McGraw-Hill book Company, 1951.

UNFCCC. Paris Agreement. United Nations Treaty Collection, Geneva, Switzerland, 2015.

U.S. Energy Information Administration, 2020. Data set accessed 2020-07-17 at `https://www.eia.gov/`.

Viswanathan, R. *Damage mechanisms and life assessment of high temperature components*. ASM international, 1989.

Viswanathan, R. and Bakker, W. Materials for ultrasupercritical coal power plants − Turbine materials: Part II. *Journal of Materials Engineering and Performance*, 10(1):96–101, 2001a.

Viswanathan, R. and Bakker, W. Materials for ultrasupercritical coal power plants—Boiler materials: Part I. *Journal of materials engineering and performance*, 10(1):81–95, 2001b.

Viswanathan, R. and Stringer, J. Failure mechanisms of high temperature components in power plants. *J. Eng. Mater. Technol.*, 122(3):246–255, 2000.

Wang, P., Cui, L., Lyschik, M., Scholz, A., Berger, C., and Oechsner, M. A local extrapolation based calculation reduction method for the application of constitutive material models for creep fatigue assessment. *International journal of fatigue*, 44:253–259, 2012.

Wu, X., Wang, M., Liao, P., Shen, J., and Li, Y. Solvent-based post-combustion CO_2 capture for power plants: A critical review and perspective on dynamic modelling, system identification, process control and flexible operation. *Applied Energy*, 257:113941, 2020.

Appendix A

Publications

Publication I

Rúa, J., Bui, M., Nord, L. O., and Mac Dowell, N. Does CCS reduce power generation flexibility? A dynamic study of combined cycles with post-combustion CO_2 capture. *International Journal of Greenhouse Gas Control*, 95:102984, 2020.

Publication II

Rúa, J., Agromayor, R., Hillestad, M., and Nord, L. O. Optimal dynamic operation of natural gas combined cycles accounting for stresses in thick-walled components. *Applied Thermal Engineering*, 170:114858, 2020.

Publication III

Rúa, J. and Nord, L. O. Optimal control of flexible natural gas combined cycles with stress monitoring: Linear vs nonlinear model predictive control. *Applied Energy*, 265:114820, 2020.

Publication IV

Rúa, J., Verheyleweghen, A., Jäschke, J., and Nord, L. O. Optimal scheduling of flexible thermal power plants with lifetime enhancement under uncertainty. *Applied Thermal Engineering*, 191:116794, 2021.

Publication V

Rúa, J., Hillestad, M., and Nord, L. O. Model predictive control for combined cycles integrated with CO_2 capture plants. *Computers & Chemical Engineering*, 146:107217, 2021.

Publication I

To date, the deployment, integration, and utilisation of intermittent renewable energy sources, such as wind and solar power, in the global energy system has been the cornerstone of efforts to combat climate change. At the same time, it is recognised that renewable power represents only one element of the portfolio of technologies that will be required to deliver a technically feasible and financially viable energy system. In this context, carbon capture and storage (CCS) is understood to play a uniquely important role, providing significant value through flexible operation. It is therefore of vital importance that CCS technology can operate synergistically with intermittent renewable power sources, and consequently ensuring that CCS does not inhibit the flexible and dispatchable nature of thermal power plants. This work analyses the intrinsic dynamic performance of the power and CO_2 capture plants independently and as an integrated system. Since the power plant represents the fast dynamics of the system and the steam extraction is the main point of integration between the CO_2 capture and power plants, disturbances with fast dynamics are imposed on the steam extraction valve during steady state and dynamic operation of a natural gas combined cycle (NGCC) to study the effects of the integration on power generation capacity. The results demonstrate that the integration of liquid-absorbent based post-combustion CO_2 capture has negligible impact on the power generation dynamics of the NGCC.

Does CCS reduce power generation flexibility? A dynamic study of combined cycles with post-combustion CO_2 capture

Jairo Rúa[a], Mai Bui[b,c], Lars O. Nord[a], Niall Mac Dowell[b,c],*

[a] Department of Energy and Process Engineering, Norwegian University of Science and Technology, Trondheim, Norway
[b] Centre for Process Systems Engineering, Imperial College London, London, UK
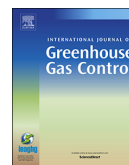[c] Centre for Environmental Policy, Imperial College London, London, UK

ARTICLE INFO

ABSTRACT

To date, the deployment, integration, and utilization of intermittent renewable energy sources, such as wind and solar power, in the global energy system has been the cornerstone of efforts to combat climate change. At the same time, it is recognized that renewable power represents only one element of the portfolio of technologies that will be required to deliver a technically feasible and financially viable energy system. In this context, carbon capture and storage (CCS) is understood to play a uniquely important role, providing significant value through flexible operation. It is therefore of vital importance that CCS technology can operate synergistically with intermittent renewable power sources, and consequently ensuring that CCS does not inhibit the flexible and dispatchable nature of thermal power plants. This work analyses the intrinsic dynamic performance of the power and CO_2 capture plants independently and as an integrated system. Since the power plant represents the fast dynamics of the system and the steam extraction is the main point of integration between the CO_2 capture and power plants, disturbances with fast dynamics are imposed on the steam extraction valve during steady state and dynamic operation of a natural gas combined cycle (NGCC) to study the effects of the integration on power generation capacity. The results demonstrate that the integration of liquid-absorbent based post-combustion CO_2 capture has negligible impact on the power generation dynamics of the NGCC.

1. Introduction

Climate change mitigation is one of the greatest challenges in the 21st century. Anthropogenic greenhouse gas emissions since the industrial revolution have resulted in increasing temperatures and changes in natural and human ecosystems (IPCC, 2014). Thus, a deep decarbonization of all sectors is necessary to meet the target of not exceeding the 1.5 °C temperature increase respect to pre-industrial levels (IPCC, 2018).

Among the different possibilities available to reduce the greenhouse gas emissions, carbon capture and storage (CCS) is a uniquely important technology for mitigating the CO_2 emissions associated with the energy sector and industry (IPCC, 2005, 2014). These two sectors account for more than 50% of the total global greenhouse gas emissions (IPCC, 2014; IEA, 2018a).

Renewable energy sources will also contribute significantly to reducing CO_2 emissions (IEA, 2018b). Future energy systems are expected to be characterized by a high penetration of intermittent renewable sources. This will result in additional costs associated with load balancing, additional firming capacity, energy storage, and interconnection capacity (Heuberger et al., 2017a,b).

Flexible dispatchable energy generation technologies such as thermal power with CCS offer a cost effective way to balance this intermittency (Heuberger et al., 2016; Kondziella and Bruckner, 2016; Montañés et al., 2016; Mac Dowell and Staffell, 2016). Consequently, thermal power plants will be exposed to cycling operation and more frequent start-ups and shut-downs (Eser et al., 2017; González-Salazar et al., 2017). Thus, to deploy CCS technology in a power market dominated by the high variability of renewable energy, it is necessary to prove its adequacy for flexible operation (Adams and Mac Dowell, 2016).

Post-combustion CO_2 capture is arguably the most mature CCS technology (IPCC, 2005; Bui et al., 2018a). Therefore, deep understanding of the dynamic performance of these capture plants integrated with thermal power plants is essential. Dynamic modelling and simulation remains the primary medium to study the interaction of these systems under transient operation due to the lack of full-scale experience (Bui et al., 2014, 2018a). Developing further detailed insight into

the process dynamics could help improve the accuracy and robustness of dynamic process control and scheduling during flexible operation, plant start-up and shut-down.

The development of dynamic CO_2 capture models was extensively reviewed by Bui et al. (2014, 2018b). Whilst the vast majority of research on flexible operation of CCS focuses on modelling the dynamics of the capture plant, there are relatively few studies that model the integrated system with a thermal power plant (Lawal et al., 2012; Mac Dowell and Shah, 2013, 2015; Wellner et al., 2016; He and Ricardez-Sandoval, 2016; Mechleri et al., 2017a,b; Garðarsdóttir et al., 2017; Montañés et al., 2017b).

Lawal et al. (2012) studied the dynamic interaction between a coal-fired power plant and a post-combustion capture plant with MEA, and showed how tight control (i.e., rapidly responds to minimize deviation between the controlled variable and its set-point) on the capture plant may interfere with the power output of the power plant. For a similar integrated system, Garðarsdóttir et al. (2017) found that power generation settling times are essentially independent of the integration of the capture plant. However, inadequate control strategies may result in unnecessary longer stabilization times. Both studies concluded that the dynamics of the capture plant are significantly slower than the power plant, leading to longer settling times in the absence of adequate control structures, which may affect power plant performance. Retrofitted coal power plants exhibit the same transient behaviour and the integration with the capture plant acts as steam storage that can be rapidly adjusted to meet peak power demands through the manipulation of the extraction valve (Wellner et al., 2016). Mac Dowell and Shah (2013, 2015), and Mechleri et al. (2017a,b) also developed integrated systems of coal-fired power plants with post-combustion capture plants to study the economic performance during flexible operation accounting for variations in the electricity market, although the dynamic interaction was not studied.

Commercial natural gas combined cycles integrated with full-scale post-combustion capture plants show similar transient performance. He and Ricardez-Sandoval (2016) and Montañés et al. (2017b) proved the faster dynamics of the power plant compared to the capture plant, which resulted in slow oscillations in the longer time-scales as a consequence of the interaction between both plants. The analysis of varying inputs in open-loop in the capture plant also showed the benefits that may be obtained from close-loop control and simultaneous scheduling of the power and CO_2 capture plant (He and Ricardez-Sandoval, 2016). Further, evaluation of several control structures in the capture plant showed that different control couplings may lead to distinct long term dynamics in the low-pressure steam turbine. Nevertheless, the short-term transient behaviour of the natural gas combined cycle is not affected as a result of the slow dynamic response of the post-combustion capture plant (Montañés et al., 2017b).

These studies on the full-scale transient performance of integrated systems showed that slow dynamic interactions between the thermal power plant with the post-combustion CO_2 capture plant do not affect notably their power production capacity, albeit the stabilization time is affected by the slow response of the capture plant. However, the dynamics of power generation are determined by the transient behaviour of the steam cycle, that is, by the fast dynamics of the integrated system. The decoupling of power generation capacity from the CCS process has the potential to significantly enhance the economic efficiency and the technical performance. Therefore, rapid dynamic disturbances must be analysed in order to determine whether the CO_2 capture plant limits the electricity production capabilities of the thermal power plant.

The aim of this study is to investigate the extent to which fast disturbances in the steam extraction affect the power generation capability of the integrated system. Building on previous work, a thorough analysis of the dynamics governing the thermal power plant, the post-combustion capture plant and the integrated system is included in Section 2 to understand the physical mechanisms dictating their transient operation. Section 3 describes the modelling of the natural gas

combined cycle integrated with the post-combustion CO_2 capture plant and the special power generation characteristic of this type of power generation systems. Results are presented and discussed in Section 4, and the conclusions are presented in Section 5.

2. Dynamic analysis of thermal power plants integrated with CCS

Thermal power plants and post-combustion capture plants exhibit distinct dynamic behaviour. This section identifies and evaluates the process and dominant dynamics that significantly influence thermal power plants integrated with post-combustion CO_2 capture plants, including passive elements that contribute to the dynamics but are not the main source.

2.1. Thermal power plants

As post-combustion capture plants are a cost effective technology to remove CO_2 from large-emission sources, they are a suitable complement for heavy-duty natural gas combined cycles and coal- and biomass-fired power plants (IPCC, 2005). Natural gas combined cycles rely on gas turbines to control and produce most of the power and a steam cycle that acts as a passive element, which utilizes the energy contained in the exhaust gas to generate extra power. In contrast, power generation from solid fuels, namely coal and biomass, using subcritical and supercritical power plant technology, produce electricity solely via the steam cycle, which is driven by the combustion process in the furnace.

Fig. 1 shows the different operation range of each thermal power plant. The minimum load of modern gas turbine is limited to 40% of its full load owing to the combustion stability of the fuel and the associated emissions (Alobaid et al., 2017; Eser et al., 2017). Therefore, since the gas turbine accounts for a large share of the total power capacity of natural gas combined cycles, this type of power plants cannot reduce its power generation below this limit. Conversely, coal and biomass power plants are not restricted by a gas turbine; and their minimum compliant load is around 25% of their full load (Hentschel et al., 2016). This broader operation range enhances the utilization of coal and biomass power plants as spinning reserves.

A common characteristic of all thermal power plants is the heat transfer in the steam generator between the combustion gases and the working fluid of the Rankine cycle. In this equipment, the combustion gases flow in a counter-current or cross-flow manner through several tube bundles where energy is transferred progressively to produce the superheated steam that drives the steam turbines. Steam generators are bulky equipment whose enormous mass of metal stores large amounts of energy due to its heat capacity. This leads to slow responses in the steam cycle and hence the power generation in the steam turbines. Thus, steam generators are the main limitation during the transient
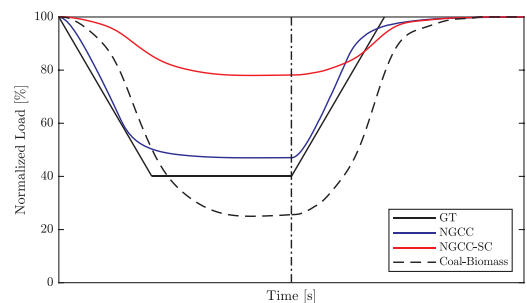

Fig. 1. Generic dynamic behaviour of different thermal power plants of similar size. Maximum and minimum loads and power generation shares depend on the power plant design. The vertical line indicates the increasing load dynamic behaviour. The nomenclature is as follows. GT: gas turbine, NGCC: natural gas combined cycle, SC: steam cycle.

operation of thermal power plants and consequently define their dominant dynamics (Alobaid et al., 2017).

Two different time-scales dictate the dynamic operation of natural gas combined cycles. Modern gas turbines are fast components that can have load ramps up to 15% per minute and whose dominant dynamics are in the order of seconds (Hentschel et al., 2016). Steam cycles are limited by the heat capacitance of the steam generator and thus their dominant dynamics are on the order of minutes. Fig. 1 represents the general dynamic behaviour of a natural gas combined cycle. The gas turbine drives the transient operation of the NGCC by changing its load, whilst the steam cycle determines the time required to reach steady-state (Kehlhofer et al., 2009). Nevertheless, natural gas combined cycles are able to meet the power demand before the steam cycle reaches steady-state by under- or over-shooting the gas turbine (Rúa et al., 2020). This unique ability of the gas turbine compensates for the slow transient performance of the steam cycle, enhancing the adequacy of NGCC for flexible operation.

Coal and biomass power plants do not have a gas turbine to control the power generation, thus governor valves are required at the inlet of the steam turbine to guarantee tight power control during transient operation. Fuel consumption is adjusted according to power demand to regulate the part-load performance, but this strategy cannot be applied in the time-scale of seconds owing to the heat capacitance of the steam generator and the slow response of the steam cycle (see Fig. 1). Consequently, the slow dynamics of the steam cycle dominate the transient operation of coal and biomass power plants, making them slower than modern NGCC and less suitable for flexible operation (Eser et al., 2017; González-Salazar et al., 2017).

2.2. Post-combustion capture plants

Capture plants are passive systems whose operation is determined by the conditions of the gas to be treated and the steam available for the reboiler. From a dynamic operation perspective, the gas is a disturbance to which the capture plant must adapt to, whereas the steam is considered a manipulated variable. The stripper condenser pressure is also a boundary condition of the capture plant, however, this is considered constant as it is rarely modified during dynamic operation.

In a post-combustion capture plant, the fastest units are the rotating machinery (i.e., blowers, compressors and pumps), as they have almost negligible dynamics with time constants in the order of a few seconds. Thus, solvent flow rates stabilize within a few minutes, depending on the size of the plant and the magnitude of the flow change (Flø et al., 2016; Montañés et al., 2018). Heat exchangers and piping lead to transport delays that do not affect the nature of the dynamics. Conversely, large vessels such as absorber and stripper sumps, reboiler hotwells or buffer tanks introduce significant inertia, which buffers and smooths the overall dynamic behaviour of the capture plant (Flø et al., 2016). Liquid hold-up in the absorber and stripper also contributes to this buffering effect, however, the effect on the solvent flow rate dynamics is small relative to that of sumps, storage tanks, etc. Therefore, the dynamics of the post-combustion capture plant are not governed by the mass balance but by the total volume of solvent, the volumetric capacity of the plant, and the solvent circulation time.

Chemical and thermal equilibrium in the absorber and stripper columns also affect the transient behaviour but has a minor influence on the stabilization time of the capture plant (Flø et al., 2016; Tait et al., 2016; Montañés et al., 2017a; Montañés et al., 2018). During open-loop operation, changes in flue gas flow rate primarily impacts the absorption section, affecting the CO_2 capture rate and shifting the temperature profile as a result of the difference in released energy from the exothermic chemical reactions (Kvamsdal and Rochelle, 2008; Bui et al., 2016; Tait et al., 2016; Montañés et al., 2018). Both changes are dominated by the chemical and thermal inertia within the absorber as the stabilization times of the absorber temperature profile and CO_2 capture rate are larger than the rise time of the flue gas flow rate

(Montañés et al., 2018).

For a given solvent flow rate, moderate changes to the exhaust gas flow rate have a minor effect on the rich CO_2 loading of the solvent (Lawal et al., 2010; Flø et al., 2016; Bui et al., 2016, 2018b; Montañés et al., 2017a; Montañés et al., 2018). However, sufficiently large variations in the feed gas CO_2 concentration or mass flow rate may lead to more pronounced effects on rich solvent loading. Changes in flue gas flow rate only affect the absorption section and the solvent loading, but the effect of these changes on the overall stabilization time of the entire capture plant is essentially negligible.

The steam flow rate to the reboiler is an important process parameter. Sufficiently large changes to the steam flow rate will vary the temperature in the reboiler, and consequently the operating conditions of the stripper column. Assuming the other process conditions remain constant or are not adequately adapted, this would result in changes to the lean CO_2 loading exiting the stripper (Lawal et al., 2010; Garðarsdóttir et al., 2015; Flø et al., 2016; Montañés et al., 2017a; Bui et al., 2020). This change in lean loading affects the amount of CO_2 the solvent can absorb, which in turn influences the energy released during the absorption reaction, the absorber column temperature profile and the CO_2 capture rate. These operation changes are expected to result in different rich loadings, which will affect the stripper transient conditions (Lawal et al., 2010; Flø et al., 2016; Bui et al., 2016; Montañés et al., 2017a; Montañés et al., 2018).

Slow and long dynamics can limit the rate of transient behaviour and increase solvent circulation time. There is a combination of factors that contribute to slow dynamics, these include (i) total volume of solvent stored or held-up in the capture plant, (ii) size of the vessels in the system which impacts residence time, and (iii) transport delay introduced by the heat exchangers and piping. There is also an observable inter-column interaction between the stripper and absorber conditions. In a plant with slow dynamics (e.g., owing to larger total liquid hold-up), changes to the solvent flow rate lead to slow variation of the rich and lean solvent loading. Thus, the slow interaction between the absorber and stripper columns due to the large liquid volumes (e.g., long solvent circulation time or slow transient behaviour) is the main bottleneck, slowing the response time during flexible operation of post-combustion capture plants.

2.3. Thermal power plants integrated with post-combustion capture plants

Several process configurations to integrate the power and capture plants have been studied (Botero et al., 2009; Lucquiaud et al., 2009; Jordal et al., 2012; Jonshagen et al., 2012; Mac Dowell and Shah, 2014), with steam extraction from the crossover between the intermediate- and low-pressure (IP-LP) steam turbines being the preferred option (Lawal et al., 2012; Montañés et al., 2017b; Garðarsdóttir et al., 2017). In this integration approach, the steam extracted from the steam turbine may be mixed with low-pressure superheated steam in NGCC, and temperature is controlled by evaporative spray cooling with pressurised water from the intermediate-pressure economizer (Montañés et al., 2017b). In contrast, temperature control in coal or biomass power plants is achieved by using feedwater downstream the condenser (Fernandez et al., 2016; Garðarsdóttir et al., 2017).

Steam availability at the IP-LP crossover does not limit the dynamic operation of integrated system. This is largely due to the steam requirements of the CO_2 capture plant being small compared to the large amount of steam produced in the Rankine cycle of the thermal power plant (Jordal et al., 2012; Rezazadeh et al., 2015). As a result, steam can always be extracted by modifying the opening of the steam extraction valve. This equipment can move from fully open to fully closed in seconds and thus their dynamics are negligible compared to those governing the thermal power plant and post-combustion capture plant.

System integration also includes the cooling and compression of the exhaust gas leaving the heat recovery steam generator. From the perspective of dynamic operability, treatment of this flue gas is not a major
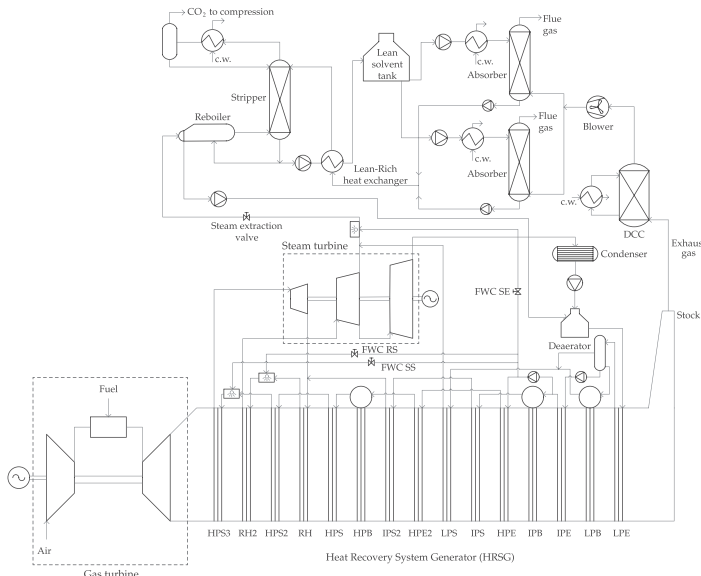
Fig. 2. Process diagram of the natural gas combined cycle integrated with the post-combustion capture plant. The nomenclature is as follows. E: economizer, B: boiler, S: superheater, R: reheater, P: pressure, L: low, I: intermediate, H: high, FWC: feed-water cooling, RS: reheated steam, SS: superheated steam, SE: steam extraction, DCC: direct contact cooler.

concern due to the fast the dynamics of the blowers utilized to overcome the absorber column pressure drop, and hence do not limit the capture plant process dynamics. The direct contact cooler only introduces time delays. Ideally, the equipment integrating the thermal power plant with the post-combustion capture plant should not slow the overall transient operation of the integrated system. However, this coupling may lead to interactions between both plants that can affect their dynamics.

As different time-scales govern the dynamic operation of thermal power plants and post-combustion capture plants, system integration must consider the distinctively different process dynamics. Whilst heat capacitance in the steam generator limits the transient behaviour of thermal power plants to an order of minutes, typically 10–20 min for power plants of several hundred MW, the large solvent volumes and long circulation time in the CO_2 capture plant may lead to stabilization times in the order of hours (Lawal et al., 2012; Montañés et al., 2017b; Garðarsdóttir et al., 2017).

The power demand defines the operation of the power plant and hence the mass flow rate of the exhaust gas. Whereas changes in the flue gas conditions do not affect the performance of the thermal power plant, such changes are a disturbance for the capture plant, which must adapt its operation to meet the CO_2 capture targets. This may lead to different steam extraction rates that also modify the operating conditions in the power plant. If steam extraction variation occurs at a slow dynamics scale, i.e., the time-scale defined by the capture plant, small fluctuations and longer stabilization times are obtained in the power generation of the low-pressure steam turbine (Lawal et al., 2012; Garðarsdóttir et al., 2017; Montañés et al., 2017b). However, this type of interaction between both plants is not critical as the thermal power plants are faster than the slow-dynamic time-scales of the CO_2 capture plant. Furthermore, steam extraction does not significantly influence the load of the power plant. On the contrary, steam extraction in the fast dynamic time-scale occurs simultaneously with the change of power plant load and may lead to dynamic interactions that compromise the power generation capacity of the system. Therefore, it is important to address this possible issue by studying the dynamic interaction between the thermal power plant and the CCS system in the fast dynamics time-scale, which are addressed in Sections 3 and 4.

3. Dynamic modelling

In this study, a physics-based model of a 615 MW NGCC integrated with a 30 wt% MEA-based post-combustion capture process was used to study the dynamic interaction of NGCC integrated with absorption CO_2 capture (Montañés et al., 2017b). Triple pressure steam cycles with reheat are the most efficient and common configuration of modern natural gas combined cycles (Alobaid et al., 2017; Kehlhofer et al., 2009). GT PRO (Thermoflow, 2014) was utilized to design the natural gas combined cycle as it provides detailed information about the geometry of the plant. Full-physics dynamic modelling was carried out in the Modelica-based (Modelica Association, 2019) software Dymola (Dassault Systemes, 2016) using the specialized Thermal Power library (Modelon, 2015).

Full-scale post-combustion capture plants are designed based on the flue gas CO_2 concentration and conditions (i.e., flow rate, temperature, pressure), the required CO_2 capture rate, the maximum pressure drops in the absorber and stripper columns, column flooding limits and a reasonable balance between capital and operational costs (Jordal et al., 2012; Dutta et al., 2017). For the natural gas combined cycle considered in this work, a capture plant with two absorber columns in parallel and one stripper for a nominal 90% CO_2 capture rate was found to meet these requirements (Montañés et al., 2017b). A dual absorber process topology was selected due to the limits in column sizing and construction (Dutta et al., 2017).

Integration of the power and capture plants was achieved by extracting steam from the crossover between the intermediate- and low-pressure steam turbines (see Section 2.3). Thus, the low-pressure section of the steam turbine was designed for nominal conditions where steam is extracted to achieve a 90% capture rate. Fig. 2 represents the layout of the natural gas combined cycle integrated with the post-combustion capture plant. Details on the design data, performance indicators, modelling assumptions and validation results are presented in the work by Montañés et al. (2017b).

The design of the power plant steam cycle includes the extraction of steam for the CO_2 capture plant. Consequently, the power generation distribution between the different turbines in this power plant differs from modern NGCC without a capture plant. Fig. 3 represents the power generation distribution at different gas turbine loads. The gas turbine
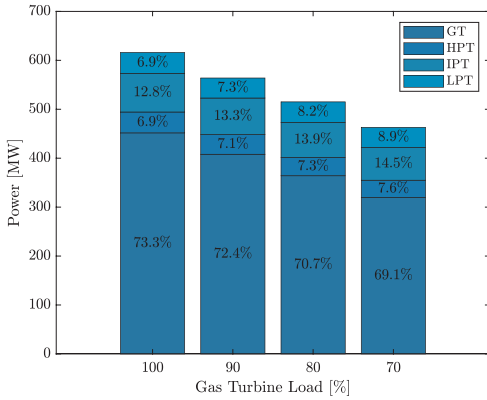
Fig. 3. Power distribution of the natural gas combined cycle with CCS at different gas turbine loads.

produces the majority of the power as in any combined cycle without steam extraction, however, the contribution to the overall power generation of the low-pressure section of the steam turbine is halved due to the steam extraction (Jordal et al., 2012; Rezazadeh et al., 2015). Therefore, the contribution of the low pressure section in electricity production and in the steam cycle diminishes as a result of the integration with the post-combustion capture system. The high- and

intermediate-pressure steam turbines contribute similarly as in NGCCs without steam extraction. This leads to larger power generation from the intermediate-pressure section because of the similar inlet temperature owing to the reheating and its larger pressure ratio.

4. Results and discussion: dynamics of a NGCC with CO_2 capture

The dynamics of the natural gas combined cycle occur in shorter time scales compared to the overall transient operation of the integrated system. Thus, to study whether the steam extraction coupling affects the power generation capacity in different dynamic operation scenarios, the variations in the opening of the extraction valve must be faster than the dominant dynamics of the thermal power plant (see Section 2). A damping sine signal was hence superimposed on the extraction valve opening to ensure fast dynamics in the interface between the NGCC and the capture plant (Ljung, 1987). This signal was characterized by an offset of 0.69 and an amplitude of 0.29, with a natural and damping frequencies of 0.01 and 0.001 Hz, respectively. These values ensure that variations in the steam extraction occur faster than the dominant dynamics of the NGCC. Albeit highly oscillating valve movements do not occur in practice during open loop operation (i.e., no feedback control), these values generate a signal that provides sufficient variation in steam extraction from the IP-LP crossover valve. This will give insight into the transient effects of variations in steam extraction on power generation.

Two different scenarios were considered to analyse the integration effect on the power generation during both steady-state and transient operation of the power plant. In the case where the NGCC is at steady-
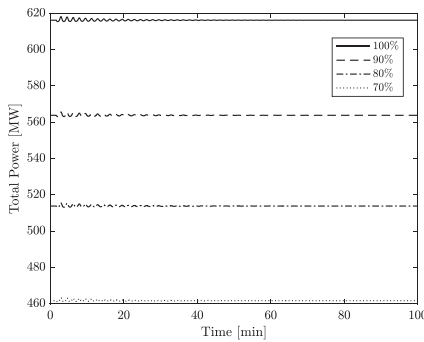
(a) Total power generation of the natural gas combined cycle.
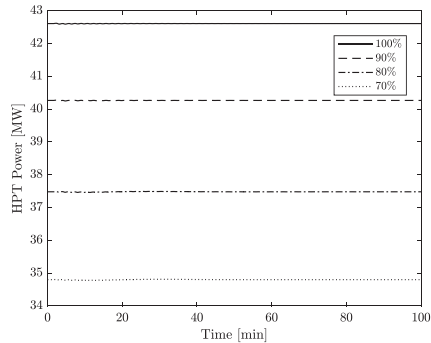
(b) Power generation of the high-pressure steam turbine.
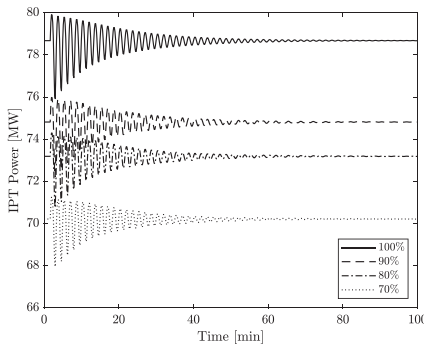
(c) Power generation of the intermediate-pressure steam turbine.
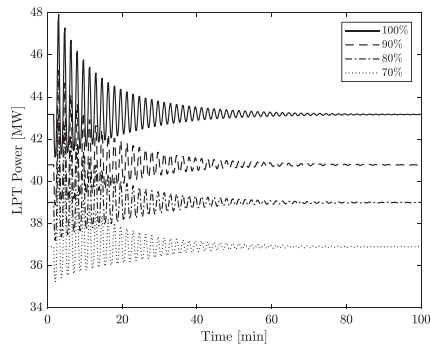
(d) Power generation of the low-pressure steam turbine.

Fig. 4. Variation in power generation in the natural gas combined cycle and the steam turbine sections (HP, IP and LP) due to the fluctuation in the steam extracted from the IP-LP crossover at different gas turbine loads.

state, the damping sine in the valve opening drives the dynamics of the system. In contrast, when there is a load change in the power plant, the dynamics are dictated by simultaneous changes occurring at the gas turbine and the steam extraction. Varying gas turbine loads directly affect power production. Secondly, steam cycle performance is influenced by change in exhaust gas conditions (e.g., temperature and mass flow rate), and variations in steam extraction.

As optimal operation of the integrated system is not the main objective of this work, the NGCC only had a regulatory control layer, which regulates the steam temperature at the steam turbine inlet, levels in drums and condenser, and the pressures in the deaerator and the low-pressure drum. In the post-combustion capture plant, the levels in the large vessels were exclusively controlled, fixing the solvent flow rate to nominal conditions. Details of the implementation of this control structure are included in the work by Montañés et al. (2017b).

4.1. Effect of steam extraction during steady state operation of the NGCC

In this study, a sinusoidal signal was imposed in the steam extraction valve during steady state operation of the NGCC to observe the effect of disturbances in the interface of the integrated system. The power generation distribution was analysed in the NGCC, whilst key performance indicators of the capture plant such the carbon capture ratio and the reboiler temperature were investigated.

4.1.1. Power generation performance

Several part-loads during steady state operation are considered in order to cover a wide operational range of the NGCC integrated with post-combustion CO_2 capture. Fig. 4 represents the variation in mechanical power production in the NGCC and the different steam turbine sections due to variation in steam extraction from the IP-LP crossover. The opening of the steam extraction valve defines the mass flow rate of working fluid available for expansion, which appears to have the greatest impact on the low pressure section in Fig. 4d. The valve opening also alters the intermediate and low pressure sections of the steam cycle, leading to deviations in power generation by the intermediate-pressure section of the steam turbine, albeit to a lesser extent compared to the low-pressure counterpart.

The variation in power generation by the intermediate- and low-pressure steam turbines has a negligible impact on the total power produced by the NGCC. The reasons for this effect is the gas turbine generates most of the total power and the average contribution from the IP and LP steam turbine sections is 20% (see Fig. 3). Therefore, the variations induced by the steam extraction valve in the NGCC power generation during steady-state operation are negligible and can be easily compensated by the power controllers included in the gas turbine. Fig. 4a demonstrates how the variation in steam extraction only creates a small disturbances in the total power generation.

4.1.2. CO_2 capture performance

Steam extraction dictates the steam flow rate to the reboiler of the post-combustion capture plant, thereby influencing the CO_2 capture performance. Fig. 5 illustrates the effect of steam flow rate on reboiler temperature, lean loading and CO_2 capture rate. The steam flow rate has an insignificant effect on the transient behaviour of the reboiler temperature, where variation is less than 0.2 °C (shown in Fig. 5d). Therefore, the operating conditions within the stripper column are relatively unaffected and the solvent lean loading (Fig. 5b) only deviates slightly from its steady-state value. This results in almost constant CO_2 capture ratios, defined as the ratio of CO_2 product over CO_2 in the feed flue gas (see Fig. 5a).

Fig. 5 shows how the effect of large fluctuations in steam mass flow rate (Fig. 5c) is dampened in the CO_2 capture system (described in Section 2.2). The dampening effect observed in these results are in line with previous dynamic operation studies discussed in Section 2.2. As steam flow rate fluctuates, the transfer of heat is limited by the heat

capacitance of the equipment and fluid. Consequently, the change in reboiler temperature is dampened (Fig. 5d), that is, very little fluctuation is observed. Hence, there is minor variation in the degree of solvent regeneration, which leads to limited change in lean loading (Fig. 5b). This contributes to the "smoothing" of the CO_2 capture ratio trend (Fig. 5a). Similarly, the volume of solvent hold-up in the plant (buffer/storage tanks, column sumps) also has a role in buffering variations in the system. Therefore, having large liquid vessels that limit the transient behaviour during slow disturbances are advantageous during fast disturbances as they buffer the dynamics and prevent departure from steady state set-points of the CO_2 capture process. However, this only occurs if the initial and final state of the disturbed variable are similar, otherwise the time required to reach a new steady-state is dictated by the large liquid hold-ups and the transport delays in the capture plant.

4.2. Effect of steam extraction during dynamic operation of the NGCC

In this case, the disturbance in the steam extraction valve was imposed simultaneously with a change of load in the gas turbine. The same parameters, i.e., power generation distribution and key performance indicators, were analysed in the NGCC and CO_2 capture plant, respectively.

4.2.1. Power generation performance

The damping sine signal in the steam extraction valve was implemented during a gas turbine load change from 100% to 70%. This demonstrates the effect of fast variations in the steam extraction during transient operation of the NGCC. Fig. 6 represents the power generation profile of the overall power plant and of each section of the steam turbine. Fig. 7 shows key process variables of the CO_2 capture plant during the transient operation of the power plant with varying steam extraction. Figs. 6 and 7 show performance with fast dynamic fluctuations in the steam extraction valve (black line), and without fluctuations (red line).

During transient operation, the change in gas turbine load dictates power generation (Fig. 6a). This is because the oscillations generated by the steam extraction valve have a negligible effect on power generation in NGCC plants. This occurs regardless of the fluctuations in the IP and LP steam turbines, represented in Fig. 6c and d respectively, due to the low contribution of these units to the total power production (see Fig. 3). As steam extraction does not have a notable effect on the total power generation, the NGCC power plant may operate independently of the capture plant without any penalty on its dynamic performance.

4.2.2. CO_2 capture performance

The transient behaviour of the CO_2 capture process is governed by the variation in flue gas conditions due to changes in gas turbine load and the steam flow rate fed to the reboiler, which depends on the steam availability in the power plant and the opening of the steam extraction valve. The gas turbine load determines steam availability for extraction at the IP-LP crossover valve, and hence dictates the dynamic performance of the reboiler and stripper. The scenario without fast dynamic fluctuations in steam extraction is represented by the red line in Fig. 7, whereas the behaviour with fast valve fluctuations is shown by the black line.

For a given steam extraction valve opening, the decrease in steam availability that arises from the change in gas turbine load results in less steam extraction (Fig. 7c), which leads to more pronounced variations in the reboiler temperature and lean loading. Unlike the fast disturbances of imposed fluctuations in the opening of the steam extraction valve, the gas turbine load change disturbance is slower. There is sufficient time for heat transfer from the steam to the reboiler fluid, thus reboiler temperature follows the same trajectory as the steam flow rate. Similarly, as the reboiler temperature dictates the degree of solvent regeneration, lean loading has the same trend. The variation in reboiler temperature and lean loading have an apparent effect on the
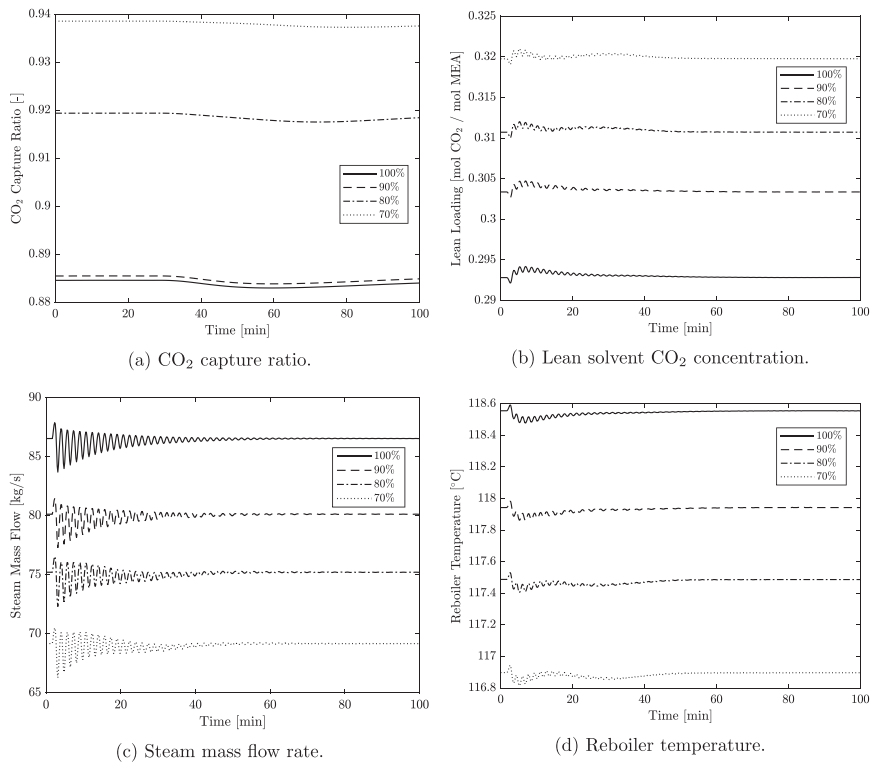
(a) CO$_2$ capture ratio.

(b) Lean solvent CO$_2$ concentration.

(c) Steam mass flow rate.

(d) Reboiler temperature.

Fig. 5. Dynamic behaviour of key process variables in the post-combustion capture plant during steady-state operation of the natural gas combined cycle. Transient operation is driven by opening variations of the steam extraction valve.

CO$_2$ capture ratio.

In contrast, fast dynamic fluctuations in the steam extraction do not disrupt the transient behaviour of the plant as the main process variables follow the same trajectory as in the scenario without fluctuations (red and black lines in Fig. 7). Thus, steam availability in the steam cycle has a more pronounced effect on the dynamic response of the CO$_2$ capture plant than the opening of the steam extraction valve.

Similar to the steady-state operation results, a smoothing effect of the fast fluctuations in steam extraction was observed during dynamic operation. Due to the fluctuations in the steam valve being so rapid, which subsequently results in equally rapid steam flow rate fluctuations, there is insufficient time for heat to transfer from the steam to the reboiler fluid. Thus, the reboiler temperature, lean loading and CO$_2$ capture rate are practically the same with and without steam valve fluctuations.

5. Conclusions

There are essentially two ways to integrate post-combustion CO$_2$ capture with thermal power plants. The first simply connects the exhaust gas with the capture process, and the energy required for solvent regeneration is supplied externally. Whilst this does present the challenge of mitigating any emissions associated with providing that energy, it does entirely avoid imposing constraints on the operability of the power plant – this form of CCS is an entirely "end of pipe" solution. The second, more commonly discussed, option involves the extraction of steam from between the intermediate and low pressure steam turbines. This avoids the challenge of having to mitigate additional emissions, but has led to concerns as to the effect this strategy might have on the operability of the power plant, since these two plants

operate in two different transient time-scales. This work seeks to address this challenge by analysing the effect of disturbances on power generation capacity, specifically disturbances with faster dynamics than the dominant dynamics of the power plant.

Transient power generation was assessed during steady-state and dynamic operation of the power plant by modifying the valve opening for steam extraction in the short time-scales defined by the power plant. Since the gas turbine generates most of the total power, fluctuations in the steam extraction valve have no impact on the power generation capacity. In steady-state power plant operation, the total power generation remains unaltered with small fluctuations around the steady-state value that are easily compensated for with small adjustments in the gas turbine. During transient operation of the power plant, the change of load in the gas turbine drives the dynamic behaviour of the NGCC. Hence, disturbances in steam extraction can be regarded as noise around the transient value dictated by the gas turbine load.

Different behaviour may be expected from power plants where the steam cycle generates most of the power, e.g., coal-fired power plants. Valve opening fluctuations in this type of power plants might lead to larger variations in the total power generation since larger steam mass flow rates are required in the steam turbine. Therefore, steam extraction from power plants dominated by the steam cycle performance has greater influence on power generation, and may add value to the flexible performance of NGCCs. However, this behaviour is yet to be demonstrated by dynamic studies.

The transient behaviour of the capture plant was similar to the power plant since its dynamics is dominated by the operating conditions in the gas turbine and steam cycle. A change in gas turbine load results in different flue gas flow rate and steam availability, thereby influencing the performance of the capture plant. The varying steam
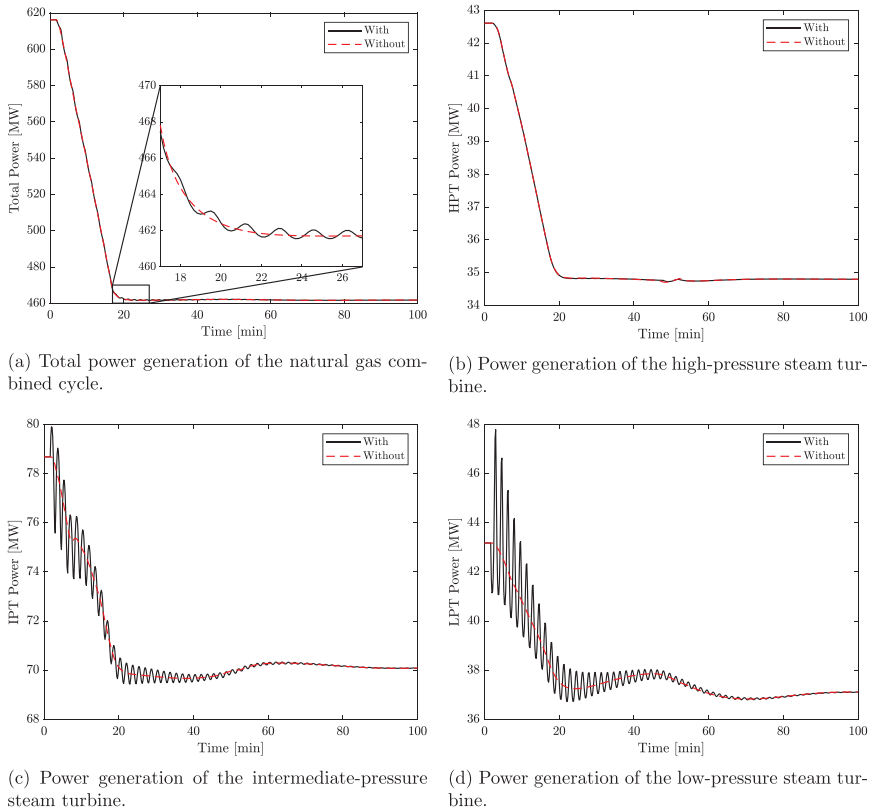
(a) Total power generation of the natural gas combined cycle.

(b) Power generation of the high-pressure steam turbine.

(c) Power generation of the intermediate-pressure steam turbine.

(d) Power generation of the low-pressure steam turbine.

Fig. 6. Power generation dynamic behaviour during a gas turbine load change from 100% to 70% with and without fast dynamic fluctuations in the steam extraction valve.

extraction only leads to small fluctuations, with the trends following the same trajectory as the profile of the scenario without valve opening variations. These small fluctuations disturb the process and are smoothed along the capture plant. This effect is demonstrated by the disturbance starting as significant fluctuations in steam flow rate, which dampen to become smaller fluctuations in reboiler temperature and lean loading, then finally resulting in a smooth CO_2 capture ratio profile. The dampening effect is attributed to the heat capacitance of the system and the buffering of the disturbance in the large liquid hold-ups. Thus, the large vessels of the capture plant are advantageous for small, fast variations as they buffer disturbances, avoiding departure from steady-state conditions. This phenomena occurs at both steady and dynamic operation of the NGCC.

These results highlight the benefits and disadvantages of having large liquid hold-ups in the capture plant. Large storage vessels allow the buffering of the fast variations in the process variables. However, these vessels also lead to slow transients, increasing the time to reach a new steady state to several hours, which will potentially limit the flexibility of the capture plant. This suggests that the post-combustion capture plants can be operated optimally and independently of the power plant. Imposing tight controls on specific variables to minimize the difference between a value and its set-point could limit the flexibility of the integrated system. Instead, the capture plant should aim at finding a new optimal operation point given the boundary conditions imposed by the power plant. This is because any changes in steam extraction to achieve optimal operating conditions would not affect power plant performance, as shown in this work. Therefore, the decarbonization of an NGCC via post-combustion CO_2 capture does not

appear to impose any limitation on the flexibility or operability of the underlying power plant in terms of power generation.

Therefore, one key research challenge is to develop control strategies and operation protocols that enable optimal operation of the capture plant that is essentially independent from the operation of the power plant rather than load following mode with fixed capture ratios (Sahraei and Ricardez-Sandoval, 2014; Bankole et al., 2018; Decardi-Nelson et al., 2018). This may lead to improvements in the financial viability of the CCS project as steam extraction fluctuations have no impact on power generation. The development of process control structures designed for flexible operation and dynamic conditions will be an important area of future research (Åkesson et al., 2012; Hauger et al., 2019). Finally, the development of reliable start-up and shut-down protocols for CCS-equipped power plants so as to avoid increasing the carbon intensity of these assets is a priority.

Authors' contribution

Jairo Rúa: methodology, model development and implementation, investigation, writing – original draft preparation.
Mai Bui: methodology, reviewing, and editing.
Lars Nord: reviewing and editing.
Niall Mac Dowell: conceptualization, methodology, reviewing, and editing.

Conflict of interest

None declared.

(a) CO_2 capture ratio.

(b) Lean solvent CO_2 concentration.

(c) Steam mass flow rate.
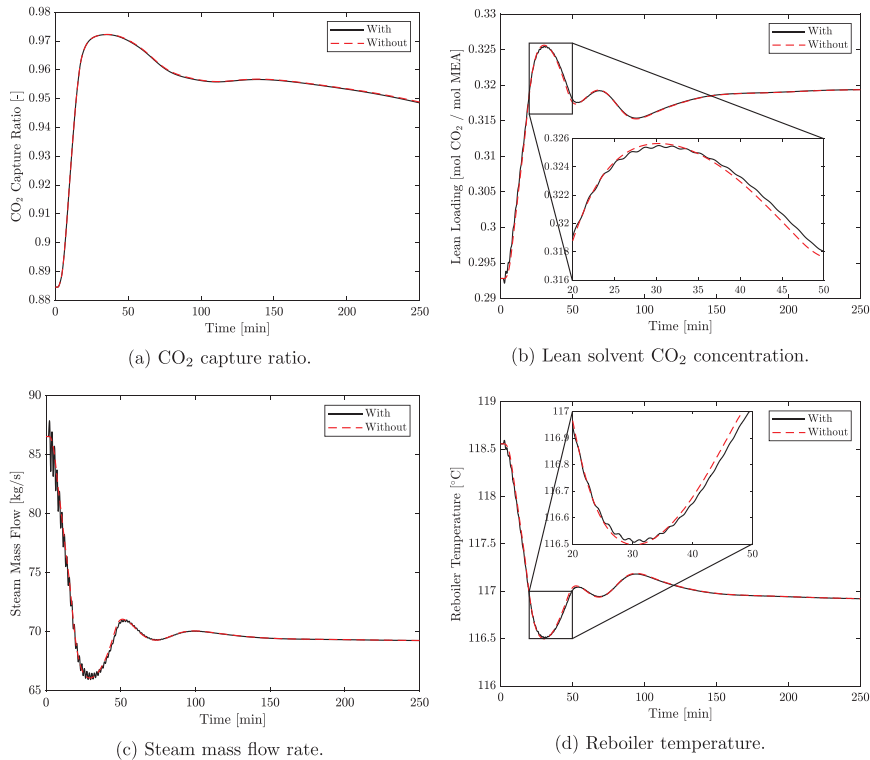
(d) Reboiler temperature.

Fig. 7. Dynamic behaviour of key process variables in the post-combustion capture plant during a gas turbine load change from 100% to 70% with and without fast dynamic fluctuations in the steam extraction valve.

Acknowledgements

References

Adams, T., Mac Dowell, N., 2016. Off-design point modelling of a 420 MW CCGT power plant integrated with an amine-based post-combustion CO_2 capture and compression process. Appl. energy 178, 681–702.

Åkesson, J., Laird, C.D., Lavedan, G., Prölß, K., Tummescheit, H., Velut, S., Zhu, Y., 2012. Nonlinear model predictive control of a CO_2 post-combustion absorption unit. Chem. Eng. Technol. 35 (3), 445–454.

Alobaid, F., Mertens, N., Starkloff, R., Lanz, T., Heinze, C., Epple, B., 2017. Progress in dynamic simulation of thermal power plants. Prog. Energy Combust. Sci. 59, 79–162.

Bankole, T., Jones, D., Bhattacharyya, D., Turton, R., Zitney, S.E., 2018. Optimal scheduling and its Lyapunov stability for advanced load-following energy plants with CO_2 capture. Comput. Chem. Eng. 109, 30–47.

Botero, C., Finkenrath, M., Bartlett, M., Chu, R., Choi, G., Chinn, D., 2009. Redesign, optimization, and economic evaluation of a natural gas combined cycle with the best integrated technology CO_2 capture. Energy Proc. 1 (1), 3835–3842.

Bui, M., Adjiman, C.S., Bardow, A., Anthony, E.J., Boston, A., Brown, S., Fennell, P.S., Fuss, S., Galindo, A., Hackett, L.A., et al., 2018a. Carbon capture and storage (CCS): the way forward. Energy Environ. Sci. 11 (5), 1062–1176.

Bui, M., Flø, N.E., de Cazenove, T., Mac Dowell, N., 2020. Demonstrating flexible operation of the Technology Centre Mongstad (TCM) CO_2 capture plant. Int. J. Greenhouse Gas Control 93, 102879.

Bui, M., Gunawan, I., Verheyen, V., Feron, P., Meuleman, E., 2016. Flexible operation of CSIRO's post-combustion CO_2 capture pilot plant at the AGL Loy Yang power station.

Int. J. Greenhouse Gas Control 48, 188–203.

Bui, M., Gunawan, I., Verheyen, V., Feron, P., Meuleman, E., Adeloju, S., 2014. Dynamic modelling and optimisation of flexible operation in post-combustion CO_2 capture plants – a review. Comput. Chem. Eng. 61, 245–265.

Bui, M., Tait, P., Lucquiaud, M., Mac Dowell, N., 2018b. Dynamic operation and modelling of amine-based CO_2 capture at pilot scale. Int. J. Greenhouse Gas Control 79, 134–153.

Dassault Systemes, 2016. https://www.3ds.com/products-services/catia/products/dymola/.

Decardi-Nelson, B., Liu, S., Liu, J., 2018. Improving flexibility and energy efficiency of post-combustion CO_2 capture plants using economic model predictive control. Processes 6 (9), 135.

Dutta, R., Nord, L.O., Bolland, O., 2017. Selection and design of post-combustion CO_2 capture process for 600 MW natural gas fueled thermal power plant based on operability. Energy 121, 643–656.

Eser, P., Chokani, N., Abhari, R., 2017. Operational and financial performance of fossil fuel power plants within a high renewable energy mix. J. Glob. Power Propul. Soc. 1, 16–27.

Fernandez, E.S., del Rio, M.S., Chalmers, H., Khakharia, P., Goetheer, E.L., Gibbins, J., Lucquiaud, M., 2016. Operational flexibility options in power plants with integrated post-combustion capture. Int. J. Greenhouse Gas Control 48, 275–289.

Flø, N.E., Kvamsdal, H.M., Hillestad, M., Mejdell, T., 2016. Dominating dynamics of the post-combustion CO_2 absorption process. Comput. Chem. Eng. 86, 171–183.

Garðarsdóttir, S.O., Montan e's, R.M., Normann, F., Nord, L.O., Johnsson, F., 2017. Effects of CO_2-absorption control strategies on the dynamic performance of a supercritical pulverized-coal-fired power plant. Ind. Eng. Chem. Res. 56 (15), 4415–4430.

Garðarsdóttir, S.Ó., Normann, F., Andersson, K., Prölß, K., Emilsdóttir, S., Johnsson, F., 2015. Post-combustion CO_2 capture applied to a state-of-the-art coal-fired power plant: the influence of dynamic process conditions. Int. J. Greenhouse Gas Control 33, 51–62.

González-Salazar, M.A., Kirsten, T., Prchlik, L., 2017. Review of the operational flexibility and emissions of gas-and coal-fired power plants in a future with growing renewables. Renew. Sustain. Energy Rev. 82, 1497–1513.

Hauger, S.O., Flø, N.E., Kvamsdal, H., Gjertsen, F., Mejdell, T., Hillestad, M., 2019. Demonstration of non-linear model predictive control of post-combustion CO_2 capture processes. Comput. Chem. Eng. 123, 184–195.

He, Z., Ricardez-Sandoval, L.A., 2016. Dynamic modelling of a commercial-scale CO_2 capture plant integrated with a natural gas combined cycle (NGCC) power plant. Int. J. Greenhouse Gas Control 55, 23–35.

Hentschel, J., Spliethoff, H., et al., 2016. A parametric approach for the valuation of power plant flexibility options. Energy Rep. 2, 40–47.

Heuberger, C.F., Rubin, E.S., Staffell, I., Shah, N., Mac Dowell, N., 2017a. Power capacity expansion planning considering endogenous technology cost learning. Appl. Energy 204, 831–845.

Heuberger, C.F., Staffell, I., Shah, N., Mac Dowell, N., 2016. Quantifying the value of CCS for the future electricity system. Energy Environ. Sci. 9 (8), 2497–2510.

Heuberger, C.F., Staffell, I., Shah, N., Mac Dowell, N., 2017b. A systems approach to quantifying the value of power generation and energy storage technologies in future electricity networks. Comput. Chem. Eng. 107, 247–256.

IEA, 2018a. CO_2 Emissions from Fuel Combustion 2018. https://www.iea.org/statistics/co2emissions/.

IEA, 2018b. World Energy Outlook 2018: Executive Summary. https://webstore.iea.org/download/summary/190?fileName=English-WEO-2018-ES.pdf.

IPCC, 2005. IPCC Special report on carbon dioxide capture and storage. In: Metz, B., Davidson, O., de Coninck, H.C., Loos, M., Meyer, L.A. (Eds.), Prepared by Working Group III of the Intergovernmental Panel on Climate Change. Cambridge University Press, Cambridge, United Kingdom and New York, NY, USA.

IPCC, 2014. Climate change 2014: synthesis report. In: Core Writing Team, Pachauri, R.K., Meyer, L.A. (Eds.), Contribution of Working Groups I, II and III to the Fifth Assessment Report of the Intergovernmental Panel on Climate Change. IPCC, Geneva, Switzerland.

IPCC, 2018. Summary for Policymakers. In: Masson-Delmotte, V., Zhai, P., Pörtner, H.O., Roberts, D., Skea, J., Shukla, P.R., Pirani, A., Moufouma-Okia, W., Péan, C., Pidcock, R., Connors, S., Matthews, J.B.R., Chen, Y., Zhou, X., Gomis, M.I., Lonnoy, E., Maycock, T., Tignor, M., Waterfield, T. (Eds.), Global Warming of 1.5 °C. An IPCC Special Report on the Impacts of Global Warming of 1.5 °C Above Pre-Industrial Levels and Related Global Greenhouse Gas Emission Pathways, in the Context of Strengthening the Global Response to the Threat of Climate Change, Sustainable Development, and Efforts to Eradicate Poverty. World Meteorological Organization, Geneva, Switzerland.

Jonshagen, K., Sammak, M., Genrup, M., 2012. Postcombustion CO_2 capture for combined cycles utilizing hot-water absorbent regeneration. J. Eng. Gas Turb. Power 134 (1), 011702.

Jordal, K., Ystad, P.A.M., Anantharaman, R., Chikukwa, A., Bolland, O., 2012. Design-point and part-load considerations for natural gas combined cycle plants with post combustion capture. Int. J. Greenhouse Gas Control 11, 271–282.

Kehlhofer, R., Hannemann, F., Rukes, B., Stirnimann, F., 2009. Combined-Cycle Gas & Steam Turbine Power Plants. Pennwell Books.

Kondziella, H., Bruckner, T., 2016. Flexibility requirements of renewable energy based electricity systems – a review of research results and methodologies. Renew. Sustain. Energy Rev. 53, 10–22.

Kvamsdal, H.M., Rochelle, G.T., 2008. Effects of the temperature bulge in CO_2 absorption from flue gas by aqueous monoethanolamine. Ind. Eng. Chem. Res. 47 (3), 867–875.

Lawal, A., Wang, M., Stephenson, P., Koumpouras, G., Yeung, H., 2010. Dynamic modelling and analysis of post-combustion CO_2 chemical absorption process for coal-fired power plants. Fuel 89 (10), 2791–2801.

Lawal, A., Wang, M., Stephenson, P., Obi, O., 2012. Demonstrating full-scale post-combustion CO_2 capture for coal-fired power plants through dynamic modelling and simulation. Fuel 101, 115–128.

Ljung, L., 1987. System Identification: Theory for the User. Prentice-hall.

Lucquiaud, M., Chalmers, H., Gibbins, J., 2009. Capture-ready supercritical coal-fired power plants and flexible post-combustion CO_2 capture. Energy Proc. 1 (1), 1411–1418.

Mac Dowell, N., Shah, N., 2013. Identification of the cost-optimal degree of CO_2 capture: an optimisation study using dynamic process models. Int. J. Greenhouse Gas Control 13, 44–58.

Mac Dowell, N., Shah, N., 2014. Dynamic modelling and analysis of a coal-fired power plant integrated with a novel split-flow configuration post-combustion CO_2 capture process. Int. J. Greenhouse Gas Control 27, 103–119.

Mac Dowell, N., Shah, N., 2015. The multi-period optimisation of an amine-based CO_2 capture process integrated with a super-critical coal-fired power station for flexible operation. Comput. Chem. Eng. 74, 169–183.

Mac Dowell, N., Staffell, I., 2016. The role of flexible CCS in the UK's future energy system. Int. J. Greenhouse Gas Control 48, 327–344.

Mechleri, E., Fennell, P.S., Mac Dowell, N., 2017a. Optimisation and evaluation of flexible operation strategies for coal-and gas-ccs power stations with a multi-period design approach. Int. J. Greenhouse Gas Control 59, 24–39.

Mechleri, E., Lawal, A., Ramos, A., Davison, J., Mac Dowell, N., 2017b. Process control strategies for flexible operation of post-combustion CO_2 capture plants. Int. J. Greenhouse Gas Control 57, 14–25.

Modelica Association, 2019. https://www.modelica.org/.

Modelon, 2015. Thermal Power Library. https://www.modelon.com/library/thermal-power-library/.

Montañés, R., Flø, N., Nord, L., 2017a. Dynamic process model validation and control of the amine plant at CO_2 Technology Centre Mongstad. Energies 10 (10), 1527.

Montañés, R.M., Flø, N.E., Nord, L.O., 2018. Experimental results of transient testing at the amine plant at Technology Centre Mongstad: Open-loop responses and performance of decentralized control structures for load changes. Int. J. Greenhouse Gas Control 73, 42–59.

Montañés, R.M., Garðarsdóttir, S.Ó., Normann, F., Johnsson, F., Nord, L.O., 2017b. Demonstrating load-change transient performance of a commercial-scale natural gas combined cycle power plant with post-combustion CO_2 capture. Int. J. Greenhouse Gas Control 63, 158–174.

Montañés, R.M., Korpås, M., Nord, L.O., Jaehnert, S., 2016. Identifying operational requirements for flexible CCS power plant in future energy systems. Energy Proc. 86, 22–31.

Rezazadeh, F., Gale, W.F., Hughes, K.J., Pourkashanian, M., 2015. Performance viability of a natural gas fired combined cycle power plant integrated with post-combustion CO_2 capture at part-load and temporary non-capture operations. Int. J. Greenhouse Gas Control 39, 397–406.

Rúa, J., Agromayor, R., Hillestad, M., Nord, L.O., 2020. Optimal dynamic operation of natural gas combined cycles accounting for stresses in thick-walled components. Appl. Therm. Eng. 114858 Elsevier.

Sahraei, M.H., Ricardez-Sandoval, L.A., 2014. Controllability and optimal scheduling of a CO_2 capture plant using model predictive control. Int. J. Greenhouse Gas Control 30, 58–71.

Tait, P., Buschle, B., Ausner, I., Valluri, P., Wehrli, M., Lucquiaud, M., 2016. A pilot-scale study of dynamic response scenarios for the flexible operation of post-combustion CO_2 capture. Int. J. Greenhouse Gas Control 48, 216–233.

Thermoflow, 2014. GT Pro 24.0. Thermoflow Inc.

Wellner, K., Marx-Schubach, T., Schmitz, G., 2016. Dynamic behavior of coal-fired power plants with postcombustion CO_2 capture. Ind. Eng. Chem. Res. 55 (46), 12038–12045.

Publication II

Flexible natural gas combined cycles will play a fundamental role in future electric markets. Stresses in thick-walled components and gas turbine load ramps are arguably the main limiting factors during transient operation. Classical control strategies as PID are not suitable to incorporate technical constraints such as stress limits. This work presents a control methodology based on model predictive control where the stress in the walls of the high pressure drum and the first high pressure steam turbine rotor are computed simultaneously with the optimal control sequence. Thus, the maximum allowable stress in this equipment can be set as a constraint and the control actions imposed in the power plant ensure that these limits are not exceeded. Two cases simulating flexible operation under realistic conditions and tight constraints on the stress limits are included. Results show that with the proposed control methodology the natural gas combined cycle can respond to load step changes of 165 MW in 300 seconds, and can operate close to the material's maximum stress limit without exceeding it. The robustness and flexibility of this methodology allows its application to different operation conditions such as start-ups and shut-downs.

Optimal dynamic operation of natural gas combined cycles accounting for stresses in thick-walled components

Jairo Rúa[a,*], Roberto Agromayor[a], Magne Hillestad[b], Lars O. Nord[a]

[a] Department of Energy and Process Engineering, Norwegian University of Science and Technology, Trondheim, Norway
[b] Department of Chemical Engineering, Norwegian University of Science and Technology, Trondheim, Norway

HIGHLIGHTS

- Maximum gas turbine's load gradient is the main limitation during load changes.
- Gas turbine under-shooting compensates the steam cycle's slow transient.
- Proposed control methodology is able to predict stresses in thick-walled components.
- Stress monitoring allows optimal and safe control sequences under tight constraints.
- Suitability of the proposed methodology for start-up and shut-down applications.

ARTICLE INFO

ABSTRACT

Flexible natural gas combined cycles will play a fundamental role in future electric markets. Stresses in thick-walled components and gas turbine load ramps are arguably the main limiting factors during transient operation. Classical control strategies as PID are not suitable to incorporate technical constraints such as stress limits. This work presents a control methodology based on model predictive control where the stress in the walls of the high pressure drum and the first high pressure steam turbine rotor are computed simultaneously with the optimal control sequence. Thus, the maximum allowable stress in this equipment can be set as a constraint and the control actions imposed in the power plant ensure that these limits are not exceeded. Two cases simulating flexible operation under realistic conditions and tight constraints on the stress limits are included. Results show that with the proposed control methodology the natural gas combined cycle can respond to load step changes of 165 MW in 300 s, and can operate close to the material maximum stress limit without exceeding it. The robustness and flexibility of this methodology allows its application to different operation conditions such as start-ups and shut-downs.

1. Introduction

Anthropogenic greenhouse emissions have continuously increased since the industrial revolution. If this tendency is maintained, global warming is expected to reach temperatures of 1.5 °C above pre-industrial levels between 2030 and 2050 [1]. Power generation is the largest source of greenhouse gas emissions, mainly because of its reliance on fossil fuels [2]. Consequently, significant progress towards the Paris Agreement objectives of limiting the temperature increase to 2 °C above pre-industrial levels can be achieved in this sector if adequate measures are taken.

Electricity is progressively gaining relevance in the energy sector. It currently accounts for 20% of the final energy global consumption and

this amount is only expected to increase [3], reaching almost 40% in 2050 [4]. Therefore, the power generation system must undergone severe modifications in order to be able to produce more electricity while reducing its emissions. Renewable energy sources will play a major role in this new energy scenario and will have large shares in the electricity mix, predicted to reach about 40% of the power generation in 2040 [3]. Nevertheless, traditional thermal power plants will remain the largest source of electricity production [3].

In this context of increasing power generation from renewable energy sources, flexibility is and will be the foundation of a reliable and efficient electric system [3–8]. The lack of dispatchability of some renewable energy sources, mainly wind and solar, requires the existence of power generation alternatives that always allow to meet the power

Nomenclature

Latin Symbols

A	System of equations matrix [–]
a	Coefficients of the responses [–]
B	System of equations vector [–]
b	Coefficients of the manipulated variables [–]
C	Specific heat capacity [J/kg K]
c	Validity function centre [–]
d	Optimization weight vector [–]
E	Young's Modulus [MPa]
e	Stochastic error [–]
h	Convection coefficient [W/m^{2}K]
k	Heat conduction coefficient [W/mK]
M	Number of local models [–]
N	Time horizon [–]
n	Number of discretizations or variables [–]
p	Pressure [bar]
Q	Optimization weight matrix [–]
r	Radius [m]
T	Temperature deviation from design [K]
t	Time [s]
U	Manipulated variable [–]
u	Displacement [m]
w	Validity function width [–]
X	System of equations solution vector [–]
$\hat{y}$	Response [–]
z	Vector of optimization variables [–]

Greek Symbols

α	Thermal diffusivity [m^2/s]
α^*	Thermal expansion coefficient [1/K]

Δx	Space discretization size [m]
γ	Current operation point [–]
κ	Current measurement vector [–]
λ	Objective function weights [–]
ω	Rotational speed [rad/s]
ρ	Density [kg/m^3]
σ	Stress [MPa]
θ	Vector of coefficients [–]
υ	Poisson's ratio [–]
ξ	Validity function [–]

Subscripts

θ	Tangential direction
0	Initial conditions
drum	High-pressure drum
eq	Equality
eql	Linearised equivalent stress
i	Inner radius
ineq	Inequality
LMN	Local model network
m	Metal
o	Outer radius
r	Radial direction
rotor	First-stage steam turbine rotor
U	Past manipulated variables
y	Past responses
z	Longitudinal direction

Superscripts

high	Higher bound
low	Lower bound

demand [9]. Energy storage is considered as a promising technology supporting decarbonisation [10], but its application in a growing electricity market in the short- and mid-term is highly limited by its cost-effectiveness, technology maturity and commercial availability at large scale. Therefore, flexible operation of thermal power plants may be arguably considered as the main complement for renewable electricity production.

In the future European energy market, high renewable penetration will significantly increase the cycling operation of thermal power plants [11]. Modern gas-fired power plants are faster, less polluting and more efficient than coal-fired units at both full and minimum complaint load [12]. Thus, and despite of their utilization as based-load units, coal power plants will be less competitive because of the increase in both coal prices and CO$_2$ taxes, and due to their lack of flexibility and low part-load efficiency. On the contrary, the high efficiency of natural gas combined cycles at part-loads and their capability to face the fast cycling of renewables will lead to an increase of their share in the future European electricity market [11].

Operational flexibility in thermal power plants is normally assessed by three criteria: mimimun complaint load, start-up time and maximum load gradient [13]. The minimum complaint load of a natural gas combined cycle depends mainly on the gas turbine, as stable combustion and acceptable emissions limits must be guaranteed. Modern heavy duty gas turbines may offer a minimum load of 40–50% of the full load, but this level is expected to decrease to 30% [12,13]. In addition, if the power plant is expected to operate for long periods at low loads, the steam cycle design may be adapted to these conditions in order to increase the overall efficiency at part-load [14]. Start-up time and load gradients are influenced by the size of the equipment and the control

strategy imposed on the system. Bulk components with high heat capacity store large amounts of energy for long periods of time and hence prolong the transient of thermal power plants, leading to slow start ups and low ramp rates. Optimal design of flexible natural gas combined cycles must address this limitation, leading to power cycles where both high efficiency and fast response are achieved. Once the power plant is designed, the implemented control determines its adequate dynamic operation aiming at reducing the transient while ensuring safe and efficient operation.

Thermal stresses in thick-walled components are the primary limiting factor in the combined cycle transient as they may reduce its expected lifetime due to creep and fatigue. Therefore, proper control strategies may reduce the start-up time and increase the load gradient without exceeding the safety limit of the materials. Traditional control strategies in thermal power plants rely on PID controllers whose objective is fast system stabilization. Alobaid et al. [15] showed that start-up times can be halved without lost of stability if the gas turbine load gradient is increased and proper control of temperatures, pressures and levels is imposed on the power plant. However, material stresses were not assessed and hence it could not be verified whether this approach can be implemented in a real unit. Kim et al. [16] analysed the thermal stress development in the steam drum of a heat-recovery steam generator under three different start-up strategies. Results showed that the selection of the wrong approach and bad operational control may lead to excessive stresses that deteriorate the equipment. Can Gülen and Kim analyzed the stresses in the rotor and high-pressure drum of a natural gas combined cycle, showing the limitations they impose during the start-up and how appropriate control routines are required to avoid damaging this equipment [17]. Improvements in boiler's start-ups can

also be achieved with suitable temperature and mass flow control [18–20].

Optimization of dynamic operation can further improve the transient performance of thermal power plants. In this approach, both start-up and load gradient are treated as dynamic optimization problems [21]. Heuristic rules may be included in this type of control strategies to reduce the computational power required [22,23], but the strength of numerical optimization is partially lost by introducing experience-based constraints. Optimal start-up sequences that do not exceed the stress limits of critical components can be computed with this approach [24,25]. Casella and Petrolani [26] proposed two strategies to reduce the start-up time or the maximum peak stress of a three-pressure combined cycle with reheat. However, these strategies cannot be considered as optimal since no dynamic optimization was utilized. Optimal load gradient profiles can also be computed, ensuring that power is varied as fast as possible without violating the imposed constraints [27].

Model predictive control (MPC) enhances the strong capabilities of dynamic optimization. In this control methodology, a dynamic optimization problem that computes the optimal control sequence over a time horizon is solved at each control step. The first control action is subsequently implemented in the power plant. Thus, optimal control actions ensuring that the operational limits are not exceeded are always imposed. Prasad et al. [28,29] and Peng et al. [30,31] implemented an MPC algorithm to limit and control the superheated and reheated steam temperatures and the steam pressure in thermal power plants, obtaining faster behaviour of the system than with traditional PID controllers. A similar approach was followed by Lu and Hogg [32], who utilized an MPC to control the drum level, the steam pressure and the power generated by a thermal power plant. Model predictive control was also tested in industrial applications, leading to improvements over traditional approaches without exceeding the maximum allowable stresses in critical components [33]. Sindareh-Esfahani et al. [34] utilized model predictive control to improve the start-up of a power plant and impose constraints that limit the deterioration of the equipment. However, these constraints were imposed on the temperature gradients in critical components and not on the stress in their walls, which is the variable related to material deterioration and the actual limiting factor. Therefore, sub-optimal load ramps may be expected from this methodology.

As thermal and mechanical stresses in thick-walled equipment of thermal power plants are the main responsible of creep and fatigue [17,35–38], conservative control strategies are traditionally implemented in these power plants. To overcome this limitation, the stresses arising in sensitive components must be considered by the control strategy. Traditional approaches such as PID controllers do not allow to incorporate stress estimation and hence optimization-based strategies are required to impose constraints on these variables. This work proposes the first control methodology, based on MPC, that determines the optimal load ramp rates in the gas turbine whilst computes both mechanical and thermal stresses in critical components and imposes constraints on them at every control step. This control methodology ensures that the fastest load changes are achieved without exceeding the maximum allowable stress in the material of the equipment and the maximum load gradient in the gas turbine.

The different models used to develop the proposed control methodology and to test its application in a thermal power plant are described in Section 2. This includes the high-fidelity dynamic model of the NGCC that replicates the operation of a real power plant, and the stress and simplified models embedded in the optimization problem of the MPC that predict, respectively, the stresses in critical equipment, and power generation, temperatures and pressures in the power plant. Section 3 discusses the control problem in modern NGCCs, the proposed control methodology that accounts for the stresses in thick-walled components, and its mathematical formulation in the form of a quadratic programming problem embedded in an MPC. The results of the tests carried out

using the proposed control methodology are presented in Section 4. Conclusions are summarized in Section 5. Supplementary Material (SM) with a thorough development of the stress and simplified models, and their integration in the optimization problem in the MPC control strategy is provided with this work for the sake of completeness and reproducibility.

2. Power plant description and stress modelling

Several models of different complexity are utilized in this study. A physics-based dynamic model of a NGCC was used to replicate the operation of a modern thermal power plant. As this type of models cannot be implemented in optimization problems due to their complexity and long computational time, simplified models that predict the future state of relevant thermodynamic variables in the NGCC were developed to be included in the optimization problem of the MPC strategy. To predict the thermal and mechanical stresses arising in the high pressure steam drum and in the rotor disk in the first stage of the high pressure steam turbine, physics-based models of these stresses were also developed and included in the optimization problem of the MPC strategy. This section describes these models and provides details about the assumptions considered during their development.

2.1. Natural gas combined cycle dynamic model

Modern natural gas combined cycles are composed of a heavy-duty gas turbine and a triple pressure steam cycle with reheating. In this work, the model also includes steam extraction from the steam turbine and the heat-recovery steam generator (HRSG). The power plant layout is represented in Fig. 1. GT PRO [39] was used to design the NGCC as it provides detailed information of the geometry of the equipment and the materials needed for the dynamic model.

The dynamic full-physics model of the NGCC was developed with the specialized Thermal Power library [40] in the software Dymola [41], based on the Modelica language [42]. As the transient behaviour of thermal power plants is highly dependent on the size of the equipment, dimensions and geometry of the components designed in GT PRO were imported to the dynamic model. Software to software validation at both full and part-load between the Thermoflow and Dymola models was performed. Results were in good agreement. Detailed description of the design, dynamic modelling, and validation of the NGCC dynamic model can be found in the work carried out by Montañés et al. [43].

2.2. Simplified models of the natural gas combined cycle

Model predictive control strategies require the periodic solution of a dynamic optimization problem. The period of time between optimizations, i.e. the sampling time of the MPC, is determined by the dominant dynamics of the system as they indicate when the majority of the transient has occurred. Good control strategies should anticipate the dominant dynamics and act frequently during this period of time. Step responses in the manipulated variables of the MPC with only the drum level controllers switched on showed that the dominant dynamics of the system occur in 250–300 s. Therefore, in order to meet the dynamics of the power plant and have enough time to carry out the dynamic optimization, a sampling time of 30 s was selected. This sampling time prevents the utilization of the dynamic full-physics model in the optimization algorithm and thus simplified models were used instead. System identification [44] was employed to develop a local network of linear ARX models that encompasses the entire power plant operation range [28,45].

System identification refers to the process of constructing dynamic data-based models [44]. Data was obtained from simulations performed in the full-physics dynamic model in Dymola. Closed-loop experiments were carried out because of its superior effectiveness for several applications, specially for control [46,47]. Among the closed-loop
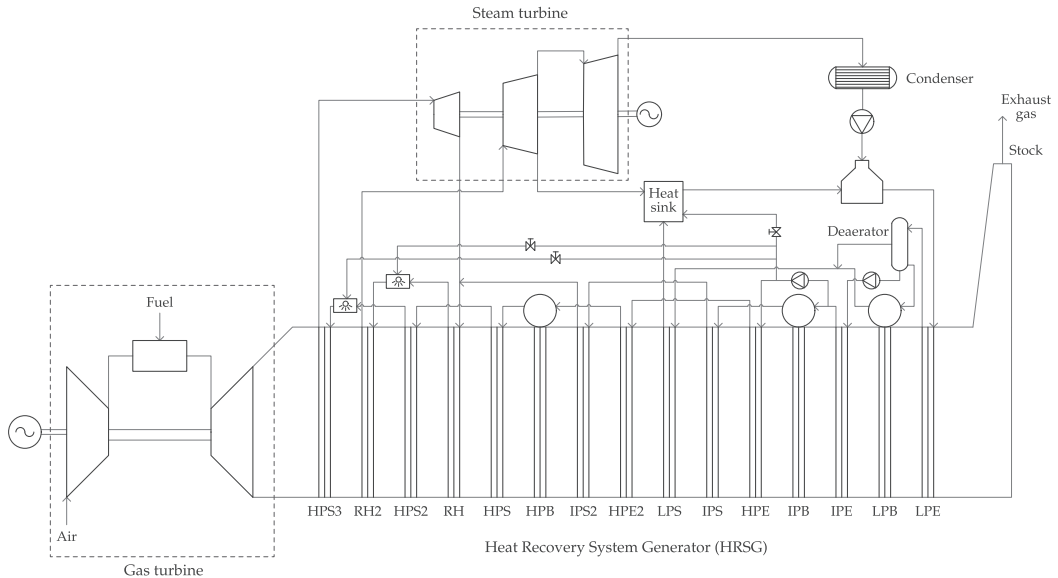
Fig. 1. Process model of the natural gas combined cycle.The nomenclature in the HRSG is as follows. E: Economizer, B: Boiler, S: Superheater, R: Reheater P: Presure, L: Low, I: Intermediate, H: High.

experiment alternatives, a direct approach was followed [44,48]. In this approach, excitation signals are superimposed in the set-points of the controllers of interest, and measurements of the inputs and outputs are collected. All inputs were imposed simultaneously as it leads to better identification of dynamics than doing it individually [49,50]. Pseudo-random binary signals (PRBS) and random Gaussian signals (RGS) were tested as they are persistently exciting and cover properly the input spectrum. Despite that PRBS signals are widely utilized due to their optimum crest factor, RGS proved to lead to better identification.

From this set of data, a model structure was fitted by varying the model parameters. Autoregressive models with exogeneous variable and without noise integration (ARX models) were selected. The general structure of an ARX model is:

$$y(t) + a_1 \, y(t-1) + \cdots + a_{n_y} \, y(t-n_y) =$$
$$b_1 \, U(t-1) + \cdots + b_{n_U} \, U(t-n_U) + e(t) \qquad (1)$$

where n_y and n_U represent the number of past outputs and inputs included in the model, and $e(t)$ is a white-noise term that enters the equation as a direct error in the difference equation. If $e(t)$ is considered as the prediction error, the predictor is given in vector form by:

$$\hat{y}(t) = \theta^{\mathrm{T}} \, \varphi(t) = \varphi(t)^{\mathrm{T}} \, \theta \qquad (2)$$

where

$$\theta = \begin{bmatrix} a_1, & a_2, ..., & a_{n_y}, & b_1, & ..., & b_{n_U} \end{bmatrix}^T$$

$$\varphi(t) = [-\hat{y}(t-1), ..., -\hat{y}(t-n_y), ..., U(t-n_U)]^T$$

ARX models are linear and cannot be used to predict the nonlinear behaviour of NGCCs. Consequently, a local model network (LMN) was used to capture and predict the high nonlinearities of the system. This simplified model relies on the development of several local linear models at different operating regimes and their interpolation according to the operating conditions. Nonlinearities can hence be captured by a set linear models with adequate interpolation. Fig. 2 represents the general structure of a local model network with several local models. This approach was firstly proposed by Johansen and Foss [45], and Prasad et al. [28] proved its efficacy for capturing the nonlinear

dynamics of a thermal power plant.

Local ARX models were developed over the operating region of interest of the NGCC. Defining such local regions is an heuristic procedure. The gas turbine load was chosen as the main criterion. Thus, linear models were utilized to predict the nonlinear behaviour around the 100%, 90%, 80%, 70%, and 60% load of the gas turbine. Since the transition among local regions is a smooth process, the local models need to be interpolated accordingly in order to predict the overall plant performance over its global operating region. Neighbouring local models should contribute more to the solution than local models of regimes far from the operating conditions. This is accomplished by
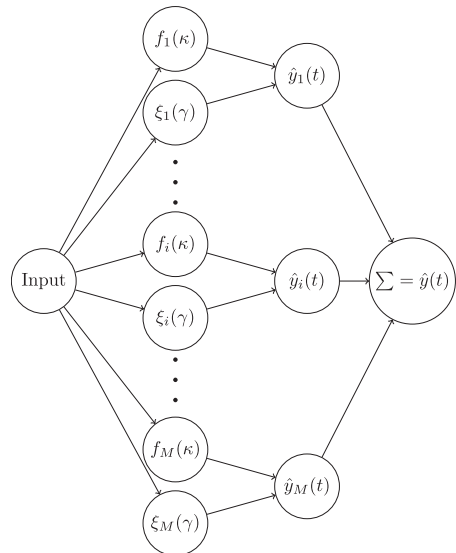

Fig. 2. Structure of a generic local model network.

associating a validity function to each local ARX model and combining all the predicted responses in the final output:

$$\hat{y}(t) = \sum_{k=1}^{M} f_i(\kappa)\,\xi_i(\gamma) \tag{3}$$

where M is the number of local models, $f_i(\kappa)$ is the evaluation of the each ARX model under the conditions defined by κ, ξ is the local validity function associated to each ARX model, and γ is the parameter defining the current operating point, which is the current GT load.

A Gaussian validity function was selected as interpolator of the local models [45]:

$$\xi_i(\gamma) = \frac{exp\left(-\frac{1}{2}\,[(\gamma - c_i)/w_i]^2\right)}{\sum_{k=1}^{M} exp\left(-\frac{1}{2}\,[(\gamma - c_i)/w_i]^2\right)} \tag{4}$$

where c_i and w_i are, respectively, the centres and widths of the local interpolation functions.

As recommended by Johansen and Foss [45] and Prasad et al. [28], the local model and validity function parameters were computed by a nonlinear optimization that aimed at minimizing the global predicting error of the local model network. Local ARX models of second order were considered suitable for predicting the temperature deviation at the outlet of the superheater and reheater. The power plant net power ARX model was selected to be of first order. Linear polynomials were defined to obtain the saturation pressure and temperature in the high pressure drum, and the pressure at the inlet of the steam turbine. Local model and validity function parameters are included in the Supplementary Material (SM).

Validation of the local model network was performed by testing its prediction and interpolation capabilities in the intermediate load ranges, i.e. at 95%, 85%, 75%, and 65% of the GT load. Random Gaussian signals were also utilized to generate the validation data. For the linear polynomials, ramp changes over the NGCC operation range were employed. Table 1 summarizes the validation results based on the R^2 value. Despite the lower values of the model predicting the net power generation of the power plant, the model is capable of predicting the dynamics of the system with high accuracy. These results may be observed in the Supplementary Material (SM) together with all the graphical representation of the validation results.

Because of the linearity of the polynomials and the local models integrating the LMN, this simplified model may be expressed as a linear system of equations. Expanding these simplified models over time, an overall system of equations representing the relation among the responses and manipulated variables in a finite time horizon is achieved. Therefore, this system can be written as:

$$A_{\mathrm{LMN}} X_{\mathrm{LMN}} = b_{\mathrm{LMN}} \tag{5}$$

where X_{LMN} is the vector containing the different predicted responses, y, and manipulated variables, U, in a time horizon. Matrix A_{LMN} and vector b_{LMN} are defined in the Supplementary Material (SM).

2.3. Thermal and mechanical stress modelling

Thick-walled components are the most sensitive equipment in NGCCs as large temperature differences that lead to thermal stresses arise in the wall. In addition, mechanical stresses are present as these components are exposed to the highest pressures of the power plant and may be subjected to rotation. Adequate control of combined cycles must hence ensure the operating conditions do not damage this critical equipment. The high pressure drum and the high pressure steam turbine rotor disk were the components considered in this work. Because of their geometry, plane strain was assumed in the steam drum and plane stress was considered in the rotor.

The temperature profile along the wall is required to compute the thermal stresses. Temperature was assumed to vary in radial direction and thus its distribution is obtained from the one-dimensional heat equation in radial direction:

$$\frac{1}{r}\frac{\partial}{\partial r}\left(r\frac{\partial T}{\partial r}\right) = \frac{1}{\alpha}\frac{\partial T}{\partial t} \tag{6}$$

An implicit Crank-Nicolson discretization scheme was utilized to compute the temperature distribution along the wall. Both drum and rotor encounter different fluids and thermodynamic states in their inner and outer surfaces. The high pressure drum is on contact with saturated water and steam on the inner surface and with air in the outer, whereas the high pressure turbine rotor is in contact with superheated steam on the outer surface and the shaft at an unknown state on the inner wall. Therefore, different boundary conditions must be imposed. The implementation of the different boundary conditions is detailed in the Supplementary Material (SM).

Thermal and mechanical stresses were modelled together following a common approach for both plane stress and plane strain. Given the constitutive equations that relate the stress with the strain and combining them with the strain-displacement relations, the stress in each direction can be expressed in terms of the displacement and the temperature in radial direction [51]. Inserting these equations into the radial equilibrium equation, an ordinary differential equation relating the displacement with the temperature gradient and the centrifugal force due to rotation is obtained [51]. Pressure enters in these equations as boundary conditions in the radial stress equation. The systems of equations for the cases of plane strain and plane stress are defined in Eqs. (2) and (3), respectively.

$$\frac{d^2 u}{dr^2} + \frac{1}{r}\frac{du}{dr} - \frac{u}{r^2} = \frac{(1+v)}{(1-v)}\alpha^*\frac{dT}{dr} - \frac{(1-2v)(1+v)}{(1-v)}\rho\omega^2 r \tag{7a}$$

$$\sigma_r = \frac{Ev}{(1-2v)(1+v)}\left[\frac{1-v}{v}\frac{du}{dr} + \frac{u}{r}\right] - \frac{E\alpha^*}{1-2v}T \tag{7b}$$

$$\sigma_\theta = \frac{Ev}{(1-2v)(1+v)}\left[\frac{du}{dr} + \frac{1-v}{v}\frac{u}{r}\right] - \frac{E\alpha^*}{1-2v}T \tag{7c}$$

$$\sigma_z = \frac{Ev}{(1-2v)(1+v)}\left[\frac{du}{dr} + \frac{u}{r}\right] - \frac{E\alpha^*}{1-2v}T \tag{7d}$$

$$\frac{d^2 u}{dr^2} + \frac{1}{r}\frac{du}{dr} - \frac{u}{r^2} = (1+v)\alpha^*\frac{dT}{dr} - \frac{1-v^2}{E}\rho\omega^2 r \tag{8a}$$

$$\sigma_r = \frac{E}{1-v^2}\left[\frac{du}{dr} + v\frac{u}{r} - (1+v)\alpha^* T\right] \tag{8b}$$

$$\sigma_\theta = \frac{E}{1-v^2}\left[v\frac{du}{dr} + \frac{u}{r} - (1+v)\alpha^* T\right] \tag{8c}$$

The stress components in the different directions are combined in an scalar measure of the overall equivalent, or effective, stress. This

Table 1

Validation R^2 results for the local network of ARX models and linear polynomials.

Variable	Symbol	GT Load				
		95%	85%	75%	65%	Ramp
Net Power	y_1	61.77%	76.11%	74.97%	73.97%	–
Superheated Steam Temperature	y_2	95.51%	98.40%	99.03%	99.14%	–
Reheated Steam Temperature	y_3	93.18%	94.65%	90.37%	92.49%	–
Turbine's Steam Inlet Pressure	y_4	–	–	–	–	86.16%
Drum's Saturation Temperature	y_5	–	–	–	–	85.22%
Drum's Saturation Pressure	y_6	–	–	–	–	86.62%

parameter can be implemented as a constraint in the optimization problem included in the MPC strategy. The von Mises equivalent stress defined in Eq. (9) is used as this measure.

$$\sigma_{eff}^2 = \sigma_r^2 + \sigma_\theta^2 + \sigma_z^2 - (\sigma_r\sigma_\theta + \sigma_\theta\sigma_z + \sigma_z\sigma_r) \qquad (9)$$

Since the von Mises equivalent stress is a nonlinear equation and linear MPC is the proposed control strategy, a linearisation of the von Mises equivalent stress is used to integrate the equivalent stress in the linear optimization algorithm:

$$\sigma_{eql}^2 = \sigma_{eql,0}^2 + \nabla\sigma_{eql,0}^2\Delta\sigma + \mathscr{O}(\Delta x^2) \qquad (10)$$

These stress equations are discretized with central finite differences and combined with the temperature distribution expressions in a common system of equations that allows to compute simultaneously the temperature, the displacement, each of the stress components and the linearised von Mises effective stress. Combining these system of equations over time, the evolution of these variables in both space and time can be obtained from a larger system of equations:

$$A_{drum|rotor}X_{drum|rotor} = B_{drum|rotor} \qquad (11)$$

where $X_{drum|rotor}$ is a vector containing the temperature difference from the design point, the displacement and the stresses in the wall discretizations over time. $A_{drum|rotor}$ and $B_{drum|rotor}$ are defined for both components in the Supplementary Material (SM).

The temperature and stress models where implemented in MATLAB [52] and validated in the specialized software ANSYS [53]. Structural steel was assumed as the material to ensure well-known physical properties in both models. A time discretization of 1 s was selected, whereas 50 and 800 spatial discretizations were chosen for the rotor and drum, respectively. Heating and cooling of both components was implemented by steam temperature ramp changes in the boundary conditions. A summary of the boundary conditions imposed during the validation is presented in Table 2. Figs. 3 and 4 represent, respectively, the drum and rotor validation results at six different radii.

3. Control methodology for optimal operation accounting for stresses

Control of thermal power plants matches generated power to the power demand from the electrical grid, and modifies adequately the temperatures, pressures and mass flows to ensure a safe, stable and efficient operation. This section presents the control problem encountered in modern NGCCs, describes the proposed methodology to optimally control the power plant whilst monitoring the stresses in critical equipment, and details its implementation as a quadratic optimization program embedded in an MPC.

3.1. Control problem

Natural gas combined cycles are integrated by two thermodynamic cycles characterized by different dynamics. Gas turbines are fast components that can adapt their operation within seconds. In contrast, steam bottoming cycles are slow units limited by the large heat capacitance of the heat-recovery steam generator, as it induces delays of 10–20 min with respect to the gas turbine operation [54,55]. Therefore,

power control in modern NGCCs is achieved by adjusting the gas turbine load. The steam cycle follows the gas turbine operation acting as a passive element that generates power with the steam available in the HRSG.

The operation of the gas turbine is determined by the performance map of its components. Automatic control is normally incorporated in these units to ensure high turbine inlet and exhaust temperatures at nominal and part-loads down to 40% [54]. This control is achieved by adapting the variable guide vanes (VGV) of the compressor, which modify the air flow rate. As gas turbines have almost negligible dynamics compared with those of the steam cycle and their operating conditions may be defined by their load, a quasi-static model is utilized in this work to represent the gas turbine. Exhaust gas mass flow and temperature are hence determined by the load control assuming immediate adjustment of fuel mass flow and VGV position. These are the boundary conditions imposed on the steam cycle [13].

The operation of the steam cycle is based on sliding pressure. In this operation strategy, the admission valves of the steam turbine are close to fully open, allowing the pressure upstream of the steam turbine to vary freely. This keeps the volume flow close to constant in the steam turbine at part load, leading to evenly distributed pressure ratios that reduce the temperature gradients within the turbine and to high isentropic efficiency at different operating conditions [56]. Sliding pressure operation may be applied until 50% load, after which throttling control is required [54]. Therefore, for the power generation changes considered in this work, steam pressure control is not necessary. Control of the steam bottoming cycle is hence reduced to inventory control of the steam drums and condenser, pressure control of the low pressure drum and the deaerator, and limiting the superheated and reheated steam temperature. Furthermore, this work proposes the control of the stresses developing in thick-walled components, as excessively fast load changes may lead to stresses that can damage this equipment.

3.2. Control methodology

A regulatory control layer is utilized in the control strategy of the natural gas combined cycle to stabilize its operation. This includes the level control of the intermediate and high pressure drums and the condenser, and the pressure control of the deaerator and the low pressure drum. Three-element controllers are normally utilized to control the drum level [54]. In this type of controller, the drum level, the feedwater flow and the live-steam flow are processed with a PID cascade structure that acts on the feedwater valves [43]. The low pressure of the cycle is controlled with a PI controller that measures the pressure in the deaerator and acts on the low pressure valve. A detailed diagram of this control structure can be found in the work by Montañés et al. [43].

Model predictive control is utilized to control the power generation of the NGCC, the superheated and reheated steam temperatures, and the maximum stresses arising in the considered components. Power generation is controlled by modifying the gas turbine load, whilst two attemperator valves are used to limit the superheated and reheated steam temperatures. Stress control is achieved by limiting the ramp changes of the gas turbine. This leads to slower changes in the steam cycle, which result in smaller temperature gradients and slower

Table 2
Validation boundary conditions.

| Component	Thermal Boundary Conditions				Mechanical Boundary Conditions		Rotation
	$T_{initial}$	Ramp	h_i	h_o	r_i	r_o	
Drum	340 [°C]	± 20	20000 [W/m²K]	0.065 [W/m²°C]	p = 150 [bar]	p = 1 [bar]	–
Rotor	590 [°C]	± 10	–	20000 [W/m²°C]	u = 0 [m]	p = 140 [bar]	3000 [rpm]

pressure variations in the high pressure drum and rotor. Therefore, the effective stress in thick-walled components is reduced by limiting the maximum load ramps of the gas turbine.

Linear quadratic control, i.e. an MPC strategy based on a quadratic programming optimization problem, was selected because of its fast computational time and convexity [57]. This type of optimization problems guarantees that global minima are found if the weight matrices are defined adequately [57]. The simplified models predicting the performance and key thermodynamic variables in the NGCC are combined with the physics-based stress models in a linear system of equations that enters the optimization problem as linear equality constraints. This methodology ensures that optimal control actions that respect the stress constraints in specific equipment and the behaviour of the NGCC are thus computed.

Since the gas turbine and steam cycle have different dynamics, an extra linear MPC that only regulates the power of the gas turbine was included. The sampling time of this control is 5 s as the gas turbine dynamics are almost negligible. This control aims at complementing the global MPC with more frequent power control and at narrowing the gap

between the demand and the production. With this overall control strategy, the global MPC defines the control actions that stabilize the NGCC every 30 s while the GT MPC adjusts the gas turbine load every 5 s. If the difference between the current stress in the critical components and the maximum allowable effective stress is less than 15%, it is considered that the steam cycle's dynamics dominate the power plant operation and hence the global MPC sets the control actions without inputs from the GT MPC. This approach ensures that when there is not enough margin between the current stress in the drum and rotor and their limit, the global MPC accounts for the stresses that may arise, whereas when the difference is large the GT MPC acts more frequently to meet the power demand.

A schematic representation of the control strategy of the NGCC is presented in Fig. 5. The physics-based NGCC dynamic model represents the operation of an actual power plant with a regulatory control layer already implemented. Measurements of key parameters, e.g. temperatures, pressures and mass flow rates, are fed into both global and GT MPC, where dynamic optimizations are carried out every 30 and 5 s. The solution of these optimization problems are the optimal control
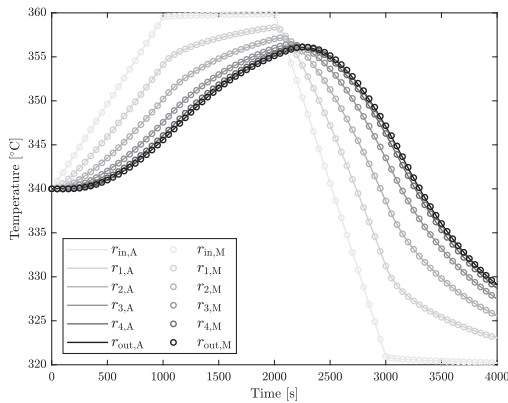
(a) Temperature along six equidistant radii. A refers to ANSYS and M to MATLAB.
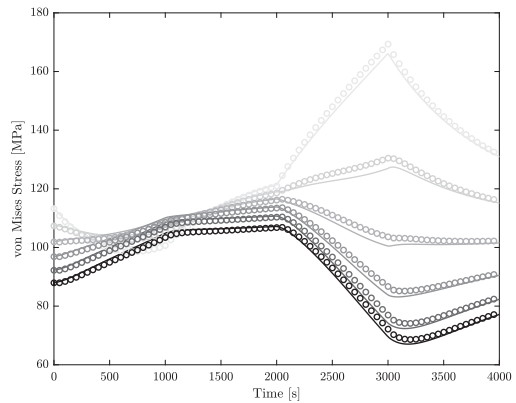
(b) von Mises equivalent stress along six equidistant radii.

Fig. 3. Validation results for the drum model.
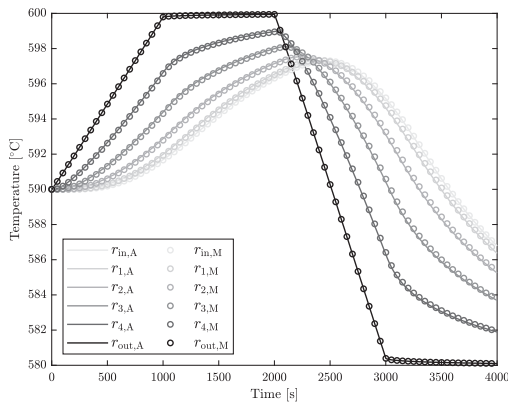
(a) Temperature along six equidistant radii. A refers to ANSYS and M to MATLAB.
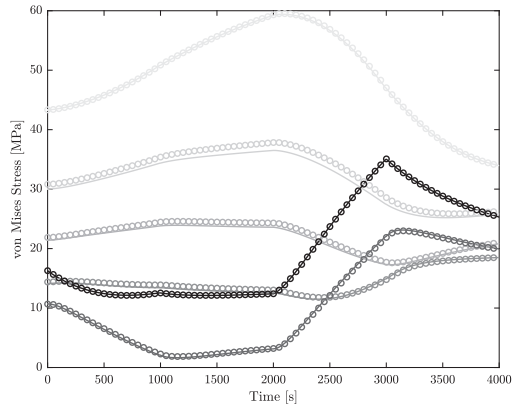
(b) von Mises equivalent stress along six equidistant radii.

Fig. 4. Validation results for the rotor model.
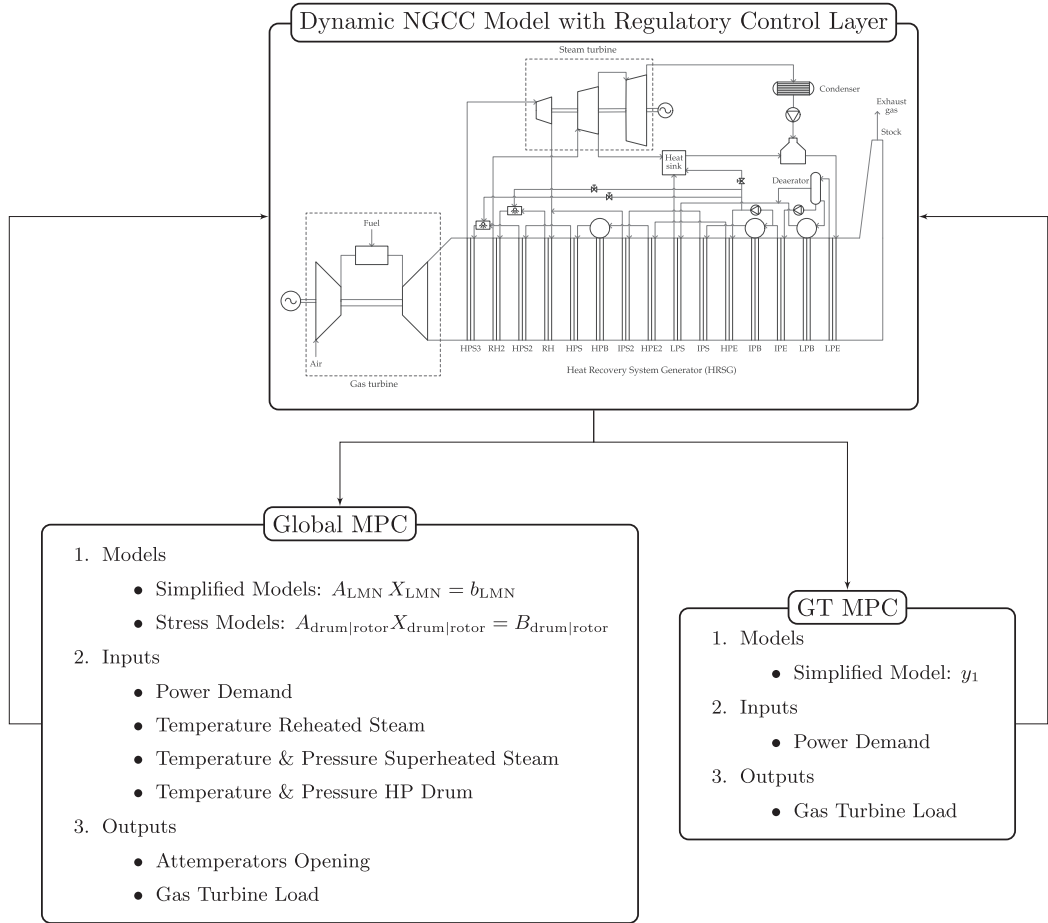
Fig. 5. Structure of the proposed control methodology accounting for stresses in critical components.

actions that must be imposed in the power plant. The novelty and strength of the proposed control methodology lies in the global MPC, as optimal control actions are computed simultaneously with the stresses arising in critical equipment in an optimization framework. This ensures that the implementation of the computed control actions will not lead to excessive stresses in the equipment of the actual NGCC.

3.3. Model predictive control formulation

The optimal quadratic programming (QP) control problem represented by both global and GT linear MPCs is formulated as:

$$\min_{z \in \mathbb{R}^n} f(z) = \frac{1}{2} z^\mathsf{T} Q z + d z \tag{12a}$$

subject to

$$A_{\text{eq}} \, z = B_{\text{eq}} \tag{12b}$$

$$A_{\text{ineq}} \, z \leqslant B_{\text{ineq}} \tag{12c}$$

$$z^{\text{low}} \leqslant z \leqslant z^{\text{high}} \tag{12d}$$

with

$$Q \geqslant 0 \tag{12e}$$

In the global MPC, vector z contains X_{LMN}, X_{drum} and X_{rotor}. It represents the optimal sequence of responses, control inputs, and temperature, displacement and stresses in both drum and rotor for several space and time discretizations calculated over a time horizon N. These variables are the dynamic optimization variables and are limited by lower and upper bounds (Eq. (12d)), ensuring that the maximum allowable stress in both drum and rotor is never exceeded. This optimization problem is subject to linear constrains (Eq. (12b)) that ensure the simplified models (Eq. (5)) and the drum and rotor stress models (Eq. (11)) are satisfied. In addition, linear inequality constraints (Eq. (12c)) are included in order to limit the load ramps in the gas turbine. The degrees of freedom included in vector z are modified throughout the optimization to minimize the objective function $f(z)$ in Eq. (12a). The objective function considered in this work aims at minimizing the difference between the power generation and demand, and the deviation of both superheated and reheated steam temperatures from their nominal value. The description of these matrices and vectors is included in the Supplementary Material (SM).

In the GT MPC, vector z includes the optimal sequence of net power generation and gas turbine loads throughout the time horizon. Therefore, the LMN for these two variables is the only equality constraint, and the maximum gas turbine load gradient is the only inequality constraint. Lower and upper bounds are also included for both
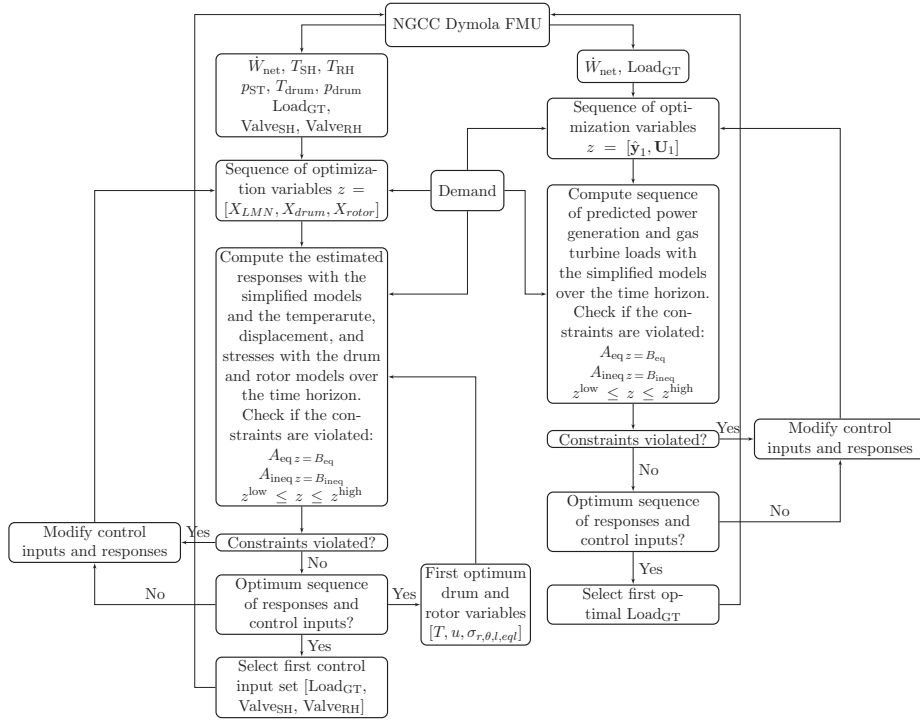
Fig. 6. Logic diagram of the MPC control strategy.

Table 3
Materials' physical and mechanical properties.

Component	Material	ρ [kg/m^3]	C_m [J/kg K]	k_m [W/m K]	α^* [m^2/s]	α [1/K]	E [MPa]	υ [–]	h_o [W/m^2 K]	h_i [W/m^2 K]	Yield stress [MPa]
Drum	SA-515 Grade 70	7850	434	47	1.3796e-05	1.36e-5	178000	0.3	5000	0.065	190
Rotor	X18CrMnMoNbVN12	7700	460	29	8.1875e-06	1.25e-5	127000	0.292	4000	–	69

variables. The detailed description of this GT MPC is also included in the Supplementary Material (SM).

A diagram representing the logic of the MPC-based control methodology for the NGCC is illustrated in Fig. 6. The full-physics dynamic

model developed in Dymola and the optimization algorithm in the MPC developed in MATLAB were merged in Simulink through a Functional Mock-up Unit (FMU). This FMU containing the detailed dynamic model of the NGCC with the regulatory control layer represents an actual
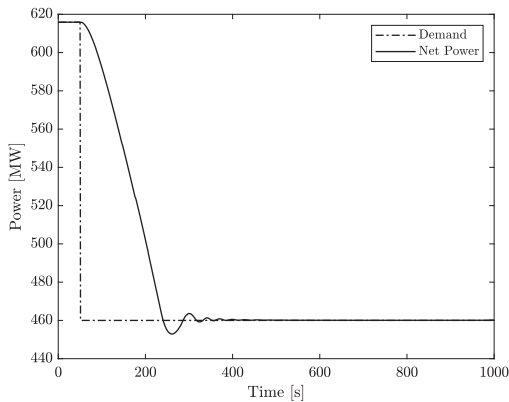
Fig. 7. Net power generation of the natural gas combined cycle.
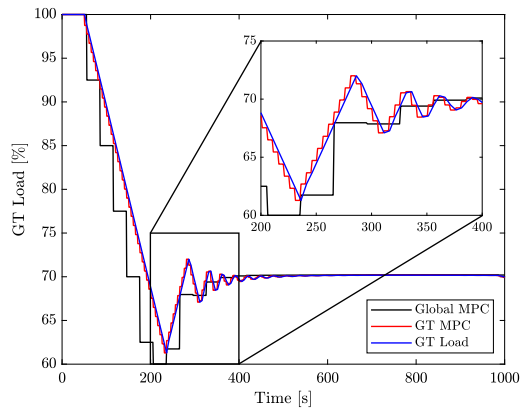
Fig. 8. Load profile of the gas turbine with MPC optimization steps.
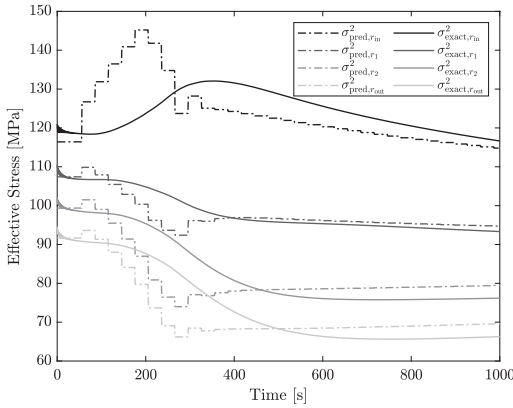
Fig. 9. Estimated and exact equivalent stress in the drum at different radii.

Fig. 10. Estimated and exact equivalent stress in the rotor at different radii.
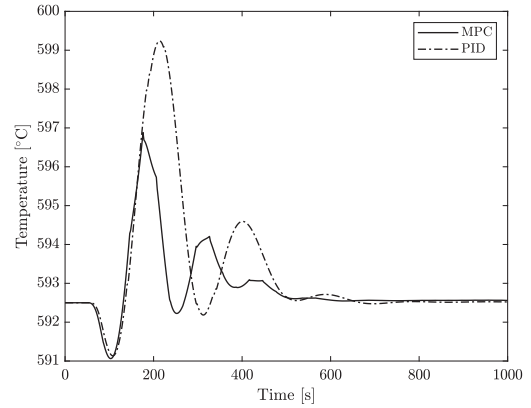
Fig. 11. Control of the superheat steam temperature.
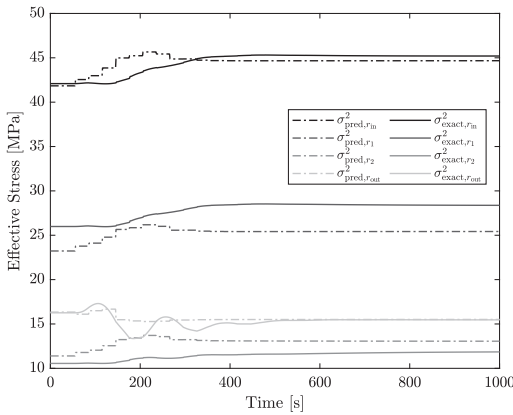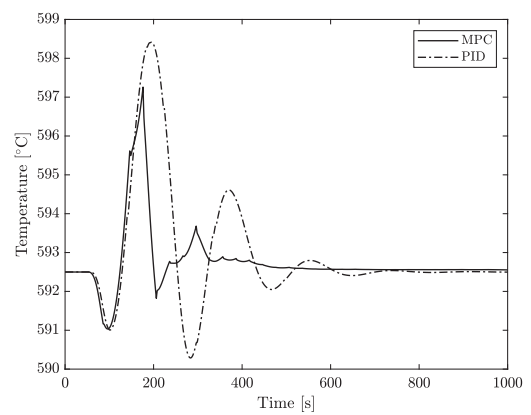
Fig. 12. Control of the reheat steam temperature.

NGCC, and provides the measurements of key parameters that are required in both MPCs to compute the optimal control actions.

4. Results and discussion

Load step change is a suitable scenario to test the control capabilities of the methodology proposed in this work. A step change in the power demand of 165 MW drives the transient operation of the natural gas combined cycle. The main goal is to minimize the difference between the power demand and generation as fast as possible while satisfying the constraints of the system. Two cases are studied in order to present the control capabilities of the proposed methodology. First, the performance of the NGCC during the load ramp is analysed under reasonable stress limitations that can be expected in current modern power plants. Subsequently, the same dynamic behaviour is studied under tight constraints on the allowable stress of the steam drum, as it represents possible scenarios as start-ups. Table 3 includes the materials considered in this work for the drum and rotor as well as their physical and mechanical properties. The yield stress of the drum utilized in the second analysis is 130 MPa instead of 190 MPa to guarantee that the constraint is active.

The weights in the matrix and vector of the objective function in the global MPC are $\lambda_{y_1} = 1$, $\lambda_{y_2} = \lambda_{y_3} = 10$, and $\lambda_{U_1} = \lambda_{U_2} = \lambda_{U_3} = 2$ (see Supplementary Material (SM)). In the GT MPC, $\lambda_{y_1} = 1$ and $\lambda_{U_1} = 0.1$. A time horizon of 30 sampling times was considered to guarantee that the

system dynamics are captured, 200 and 50 spatial discretizations were used in the drum and rotor walls respectively, and 3 time discretizations per sampling time were utilized.

4.1. Optimal dynamic operation with realistic constraints

In this first case the transient performance of the NGCC is studied by imposing constraints that may be expected in modern power plants. This includes gas turbine load ramping rates up to 15% per minute, and complex alloys for the rotor material capable of withstanding the high temperature and pressure at the inlet of the steam turbine [58].

With these constraints imposed, the NGCC is able to meet the power demand in 300 s (see Fig. 7). Since this time is half the stabilization time of the steam cycle, it is clear that the gas turbine compensated the slow response of the HRSG. This behaviour is represented in Fig. 8. The gas turbine load is under-shot in order to compensate the slow transient of the steam cycle and meet the power demand faster. As the steam cycle reaches steady-state at part-load, the gas turbine increases progressively its load to keep the power generation constant. The GT stops fluctuating after 600 s, which coincides with the stabilization time of the steam cycle.

From a dynamic optimization perspective, the load of the gas turbine is always dictated by the GT MPC, which finds a different and smoother optimal trajectory than the global MPC as it is evaluated more frequently. This is possible since the difference between the equivalent
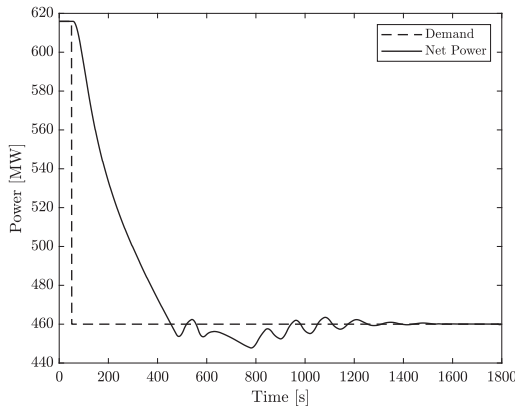
Fig. 13. Net power generation of the natural gas combined cycle.
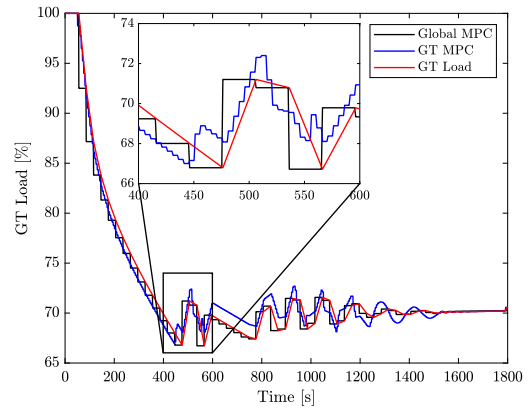
Fig. 14. Load profile of the gas turbine with MPC optimization steps.

stress in both drum and rotor and the maximum allowable stress is always bigger than 15%. Figs. 9 and 10 show the stresses predicted by the global MPC at each sampling time during the transient operation of the NGCC.

The stress in both components was calculated with the exact profile of temperatures and pressures from the dynamic high-fidelity model and compared with the linearized equivalent stresses predicted during the dynamic optimizations (see Figs. 9 and 10). Despite the predicted stress overestimates slightly the equivalent stress in both components, both in time and magnitude, it predicts adequately their tendency and the largest value, ensuring that the components do not exceed the maximum allowable limit. This discrepancy may be generated by the utilization of simplified models and the lack of detailed wall temperatures from the dynamic high-fidelity model. The simplified models might over-predict the rate of change of the temperature and pressure in both components, leading to faster dynamics than those encountered in the detailed model. However, the the lack of detailed wall temperature in the dynamic high-fidelity model may influence more the difference between the predicted and exact stresses, as it prevents the utilization of actual wall temperatures and forces the estimation of the initial conditions along the wall at each optimization. Having detailed data of the wall temperature every sampling time would smear out the fluctuations of the stress predictions.

Superheat and reheat steam temperature profiles with PID controllers in the attemperators were also calculated by imposing the gas turbine load profile in the detailed dynamic model. The results are represented in Figs. 11 and 12. Albeit being more aggressive, MPC outperforms the PID temperature controllers as it is able to stabilize the superheated and reheated steam temperatures faster and with smaller deviations from their set-point.

During this transient response the inequality constraint limiting the maximum gas turbine load gradient is always active for both MPC controllers. Therefore, it is the gas turbine and not the stresses in thick-walled components the main limitation for faster and more flexible operation of natural gas combined-cycles during load changes. On the contrary, during the start-up of the power plant, it is expected that the stresses in these components are the limiting factor for faster operation. Consequently, in order to prove that this control methodology is suitable also for start-up of natural gas combined cycles, the same scenario is studied but ensuring that the maximum allowable stress is reached in the steam drum. This was done by reducing the yield stress limit to 130 MPa.

4.2. Optimal dynamic operation with tight stress constraints

This case aims at showing the capabilities of the methodology

proposed in this work to control the power generation of the NGCC under tight constraints imposed on the material of the equipment. Fig. 13 shows the net power generation of the NGCC for these tight constraints. As expected, the power plant requires more time to meet the power demand since the stress limitation in the drum inhibits large changes in the gas turbine load. Thus, and since the stabilization time is longer than the 600 s required by the steam cycle, the stress in the high pressure drum is the limiting factor during the transient operation of the NGCC.

The slow transient response of the gas turbine is represented in Fig. 14. In contrast with the previous case, the gas turbine load is dictated by the global MPC, which leads in this case to a smoother gas turbine control. As the margin between the maximum allowable stress and the stress predicted by the global MPC is small, the GT MPC does not influence the power plant operation.

From Fig. 15 can be observed that the constraint on the maximum effective stress in the drum is active for a period of time during the transient. This indicates that the MPC control strategy is able to adequately predict the stress in the steam drum and obtain an optimal control sequence that does not exceed the material allowable limits. The comparison of the exact and the predicted effective stress in Figs. 15 and 16 shows better agreement than in the previous case. This is a result of the slower gas turbine load changes, leading to more uniform conditions in the wall, which, in turn, make the predictions of the initial conditions in the drum more accurate. This fact points out the necessity of incorporating models to calculate the temperature profile along the components wall in the dynamic high-fidelity models. As occurred in the previous case, the abrupt step occurring in the effective drum stress at the first instant after the step change in the power demand may be originated by the simplified models, which over-estimate the dynamic response of the pressure and temperature on the inner surface of the drum.

5. Conclusions

This work proposes a control methodology based on linear MPC with stress control. In the proposed methodology, the effective stress in the high pressure drum and steam turbine inlet rotor are computed and predicted together with relevant thermodynamic variables in specific locations of the steam cycle in an optimization framework. Constraints on the effective stress arising in critical equipment can be imposed with this approach, which allows to compute optimal control actions that do not exceed these material limitations.

Temperature and stress models for the wall of the drum and rotor were developed and validated with finite element method software, whilst simplified ARX and linear polynomial models were created to

Fig. 15. Estimated and exact equivalent stress in the drum at different radii.

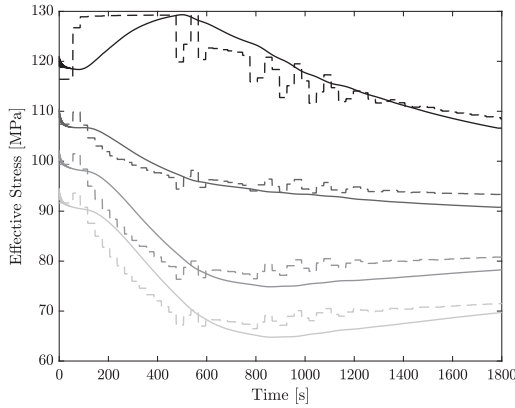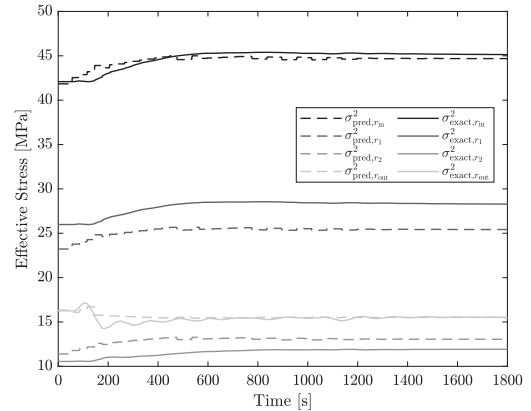**Fig. 16.** Estimated and exact equivalent stress in the rotor at different radii.

predict key thermodynamic variables in the steam cycle such as temperatures and pressures during the optimization. The stress and simplified power plant models were embedded as linear equality constraints in the quadratic optimization algorithm within the MPC strategy, which computes the optimal set of control actions and implements them in the thermal power plant every sampling time.

Two cases that simulated load step changes of the NGCC were presented. The first case imposed constraints equivalent to those encountered in modern combined cycles, whereas the second case drastically reduced the maximum allowable stress in the steam drum. The results showed the NGCC is able to reduce the load by 165 MW in 300 s by under-shooting the GT load to compensate the slow transient behaviour of the steam cycle. In this case, the GT MPC defined the load profile of the gas turbine because of the broad margin between the effective and maximum allowable stress in the critical equipment. When the stress limitations were tighter as in the second case, the global MPC defined the gas turbine load profile as the maximum allowable stress limited the ramping capabilities of the NGCC. These results demonstrate that the maximum gas turbine load gradient, and not the stresses in critical components, is the main limitation of flexible natural gas combined cycles during load changes. Therefore, improvements towards enhanced flexibility of this type of thermal power plants requires gas turbines capable of ramping up and down faster.

A comparison in these two cases between the exact and predicted linearised equivalent stress in both drum and rotor showed a good agreement of the results. Despite the simplified models may lead to over-prediction in the initial stress dynamics, it is considered that the discrepancy between predicted and exact effective stresses was originated by the lack of detailed wall temperatures from the dynamic high-fidelity model and thus the need of estimating these initial optimization conditions. Nevertheless, the exact stress never exceeded the stress predicted by the MPC. Thus, the proposed methodology proved to be an effective control strategy suitable to incorporate technical constraints as stress limits in different components and with a faster response and less overshooting in process variables than traditional feedback control strategies.

This control methodology based on MPC with stress control can be extended to other components such as pipes, headers, downcomers, casings or combustors, if stress models for these components are available. The main limitation is the computational time, as more models add more optimization variables to the dynamic optimization problem, which has to be solved within the sampling time spam. Furthermore, the methodology can only handle linear or linearised constraints and nonlinear stress models cannot be included. The methodology proposed in this work could be extended to nonlinear MPC. This is a research gap that must be considered for complicated

geometries that lead to nonlinear stress models.

The application of this methodology to start-ups and shut-downs of thermal power plants to obtain optimal operating sequences is a promising future research step, as stress limitations dominate the time required in this type of operation. Moreover, the flexibility of this methodology allows to tune the objective function to explore different control actions, include online model estimation to account for changes in the power plant such as fouling, and easily include Kalman filters or additional variables that may be needed during the start-up as, for instance, bypass valves and steam mass flow and temperature prediction models in different location of the steam cycle. This methodology could also be combined with fatigue analysis in an economic MPC, where the objective may be to find a trade-off between the damage in specific equipment and the economic revenue from gas turbine ramps or start-ups and shut-downs. Scheduling will be a relevant issue in future power markets, and combining stress and fatigue analyses with power plant control and damage studies can lead to economic benefits.

Declaration of Competing Interest

The authors declare that they have no known competing financial interests or personal relationships that could have appeared to influence the work reported in this paper.

Acknowledgements

Appendix A. Supplementary material

Supplementary data associated with this article can be found, in the online version, at https://doi.org/10.1016/j.applthermaleng.2019.114858.

References

[1] IPCC, Summary for Policymakers, in: Global warming of 1.5C. An IPCC Special Report on the impacts of global warming of 1.5C above pre-industrial levels and related global greenhouse gas emission pathways, in the context of strengthening the global response to the threat of climate change, sustainable development, and efforts to eradicate poverty, [V. Masson-Delmotte, P. Zhai, H.O. Pörtner, D. Roberts, J. Skea, P.R. Shukla, A. Pirani, W. Moufouma-Okia, C.Péan, R. Pidcock, S. Connors,

J.B.R. Matthews, Y. Chen, X. Zhou, M.I. Gomis, E. Lonnoy, T. Maycock, M. Tignor, T. Waterfield (eds.)]. World Meteorological Organization, Geneva, Switzerland, 2018.

[2] IPCC, Climate Change 2014: Synthesis Report, Contribution of Working Groups I, II and III to the Fifth Assessment Report of the Intergovernmental Panel on Climate Change [Core Writing Team, R.K. Pachauri and L.A. Meyer (eds.)], IPCC, Geneva, Switzerland, 2014.

[3] International Energy Agency – IEA, World Energy Outlook 2018: Executive Summary, 2018. https://webstore.iea.org/download/summary/190?fileName= English-WEO-2018-ES.pdf.

[4] European Commission, Energy Roadmap 2050, 2011. https://eur-lex.europa.eu/ LexUriServ/LexUriServ.do?uri=COM:2011:0885:FIN:EN:PD.

[5] J. Bertsch, C. Growitsch, S. Lorenczik, S. Nagl, Flexibility in Europe's power sector: an additional requirement or an automatic complement? Energy Econ. 53 (2016) 118–131.

[6] M. Huber, D. Dimkova, T. Hamacher, Integration of wind and solar power in Europe: assessment of flexibility requirements, Energy 69 (2014) 236–246.

[7] H. Kondziella, T. Bruckner, Flexibility requirements of renewable energy based electricity systems–a review of research results and methodologies, Renew. Sustain. Energy Rev. 53 (2016) 10–22.

[8] R.M. Montañés, M. Korpås, L.O. Nord, S. Jaehnert, Identifying operational requirements for flexible CCS power plant in future energy systems, Energy Procedia 86 (2016) 22–31.

[9] J. Oswald, M. Raine, H. Ashraf-Ball, Will British weather provide reliable electricity? Energy Policy 36 (8) (2008) 3212–3225.

[10] International Energy Agency – IEA, Technology Roadmap, Energy storage, 2014. https://www.iea.org/publications/freepublications/publication/ TechnologyRoadmapEnergystorage.pdf.

[11] P. Eser, N. Chokani, R. Abhari, Operational and financial performance of fossil fuel power plants within a high renewable energy mix, J. Glob. Power Propul. Soc. 1 (2017) 16–27.

[12] M.A. González-Salazar, T. Kirsten, L. Prchlik, Review of the operational flexibility and emissions of gas-and coal-fired power plants in a future with growing renewables, Renew. Sustain. Energy Rev. 82 (2017) 1497–1513.

[13] F. Alobaid, N. Mertens, R. Starkloff, T. Lanz, C. Heinze, B. Epple, Progress in dynamic simulation of thermal power plants, Prog. Energy Combust. Sci. 59 (2017) 79–162.

[14] L. Riboldi, L.O. Nord, Optimal design of flexible power cycles through Kriging-based Surrogate models, in: ASME Turbo Expo 2018: Turbomachinery Technical Conference and Exposition, American Society of Mechanical Engineers, 2018, p. V003T08A002.

[15] F. Alobaid, R. Postler, J. Ströhle, B. Epple, H.-G. Kim, Modeling and investigation start-up procedures of a combined cycle power plant, Appl. Energy 85 (12) (2008) 1173–1189.

[16] T. Kim, D. Lee, S. Ro, Analysis of thermal stress evolution in the steam drum during start-up of a heat recovery steam generator, Appl. Therm. Eng. 20 (11) (2000) 977–992.

[17] S.C. Gülen, K. Kim, Gas turbine combined cycle dynamic simulation: a physics based simple approach, J. Eng. Gas Turbines Power 136 (1) (2014) 011601.

[18] P. Dzierwa, J. Taler, Optimum heating of pressure vessels with holes, J. Pressure Vessel Technol. 137 (1) (2015) 011202.

[19] J. Taler, P. Dzierwa, D. Taler, P. Harchut, Optimization of the boiler start-up taking into account thermal stresses, Energy 92 (2015) 160–170.

[20] J. Taler, B. Weglowski, D. Taler, T. Sobota, P. Dzierwa, M. Trojan, P. Madejski, M. Pilarczyk, Determination of start-up curves for a boiler with natural circulation based on the analysis of stress distribution in critical pressure components, Energy 92 (2015) 153–159.

[21] J. Bausa, G. Tsatsaronis, Dynamic optimization of startup and load-increasing processes in power plants – Part I: Method, J. Eng. Gas Turbines Power 123 (1) (2001) 246–250.

[22] T. Akiyama, H. Matsumoto, K. Asakura, Dynamic simulation and its applications to optimum operation support for advanced combined cycle plants, Energy Convers. Manage. 38 (15–17) (1997) 1709–1723.

[23] H. Matsumoto, Y. Ohsawa, S. Takahasi, T. Akiyama, H. Hanaoka, O. Ishiguro, Startup optimization of a combined cycle power plant based on cooperative fuzzy reasoning and a neural network, IEEE Trans. Energy Convers. 12 (1) (1997) 51–59.

[24] M. Shirakawa, M. Nakamoto, S. Hosaka, Dynamic simulation and optimization of start-up processes in combined cycle power plants, JSME Int. J. Ser. B Fluids Therm. Eng. 48 (1) (2005) 122–128.

[25] C. Albanesi, M. Bossi, L. Magni, J. Paderno, F. Pretolani, P. Kuehl, M. Diehl, Optimization of the start-up procedure of a combined cycle power plant, in: 2006 45th IEEE Conference on Decision and Control, IEEE, 2006, pp. 1840–1845.

[26] F. Casella, F. Pretolani, Fast start-up of a combined cycle power plant: a simulation study with modelica, 5th International Modelica Conference, Vienna, Austria,

September, 2006, pp. 3–10.

[27] J. Bausa, G. Tsatsaronis, Dynamic optimization of startup and load-increasing processes in power plants – Part II: Application, J. Eng. Gas Turbines Power 123 (1) (2001) 251–254.

[28] G. Prasad, E. Swidenbank, B. Hogg, A local model networks based multivariable long-range predictive control strategy for thermal power plants, Automatica 34 (10) (1998) 1185–1204.

[29] G. Prasad, E. Swidenbank, B. Hogg, A neural net model-based multivariable long-range predictive control strategy applied in thermal power plant control, IEEE Trans. Energy Convers. 13 (2) (1998) 176–182.

[30] H. Peng, J. Wu, G. Inoussa, Q. Deng, K. Nakano, Nonlinear system modeling and predictive control using the RBF nets-based quasi-linear ARX model, Control Eng. Pract. 17 (1) (2009) 59–66.

[31] H. Peng, T. Ozaki, Y. Toyoda, K. Oda, Exponential ARX model-based long-range predictive control strategy for power plants, Control Eng. Pract. 9 (12) (2001) 1353–1360.

[32] S. Lu, B.W. Hogg, Predictive co-ordinated control for power-plant steam pressure and power output, Control Eng. Pract. 5 (1) (1997) 79–84.

[33] F.J. D'Amato, Industrial application of a model predictive control solution for power plant startups, in: Computer Aided Control System Design, 2006 IEEE International Conference on Control Applications, 2006 IEEE International Symposium on Intelligent Control, 2006 IEEE, IEEE, 2006, pp. 243–248.

[34] P. Sindareh-Esfahani, S.S. Tabatabaei, J.K. Pieper, Model predictive control of a heat recovery steam generator during cold start-up operation using piecewise linear models, Appl. Therm. Eng. 119 (2017) 516–529.

[35] R. Viswanathan, J. Stringer, Failure mechanisms of high temperature components in power plants, J. Eng. Mater. Technol. 122 (3) (2000) 246–255.

[36] S. Barella, M. Bellogini, M. Boniardi, S. Cincera, Failure analysis of a steam turbine rotor, Eng. Fail. Anal. 18 (6) (2011) 1511–1519.

[37] A. Mirandola, A. Stoppato, E.L. Casto, Evaluation of the effects of the operation strategy of a steam power plant on the residual life of its devices, Energy 35 (2) (2010) 1024–1032.

[38] A. Benato, A. Stoppato, S. Bracco, Combined cycle power plants: a comparison between two different dynamic models to evaluate transient behaviour and residual life, Energy Convers. Manage. 87 (2014) 1269–1280.

[39] Thermoflow Inc, GT PRO 24.0, 2014.

[40] Modelon, Thermal Power Library. https://www.modelon.com/library/thermal-power-library/.

[41] Dassault Systemes. https://www.3ds.com/products-services/catia/products/ dymola/.

[42] Modelica Association. https://www.modelica.org/.

[43] R.M. Montañés, S.Ó. GarDarsdóttir, F. Normann, F. Johnsson, L.O. Nord, Demonstrating load-change transient performance of a commercial-scale natural gas combined cycle power plant with post-combustion CO₂ capture, Int. J. Greenhouse Gas Control 63 (2017) 158–174.

[44] L. Ljung, System Identification: Theory for the User, Prentice-hall, 1987.

[45] T.A. Johansen, B. Foss, Constructing NARMAX models using ARMAX models, Int. J. Control 58 (5) (1993) 1125–1153.

[46] M. Gevers, Identification for control: from the early achievements to the revival of experiment design, Eur. J. Control 11 (2005) 1–18.

[47] M. Gevers, L. Ljung, Optimal experiment designs with respect to the intended model application, Automatica 22 (5) (1986) 543–554.

[48] U. Forssell, L. Ljung, Closed-loop identification revisited, Automatica 35 (7) (1999) 1215–1241.

[49] L. Mišković, A. Karimi, D. Bonvin, M. Gevers, Closed-loop identification of multivariable systems: with or without excitation of all references? Automatica 44 (8) (2008) 2048–2056.

[50] M. Gevers, L. Mišković, D. Bonvin, A. Karimi, Identification of multi-input systems: variance analysis and input design issues, Automatica 42 (4) (2006) 559–572.

[51] S. Timoshenko, J.N. Goodier, Theory of Elasticity, McGraw-Hill book Company, 1951.

[52] Mathworks Inc, MATLAB version R2018a, 2018.

[53] ANSYS, ANSYS Academic Research Thermal and Mechanical, Release 19.2, ANSYS Inc, 2018.

[54] R. Kehlhofer, F. Hannemann, B. Rukes, F. Stirnimann, Combined-cycle Gas & Steam Turbine Power Plants, Pennwell Books, 2009.

[55] P.J. Dechamps, Modelling the transient behaviour of heat recovery steam generators, Proc. Inst. Mech. Eng., Part A: J. Power Energy 209 (4) (1995) 265–273.

[56] K. Jonshagen, M. Genrup, Improved load control for a steam cycle combined heat and power plant, Energy 35 (4) (2010) 1694–1700.

[57] J. Nocedal, S.J. Wright, Numerical Optimization, Springer, 2006.

[58] R. Viswanathan, W. Bakker, Materials for ultrasupercritical coal power plants - Turbine materials: Part II, J. Mater. Eng. Perform. 10 (1) (2001) 96–101.

Publication III

In future energy markets, traditional thermal power plants will have to cycle more to adapt their operation to the intermittent power generation of renewable energy sources. Gas turbine load ramps and stresses in thick-walled equipment are arguably the main limitations in the flexible operation of natural gas combined cycles. This work proposes a control strategy based on model predictive control with stress monitoring to overcome both limitations and enhance the flexible operation of thermal power plants. The linear and nonlinear formulation of the optimization problem included in the model predictive control strategy are described, and two different modelling approaches for the stresses in the high pressure drum and rotor are presented. The results demonstrate that the proposed control strategy is capable of computing optimal control sequences without exceeding the maximum allowable stress in critical components and the ramp rates of the gas turbine. The comparison between the linear and nonlinear formulation shows the superior performance of linear model predictive control and suggests that the nonlinear formulation should only be used when the stress models can not be expressed as a linear system of equations.
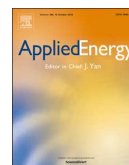
Optimal control of flexible natural gas combined cycles with stress monitoring: Linear vs nonlinear model predictive control☆

Jairo Rúa*, Lars O. Nord

Department of Energy and Process Engineering, Norwegian University of Science and Technology, Trondheim, Norway

HIGHLIGHTS

- Maximum gas turbine load gradient is the main limitation during load changes
- Linear MPC shows superior performance than nonlinear MPC
- Possible to resort to nonlinear MPC when linear stress modelling is not feasible
- Proposed control methodology is able to predict stresses in thick-walled components
- Stress monitoring allows optimal and safe control sequences under tight constraints

ABSTRACT

In future energy markets, traditional thermal power plants are expected to cycle more to adapt their operation to the intermittent power generation of renewable energy sources. Gas turbine load ramps and stresses in thick-walled equipment of the steam cycle are arguably the main limitations in the flexible operation of natural gas combined cycles. This work proposes a control strategy based on model predictive control with stress monitoring to overcome both limitations and enhance the flexible operation of thermal power plants. The linear and non-linear formulation of the problem included in the model predictive control strategy are described, and two different modelling approaches for the stresses in the high pressure drum and steam turbine rotor are presented. The results demonstrate that the proposed control strategy is capable of computing optimal control sequences without exceeding the maximum allowable stress in critical components and the ramp rates of the gas turbine. The comparison between the linear and nonlinear formulations shows the superior performance of linear model predictive control and suggests that the nonlinear formulation should only be used when the stress models can not be expressed as a linear system of equations.

1. Introduction

Atmospheric concentrations of greenhouse gases are increasing as a result of the anthropogenic emissions since the industrial revolution [1]. According to the Intergovernmental Panel on Climate Change (IPCC), the temperature increase with respect to pre-industrial levels must not exceed 1.5 °C to limit the consequences of global warming in natural and human ecosystems [2]. Thus, a major reduction of greenhouse emissions in all sectors is necessary to migate the effects of climate change [2].

The energy sector is the main contributor to the global CO_2 emissions owing to its reliance on fossil fuels [3]. Renewable energy sources have increased their contribution in recent years in an effort to reduce the greenhouse emissions in this sector [3]. In line with this trend, more capacity will be installed with the objective of reaching 40% power generation from renewable energy sources by 2050 [4]. Consequently, thermal power plants will likely need to compensate the intermittency of renewable power generation and partly balance the load in the grid [5–9].

Flexible operation of thermal power plants will require enhanced cycling capabilities and more frequent start-ups and shut-downs [10–12]. Natural gas combined cycles (NGCC) offer the fastest operation with higher performance and lower emissions than traditional coal-fired power plants [13]. Therefore, NGCCs are expected to increase

---

Nomenclature

Latin Symbols

A	system of equations matrix –
a	responses coefficients –
B	system of equations vector–
b	manipulated variables coefficients–
C	specific heat capacity J/kg K
c	nonlinear constraints–
cv	validity function centre –
d	QP optimization weight vector–
E	Young's Modulus MPa
e	stochastic error –
f	nonlinear objective function –
h	convection coefficient W/m^{2}K
k	heat conduction coefficient W/m K
M	number of local models –
N	time horizon –
p	pressure bar
Q	QP optimization weight matrix–
r	radius m
T	temperature deviation from design K
t	time s
U	manipulated variable –
u	displacement m
$\dot{W}$	mechanical power generation MW
w	validity function width –
$\hat{y}$	predicted response –
y	response –
z	vector of optimiaztion variables –

Greek Symbols

α	thermal diffusivity m^2/s
α^*	thermal expansion coefficient 1/K

γ	current operation point –
κ	current measurement vector –
λ	objective function weights –
ω	rotational speed rad/s
ρ	density kg/m^3
σ	stress MPa
υ	Poisson's ratio –
ξ	validity function –

Subscripts

θ	tangential direction
n_U	number past manipulated variables
n_y	number past responses
0	initial conditions
dist	displacement formulation
drum	high-pressure drum
eff	effective von Mises stress
effl	linearised von Mises stress
eq	equality
i	inner radius
ineq	inequality
int	integral formulation
m	metal
o	outer radius
r	radial direction
RH	reheated steam
SH	superheated steam
turb	first-stage steam turbine rotor
wall	wall of the equipment
z	longitudinal direction

Superscripts

high	higher bound
low	lower bound

---

their share in future energy markets [10].

Gas turbine load ramps and stresses in thick-walled components of the steam cycle are arguably the main limitations during the dynamic operation of NGCCs [14]. Fast load ramps may lead to combustion issues in the gas turbine, whilst excessive stress levels generate creep and fatigue in the walls of the equipment and reduce their expected operational lifetime. The maximum gas turbine load ramps are determined by the manufacturer and depend exclusively on the gas turbine model. In contrast, the stresses arising on the walls of the power plant equipment depend mainly on temperature gradients, inner and outer pressures, and centrifugal forces. These stresses can be limited by an adequate control strategy [15].

Monitoring the stress development on thick-walled components (e.g. high pressure steam turbine rotor and high pressure drum) is fundamental to enhance the flexible operation of thermal power plants and ensure their integrity [16–20]. Kim et al. [16] and Taler et al. [19,20] demonstrated how the adequate control of temperature and mass flow rates can limit the stress in a steam drum, whereas Can Gülen and Kim [18] showed the stress development in the high pressure drum and rotor of a combined cycle during the start-up sequence, pointing out the critical stresses that arise in this equipment. Alobaid et al. [17] proved that the start-up time can be reduced with adequate control strategies using PID controllers. As a result, larger temperature gradients and pressure differences built up in the equipment, leading to stresses that could damage these components. Stress monitoring was recommended to ensure that the proposed control did not exceed the limits of the material but was not included in their analysis.

Traditional PID control is not suitable for flexible operation of thermal power plants with stress prediction and monitoring as it is not possible to impose constraints on the controlled variables. Dynamic optimisation is a more advanced control approach where the control sequence is the result of an optimisation problem [21]. Therefore, the stress development can be computed simultaneously with the control actions where constraints may be imposed. As a result, optimal start-up sequences and load gradients that do not exceed the stress limits can be obtained with this approach [22–24].

Model predictive control (MPC) is a control methodology based on the periodic solution of a dynamic problem and the update of the optimal control actions. MPC predicts the performance of the power plant and selects the best control action based on the current state of the system. This control strategy can adjust the operation of the power plant to disturbances and demand changes by solving a dynamic optimisation problem periodically. In thermal power plants, MPC leads to better temperature, pressure and level control than traditional PID controllers or control strategies based on single dynamic problems [25–29]. In addition, Sindareh et al. [30] demonstrated the MPC capacity to control the temperature gradient in the steam turbine rotor and reduce its deterioration. However, the application of this control strategy is limited since deterioration depends on the stresses and not on the temperature gradient.

The first control methodology that included stress and load ramp limitation in the MPC control strategy of an NGCC was proposed by Rúa et al. [15]. Linear MPC was utilized for temperature control in the power plant and limit the stresses in the high pressure drum and the

high pressure steam turbine rotor. The results demonstrated that the proposed methodology was capable of computing the optimal control actions without exceeding the maximum allowable stresses.

This work complements and expands the previous work by proposing a novel stress modelling for both high pressure drum and rotor, and formulating the problem linearly and nonlinearly. Since thermal power plants are highly integrated by equipment with complex and different geometries, stress modelling may lead to nonlinear systems where linearisation is not accurate. Therefore, linear MPC is not suitable and nonlinear formulations of the optimal control problem with stress monitoring are necessary to ensure a safe yet efficient operation of thermal power plants. The two formulations proposed in this study ensure that this methodology can be applied to all control problems and any stress model can be embedded in the control strategy. This enhances the applicability range of the proposed methodology, as stress modelling of difficult geometries can be included in a nonlinear MPC for their application in control. Section 2 describes the dynamic model of the case study power plant, the simplified models implemented in the MPC, and the stress models of the drum and rotor. The control strategy and its mathematical formulation are described in Section 3. A comparison between the computational performance of the linear and nonlinear MPC formulations is presented in Section 4 with a case study that demonstrates the capability of the proposed control methodology to limit the stress development in the NGCC. Section 5 summarizes the main findings of this study.

2. Power plant and stress modelling

This work utilizes several models of different complexity to describe the stress in the equipment, predict the power plant performance and simulate the MPC application in a modern NGCC. This section describes the dynamic high-fidelity model utilized to replicate the transient behaviour of a thermal power plant, the simplified models implemented in the MPC to estimate the future thermodynamic state of the power plant at specific locations, and the stress models that are also embedded in the MPC optimisation problem to avoid that the limits of the materials are exceeded.

2.1. Natural gas combined cycle dynamic model

Natural gas combined cycles with triple pressure steam cycles and reheating are the thermal power plants that offer the highest efficiency with the lowest emissions [14,31]. A dynamic high-fidelity model of a modern NGCC is utilized in this work to study the performance of the proposed MPC methodology on this type of power plants and replicate the behaviour of a real NGCC. Fig. 1 represents the configuration of the NGCC considered in this work. The steady state design was carried out in GT PRO [32] because it provides detailed information of the geometry of the equipment that is necessary for the dynamic model, e.g. the dimensions, materials and number of units of the different components.

The dynamic high-fidelity model of the NGCC was constructed using the Thermal Power library [33] in the software Dymola [34], which is based on the Modelica language [35]. This dynamic model is based on first principle equations for fluid flow, includes thermodynamic properties for the different fluids in the NGCC, and switches among different pressure and heat transfer correlations depending on the fluid state. Pump modelling is based on maps of performance from operation data, whilst the steam turbine model is defined by Stodola cone law. Since the gas turbine transient performance is orders of magnitude faster than the steam cycle, a quasi-steady state model was used to provide the mechanical power output, and the temperature and pressure of the exhaust gas. Software to software validation at design and off-design operation demonstrated the accuracy and reliability of the dynamic NGCC model. A thorough description of the modelling approach and validation of the NGCC model is presented in the work by Montañés et al. [36].

2.2. Simplified models of the natural gas combined cycle

Good control strategies must be capable of anticipating the dominant dynamics of the system to maintain a stable and efficient operation. Therefore, the dominant dynamics of the system dictate the frequency of the control actions. For control strategies based on MPC, computational speed is the main limitation. As model predictive control
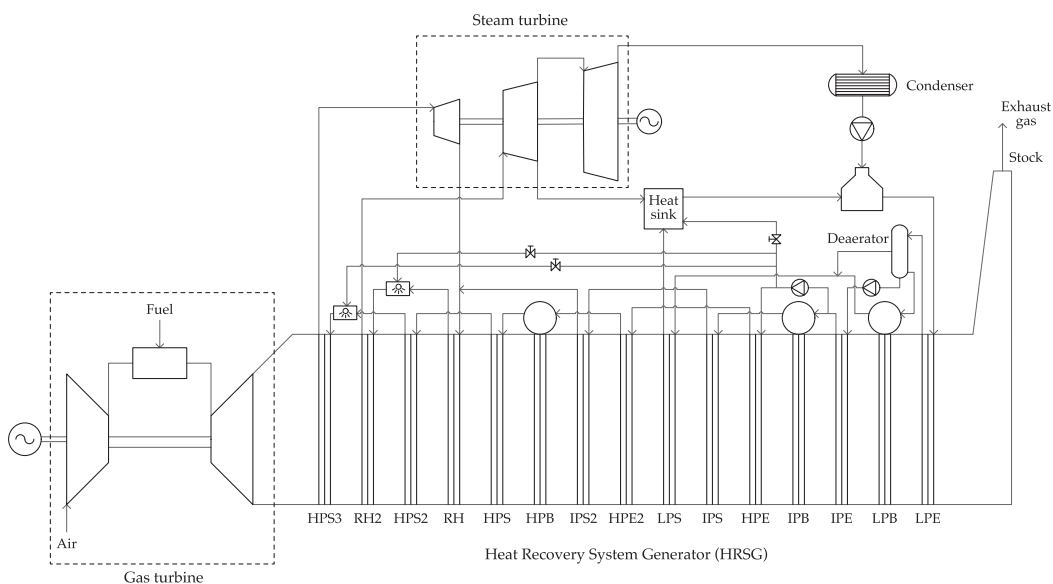

Fig. 1. Process model of the natural gas combined cycle. The nomenclature in the HRSG is as follows. E: Economizer, B: Boiler, S: Superheater, R: Reheater P: Pressure, L: Low, I: Intermediate, H: High.

relies on the periodic solution of a dynamic optimisation, fast dominant dynamics require fast online optimisation and control. The dominant dynamics of modern NGCCs with 600 MW power output occur approximately in 300 s. Thus, the control actions should be imposed every 15–30 s to anticipate and meet the transient operation of the power plant. A sampling time of 30 s was found as a reasonable trade-off between controllability and computational time for the dynamic optimisation. The dynamic high-fidelity model cannot be used in the MPC strategy because it would lead to excessively high optimisation times for online operation with current computational power, owing to its complexity. Simplified models that predict the behaviour of key thermodynamic variables in the power plant must be used instead.

Autoregressive models with exogenous variables (ARX) are linear data-based models that can predict the dynamic performance of a system. These models are suitable for dynamic optimisation because of their simplicity and accuracy within the training data range [37]. System identification was the approach followed to develop the ARX models and combined them in a local model network that can predict nonlinear behaviour with a set of linear local models [25,38].

The data to train and test the ARX models was obtained by superimposing random gaussian signals (RGS) in the controllers of the dynamic high-fidelity model in closed-loop [39–42]. Different sets of data were generated for each operation regime and variable, and least squares were used to fit the training data to the general ARX model structure:

$$y(t) + a_1 \, y(t-1) + \cdots + a_{n_y} \, y(t - n_y) =$$
$$b_1 \, U(t-1) + \cdots + b_{n_U} \, U(t - n_U) + e(t) \tag{1}$$

where n_y and n_U denote the order of the model, y represents the predicted variable, U are independent variables, and $e(t)$ is a white-noise term that enters in the regression as prediction error.

The operation regime defines the prediction range of each linear local model. Several local models are necessary to cover the operation range of a variable in the high-fidelity model, which normally exhibits nonlinear behaviour. A local model network combines the local models and interpolates their prediction according to the operating point of the NGCC. The interpolation is achieved by associating to each local model a validity function, which weights the contribution of the local models to the final output depending on the operating point. This approach ensures that neighbouring local models contribute more to the final output than local models for distant operation regimes [25,38]. Fig. 2 represents the structure of a generic local model network.

A Gaussian validity function was selected to interpolate the different local models of each variable [38]:

$$\xi_i(\gamma) = \frac{exp\left(-\frac{1}{2} \, [(\gamma - cv_i)/w_i]^2\right)}{\sum\limits_{k=1}^{M} exp\left(-\frac{1}{2} \, [(\gamma - cv_i)/w_i]^2\right)} \tag{2}$$

where cv_i and w_i are, respectively, the centres and widths of the local Gaussian interpolation functions.

The final output of the local model network is a combination of all local outputs:

$$\hat{y}(t) = \sum_{i=1}^{M} \hat{y}_i(\kappa) \, \xi_i(\gamma) \tag{3}$$

where M is the number of local models, $\hat{y}_i(\kappa)$ represents the outputs of the local ARX models under the conditions defined by the inputs κ, ξ is the local validity function associated to each ARX model, and γ is the parameter defining the current operating point.

In this work, the variable defining the operating point (γ) was the gas turbine load and 5 equidistant local models in the range 100–60% were defined for each of the predicted variables. The mechanical net power generation of the NGCC, and the superheated and reheated steam temperatures were the predicted variables using local model
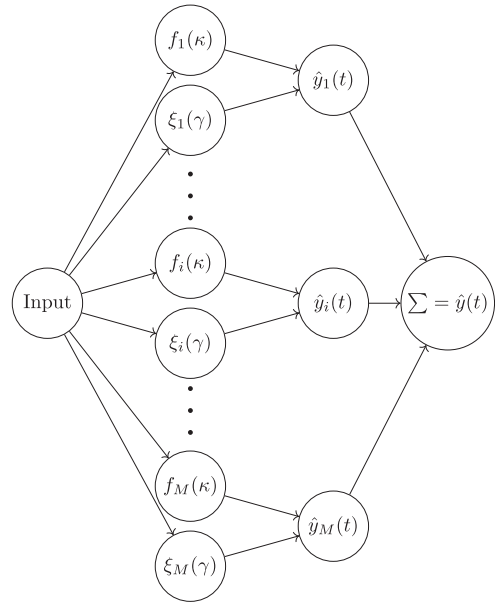
Fig. 2. Structure of a generic local model network.

networks. The parameters of the Gaussian validity function were selected by a nonlinear optimisation [25,38]. A screening of different model orders, n_y and n_U, defined the ARX model structure that better predicted the testing data for 1 and 20 steps-ahead prediction (Fig. 3).

In addition, simplified models for the saturation temperature and pressure in the steam drum and the inlet pressure in the steam turbine were also developed. Linear polynomials as in Eq. (4) are suitable models for these variables as they can be directly related to the gas turbine load.

$$\hat{y}(t) = a_0 + b_1 \, U(t-1) \tag{4}$$

Table 1 summarizes the structure and main validation results of the models implemented in the MPC strategy. From these results, accurate predictions can be expected throughout the time horizon in the dynamic optimisation.
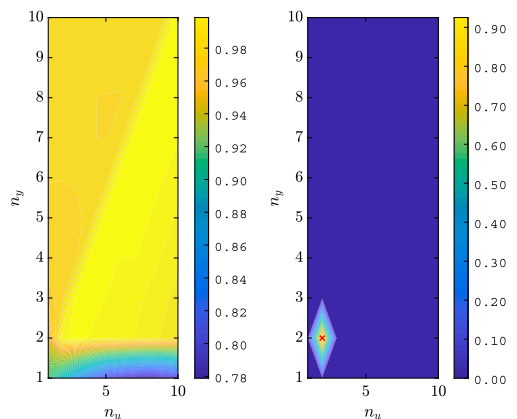
Fig. 3. Screening of different orders for the simplified model of the superheated steam temperature. One step-ahead prediction in the left and 20 step-ahead prediction in the right.

Table 1
Structure and 20 step-ahead validation results of the simplified models.

Variable	Model	Order	R_{20}^2
$\dot{W}_{net}$	LMN	(1,1)	99.95%
T_{SH}	LMN	(2,2)	76.97%
T_{RH}	LMN	(2,2)	92.82%
T_{drum}	Polynomial		86.16%
p_{drum}	Polynomial		85.22%
p_{turb}	Polynomial		86.62%

2.3. Stress modelling

Equipment with thick walls normally suffers the largest stresses in the thermal power plant. The main causes of these stresses are the large temperature gradients along the walls, the centrifugal forces due to rotation, and the high pressures this equipment must withstand. The high pressure drum and the rotor disk in the first stage of the high pressure steam turbine are arguably the most sensitive equipment in an NGCC [14,18]. Therefore, it is critical to ensure that the maximum allowable stress in those components is not exceeded during transient operation.

Thermal stresses depend on the temperature gradients along the wall. Thus, the temperature distribution is necessary to compute the thermal component of the stress in both drum and rotor. The temperature was assumed to vary exclusively in radial direction, reducing the modelling of the temperature distribution to the one-dimensional heat equation:

$$\frac{1}{r}\frac{\partial}{\partial r}\left(r\frac{\partial T}{\partial r}\right) = \frac{1}{\alpha}\frac{\partial T}{\partial t} \tag{5}$$

where T refers to the temperature difference respect to the equipment design temperature, r is a generic radius, and α is the thermal diffusivity of the material.

An implicit Crank-Nicolson scheme was used to discretize Eq. (5) and compute the temperature distribution along the walls. Different boundary conditions apply to the steam drum and rotor disk. The implementation of these boundary conditions and the mathematical development to express Eq. (5) as a linear system of equations are detailed in the work by Rúa et al. [15].

Stress modelling in the rotor and drum assumes plane strain and plane stress, respectively. These assumptions are valid because the longitudinal length of the steam drum is notably larger than in the other two directions, and negligible in the case of the rotor disk [43].

This work proposes and compares two different physical approaches to model the thermal and mechanical stresses with the considered assumptions. Both methods rely on the constitutive equations that relate the stress and strain, the strain-displacement relations, and the radial equilibrium equation. In addition, the mechanical stress due to the centrifugal force originated by the rotation enters as a body force, and the mechanical stress due to pressure appears as a boundary condition. The first modelling approach combines these equations to express the stress components in terms of the radial temperature distribution and the displacement. These expressions and a thorough description of the process to transform them in a linear system of equations can be found in the work by Rúa et al. and the supplementary material included therein [15].

In the second modelling approach, the ordinary differential equation obtained for the displacement is solved analytically. Thus, the displacement is not a computed variable and the stress components only depend on the temperature distribution, the rotational speed and the pressure. The stress components of the drum and rotor are defined in Eqs. (6) and (7), respectively.

$$\sigma_r = \left(1 - \frac{r_i^2}{r^2}\right)\frac{E\,\alpha}{(1+\upsilon)(1-2\upsilon)}\int_{r_i}^{r_o} rT\,dr - \frac{E\,\alpha}{(1-\upsilon)}\int_{r_i}^{r} rT\,d$$
$$r + \left[\frac{r_o^2 r_i^2}{(r_o^2-r_i^2)r^2} - \frac{r_o^2}{(r_o^2-r_i^2)}\right](p_o - p_i) - p_i \tag{6a}$$

$$\sigma_\theta = \left(1 + \frac{r_i^2}{r^2}\right)\frac{E\,\alpha}{(1-\upsilon)(r_o^2-r_i^2)}\int_{r_i}^{r_o} rT\,dr + \frac{E\,\alpha}{1-\upsilon}\left(\frac{1}{r^2}\int_{r_i}^{r} rT\,dr - T\right)$$
$$+ \left[\frac{r_o^2 r_i^2}{(r_o^2-r_i^2)r^2} + \frac{r_o^2}{(r_o^2-r_i^2)}\right](p_i - p_o) - p_i \tag{6b}$$

$$\sigma_z = \frac{2\upsilon E\,\alpha}{(r_o^2-r_i^2)(1-\upsilon)}\int_{r_i}^{r_o} rT\,dr - \frac{E\,\alpha}{1-\upsilon}T$$
$$+ p_i\left(\frac{2\upsilon r_o^2}{r_o^2-r_i^2} - 2\upsilon\right) - p_o\frac{2\upsilon r_o^2}{r_o^2-r_i^2} \tag{6c}$$

$$\sigma_r = \left[1 + \upsilon + \frac{(1-\upsilon)r_i^2}{r^2}\right]\frac{r_o^2}{(1+\upsilon)r_o^2 + (1-\upsilon)r_i^2}\left(\frac{E\,\alpha}{r_o^2}\int_{r_i}^{r_o} rT\,dr - p_o\right) - \frac{E\,\alpha}{r^2}\int_{r_i}^{r} rT\,dr + \frac{\rho\,\omega^2 r_o^2(1+\upsilon)}{8\left[(1+\upsilon)r_o^2 + (1-\upsilon)r_i^2\right]}\left[r_o^2(3+\upsilon) - r_i^2(1+\upsilon)\right]$$
$$+ \frac{\rho\,\omega^2}{8}\left[(1+\upsilon)r_i^2 - (3+\upsilon)r^2\right] + \frac{\rho\,\omega^2 r_o^2 r_i^2(1-\upsilon)}{8\,r^2\left[(1+\upsilon)r_o^2 + (1-\upsilon)r_i^2\right]}\left[r_o^2(3+\upsilon) - r_i^2(1+\upsilon)\right] \tag{7a}$$

$$\sigma_\theta = \left[1 + \upsilon - \frac{(1-\upsilon)r_i^2}{r^2}\right]\frac{r_o^2}{(1+\upsilon)r_o^2 + (1-\upsilon)r_i^2}\left(\frac{E\,\alpha}{r_o^2}\int_{r_i}^{r_o} rT\,dr - p_o\right) + E\,\alpha\left(\frac{1}{r^2}\int_{r_i}^{r_o} rT\,dr - T\right) + \frac{\rho\,\omega^2 r_o^2(1+\upsilon)}{8\left[(1+\upsilon)r_o^2 + (1-\upsilon)r_i^2\right]}\left[r_o^2(3+\upsilon) - r_i^2(1+\upsilon)\right]$$
$$+ \frac{\rho\,\omega^2}{8}\left[(1+\upsilon)r_i^2 - (1+3\upsilon)r^2\right] + \frac{\rho\,\omega^2 r_o^2 r_i^2(1-\upsilon)}{8\,r^2\left[(1+\upsilon)r_o^2 + (1-\upsilon)r_i^2\right]}\left[r_i^2(1+\upsilon) - r_o^2(3+\upsilon)\right] \tag{7b}$$

Table 2
Validation boundary conditions.

Component	Thermal Boundary Conditions				Mechanical Boundary Conditions		Rotation
	$T_{initial}$	Ramp	h_i	h_o	r_i	r_o	
Drum	340 [°C]	± 20	20000 [W/m²K]	0.065 [W/m²°C]	$p = 150$ [bar]	$p = 1$ [bar]	–
Rotor	590 [°C]	± 10	-	20000 [W/m²°C]	$u = 0$ [m]	$p = 140$ [bar]	3000 [rpm]

(a) von Mises equivalent stress along six equidistant radii of the drum.

(b) von Mises equivalent stress along six equidistant radii of the rotor disk.

Fig. 4. Validation results of the stress models for the two proposed approaches. *A* refers to the results obtained in ANSYS, Dis refers to the modelling approach based on computing the displacement, and Int to the approach based on applying the trapezoidal rule to the integrals in Eqs. (6) and (7).

Linear MPC requires that the models implemented in the dynamic optimisation problem are linear. Therefore, the trapezoidal rule was applied to Eqs. (6) and (7) so they can be expressed as a linear system of equations.

The von Mises equivalent, or effective, stress defined in Eq. (8) is a scalar measure of the overall effective stress, as it is combination of the different stress components. Therefore, a constraint is imposed on the von Mises equivalent stress in the optimisation problem to ensure that the maximum effective stress is not exceeded. A linearisation of the von Mises stress, defined in Eq. (9), is used in the linear MPC formulation.

$$\sigma_{eff}^2 = \sigma_r^2 + \sigma_\theta^2 + \sigma_z^2 - (\sigma_r \sigma_\theta + \sigma_\theta \sigma_z + \sigma_z \sigma_r) \tag{8}$$

$$\sigma_{eff}^2 = \sigma_{eff,0}^2 + \nabla \sigma_{eff,0}^2 \Delta\sigma + \mathcal{O}(\Delta x^2) \tag{9}$$

Model validation of the two approaches considered in this work was carried out with the specialized software ANSYS [44]. Table 2 summarizes the boundary conditions imposed to the models during the validation procedure. Structural steel was the material assumed for both drum and rotor as it has well-known properties. A comparison between the accuracy of both approaches is presented in Fig. 4.

3. Control methodology with stress monitoring

Natural gas combined cycles exhibit two different dominant dynamics. Gas turbines have negligible dynamics and can change their operation point within a few seconds. In contrast, the large metal mass of the heat recovery steam generator (HRSG) in the steam cycle limits its transient operation. The heat capacity of this bulk component leads to dominant dynamics between 10 and 20 min, depending on the size of the NGCC. Power generation is however not limited by the slow dynamics of the steam cycle as gas turbines can over- and under-shoot to compensate its slow response, leading to tight power generation control [15].

As power control relies mainly on the gas turbine, the steam cycle normally operates in sliding pressure mode due to the higher efficiency of this strategy [31,45]. This type of operation keeps the admission valves of the steam turbine close to fully open to maintain the volume flow constant whilst the pressure of the steam cycle can vary freely. Throttling at the inlet of the steam turbine is hence avoided until about 50% load, where it becomes necessary for the HRSG operation [31].

The control of the steam cycle between 100% and 50% load reduces to limiting the steam temperature at the inlet of the steam turbine, and

control of the fluid inventory and low pressure in the cycle. Both traditional PID controllers and more advanced MPC strategies can be used to ensure the adequate operation of the steam cycle [27–29,46]. In this work, inventory and low pressure control in the steam cycle was carried out by PID controllers [36], whereas MPC was implemented to control the power generation of the NGCC and limit the superheated and reheated steam temperature at the inlet of the steam turbine. Attemperator valves regulate the temperature of the steam at the inlet of the steam turbine, and the gas turbine load controls the power generation of the NGCC. In addition, stress monitoring and control was included in the MPC strategy to ensure that the maximum allowable stress in the high pressure drum and rotor disk were not exceeded during the transient operation of the NGCC. Stress levels close to the limit of the material impose restrictions on the load change of the gas turbine and may slow down the NGCC.

In some cases, stresses in different equipment might only be expressed as nonlinear models; whereas linear formulations are exclusively used in other applications. Therefore, both linear and nonlinear formulations of the dynamic optimisation problem in the MPC strategy are presented so any stress model can be implemented. This expands the applicability range of the proposed control methodology to any type of control problem with stress monitoring.

3.1. Linear MPC formulation

Linear MPC solves a dynamic quadratic programming (QP) problem every sampling time. The mathematical formulation of this optimisation problem is:

$$\min_{z \in \mathbb{R}^n} f(z) = \frac{1}{2} z^T Q z + d z \tag{10a}$$

subject to

$$A_{eq} z = B_{eq} \tag{10b}$$

$$A_{ineq} z \leqslant B_{ineq} \tag{10c}$$

$$z^{low} \leqslant z \leqslant z^{high} \tag{10d}$$

with

$$Q \succcurlyeq 0 \tag{10e}$$

Vector z represents the optimisation variables of the optimisation problem. These are the manipulated variables defining the control

actions (U in Eqs. (1) and (4)), the responses $\hat{y}$ associated to them, and the temperature distribution, stress components and linearised equivalent stress in the wall of the drum and rotor disk. Eq. (10d) includes the lower and upper bounds of these optimisation variables, including the maximum allowable stress that the material of the equipment can withstand.

The simplified models and the stress linear system of equations developed in Section 2 enter in the optimisation problem as linear equality constraints in Eq. (10b). This ensures that the solution respects the stress physics and the thermodynamic behaviour of the NGCC. Similarly, the limitation in the maximum load ramp of the gas turbine is implemented in Eq. (10c).

During the dynamic optimisation, the degrees of freedom, i.e. the manipulated variables of the system, are continuously modified until a set of optimisation variables z that minimizes the objective function defined by Eq. (10a) is obtained. Minimizing the difference between power generation and demand, and the deviation of the superheated and reheated steam temperature from their set-points were the objectives in this work. Q and d are a weight matrix and vector, respectively. The description of the matrices and vectors in Eq. (10) with the stress modelling approach including the displacement can be found in the work by Rúa et al. [15].

3.2. Nonlinear MPC formulation

The nonlinear programming (NLP) problem used in the nonlinear MPC strategy is mathematically formulated as:

$$\min_{z \in \mathbb{R}^n} f(z) \tag{11a}$$

subject to

$$c_{\text{eq}}(z) = 0 \tag{11b}$$

$$c_{\text{ineq}}(z) \leqslant 0 \tag{11c}$$

$$A_{\text{eq}}\, z = B_{\text{eq}} \tag{11d}$$

$$A_{\text{ineq}}\, z \leqslant B_{\text{ineq}} \tag{11e}$$

$$z^{\text{low}} \leqslant\ z\ \leqslant z^{\text{high}} \tag{11f}$$

where z represents the vector of optimisation variables with lower and upper bounds defined in Eq. (11f), c_{eq} and c_{ineq} are, respectively, nonlinear equality and inequality constraints, and Eqs. (11b) and (11c) are their linear counterparts. The objective function $f(z)$ defined in Eq. (11a) can be any linear or nonlinear function.

This mathematical formulation adds modelling flexibility as the simplified and stress models can enter the dynamic optimisation in Eqs. (11b) or (11d), and ensures that the physics of the system and the stresses are always met regardless of the linearity of the models. Eqs. (11c) and (11e) provide the same benefits with the inequality constraints.

The same simplified models and linear system of equations describing the stresses were implemented in the nonlinear optimisation problem to compare the linear and nonlinear MPC formulation and the two proposed approaches to model the stresses in the drum and rotor disk. Therefore, the simplified models enter as a linear equality constraint in Eq. (11d) and the constraint in the gas turbine load ramp as a linear inequality constraint in Eq. (11e). In the NLP problem, the von Mises equivalent stress defined in Eq. (8) is used instead of the linearized version defined in Eq. (9) and implemented in the QP problem. This model represents a nonlinear constraint in the nonlinear dynamic optimisation problem.

Albeit the only difference between the linear and nonlinear MPC formulation is the utilization of a different equation to calculate the equivalent von Mises stress, the optimisation problem changes notably. In the QP optimisation problem, the linearized von Mises equivalent stress is expressed together with the models of the temperature

distribution, displacement (if the first modelling approach is considered) and stress components in a linear system of equations. All these variables are hence optimisation variables since this system of equations is implemented in the optimisation problem as a linear equality constraint. In contrast, the only optimisation variable in the NLP problem is the von Mises equivalent stress. As the nonlinear inequality constraint in Eqs. (11c) does not require an entire system of equations, only the variables of interest may be defined as optimisation variables.

Therefore, the QP optimisation problem in the linear MPC formulation has more optimisation variables than the NLP problem. However, checking whether the nonlinear constraints are satisfied requires more evaluations of the stress models than in the QP problem. Section 4 illustrates which of these two optimisation problems, and thus MPC formulations, leads to better computational performance.

4. Results and discussion

Linear and nonlinear MPC with stress control differ on the number of optimisation variables and how evaluate the stress models. The computational performance of the QP and NLP optimisation problems is crucial for the utilization of MPC as control strategy due to the limited time to carry out the dynamic online optimisation. Thus, the computational time required by both formulations with the two stress modelling approaches proposed in this work was compared for a single optimisation.

The proposed control methodology was also tested in a case study where tight limitations on the maximum allowable stress in the drum were included. This reduced the operational margin of the NGCC and forced the MPC controller to adequate the control actions imposed on the manipulated variables. These scenarios are specially relevant in power markets dominated by the large deployment of renewable energy sources, where thermal power plants will most likely balance the grid, leading to more frequent start-ups, shut-downs and faster load ramps that will narrow the operational limits.

4.1. Computational time analysis

A dynamic optimisation with the simplified models defined in Section 2 and a time horizon of 30 sampling times was the test case used to compare the computational time of the QP and NLP optimisation problem. In addition, the stress models defined with the two proposed approaches were included in order to compare their effect on the computational cost. Table 3 summarizes the computational time for each formulation and stress modelling approach relative to the fastest optimisation.

Quadratic programming shows superior computational performance independently of the stress modelling that is implemented. This demonstrates that, albeit having less optimisation variables, the evaluation of the objective function gradients and the stress models as nonlinear constraints suppose big penalties on the computational cost that lead to longer computational times. The gradients of the objective function in the QP optimisation problem are computed analytically, whilst in the NLP case the gradients are calculated numerically by finite differences. This leads to an increase of performance of the linear formulation. As a result, linear MPC can carry out more optimisations in a

Table 3
Relative computational time for the both MPC formulations and stress modelling approaches. Disp refers to the stress model based on the displacement calculation and Int to the integral stress model.

Formulation	Linear		Nonlinear	
Stress Model	Disp	Int	Disp	Int
Relative Time	1.88	1	41.02	27.19

given period of time, which allows to increase the time horizon during the optimisation, reduce the sampling time, or include more models in the constraints of the QP problem. These modifications would result in tighter and more frequent control actions that would improve performance of the power plant, and could expand the stress monitoring to other components that can also be critical in scenarios such start-ups and shut-downs.

The stress modelling approach does not have a strong effect on the computational time. The model based on the integral definitions of the stress components leads to slightly faster results than those obtained from the model additionally computing the displacement. This behaviour may be explained by the reduction of optimisation variables in the integral-based approach as the displacement is not computed. However, this approach leads to denser matrices in the linear system of equations than those obtained with the displacement-based approach, which are more sparse. The number of spatial discretizations along the wall of the components is also different for each of these two modelling approaches. Since the matrices obtained from the integral stress equations are denser due to the extra analytical development integrating the ordinary differential equations, they have more information and hence less spatial discretizations are needed. In contrast, the sparsity of the matrices obtained from the displacement-based models require more discretizations to capture the physics on the wall of the drum and rotor. Therefore, the computational time of the dynamic optimisation is affected by the number of spatial discrezations. Because of their similar accuracy (see Fig. 4), the relative small difference in computational time, and the difference in space discretizations needed by each model, both stress modelling approaches are suitable for utilization in MPC strategies.

4.2. Flexible operation with stress limitation

A load step change of 25% was the selected scenario to test the control methodology proposed in this work. This simulates a reduction in the power demand of 165 MW that the NGCC needs to compensate by decreasing its power generation as fast as possible without exceeding the maximum allowable stress in the steam drum and rotor disk, and limiting the maximum temperature at the inlet of the steam turbine.

These operational limitations were implemented in the optimisation problem of the MPC strategy as the objective function and constraints (see Section 3). The weights in the matrix Q and vector d of the objective function used in this simulation were $\lambda_{y_1} = 1$ for the power generation, and $\lambda_{y_2} = \lambda_{y_3} = 10$ for the temperature deviations from the set-point. The penalties in the manipulated variables, i.e. gas turbine load and attemperator valves, were $\lambda_{U_1} = \lambda_{U_2} = \lambda_{U_3} = 2$. The time horizon was 30 to guarantee that the system dynamics were captured, and a sampling time of 30 ensured that the control actions were implemented with enough frequency to anticipate the dominant dynamics of the system. For the stress models of the high pressure drum and rotor disk, 200 and 50 spatial discretizations were selected, respectively, whilst 3 time discretizations per sampling time were used.

Table 4 summarizes the physical and mechanical properties considered for the drum and rotor disk [47]. Since the maximum allowable stress presented in Table 4 was not reached with a realistic value during the considered scenario, a reduced value of the yield stress of 125 MPa was used to demonstrate the capability of the control methodology to predict the stress and adapt the operation of the power plant. Both simulations limited the maximum gas turbine load ramp to 15% per minute. Table 5 includes the lower and upper bounds of the optimisation variables.

Stress constraints may notably affect the operation of thermal power plants. Fig. 5 shows how the maximum allowable stress in the high pressure steam drum slows down the reduction in mechanical power generation. Lower limits in the equivalent stress of the equipment reduce the operating region of the NGCC. The MPC strategy is still able to compute optimal control sequences but the power ramp down is slower than in the case with looser constraints. Fig. 6 presents the two optimal load profiles of the gas turbine that the MPC computed for the two scenarios with different stress limits on the steam drum. Albeit the gas turbine load varies identically in the first seconds, the stress development due to the transient operation of the NGCC forces the MPC strategy to reduce the rate of change of the gas turbine load and hence the reduction of power generation.

The stress in three equidistant radii of the wall of the steam drum and rotor disk during the change of operation of the NGCC is represented in Figs. 7 and 8, respectively. Lower stress limits change the stress development profiles in the wall of this equipment because of the different transient operation determined by the MPC strategy. Fig. 7 illustrates how the dynamic optimisation problem in the MPC strategy reaches the maximum allowable stress constraint in the drum, which is active during 300–400 s, thus inhibiting larger changes in the gas turbine load and slowing the transient operation of the NGCC. The stress profile where the maximum allowable stress is 190 MPa (black lines) demonstrates that higher limits on the material allow larger stress developments and enhance the flexible operation of the NGCC. Therefore, the power plant can ramp down faster and meet the power demand in less than 300 s by under-shooting the gas turbine to compensate the slowness of the steam cycle.

Both the stress estimated during the optimisation in the MPC strategy and the exact stress computed with the true temperature and pressure profiles are compared in Figs. 7 and 8. The stress prediction during the dynamic optimisation captures the tendency of the stress development, as the different between the true stress and this prediction is small. However, the stress models over-predict the effective stress when the transient operation starts, specially in the steam drum. This behaviour may be explained by the lack of detailed data of the temperature distribution in the high-fidelity NGCC model, which forces the MPC controller to estimate the initial temperature along the walls of the equipment and provide this information to the dynamic optimisation problem. Stress prediction during the control of the NGCC operation would improve if the actual temperature distribution was provided by the detailed dynamic model of the NGCC.

Temperature control is also affected by the limitations imposed by the maximum allowable stress. Figs. 9 and 10 show the different temperature profiles obtained during the two test cases. Tighter stress limits lead to slower ramps in the gas turbine and more progressive changes in the steam cycle. Slower temperature variations are thus observed in the superheated and reheated steam. Consequently, tighter limits on the effective stress in the equipment of the NGCC ease the temperature control. Nevertheless, the proposed MPC strategy can rapidly limit the steam temperature variation without exceeding the temperature limitations in both test cases.

Table 4
Physical and mechanical properties of the materials considered for the drum and rotor disk.

Component	Material	ρ [kg/m³]	C_m [J/kg K]	k_m [W/m K]	α^* [m²/s]	α [1/K]	E [MPa]	υ [—]	h_o [W/m² K]	h_i [W/m² K]	Yield stress [MPa]
Drum	SA-515 Grade 70	7850	434	47	$1.3796e-05$	$1.36e-5$	178000	0.3	5000	0.065	190
Rotor	X18CrMnMoNbVN12	7700	460	29	$8.1875e-06$	$1.25e-5$	127000	0.292	4000	–	69

Table 5
Lower and upper bounds of the optimisation variables.

	LMN			Drum			Rotor	
Lower	Variable	Upper	Lower	Variable	Upper	Lower	Variable	Upper
400	$\dot{W}$	615.867	$-\infty$	T_{wall}	∞	$-\infty$	T_{wall}	∞
-10	T_{SH}	15	-0.001	u	0.001	-0.001	u	0.001
-10	T_{RH}	15	$-\infty$	σ_r	∞	$-\infty$	σ_r	∞
$-\infty$	p_{turb}	∞	$-\infty$	σ_θ	∞	$-\infty$	σ_θ	∞
$-\infty$	T_{drum}	∞	$-\infty$	σ_z	∞	0	σ_{eql}	69
$-\infty$	p_{drum}	∞	0	σ_{eql}	190/125			
60	U_1	100						
-0.01655	U_2	0.97345						
-0.06882	U_3	0.92188						

Fig. 5. Mechanical power generation with different stress constraints in the drum.
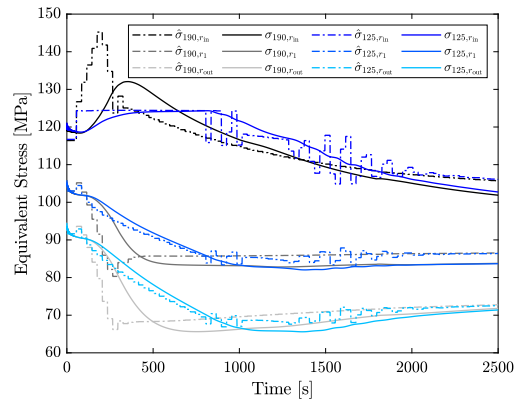
Fig. 6. Gas turbine load profile with different stress constraints in the drum.

Fig. 7. Equivalent stress in the high pressure steam drum along three equidistant radii.
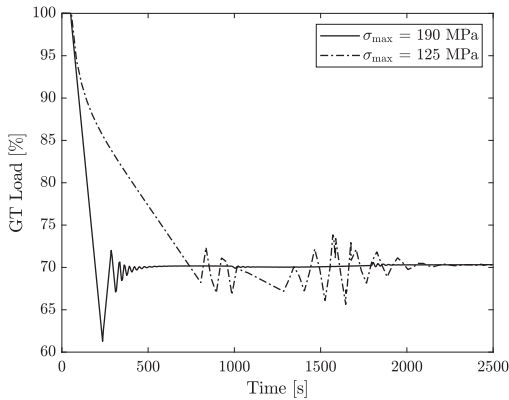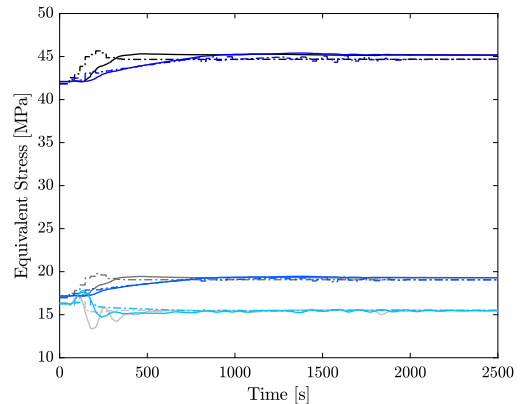
Fig. 8. Equivalent stress in the high pressure rotor disk along three equidistant radii.

5. Conclusions

Thermal power plants will need to ramp faster and more frequently to balance the intermittent power generation from renewable energy sources in the future energy sector. Gas turbine load ramps and thermal stresses limit the power generation rate. This work addresses both limitations by proposing a control strategy based on model predictive control with stress monitoring.

Two modelling approaches for the stresses in the walls of the high pressure steam drum and the rotor disk of the first stage of the steam turbine were proposed. Furthermore, both linear and nonlinear MPC formulations were described to cover all possible control problems and modelling approaches of the stresses in different equipment. Local model networks of simplified models were also developed to predict specific thermodynamic variables of the NGCC during the dynamic optimisation.

A comparison of the computational cost of the linear and nonlinear dynamic optimisation problems proved the superior performance of the linear MPC formulation. Nonlinear MPC requires more evaluations of
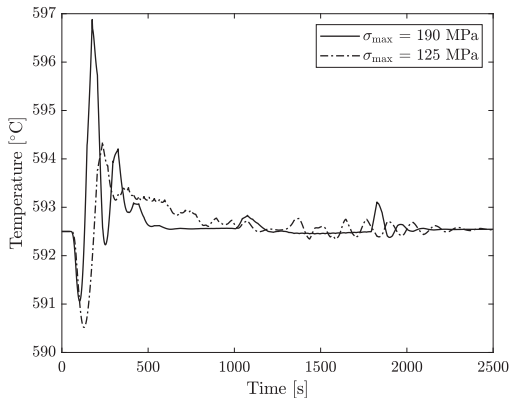
Fig. 9. Superheated steam temperature with different stress constraints in the drum.
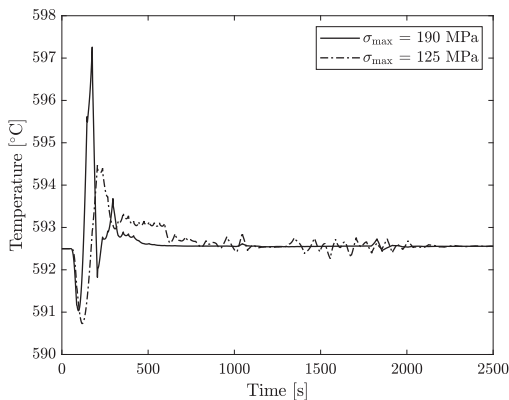
Fig. 10. Reheated steam temperature with different stress constraints in the drum.

the stress models than the linear formulation to compute numerically the gradients of the optimisation problem by finite differences, leading to longer computational times despite having less optimisation variables. Thus, linear MPC is more advantageous when is possible to employ linear models to predict the thermodynamic variables of the NGCC and the stress development in the walls of the selected equipment. It is possible to resort to nonlinear MPC when modelling of the stresses or simplified models cannot be carried out with linear formulations.

The two proposed modelling approaches to estimate the equivalent stress in the walls of the steam drum and rotor disk proved similar accuracy during their validation. Both stress models led to similar computational times during the dynamic optimisation. The difference showed in Table 3 is originated by the different spatial discretizations. Since these two modelling approaches lead to linear system of equations with different sparsity in the matrices, different spatial discretizations are required. However, both models result in similar computational time for equivalent accuracy, pointing out that the distinguishing factor is the linearity of the optimisation problem.

To test the controlling capability of the proposed MPC methodology, two test cases with different maximum allowable stresses in the steam drum were studied. The stress limit in the first case assumed maximum stresses according to the utilization of modern alloys, whilst the second test case imposed tight limits on the maximum stress to ensure that this limit was reached. The MPC strategy with stress monitoring was able to compute the optimal control actions without exceeding the imposed

constraints. The gas turbine ramp rate limited the operation in the first case as the stress limits were not reached. In the second test, the constraint on the effective stress was active during a period of time. These two studies demonstrate the suitability of the proposed MPC strategy to optimally control flexible NGCC with stress monitoring.

Low stress limits reduce the power generation flexibility of the NGCC. When the maximum allowable stress was reached, the control strategy decreased the gas turbine load ramps to ensure that larger temperature gradients did not arise. As a result, the load change required more time compared to the test case where stress limits for modern alloys were considered.

Temperature control was also accomplished with the MPC methodology, limiting the maximum temperature variation to below 5 °C. Lower stress limits eased the control of the superheated and reheated steam temperature. Since lower maximum allowable stress constraints lead to slower ramp rates, the temperature fluctuation in the steam was reduced.

This work proposes a optimal control methodology with both linear and nonlinear formulations for control of flexible thermal power plants with stress monitoring. Overall, this study demonstrates that (1) MPC is an adequate control strategy to include stress monitoring; (2) both linear and nonlinear formulations can limit the maximum effective stress in different components, and thus the proposed methodology can be applied to any geometry (e.g. turbine blades and rotor, steam turbine casings, piping, headers) and power system; and (3) the linear formulation shows superior computational performance and should be preferred over the nonlinear case if linear stress models are available. Furthermore, the proposed MPC methodology with stress monitoring can be applied to start-ups and shut-downs, as these are procedures where large stresses arise owing to the large temperature gradients.

Acknowledgements

References

[1] IPCC, Climate Change 2014: Synthesis Report, Contribution of Working Groups I, II and III to the Fifth Assessment Report of the Intergovernmental Panel on Climate Change [Core Writing Team, R.K. Pachauri and L.A. Meyer (eds.)], IPCC, Geneva, Switzerland; 2014.

[2] IPCC, Summary for Policymakers. In: Global warming of 1.5 C. An IPCC Special Report on the impacts of global warming of 1.5 C above pre-industrial levels and related global greenhouse gas emission pathways, in the context of strengthening the global response to the threat of climate change, sustainable development, and efforts to eradicate poverty, [Masson-Delmotte V, Zhai P, Pörtner HO, Roberts D, Skea J, Shukla PR, et al., editors]. World Meteorological Organization, Geneva, Switzerland; 2018.

[3] International Energy Agency - IEA, World Energy Outlook 2018: Executive Summary, <https://webstore.iea.org/download/summary/190?fileName=English-WEO-2018-ES.pdf>; 2018.

[4] European Commission, Energy Roadmap 2050. <https://eur-lex.europa.eu/LexUriServ/LexUriServ.do?uri=COM:2011:0885:FIN:EN:PDF>; 2011.

[5] Heuberger CF, Rubin ES, Staffell I, Shah N, Mac Dowell N. Power capacity expansion planning considering endogenous technology cost learning. Appl Energy 2017;204:831–45.

[6] Bertsch J, Growitsch C, Lorenczik S, Nagl S. Flexibility in Europe's power sector: an additional requirement or an automatic complement? Energy Econ 2016;53:118–31.

[7] Huber M, Dimkova D, Hamacher T. Integration of wind and solar power in Europe: assessment of flexibility requirements. Energy 2014;69:236–46.

[8] Kondziella H, Bruckner T. Flexibility requirements of renewable energy based electricity systems–a review of research results and methodologies. Renew Sustain Energy Rev 2016;53:10–22.

[9] Monta nés RM, Korpås M, Nord LO, Jaehnert S. Identifying operational requirements for flexible CCS power plant in future energy systems. Energy Proc 2016;86:22–31.

[10] Eser P, Chokani N, Abhari R. Operational and financial performance of fossil fuel power plants within a high renewable energy mix. J Global Power Propul Soc

2017;1:16–27.

[11] González-Salazar MA, Kirsten T, Prchlik L. Review of the operational flexibility and emissions of gas-and coal-fired power plants in a future with growing renewables. Renew Sustain Energy Rev 2017;82:1497–513.

[12] IEACCC - International Energy Agency Clean Coal Centre, Power plant design and managment for unit cycling, <https://www.iea-coal.org/>; 2019.

[13] Hentschel J, Spliethoff H, et al. A parametric approach for the valuation of power plant flexibility options. Energy Rep 2016;2:40–7.

[14] Alobaid F, Mertens N, Starkloff R, Lanz T, Heinze C, Epple B. Progress in dynamic simulation of thermal power plants. Prog Energy Combust Sci 2017;59:79–162.

[15] Rúa J, Agromayor R, Hillestad M, Nord LO. Optimal dynamic operation of natural gas combined cycles accounting for stresses in thick-walled components. Appl Therm Eng 2020;114858.

[16] Kim T, Lee D, Ro S. Analysis of thermal stress evolution in the steam drum during start-up of a heat recovery steam generator. Appl Therm Eng 2000;20(11):977–92.

[17] Alobaid F, Postler R, Ströhle J, Epple B, Kim H-G. Modeling and investigation start-up procedures of a combined cycle power plant. Appl Energy 2008;85(12):1173–89.

[18] Gülen SC, Kim K. Gas turbine combined cycle dynamic simulation: a physics based simple approach. J Eng Gas Turb Power 2014;136(1):011601.

[19] Taler J, Dzierwa P, Taler D, Harchut P. Optimization of the boiler start-up taking into account thermal stresses. Energy 2015;92:160–70.

[20] Taler J, Weglowski B, Taler D, Sobota T, Dzierwa P, Trojan M, et al. Determination of start-up curves for a boiler with natural circulation based on the analysis of stress distribution in critical pressure components. Energy 2015;92:153–9.

[21] Bausa J, Tsatsaronis G. Dynamic optimization of startup and load-increasing processes in power plants - Part I: method. J Eng Gas Turb Power 2001;123(1):246–50.

[22] Bausa J, Tsatsaronis G. Dynamic optimization of startup and load-increasing processes in power plants - Part II: application. J Eng Gas Turb Power 2001;123(1):251–4.

[23] Shirakawa M, Nakamoto M, Hosaka S. Dynamic simulation and optimization of start-up processes in combined cycle power plants. JSME Int J Ser B Fluids Therm Eng 2005;48(1):122–8.

[24] Albanesi C, Bossi M, Magni L, Paderno J, Pretolani F, Kuehl P, et al. Optimization of the start-up procedure of a combined cycle power plant. In: Decision and control, 2006 45th IEEE Conference on, IEEE; 2006. p. 1840–45.

[25] Prasad G, Swidenbank E, Hogg B. A local model networks based multivariable long-range predictive control strategy for thermal power plants. Automatica 1998;34(10):1185–204.

[26] Prasad G, Swidenbank E, Hogg B. A neural net model-based multivariable long-range predictive control strategy applied in thermal power plant control. IEEE Trans Energy Convers 1998;13(2):176–82.

[27] Peng H, Ozaki T, Toyoda Y, Oda K. Exponential ARX model-based long-range predictive control strategy for power plants. Control Eng Pract

[28] Peng H, Wu J, Inoussa G, Deng Q, Nakano K. Nonlinear system modeling and predictive control using the RBF nets-based quasi-linear ARX model. Control Eng Pract 2009;17(1):59–66.

[29] Lu S, Hogg BW. Predictive co-ordinated control for power-plant steam pressure and power output. Control Eng Pract 1997;5(1):79–84.

[30] Sindareh-Esfahani P, Tabatabaei SS, Pieper JK. Model predictive control of a heat recovery steam generator during cold start-up operation using piecewise linear models. Appl Therm Eng 2017;119:516–29.

[31] Kehlhofer R, Hannemann F, Rukes B, Stirnimann F. Combined-cycle gas & steam turbine power plants. Pennwell Books; 2009.

[32] Thermoflow, GT PRO 24.0, Thermoflow Inc.

[33] Modelon, Thermal Power Library, <https://www.modelon.com/library/thermal-power-library/>.

[34] Dassault Systemes, <https://www.3ds.com/products-services/catia/products/dymola/>.

[35] Modelica Association, <https://www.modelica.org/>.

[36] Monta nés RM, GarDarsdóttir SÓ, Normann F, Johnsson F, Nord LO. Demonstrating load-change transient performance of a commercial-scale natural gas combined cycle power plant with post-combustion CO2 capture. Int J Greenhouse Gas Control 2017;63:158–74.

[37] Ljung L. System identification: theory for the user. Prentice-hall; 1987.

[38] Johansen TA, Foss B. Constructing NARMAX models using ARMAX models. Int J Control 1993;58(5):1125–53.

[39] Gevers M, Ljung L. Optimal experiment designs with respect to the intended model application. Automatica 1986;22(5):543–54.

[40] Gevers M. Identification for control: from the early achievements to the revival of experiment design. Eur J Control 2005;11:1–18.

[41] Gevers M, Mišković L, Bonvin D, Karimi A. Identification of multi-input systems: variance analysis and input design issues. Automatica 2006;42(4):559–72.

[42] Mišković L, Karimi A, Bonvin D, Gevers M. Closed-loop identification of multi-variable systems: with or without excitation of all references? Automatica 2008;44(8):2048–56.

[43] Timoshenko S, Goodier JN. Theory of elasticity. McGraw-Hill book Company; 1951.

[44] ANSYS, ANSYS Academic Research Thermal and Mechanical, Release 19.2, ANSYS Inc.

[45] Jonshagen K, Genrup M. Improved load control for a steam cycle combined heat and power plant. Energy 2010;35(4):1694–700.

[46] Aske EMB, Skogestad S. Consistent inventory control. Industr Eng Chem Res 2009;48(24):10892–902.

[47] Viswanathan R, Bakker W. Materials for ultrasupercritical coal power plants - turbine materials: Part II. J Mater Eng Perform 2001;10(1):96–101.

Publication IV

Renewable energy sources have been the focal point to decarbonise the power sector. The large deployment of these intermittent power generation units requires mechanisms to balance the grid. Thermal power plants can provide this service by increasing the number of start-ups, shut-downs, and intraday ramps at the expense of higher deterioration in critical equipment, including high-pressure steam drums, turbine rotors and blades, and high-temperature heat exchangers and pipes. This work proposes a method to formulate the power generation scheduling of thermal power plants as a stochastic optimisation problem with limitations on the maximum damage in critical components. This method models the uncertainty associated with intermittent power generation from renewable sources with a scenario-tree whilst computing the deterioration of the equipment in each scenario to limit the maximum damage. Scheduling of a flexible natural gas combined cycle demonstrated how this methodology can reduce the deterioration of the superheating heat exchanger of the power plant with minimum detriment in power generation and revenue. Furthermore, the effect of the design temperature of the material on the total damage was analysed for a broad range of temperatures and operating profiles, showing how adequate selection of design temperature can reduce the deterioration of the equipment and enhance its lifetime.

Optimal scheduling of flexible thermal power plants with lifetime enhancement under uncertainty

Jairo Rúa [a],[*], Adriaen Verheyleweghen [b], Johannes Jäschke [b], Lars O. Nord [a]

[a] Department of Energy and Process Engineering, Norwegian University of Science and Technology, Trondheim, Norway
[b] Department of Chemical Engineering, Norwegian University of Science and Technology, Trondheim, Norway

ARTICLE INFO

ABSTRACT

Renewable energy sources have been the focal point to decarbonise the power sector. The large deployment of these intermittent power generation units requires mechanisms to balance the grid. Thermal power plants can provide this service by increasing the number of start-ups, shut-downs, and intraday ramps at the expense of higher deterioration in critical equipment, including high-pressure steam drums, turbine rotors and blades, and high-temperature heat exchangers and pipes. This work proposes a method to formulate the power generation scheduling of thermal power plants as a stochastic optimisation problem with limitations on the maximum damage in critical components. This method models the uncertainty associated with intermittent power generation from renewable sources with a scenario-tree whilst computing the deterioration of the equipment in each scenario to limit the maximum damage. Scheduling of a flexible natural gas combined cycle demonstrated how this methodology can reduce the deterioration of the superheating heat exchanger of the power plant with minimum detriment in power generation and revenue. Furthermore, the effect of the design temperature of the material on the total damage was analysed for a broad range of temperatures and operating profiles, showing how adequate selection of design temperature can reduce the deterioration of the equipment and enhance its lifetime.

1. Introduction

The decarbonisation of the power sector is a fundamental measure to reduce global anthropogenic greenhouse gas emissions and mitigate climate change [1,2]. There exists a broad portfolio of technologies that can deliver low-carbon electricity whilst meeting the increasing power demand associated with the growing population and electrification of other economic sectors. Among the different available alternatives, renewable energy sources, mainly wind and solar, have concentrated most of the efforts to reduce CO_2 emissions in this sector [2]. However, it is also recognised that the intermittent power generation nature of these renewable energy sources requires an heterogeneous and flexible power system to balance such variability and guarantee reliable, clean and efficient generation of electricity [3–5].

Thermal power plants, especially natural gas combined cycles (NGCCs), are expected to play a fundamental role in the future power sector since they can accommodate large power fluctuations in a short period of time [6,7]. These power plants are thus arguably considered as an important complement for intermittent renewable energy sources.

Furthermore, if carbon capture and storage (CCS) is integrated with thermal power plants, low carbon electricity can be provided whilst balancing the power grid [8].

In a power system dominated by rapid and large deployment of renewable energy, thermal power plants will face more frequent start-ups and shut-downs, and faster ramping rates in order to balance the grid [6,9,10]. This aggressive operation will originate larger and more periodic thermal and mechanical stresses in the equipment of thermal power plants, which may lead to irreversible damages if the maximum stress limits of the material are exceeded. High-pressure steam drums, boiler tubes with superheated and reheated steam, headers, and first-stage rotor disks, blades and casings of high-pressure steam turbines are some of the equipment that endures the highest stress levels during start-ups, shut-downs and ramping operation [11–19].

There are several procedures and control methodologies to avoid exceeding the maximum allowable stresses in these critical components. Bypassing a fraction of the flue gas is a common and effective start-up procedure to limit the maximum stress in the steam drums and boiler tubes during the start-up of a power plant, as it reduces the temperature gradient in the walls and hence the effective stress peaks [13,15]. This

Nomenclature

Latin symbols

a	Coefficients of polynomials [–]
b	Coefficients of polynomials [–]
C	Specific heat capacity [J/kg K]
D	Damage [–]
d	Uncertainty realisation [–]
E	Young's Modulus [MPa]
E^*	Non-anticipativity matrix [-]
h	Convection coefficient [W/m^2 K]
k	Heat conduction coefficient [W/m K]
M	Number of uncertainty realisations [–]
N_r	Robust time horizon [–]
N	Time horizon [–]
n	Number of cycles [–]
P	Price [–]
p	Pressure [MPa]
r	Radius m
S	Number of scenarios [–]
T^*	Temperature deviation from design [°C]
T	Temperature [°C]
t	Time [s]
u	Manipulated variable [–]
x	Estimated thermodynamic variables [–]

Greek symbols

α	Thermal diffusivity [m^2/s]
α^*	Thermal expansion coefficient [1/K]
$\Delta \varepsilon$	Strain amplitude [m]
ω	Scenario weights [–]
ρ	Density [kg/m^3]

σ	Stress [MPa]
σ'_f	Tensile strength coefficient [MPa]
υ	Poisson's ratio [–]
ε	Strain [–]
ε'_f	Ductility coefficient [–]

Subscripts

θ	Tangential direction
creep	Creep damage
design	Design
e	Elastic
eff	Effective stress
exp	Experimental
f	Failure
fatigue	Fatigue damage
i	Inner radius
ineq	Inequality
init	Initial conditions
m	Metal
max	Maximum
o	Outer radius
oper	Operation
p	Plastic
r	Radial direction
wall	Wall of the tubes
z	Longitudinal direction

Superscripts

b	Elastic fitting parameter
c	Plastic fitting parameter
low	Lower bound
up	Upper bound

enables the control of the heating rate within the boiler, which can be progressively modified to achieve faster warm-ups with limited maximum stresses [16,17]. A similar procedure is followed in the steam turbine, where the steam is initially bypassed to accommodate the warm up of the steam turbine and avoid excessively high thermal stresses [14,15,19]. The maximum allowable stress in this critical equipment can also be embedded in optimisation-based control strategies so the constraints imposed by the material can be considered when computing the control actions [20,21]. Therefore, this type of methodologies allow computation of optimal control sequences that never exceed the maximum stress levels the equipment can tolerate and enhance the flexible operation of thermal power plants.

Nevertheless, regular operation induces damage in the equipment of thermal power plants that reduces its lifetime even if these procedures and control strategies keep the stress levels within safe limits. Creep and fatigue are arguably the main damage mechanisms that initiate and grow cracks in highly loaded components, ultimately leading to lack of reliability and failures due to fractures or large deformations [11,12]. Creep refers to the damage originated by the continuous operation at specific temperature and stress levels, which can result in deformations in the short term, and crack growth and cavitation in the long term [12,22,23]. Fatigue is the progressive and persistent structural damage originating from cyclic loading in the material [11,12,24]. Low-cycle fatigue occurs in the components of thermal power plants that operate at high temperature and pressure (e.g. headers, superheater and reheater tubes, steam turbine rotors), whereas high-cycle fatigue affects the equipment that experiences vibration (e.g. turbomachinery components) [11,12,25]. Additional damage phenomena that can affect the residual lifetime operation of thermal power plants are corrosion, embrittlement, oxidation, pitting and erosion [11].

Damage and degradation of thermal power plant components are normally generated by a combination of mechanisms. Barella et al. [26] studied the failure of a steam turbine rotor with finite element methods (FEMs), concluding that high thermal stress concentration initiated the cracks that were propagated by mechanical fatigue. Similar crack developments can be observed in the failure of steam turbine blades [27]. Mechanical fatigue is also the propagation mechanism of the crack, whereas crack initiation can occur by corrosion. Creep is another damage phenomena that can initiate cracks in the rotors of steam turbines because of the high temperatures and stresses this type of components must withstand. Thus, the combination of creep and fatigue is a common failure mechanism in steam turbines [12,28,29]. Creep and creep-fatigue damage is also typical in the tubes of superheaters and reheaters because of their operating conditions, with high inner and outer temperatures and high pressure steam flowing inside the tubes. Furthermore, these components experience large and frequent temperature gradients owing to the ramping operation of thermal power plants, which generates larger stresses and more cyclic loading that enhance the damage through creep and thermo-mechanical fatigue [30]. The operation profile hence influences the damage in the equipment and its lifetime reduction. Benato et al. [31,32] compared different flexible operation profiles for a three pressure level heat recovery steam generator (HRSG) and a combined cycle, and observed that the faster ramp rates substantially increased the degradation of the superheater tubes. These components are also sensitive to the composition of the exhaust gas as it may contain chemical components that generate hot corrosion in the presence of certain elements, which results in wall thinning and premature failure without the adequate maintenance [33].

Whilst the limitation of maximum stress levels occurs in the short timescales (i.e. orders of seconds and minutes) and depends on the
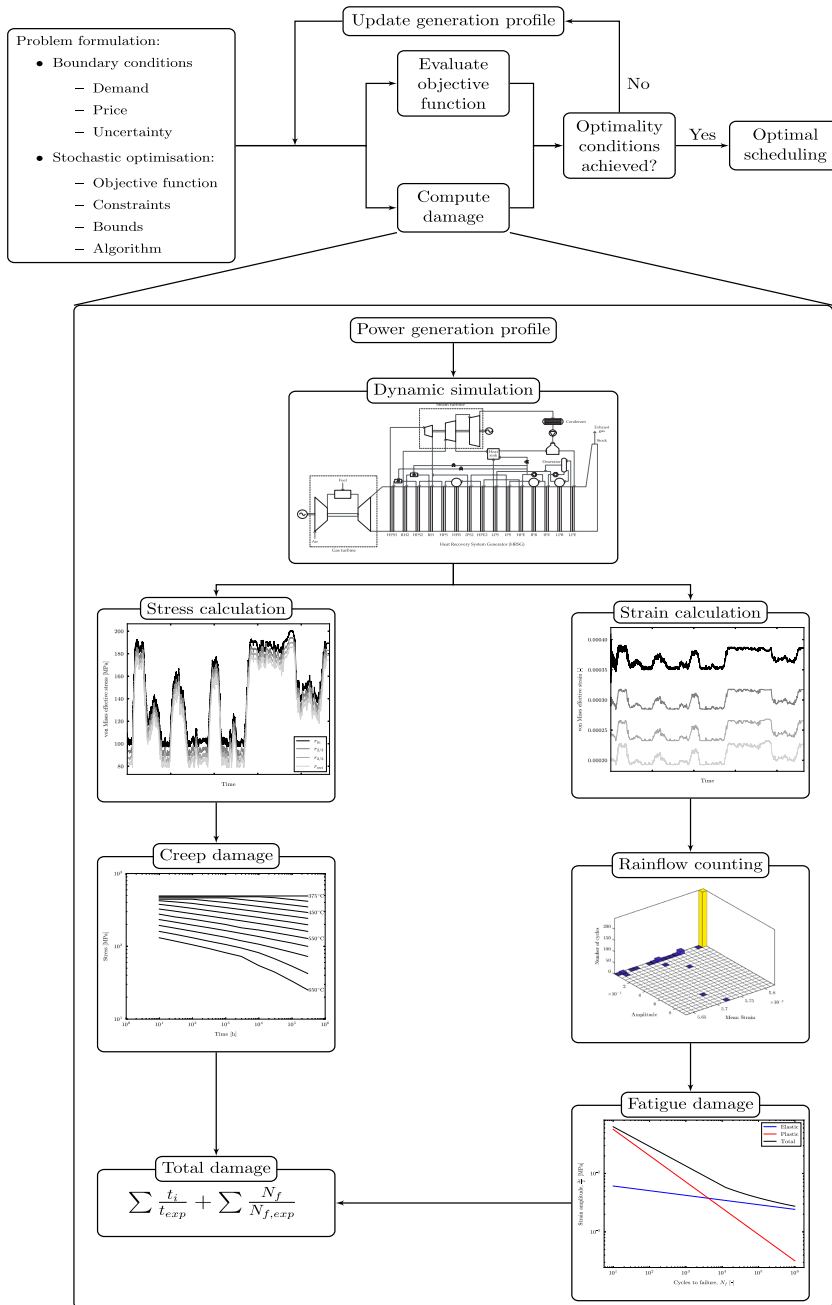
Fig. 1. Method to optimally schedule the power generation profile of thermal power plants with lifetime enhancement under uncertainty.

regulatory and supervisory control layers [20,21], the evaluation of creep and fatigue damage and the associated reduction of operational lifetime in critical equipment owing to the operation of thermal power plants befall in longer time scales (i.e. days, weeks and months), or once the failure has already occurred. Damage in critical equipment may also be monitored online to quantify its deterioration and allow more

accurate assessments of possible repairs and maintenance [28,34]. Nevertheless, online monitoring of the damage is only valid for failure prevention since the power generation profile, which determines the operation and hence the damage in the equipment of thermal power plants, is normally defined one day ahead in deregulated power markets.

Therefore, scheduling of daily and weekly operation of thermal
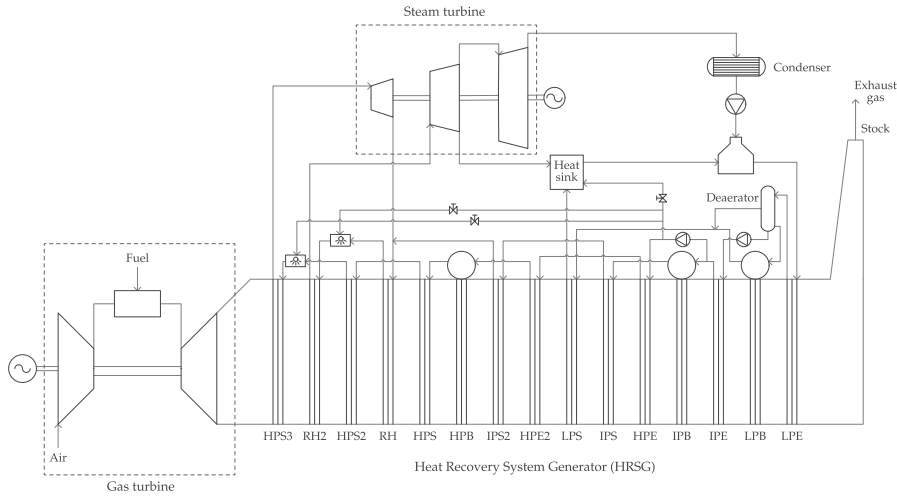
Fig. 2. Process model of the natural gas combined cycle.The nomenclature in the HRSG is as follows. E: Economiser, B: Boiler, S: Superheater, R: Reheater P: Pressure, L: Low, I: Intermediate, H: High.

power plants in power markets with large shares of renewable energy confronts three main challenges: (1) adapt the operation profile to intermittent power generation from renewable energy sources and demand variations, (2) consider the uncertainty associated with this type of technology, and (3) limit the deterioration of critical equipment because of the flexible operation required to balance power generation and demand. Traditional scheduling methods focus on point (1), with modern approaches progressively including the uncertainty from renewable power generation and demand fluctuation [35–37], whereas damage analysis is decoupled from the scheduling stage and carried out once the fault has already occurred.

This study presents a methodology that addresses these three requirements. In this scheduling strategy, power generation profiles of thermal power plants are the result of an optimisation problem where the maximum deterioration of the equipment by different damage phenomena is limited. Furthermore, this optimisation is formulated as a scenario-tree stochastic optimisation problem to consider the uncertainty associated with the intermittent renewable energy sources. Thus, the main contribution of this work is the combination of the scheduling process with the uncertainty associated with renewable energy sources and the deterioration of the equipment in a stochastic optimisation framework. This approach enables thermal power plants to balance the grid under different scenarios whilst enhancing the lifetime of sensitive equipment and maximising their economical performance.

This methodology involves several models that are merged in an optimisation framework, whereas its formulation allows including different types of uncertainty and deterioration mechanisms. The structure of this work follows a modular approach to show how this methodology can be easily adapted to different applications and scenarios. Section 2 describes the overall method and presents the different models required during the optimisation to estimate the dynamic power plant behaviour, the stress and strain arising in different equipment, and the damage caused by different phenomena. Section 3 presents the mathematical formulation of the proposed scheduling method, and details how these models are combined in a scenario-tree stochastic optimisation problem that limits the damage in the equipment. A case study analysed in Section 4 illustrates the application of the proposed methodology to the scheduling of a day-ahead power generation profile for a natural gas combined cycle and discusses the importance of adequate selection of design temperatures in the equipment. Conclusions and final remarks are included in Section 5.

2. Method for stochastic scheduling with lifetime enhancement

Flexible operation of thermal power plants may result in a substantial reduction of their operational lifetime. It is thus fundamental to consider the deterioration generated by this type of operation to assess the economic viability of these power generation systems. The methodology presented in this paper aims at limiting the damage in the components of a power plant whilst optimally scheduling the power generation profile. Moreover, the uncertainty in the power demand and the power generation from intermittent renewable energy sources is considered by formulating the scheduling of power generation as a stochastic optimisation problem. Fig. 1 summarises the methodology proposed in this study.

In deregulated power markets, one-day ahead predictions of the demand are available so the power producers can schedule their operation and offer a selling price for the produced electricity. The proposed methodology considers hence that an estimation of the demand and the uncertainty attached to this prediction are known. In addition, a price profile for the given demand is also assumed, albeit several prices with different uncertainties may be considered to cover a broad range of scenarios where the plant operator can adjust the electricity price to obtain more revenue or be more competitive. These demand and price profiles and their associated uncertainties are used to define a stochastic optimisation problem to schedule a power generation profile that maximises revenue and does not exceed the maximum allowable damage in the components of the thermal power plant.

In this optimisation process, the deterioration of the different components of the power plant is a constraint. Therefore, the different power generation profiles computed by the optimisation algorithm are used to calculate the damage in specific equipment and check if the constraints are satisfied (see Fig. 1). The damage calculation is a sequential procedure where the possible optimal power generation profile is utilised to carry out a dynamic simulation that attempts to recreate the behaviour of an actual thermal power plant. Stresses and strains throughout the operation period can thus be obtained for the equipment of interest. Damage is subsequently computed by considering these stresses and strains and the adequate experimental data for the material of the considered equipment. The total deterioration owing to the different damage mechanisms is the result of a linear summation rule. This procedure to compute the damage generated by different phenomena from the operation profile of a thermal power plant is illustrated in Fig. 1.

Damage estimation is a procedure that requires several types of models. The remainder of this section includes the description of the dynamic models that replicate the operation of an actual thermal power plant in Section 2.1, the modelling approach to compute the stresses and strains in the equipment in Section 2.2, and the methods to estimate the damage depending on different mechanisms in Section 2.3.

2.1. Dynamic modelling of a natural gas combined cycle

This study considers a natural gas combined cycle with three-pressure levels and reheating. This type of thermal power plant is the most efficient, flexible and less polluting fossil-fueled plant available [18,38]. Thus, they are expected to ramp more frequently to balance the intermittent power generation from renewable energy sources [6,7]. Deterioration of these thermal power plants may become an issue without the adequate scheduling, and hence a modern NGCC is used to demonstrate the application of the proposed methodology.

The design of the NGCC was performed with GT PRO [39] because it provides details about the material of the equipment, the geometry and dimensions of individual components, maps of performance for the pumps, and experimental data for the exhaust conditions and power generation of the gas turbine. Fig. 2 represents the process layout of the NGCC considered in this work. The dynamic model of the NGCC was developed with the specialised thermal power library [40] in the software Dymola [41], which is based on the Modelica language [42]. This model relies on conservation laws, detailed heat transfer and pressure drop correlations, maps of performance and experimental data to adequately simulate the dynamic operation of the NGCC. A thorough description of the modelling principles and validation results of this dynamic model can be found in the work by Montañés et al. [43].

High-fidelity dynamic models representing large energy systems are not suitable for optimisation because of their high computational cost. Simplified models that capture the dynamic behaviour of thermodynamic variables of interest must thus be used instead. System identification can be implemented to obtain dynamic data-based models that predict the overall transient performance of specific variables [44]. However, since scheduling captures the long-term dynamic behaviour of thermal power plants, quasi-steady state models may be used without excessive loss of accuracy and standard regression approaches can be applied.

Temperatures and pressures in the equipment of interest are normally the thermodynamic variables estimated by simplified models, as they are the boundary conditions of the stress models that allow computation of creep and fatigue damage. If other deterioration mechanisms such as hot corrosion are considered, simplified models to estimate the composition of specific chemical components in the flue gas could also be developed and implemented in the proposed methodology. In addition, a simplified model for predicting the power generation of the thermal power plant is also needed.

The tubes in the superheating section of the heat-recovery steam generator (HRSG) of the NGCC are considered. Creep is a major issue for this type of components because they experience many drastic operation changes during regular operation of NGCCs as a result of the frequent ramping, start-ups and shut-downs [11,12]. Therefore, the tubes in the superheaters are a suitable and illustrative example to demonstrate the lifetime enhancement capability of the methodology proposed in this work.

Table 1
Fitting parameters of the simplified models and coefficient of determination R^2.

x	a	b	R^2[%]
Power	90	5.25	99.95
Inner pressure	6.48	0.08	99.88
Inner temperature	377.17	1.83	95.58
Outer temperature	768.57	−1.45	93.43

This component only requires simplified models to predict the inner temperature and pressure, and outer temperature since creep is the unique failure phenomenon. The outlet pressure in the HRSG is almost constant because of the minimal changes in the pressure drop of the exhaust gas. A direct relation may be established between the gas turbine load and the quasi-steady state value of these variables. Therefore, linear polynomials with the structure presented in Eq. (1) lead to adequate estimations, where x represents the different predicted variables (i.e. mechanical power generation, and inner and outer pressure and temperature in the superheated tubes), u is the manipulated variable, which is the gas turbine load as it dictates the operation profile of the NGCC, and parameters a and b are fitted to the high-fidelity model for each variable. Table 1 summarises the fitting parameters of each variable and presents the coefficient of determination R^2 that measures the agreement between the high-fidelity and simplified models. Fig. A.11 presents a comparison between the high-fidelity and simplified models for the considered temperatures and pressure.

$$x = a + bu \tag{1}$$

2.2. Stress and strain modelling

In thermal power plants, there are several components that must withstand high temperatures and pressures. These operating conditions originate both thermal and mechanical stresses, which lead to the progressive deterioration of the equipment. Thermal stresses depend on the temperature gradient along the wall of the component and the design temperature of the material, whereas the mechanical contribution is proportional to the applied mechanical forces (e.g. pressure or centrifugal force). The temperature distribution along the wall of any circular equipment (e.g. pipes, tubes or rotors) is obtained with the heat equation assuming that heat transfer occurs exclusively in the radial direction:

$$\frac{1}{r}\frac{\partial}{\partial r}\left(r\frac{\partial T^*}{\partial r}\right) = \frac{1}{\alpha}\frac{\partial T^*}{\partial t} \tag{2}$$

where r is a generic radius, α is the thermal diffusivity of the material, and T^* refers to the temperature difference respect to the design temperature of the equipment.

The temperatures in the inner and outer surfaces are the boundary conditions that define the temperature distribution in the wall. Thermal stresses can hence be computed considering this temperature profile. The method to calculate these stresses depends on the geometry of the component. Plane strain is a suitable modelling approach for equipment where the longitudinal dimension is notably larger than in the radial or tangential directions [45]. Pipes, drums, headers, downcomers and any component with a cylindrical shape can be modelled under the plain strain assumption. In contrast, if the longitudinal dimension is almost negligible compared to the other two dimensions, plane stress can be assumed to model the stress [45]. This modelling approach describes the stresses that arise in the rotor disks of the steam turbines (see, e.g., the work by Rúa et al. [20,21]). More detailed and intricate stress modelling approaches, or even finite element methods (FEMs), may be necessary to determine the stress generated in complex geometries such as turbine blades.

$$\sigma_r = \left(1 - \frac{r_i^2}{r^2}\right)\frac{E\alpha^*}{(1+v)(1-2v)}\int_{r_i}^{r_o} rT^*\,\mathrm{d}r - \frac{E\alpha^*}{(1-v)}\int_{r_i}^{r} rT^*\,\mathrm{d}r$$
$$+ \left[\frac{r_o^2 r_i^2}{(r_o^2 - r_i^2)r^2} - \frac{r_o^2}{(r_o^2 - r_i^2)}\right](p_o - p_i) - p_i \tag{3a}$$

$$\sigma_\theta = \left(1 + \frac{r_i^2}{r^2}\right)\frac{E\alpha^*}{(1-v)(r_o^2 - r_i^2)}\int_{r_i}^{r_o} rT^*\,\mathrm{d}r + \frac{E\alpha^*}{1-v}\left(\frac{1}{r^2}\int_{r_i}^{r} rT^*\,\mathrm{d}r - T^*\right)$$
$$+ \left[\frac{r_o^2 r_i^2}{(r_o^2 - r_i^2)r^2} + \frac{r_o^2}{(r_o^2 - r_i^2)}\right](p_i - p_o) - p_i \tag{3b}$$

$$\sigma_z = \frac{2 \upsilon E \alpha^*}{(r_o^2 - r_i^2)(1 - \upsilon)} \int_{r_i}^{r_o} r T^* \, dr - \frac{E \alpha^*}{1 - \upsilon} T^* + p_i \left(\frac{2 \upsilon r_o^2}{r_o^2 - r_i^2} - 2\upsilon \right) - p_o \frac{2 \upsilon r_o^2}{r_o^2 - r_i^2} \tag{3c}$$

Both modelling approaches are based on the stress–strain constitutive equations, the strain–displacement relations and the radial equilibrium equation. Expressions for the principal stress components are obtained if these relations are combined and the ordinary differential equation that determines the displacement is solved analytically. The mechanical stresses enter these expressions by including the inner and outer pressure as boundary conditions and the centrifugal force as an additional term in the radial equilibrium equation. A detailed development of the equations describing the principal stresses under the assumptions of plane strain and strain can be found in the work by Rúa et al. [20,21]. Eq. (3) defines the principal stress components under the plane strain assumption, which is the modelling approach that describes the stresses arising in the tubes of the superheater. Thermal stresses arise when the temperature distribution in the wall is different from the design temperature at which the component was produced. Therefore, the temperature T^* in any stress or strain expression refers to the deviation with respect to that initial temperature.

The von Mises equivalent, or effective, stress is a scalar measure that represents the overall effect of the principal stress components. This variable, defined in Eq. (4), is therefore suitable to estimate the overall damage induced by a power generation profile.

$$\sigma_{eff}^2 = \sigma_r^2 + \sigma_\theta^2 + \sigma_z^2 - (\sigma_r \sigma_\theta + \sigma_\theta \sigma_z + \sigma_z \sigma_r) \tag{4}$$

Strains are computed from the temperature profile along the wall, the principal stress components and the stress–strain constitutive relations [45]. If plane strain is assumed to model the stresses and strains in a component, the strain in the longitudinal direction is zero. Thus, the strains for the tubes in the superheater are:

$$\varepsilon_r = \frac{1}{E} (\sigma_r - \upsilon(\sigma_\theta + \sigma_z)) - \alpha^* T^* \tag{5a}$$

$$\varepsilon_\theta = \frac{1}{E} (\sigma_\theta - \upsilon(\sigma_r + \sigma_z)) - \alpha^* T^* \tag{5b}$$

Similar to the stress models, an overall effective strain can be defined following the von Mises criteria [24]:

$$\varepsilon_{eff}^2 = \varepsilon_r^2 + \varepsilon_\theta^2 + \varepsilon_z^2 - (\varepsilon_r \varepsilon_\theta + \varepsilon_\theta \varepsilon_z + \varepsilon_z \varepsilon_r) \tag{6}$$

These temperature, stress and strain models were validated using high-fidelity finite element methods for the same operating conditions. Fig. A.12 illustrates the agreement between the stresses and strains of the proposed models and the FEM analysis.

2.3. Damage estimation methods

Deterioration of the equipment in thermal power plants occurs as a result of a combination of different damage phenomena [11,12]. Creep and low cycle fatigue are arguably the most common and relevant failure mechanisms caused by the cyclic operation of flexible power plants [12,31,32]. Therefore, this work describes the main methods to estimate the deterioration caused by both phenomena.

The calculation of damage relies on experimental data obtained by the repetition of different tests in samples of specific materials [11,24]. Different procedures are hence applied to obtain this data depending on the damage mechanisms. Creep is normally computed with charts as in Fig. 3 that relate the operating stress level and temperature with the maximum operating time at these conditions before failure [11]. Thus, the total creep damage generated during the operation of a thermal power plant is:

$$D_{creep} = \sum_{i=1}^{m} \frac{t_{oper}}{t_{exp}} \tag{7}$$
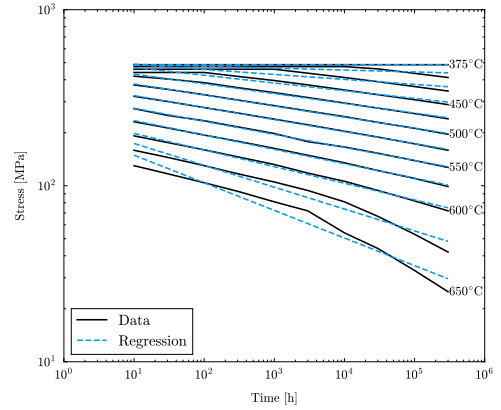
Fig. 3. Diagram with experimental data to estimate the creep damage. The black lines represent the data obtained experimentally whereas the blue lines are linear regression models used during the optimisation.

where t_{oper} is the time that a component of the power plant operates at a specific temperature and stress level, t_{exp} is the maximum operational time obtained experimentally at those levels, and m is the number of considered operation points.

Experimental data are discrete. Therefore, the computation of creep damage given the operating temperature and stress profiles from the models described in Section 2.1 and Section 2.2, respectively, requires a two-dimensional interpolation to obtain the experimental time that the equipment can operate at such conditions. Interpolation is not suitable for optimisation since different iterations may lead to points that lay outside the experimental data set and hence to convergence issues. Linear models of the experimental data were thus developed by standard least-squares to have continuous models that ease the convergence of the optimisation. The creep data estimated by the regression models is compared to the experimental data in Fig. 3.

Fatigue depends on the cyclic loading that the equipment undergoes during regular operation. Rotating machinery can experience vibrations and hence high cycle fatigue. In contrast, high-temperature components in thermal power plants suffer low cycle fatigue because of the low frequency of the operation changes [11,12,24,31,32]. Damage originated by both fatigue mechanisms is also calculated with procedures based on experimental data, although stress profiles are normally used to correlate the operating conditions with the high cycle fatigue deterioration and strain profiles to compute the low cycle fatigue damage [24,46].

The stress and strain profiles are not uniform since they depend on the operation of the thermal power plants. However, the experimental data utilised to compute the fatigue damage is obtained by applying uniform cyclic loading to the samples of material. Standardisation techniques that transform the variable spectrum of stresses and strains into uniform loading profiles are therefore required to calculate the fatigue damage. Rainflow counting is a procedure that extracts the hysteris cycles from the loading spectrum and generates uniform loading cycles from non-uniform stress and strain profiles [24,47–50]. This results in a set of amplitudes and mean stress or strain ranges with an associated number of cycles (see Fig. 1). The fatigue damage is calculated by comparing the number of cycles obtained from the rainflow counting procedure and the experimental maximum number of cycles for a specific amplitude and mean stress/strain [24,46]. Eq. (8) represents the computation of the fatigue damage following the linear cumulative damage hypothesis formulated by Miner-Pålmgren [46,51,52]:

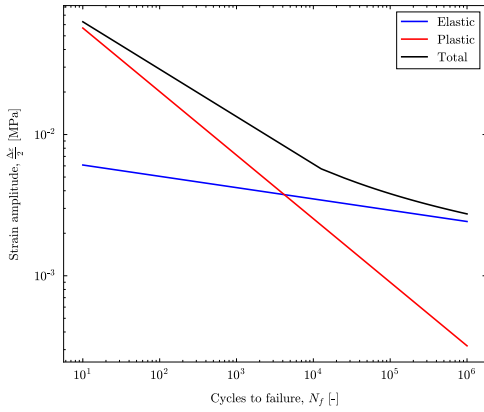$$D_{fatigue} = \sum_{i=1}^{n_r} \frac{n_{oper}}{n_f} \tag{8}$$

Fig. 4. Diagram with experimental data to estimate the fatigue damage. The black line represents the maximum experimental number of cycles to failure given that a strain amplitude is a combination of elastic and plastic effects.

where n_{oper} is the number of operation cycles for a given strain amplitude and mean strain, n_r is the number of the different considered ranges, and n_f is the experimental data for the maximum number of cycles before failure. This experimental data is normally represented by the Coffin-Manson equation [24,46]:

$$\frac{\Delta \varepsilon}{2} = \frac{\Delta \varepsilon_e}{2} + \frac{\Delta \varepsilon_p}{2} = \frac{\sigma_f'}{E} \left(2 n_f\right)^b + \varepsilon_f' \left(2 n_f\right)^c \tag{9}$$

with σ_f' and ε_f' being, respectively, the tensile strength and ductility coefficient scaled to fit the experimental data, and b and c are fitting parameters. The elastic contribution to the overall strain amplitude is $\Delta \varepsilon_e / 2$, whereas $\Delta \varepsilon_p / 2$ is the plastic component. Fig. 4 illustrates the experimental fatigue data fitted to the Coffin-Manson equation.

Experimental fatigue data represents the effect of uniaxial loading in

the deterioration of samples of a specific material. The equipment of thermal power plants is however exposed to multiaxial loading. Therefore, to estimate the fatigue damage with uniaxial experimental data, the effective values of the stress and strain defined in Eqs. (4) and (6) are used [24,53,54]. This allows the utilisation of available experimental uniaxial data to compute the fatigue damage from complex multiaxial loading.

The total damage of a component results from the summation of the individual contributions of the different damage phenomena:

$$D = D_{\text{creep}} + D_{\text{fatigue}} \tag{10}$$

This method to compute the deterioration of the equipment in thermal power plants eases the inclusion of different damage mechanisms. For instance, hot corrosion could be added by developing a model that predicted the deposition of eroding elements in the equipment and a expression that correlated this deposition with the operating conditions and the generated damage.

3. Scheduling as a stochastic optimisation problem

Scheduling of thermal power plants in deregulated markets is a challenging procedure because of the large deployment of intermittent renewable energy sources. The intrinsic uncertainty associated with the power generation from solar and wind power sources imposes drastic operation profiles on traditional thermal power plants to balance the grid. This work proposes the utilisation of scenario-based multistage optimisation to consider the uncertainty associated with renewable power generation and schedule the operation of flexible thermal power plants whilst limiting the maximum damage in their critical components. The scheduling problem becomes hence a stochastic optimisation problem where the different scenarios represent the uncertainty in the power demand and the deterioration of the equipment is a constraint. This section describes the mathematical formulation of the method illustrated in Fig. 1.

Scenario-based multistage optimisation models the uncertainty of a process as discrete realisations of a probability density function representing such uncertainty, considers the different possible combinations of these realisations, and integrates them in an optimisation framework that
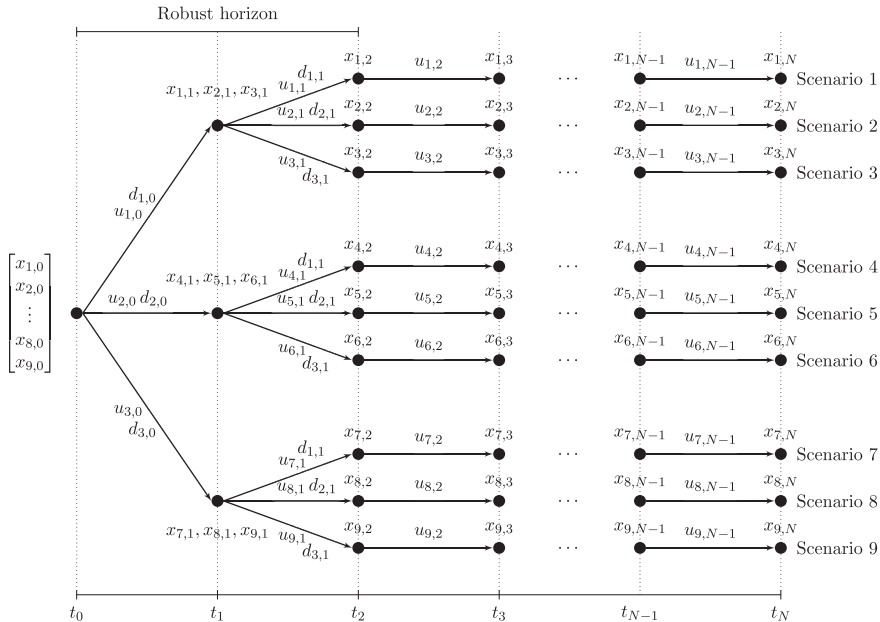

Fig. 5. Schematic representation of a scenario-tree with $M = 3$ uncertainty realisations and a robust time horizon $N_r = 2$.

aims at finding the optimal solution of all possible uncertain scenarios [55]. Therefore, its application to the one-day ahead scheduling of power generation from thermal power plants in flexible power markets may enhance the optimal utilisation of this type of power plants. Furthermore, since the scheduling problem is expressed as a stochastic optimisation problem, the maximum damage induced by the regular operation of the power plant can be included as a constraint, which may expand the lifetime of traditional thermal power plants. Fig. 5 represents the scenario-tree evolution embedded in the optimisation problem. Given a known initial operation point, M different uncertainty realisations, d, consider the power generation uncertainty of the intermittent renewable energy sources. These realisations represent possible power demands that the thermal power plant must balance by modifying its manipulated variable, u, which is the gas turbine load in NGCCs and the fuel input in coal and biomass power plants, to produce the adequate amount of power.

The robust time horizon, N_r, limits the extension to which the uncertainty is considered, as the size of the optimisation problem, i.e. the number of scenarios, increases exponentially, $S = M^{N_r}$, with this horizon. In contrast to design problems, where the stochastic optimisation problem is solved only once, this scheduling method may re-solve the optimisation problem continuously with updated information (e.g. every two hours). This means that it is not necessary to branch the scenario tree until the end of the prediction horizon. Instead, the expansion of the scenario tree might be stopped after a robust horizon, and from this point on consider the uncertainty unchanging. The main reasoning is that information about the far future need not be accurately represented at the time when the decision is made, because the decisions will be refined in the next optimisation, when the scheduling problem is solved again with new information.

The mathematical formulation of the scheduling problem as a scenario-tree optimisation problem is:

$$\min_{x_{i,j}, u_{i,j}} \sum_{i=1}^{S} \omega_i \sum_{j=0}^{N-1} \ell(x_{i,j}, u_{i,j}, P_j) \tag{11a}$$

subject to
$$x_{i,0} = x_{\text{init}} \quad \forall i \in \mathscr{S} \tag{11b}$$

$$x_{i,j} = f(x_{i,j}, u_{i,j}, d_{i,j}) \quad \forall i \in \mathscr{S}, \forall j \in \mathscr{N} \tag{11c}$$

$$c_{\text{ineq}}(x_{i,j}, u_{i,j}) \leqslant D_{\max} \quad \forall i \in \mathscr{S}, \forall j \in \mathscr{N} \tag{11d}$$

$$(x_{i,j}, u_{i,j})^{\text{low}} \leqslant (x_{i,j}, u_{i,j}) \leqslant (x_{i,j}, u_{i,j})^{\text{up}} \quad \forall i \in \mathscr{S}, \forall j \in \mathscr{N} \tag{11e}$$

$$\sum_{i=1}^{S} E_i^* u_i = 0 \quad \forall i \in \mathscr{S} \tag{11f}$$

where the subscripts $(\cdot)_{i,j}$ refer to the ith scenario at the jth sample time, $\mathscr{S}$ is the set of scenarios $\mathscr{S} := \{1, ..., S\}$, and $\mathscr{N}$ denotes the set of indices j defining the sampling time such $\mathscr{N} := \{1, ..., N\}$. The cost function in Eq. (11a) is a weighted average of the individual cost functions of each scenario, where ω_i is the coefficient that determines the weight of each scenario. Since scheduling problems aim at maximising the operating profit, the cost function is defined as:

$$\ell(x_{i,j}, u_{i,j}, P_j) = -x_{i,j}^{\text{T}} P_j \tag{12}$$

with P_j representing the price of the generated power and $x_{i,j}$ the scheduled power generation, which is a vector including the discrete sequence of operation points that define the quasi-steady state net power production of the NGCC throughout each scenario.

The equality constraints in Eq. (11c) ensure that the models describing the behaviour of the thermal power plant (i.e. the simplified models for power generation, inner pressure and temperature, and outer temperature in Eq. (1) and Table 1 are satisfied for all uncertainty

realisations $d_{i,j}$. In contrast to the original model predictive control application where the equality constraints predict future dynamic behaviour of the system [55], Eq. (11c) only guarantees that the solution satisfies the quasi-steady state performance of the power plant but does not include any prediction, as each point of the sequence defining the power generation profile is independent. The inequality constraints represented by Eq. (11d) include the computation of the damage in the equipment over the time horizon N and limit its value to a maximum allowable level specified by $D_{\max}$, whereas Eq. (11e) defines the lower and upper bounds of the computed thermodynamic variables in the equipment x (i.e. temperatures, pressure and power) and the manipulated variable u. Eq. (11b) sets the initial conditions of the power plant, which are common for all scenarios.

Scenario-tree optimisations include the uncertainty in the process by the continuous branching of different scenarios. This approach hence considers a broader range of operating conditions, but it also imposes extra restrictions during the optimisation. As the disturbances associated with the uncertainty cannot be predicted, the control inputs must not anticipate them and the power plant states x in every node must be equal. This implies that the control inputs leading to a node within the robust horizon are equal for the different scenarios branching from that node [55–58]. These restrictions are the non-anticipativity constraints, and are enforced in the optimisation problem by Eq. (11f), where $u_i = [u_{i,0}, u_{i,1}, u_{i,2}, ..., u_{i,N-1}] \in \mathbb{R}^N$.

4. Optimal scheduling of flexible natural gas combined cycles: a case study

The scheduling of a flexible NGCC was considered to illustrate the application of the methodology proposed in this work. Section 4.1 presents a case study where the maximum creep damage in the tubes of the superheater is limited whilst maximising the power generation of the NGCC. Moreover, since stress, and consequently creep damage, are profoundly affected by the design temperature of the equipment, the effect of this parameter on both effective stress and deterioration is studied for a broad range of temperatures in Section 4.2.

4.1. Optimal scheduling with lifetime enhancement

The power demand profile estimated by the grid operator and scaled to the power generation range of the actual power plant is represented in Fig. 6. This demand was simplified to a coarser profile since scheduling aims at defining overall power generation profiles and NGCCs can respond within seconds to small, unscheduled variations in power
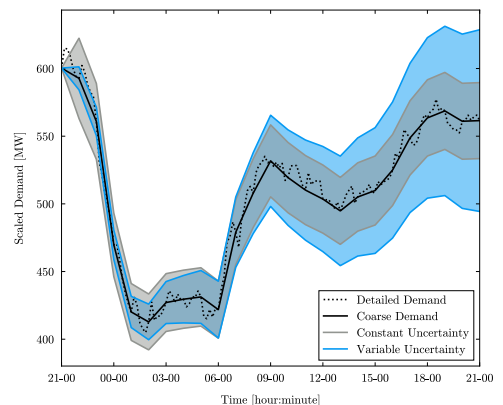

Fig. 6. Demand profile estimated in day-ahead markets with a coarse simplification and intervals for constant and increasing uncertainty.

Table 2
Physical and mechanical properties of T91 martensitic steel.

ρ [kg/m^3]	C_m [J/kgK]	k_m [W/mK]	α^* [m^2/s]	α [1/K]	E [MPa]	υ [−]	h_o [W/m^{2}K]	h_i [W/m^{2}K]
7750	770	33	5.53e−05	1.3e−5	180000	0.3	2000	400

demand [20,21]. Furthermore, Fig. 6 illustrates two different types of uncertainty that can be included in the stochastic optimisation. This work assumed a ±5% constant uncertainty in the estimated power demand (grey area in Fig. 6). The time and robust horizons were, respectively, 24 and 2 h, with a sampling time of 1 h, whereas 3 uncertainty realisations were considered, leading to a total of 9 scenarios that were equally weighted. Fig. 5 represents this stochastic problem for the considered realisations and robust time horizon. This number of uncertainty realisations and robust time horizon was considered a reasonable trade-off between adequate consideration of uncertainty and computational cost. The price of electricity is shown in Fig. B.13.

Scheduling of the power generation from the NGCC was first carried out *without* damage constraints to obtain an operation profile benchmark that maximised the revenue. The sequential least-squares quadratic programming (SLSQP) algorithm [59,60] included in the nonlinear optimisation package NLOPT [61] was used in the optimisation. A maximum total damage $D_{max} = 0.00017$ was then included in the stochastic optimisation problem. This allows identifying the main restrictions imposed by the constraint in the maximum damage and points out its effect on the shape of the power generation profiles in different scenarios. This study only considers creep damage in the tubes of the superheater as this is the main deterioration mechanism in this type of components [11,12]. The material of the tubes was T91, a martensitic steel for high temperature applications with its physical and mechanical properties summarised in Table 2 [62]. The design temperature of the tubes considered in this case study was 510 °C.

The nomenclature referring to the different scenarios in the stochastic optimisation problem is based on the sequence of uncertainty realisations, where H, M and L indicate the high (105%), medium (100%) and low (95%) values of the power demand estimated by the grid operator. Since the robust time horizon considered in this work is 2, a pair of letters defines each scenario. The first letter refers to the uncertainty realisation in the first sampling time and the second letter indicates the next one. For instance, the pair HL refers to the scenario where the scheduled power considers the highest demand in the first sampling time, and the lowest in the second. Moreover, the letter X is used to indicate all uncertainty realisations (e.g. XH refers to all scenarios where the second uncertainty realisation represents the higher demand profile, independently of the first realisation).

Fig. 7 shows the scheduled power for each scenario and the time distribution of the associated wall temperature, von Mises stress and the creep damage in the tubes of the superheater. Fig. 8 represents the accumulated deterioration for the scheduled power generation profiles. The maximum damage limitation, $D_{max} = 0.0017$, only affected the HX scenarios since they produced a higher deterioration in the unconstrained[1] case. Despite the reduction in the deterioration of the equipment to meet the maximum damage constraint could be also achieved in the final hours of operation (Fig. 7g and h), the scheduling methodology performed the entire damage reduction in the first operating period since the electricity price was lower. A change in the operation profile of the NGCC (Fig. 7a and b) lead to different operating conditions that resulted in lower temperature (Fig. 7c and d) and effective stress (Fig. 7e and f) in the wall of the superheater tubes, and hence in smaller creep damage because of the combined effect of a reduction in both variables (see Fig. 3).

Modifying the power generation profile in the HH scenario to meet

the damage constraint also affected the HM and HL scenarios. This coupling occurs because of the non-anticipativity constraints in Eq. (11f), which enforces the set of scenarios HX to coincide in the first uncertainty realisation. Therefore, all HX scenarios consider the same uncertainty level in the first sampling time of the robust horizon. The HL scenario hence changes when the constraint in the damage is imposed, albeit it had not reached this limit in the unconstrained case. This illustrates the effects of combining in a stochastic optimisation problem the damage limitation of the equipment with the uncertainty in the estimated power demand.

A comparison between the accumulated revenue for all scenarios and the unconstrained and constrained problems is presented in Fig. 9. Revenue did not change in the MX and LX scenarios since the damage limitation was not exceeded in the unconstrained case. In contrast, the change in the power generation profile of the HX scenarios reduced the accumulated revenue owing to the constraint on the maximum allowable deterioration. However, this reduction is almost negligible (0.11% in the HH scenario) because of the limited change in the operation profile and the mid-range prices where it occurred. This proves the suitability and advantages provided by the scheduling methodology presented in this work. The formulation of the scheduling problem with lifetime enhancement as a stochastic optimisation problem allows the limitation of damage in the equipment by modifying the power generation profiles where it has the largest effect on damage reduction and the minimum decrease in revenue. This is specially relevant when there is creep damage, as this deteriorating phenomena concentrates at specific periods of time where the operation of the thermal power plant originates high level of temperature and stress that may be largely reduced by small changes in the operation of the thermal power plant. Moreover, the intrinsic uncertainty attached to renewable energy sources can be included, and thus maximum profits can be achieved under different conditions.

4.2. Effect of design temperature on effective stress and creep damage

Creep damage depends on the temperature and stress of the equipment. Whilst the wall temperature is an absolute variable that only varies with the operation of the power plant, the thermal stresses that contribute to the effective stress are computed relatively to a design temperature where the material is free of this type of stress. Therefore, the damage of the power plant equipment is highly affected by its design temperature. Fig. 10 shows how the design temperature modifies the shape and magnitude of the effective stress in the unconstrained HH scenario. Higher design temperatures than that encountered in the wall of the superheater tubes generate inverse profiles of temperature and von Mises effective stress (see, e.g., the lines for 590 °C and 570 °C in Fig. 10). In contrast, the wall temperature and effective stress profiles follow the same tendency if the design temperature is lower than the wall temperature (see, e.g., the lines for 510 °C and 490 °C in Fig. 10). When the design temperature is between the maximum and minimum temperature of the wall for a given operation profile, the von Mises effective profile is a combination of both trajectories depending on whether the current wall temperature is above or below the design temperature (lines for 550 °C and 530 °C in Fig. 10).

Moreover, the inverse trajectories between the wall temperature and the effective stress for design temperatures above the maximum wall temperature reveal that the power generation profile that maximises the revenue also minimises the damage if there is a direct relation between the power generation and the wall temperature, i.e. more power leads to higher wall temperatures. When this condition is met and the design temperature of the equipment is above the peak of the wall temperature,

---

[1] In this context, unconstrained refers to the case where there is no limitation on the maximum damage. However, the remaining equality and inequality constraints are still included.

(a) Optimal scheduled power without damage constraints.

(b) Optimal scheduled power with damage constraints.

(c) Wall temperature for the optimal operation profiles without damage constraints.

(d) Wall temperature for the optimal operation profiles with damage constraints.

(e) Maximum von Mises stress for the optimal operation profiles without damage constraints.

(f) Maximum von Mises stress for the optimal operation profiles with damage constraints.

(g) Damage for the optimal operation profiles without damage constraints.

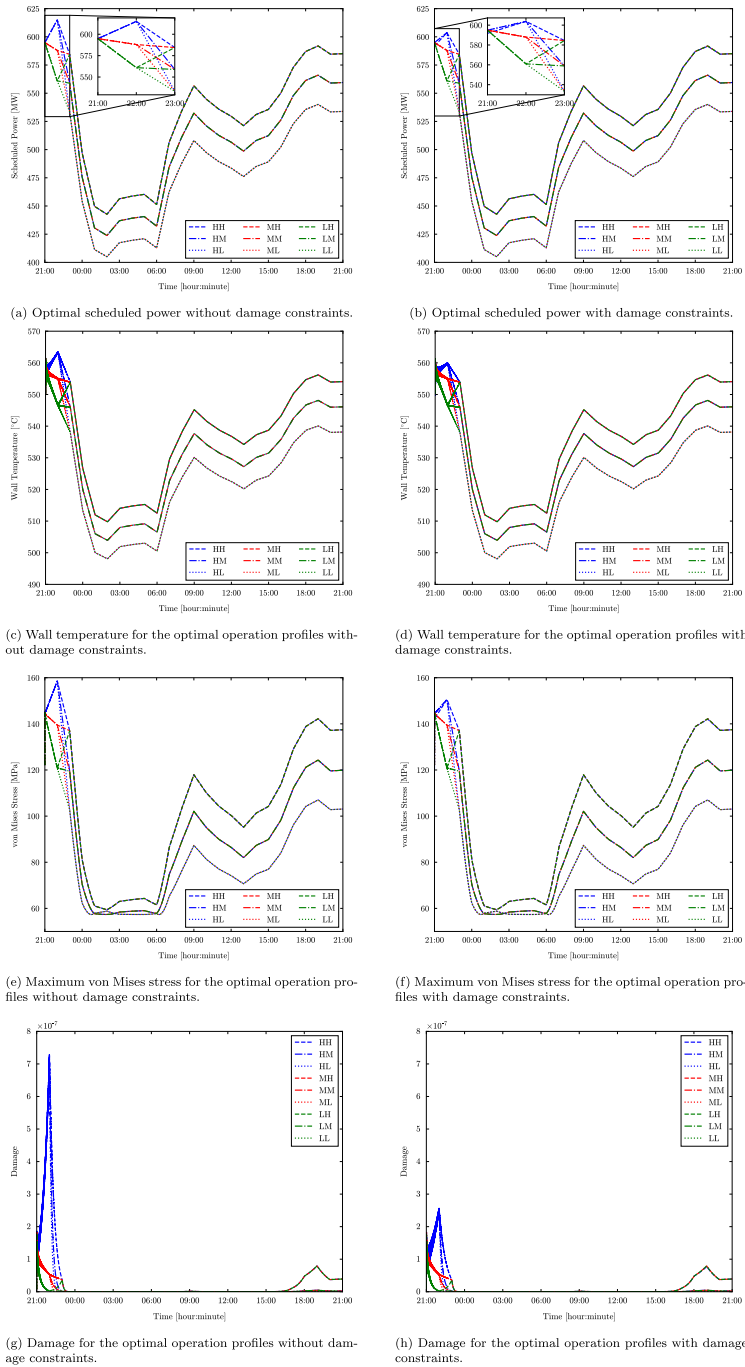(h) Damage for the optimal operation profiles with damage constraints.

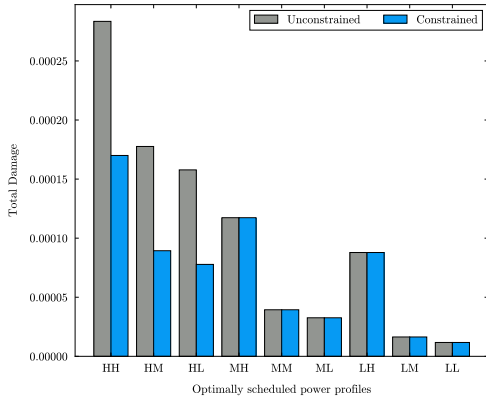**Fig. 7.** Optimal scheduling of a flexible NGCC with and without damage limitation under uncertainty.

Fig. 8. Total creep damage in the tubes of the superheater for the different scenarios considered in the stochastic optimisation.

Fig. 10. Effective stress in the unconstrained HH scenario for different design temperatures. The maximum wall temperature for this scenario is included for shape comparison.
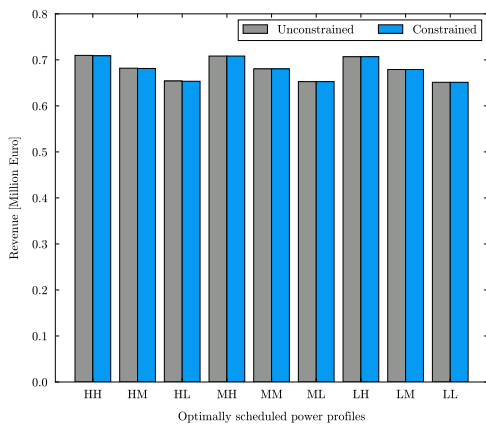

Fig. 9. Revenue for the different scenarios considered in the stochastic optimisation.

e.g. lines for 590 °C and 570 °C in Fig. 10, reducing the power generation leads to lower wall temperatures and thus higher temperature differences. As a result, the thermal stresses and the associated creep damage increase. Therefore, the optimal solution is the upper bound of the power generation, a limit where the creep damage cannot be further reduced. This solution does not hold if the wall temperature does not exhibit a proportional relation with the power generation, in which case the proposed methodology can find an operating profile that reduces the damage compared to the upper bound of the power generation.

The design temperature also influences the maximum value of the effective stress and temperature of the wall at which it occurs. Thus, the selection of an adequate design temperature can reduce notably the creep damage owing to the combined effect of these two variables. Table 3 compares the maximum effective stress value, the associated wall temperature at the instant it occurs and the accumulated damage, for three different scenarios and a broad range of design temperatures. These results demonstrate the trade-off existing between wall temperature and effective stress, since the lowest accumulated damage at each scenario occurred at the lowest combination of both variables, and not at

the smallest value of the maximum stress. Design temperatures closer to the highest wall temperature cause the maximum stress at the lowest wall temperatures because of the larger temperature difference (e.g. rows for design temperatures in the range 570–550 °C in Table 3), whilst design temperatures similar to the mean of the wall temperature reduce the overall temperature difference throughout the operation of the power plant but have the peak of stress at higher wall temperatures (rows 550–520 °C in Table 3).

5. Conclusions

Thermal power plants are expected to cycle more frequently and increase their number of start-ups and shut-downs in order to balance the intermittent power generation from renewable energy sources. In the long term, this type of operation may lead to larger deterioration of the equipment. Adequate scheduling of the power dispatched by flexible thermal power plants must hence consider the uncertainty associated to the increasing renewable energy sources whilst limiting the damage generated by the flexible operation of these thermal power units. This work seeks to address this challenge by proposing a methodology where the scheduling of power generation is formulated as a stochastic optimisation problem that considers the uncertainty in the power demand and limits the maximum deterioration of specific equipment.

Uncertainty in the power demand owing to the intermittent power generation of renewable energy sources was included in this methodology by formulating the scheduling problem as a scenario-tree based optimisation. This method considers several discrete realisations of the uncertainty associated to renewable power generation and combines them over time in a set of different scenarios that represent alternative profiles of power demand. Therefore, this optimisation problem aims at finding a set of optimal solutions that maximise the weighted sum of scenario revenues.

Deterioration of the equipment is embedded in the optimisation problem as a nonlinear constraint. This is achieved by a sequential procedure that calculates the damage over the considered operation time. During every iteration of the optimisation problem, the computed power generation profiles for each scenario are used to simulate the dynamic behaviour of the thermal power plant, which allows the estimation of temperature, pressure, stress and strain in specific equipment. Damage owing to different deterioration phenomena can subsequently be computed with these variables and experimental data. Since this is a general and sequential procedure, any damage mechanism (e.g. hot

Table 3
Effect of design temperature on the maximum effective stress, wall temperature at which occurs and total damage for different scenarios. Data for the HH scenario may be compared with Fig. 10.

T_{design} [°C]	HH			MM			LL		
	$\sigma_{eff,max}$ [MPa]	T_{wall} [°C]	Damage	$\sigma_{eff,max}$ [MPa]	T_{wall} [°C]	Damage	$\sigma_{eff,max}$ [MPa]	T_{wall} [°C]	Damage
590	196.75	509.77	$7.08 \cdot 10^{-5}$	210.39	503.92	$1.09 \cdot 10^{-4}$	224.13	498.07	$1.6 \cdot 10^{-4}$
570	146.09	509.77	$5.44 \cdot 10^{-7}$	159.19	503.92	$9.95 \cdot 10^{-7}$	172.50	498.07	$1.74 \cdot 10^{-6}$
560	123.98	509.77	$4.54 \cdot 10^{-8}$	136.61	503.92	$8.12 \cdot 10^{-8}$	149.57	498.07	$1.55 \cdot 10^{-7}$
550	102.96	509.77	$3.39 \cdot 10^{-8}$	114.82	503.92	$8.34 \cdot 10^{-9}$	127.22	498.07	$1.14 \cdot 10^{-8}$
540	96.12	563.34	$3.38 \cdot 10^{-7}$	94.38	503.92	$3.10 \cdot 10^{-8}$	105.84	498.07	$9.21 \cdot 10^{-9}$
530	115.53	563.34	$3.84 \cdot 10^{-6}$	104.35	554.72	$3.85 \cdot 10^{-7}$	104.23	554.65	$1.09 \cdot 10^{-7}$
520	136.57	563.34	$3.68 \cdot 10^{-5}$	124.14	554.72	$4.34 \cdot 10^{-6}$	124.02	554.65	$1.26 \cdot 10^{-6}$
510	158.60	563.34	$2.84 \cdot 10^{-4}$	144.92	554.72	$3.94 \cdot 10^{-5}$	144.79	554.65	$1.17 \cdot 10^{-5}$
500	181.32	563.34	$1.77 \cdot 10^{-3}$	168.60	562.40	$2.86 \cdot 10^{-4}$	168.40	562.32	$8.74 \cdot 10^{-5}$
490	204.46	563.34	$9.22 \cdot 10^{-3}$	192.95	562.40	$1.70 \cdot 10^{-3}$	192.74	562.32	$5.30 \cdot 10^{-4}$

corrosion, vibration, erosion, oxidation) can be included if the necessary variables to estimate the deterioration of the component can be obtained from the dynamic simulation of the thermal power plant.

Scheduling of a flexible natural gas combined cycle with limitation of creep damage in the tubes of the superheater demonstrated that the proposed methodology can enhance the lifetime operation of critical equipment by controlling its deterioration whilst maximising the economic revenue. This was achieved by modifying the set of power generation profiles in the time periods where the smaller changes in operation and revenue generation lead to the largest reduction in the damage. Therefore, the application of the proposed methodology to thermal power plants in deregulated power markets with a large deployment of renewable energy sources can enhance their lifetime with minimal detriment in the revenue.

The scheduling of the NGCC showed that the design temperature of the material notably affected the creep damage in the equipment. A comparison of its effect on the maximum effective stress, wall temperature and deterioration for a broad range of temperatures demonstrated that design temperatures close to the mean and peak values of the wall temperature in the tubes of the superheater substantially reduce the total damage generated by a given power generation profile, provided that the wall temperature and power generation are directly related (i.e. both increase or decrease simultaneously). In contrast, design temperatures larger than the maximum wall temperature lead to the trivial solution where the maximum power generation minimises the overall creep damage.

These results highlight the benefit of the scheduling methodology proposed in this work. Damage can be limited and controlled with minor modifications on the scheduled power generation profile and economic revenue, which enhances the operational lifetime and profitability of the power units. Furthermore, this methodology may ease the selection of adequate design temperatures of materials for critical equipment in the design phase of the thermal power plant. Scheduling of start-ups and shut-downs can also be carried out provided they can be simulated within the optimisation framework.

Declaration of Competing Interest

The authors declare that they have no known competing financial interests or personal relationships that could have appeared to influence the work reported in this paper.

Acknowledgements

Appendix A. Model validation

This section presents the validation results of the models developed throughout this work. Fig. A.11 compares the high-fidelity and simplified models for the considered temperatures and pressure, whereas Fig. A.12 shows the agreement between the stresses and strains of the proposed models and the FEM analysis.
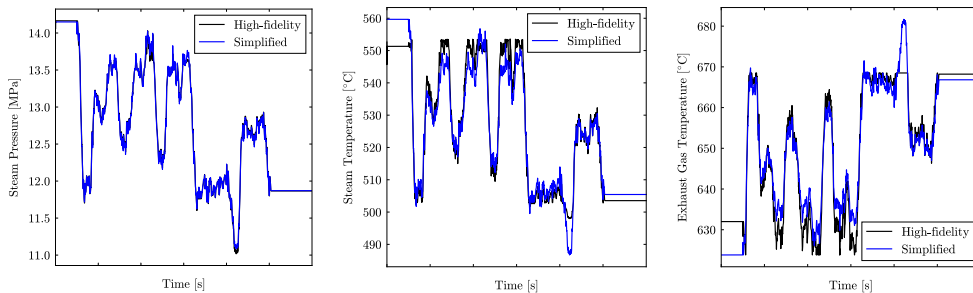
(a) Pressure of the steam inside the superheating tubes.

(b) Temperature of the steam inside the superheating tubes.

(c) Temperature of the exhaust gas outside the superheating tubes.

Fig. A.11. Comparison between the high-fidelity and simplified model predictions.

(a) von Mises stress at six equidistant radii.

(b) von Mises strain at six equidistant radii.
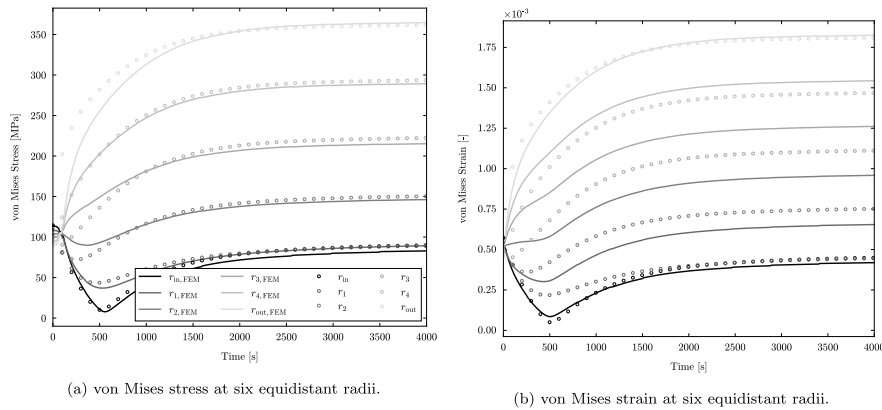
Fig. A.12. Validation of stress and strain models under the assumption of plain strain.

Appendix B. Power demand and price

Fig. B.13 presents the day-ahead demand profile used in the case study in Section 4, its coarse simplification, and the deterministic electricity price throughout the considered scheduling range.
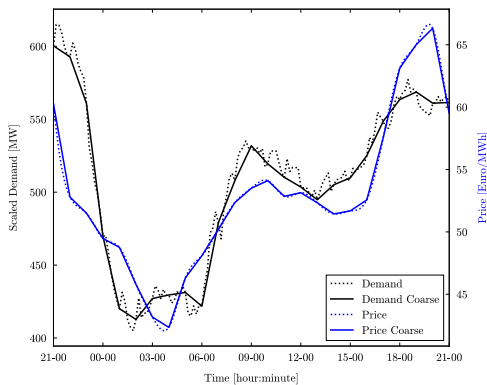
Fig. B.13. Demand profile estimated in day-ahead markets with a coarse simplification and deterministic electricity prices.

References

[1] IPCC, Summary for Policymakers. In: Global warming of 1.5C. An IPCC Special Report on the impacts of global warming of 1.5C above pre-industrial levels and related global greenhouse gas emission pathways, in the context of strengthening the global response to the threat of climate change, sustainable development, and efforts to eradicate poverty, [V. Masson-Delmotte, P. Zhai, H.O. Pörtner, D. Roberts, J. Skea, P.R. Shukla, A. Pirani, W. Moufouma-Okia, C.Péan, R. Pidcock, S. Connors, J.B.R. Matthews, Y. Chen, X. Zhou, M.I. Gomis, E. Lonnoy, T. Maycock, M. Tignor, T. Waterfield (eds.)]. World Meteorological Organization, Geneva, Switzerland, 2018.

[2] IEA, World Energy Outlook 2019: Executive Summary, https://iea.blob.core. windows.net/assets/1f6bf453-3317-4799-ae7b-9cc6429c81d8/English-WEO-2019-ES.pdf, 2019.

[3] J. Oswald, M. Raine, H. Ashraf-Ball, Will British weather provide reliable electricity? Energy Policy 36 (8) (2008) 3212–3225.

[4] M. Huber, D. Dimkova, T. Hamacher, Integration of wind and solar power in Europe: Assessment of flexibility requirements, Energy 69 (2014) 236–246.

[5] J. Bertsch, C. Growitsch, S. Lorenczik, S. Nagl, Flexibility in Europe's power sector: An additional requirement or an automatic complement? Energy Econ. 53 (2016) 118–131.

[6] P. Eser, N. Chokani, R. Abhari, Operational and financial performance of fossil fuel power plants within a high renewable energy mix, J. Global Power Propul. Soc. 1 (2017) 16–27.

[7] M.A. González-Salazar, T. Kirsten, L. Prchlik, Review of the operational flexibility and emissions of gas-and coal-fired power plants in a future with growing renewables, Renew. Sustain. Energy Rev. 82 (2017) 1497–1513.

[8] J. Rúa, M. Bui, L.O. Nord, N. Mac Dowell, Does CCS reduce power generation flexibility? A dynamic study of combined cycles with post-combustion CO₂ capture, Int. J. Greenhouse Gas Control 95 (2020) 102984.

[9] R.M. Montañés, M. Korpås, L.O. Nord, S. Jaehnert, Identifying operational requirements for flexible CCS power plant in future energy systems, Energy Proc. 86 (2016) 22–31.

[10] H. Kondziella, T. Bruckner, Flexibility requirements of renewable energy based electricity systems–a review of research results and methodologies, Renew. Sustain. Energy Rev. 53 (2016) 10–22.

[11] R. Viswanathan, Damage mechanisms and life assessment of high temperature components, ASM International, 1989.

[12] R. Viswanathan, J. Stringer, Failure mechanisms of high temperature components in power plants, J. Eng. Mater. Technol. 122 (3) (2000) 246–255.

[13] T. Kim, D. Lee, S. Ro, Analysis of thermal stress evolution in the steam drum during start-up of a heat recovery steam generator, Appl. Therm. Eng. 20 (11) (2000) 977–992.

[14] F. Alobaid, R. Postler, J. Ströhle, B. Epple, H.-G. Kim, Modeling and investigation start-up procedures of a combined cycle power plant, Appl. Energy 85 (12) (2008) 1173–1189.

[15] S.C. Gülen, K. Kim, Gas turbine combined cycle dynamic simulation: a physics based simple approach, J. Eng. Gas Turbines Power 136 (1) (2014) 011601.

[16] P. Dzierwa, J. Taler, Optimum heating of pressure vessels with holes, J. Pressure Vessel Technol. 137 (1) (2015) 011202.

[17] J. Taler, P. Dzierwa, D. Taler, P. Harchut, Optimization of the boiler start-up taking into account thermal stresses, Energy 92 (2015) 160–170.

[18] F. Alobaid, N. Mertens, R. Starkloff, T. Lanz, C. Heinze, B. Epple, Progress in dynamic simulation of thermal power plants, Prog. Energy Combust. Sci. 59 (2017) 79–162.

[19] A.B. Ata, F. Alobaid, C. Heinze, A. Almoslh, A. Sanfeliu, B. Epple, Comparison and validation of three process simulation programs during warm start-up procedure of a combined cycle power plant, Energy Convers. Manage. 207 (2020) 112547.

[20] J. Rúa, R. Agromayor, M. Hillestad, L.O. Nord, Optimal dynamic operation of natural gas combined cycles accounting for stresses in thick-walled components, Appl. Therm. Eng. 170 (2020) 114858.

[21] J. Rúa, L.O. Nord, Optimal control of flexible natural gas combined cycles with stress monitoring: Linear vs nonlinear model predictive control, Appl. Energy 265 (2020) 114820.

[22] R. Viswanathan, W. Bakker, Materials for ultrasupercritical coal power plants–Boiler materials: Part I, J. Mater. Eng. Perform. 10 (1) (2001) 81–95.

[23] R. Viswanathan, W. Bakker, Materials for ultrasupercritical coal power plants–Turbine materials: Part II, J. Mater. Eng. Perform. 10 (1) (2001) 96–101.

[24] S. Suresh, Fatigue of materials, Cambridge University Press, 1998.

[25] N. Mukhopadhyay, S.G. Chowdhury, G. Das, I. Chattoraj, S. Das, D. Bhattacharya, An investigation of the failure of low pressure steam turbine blades, Eng. Fail. Anal. 5 (3) (1998) 181–193.

[26] S. Barella, M. Bellogini, M. Boniardi, S. Cincera, Failure analysis of a steam turbine rotor, Eng. Fail. Anal. 18 (6) (2011) 1511–1519.

[27] G. Das, S.G. Chowdhury, A.K. Ray, S.K. Das, D.K. Bhattacharya, Turbine blade failure in a thermal power plant, Eng. Fail. Anal. 10 (1) (2003) 85–91.

[28] I. Paterson, J. Wilson, Use of damage monitoring systems for component life optimisation in power plant, Int. J. Pressure Vessels Piping 79 (8–10) (2002) 541–547.

[29] P. Wang, L. Cui, M. Lyschik, A. Scholz, C. Berger, M. Oechsner, A local extrapolation based calculation reduction method for the application of constitutive material models for creep fatigue assessment, Int. J. Fatigue 44 (2012) 253–259.

13

[30] A. Benato, A. Stoppato, S. Bracco, Combined cycle power plants: A comparison between two different dynamic models to evaluate transient behaviour and residual life, Energy Convers. Manage. 87 (2014) 1269–1280.

[31] A. Benato, A. Stoppato, A. Mirandola, Dynamic behaviour analysis of a three pressure level heat recovery steam generator during transient operation, Energy 90 (2015) 1595–1605.

[32] A. Benato, S. Bracco, A. Stoppato, A. Mirandola, Dynamic simulation of combined cycle power plant cycling in the electricity market, Energy Convers. Manage. 107 (2016) 76–85.

[33] D. Ghosh, H. Roy, S. Ray, A. Shukla, High temperature corrosion failure of a secondary superheater tube in a thermal power plant boiler, High Temp. Mater. Process. 28 (1–2) (2009) 109–114.

[34] N. Mukhopadhyay, B. Dutta, H. Kushwaha, On-line fatigue–creep monitoring system for high-temperature components of power plants, Int. J. Fatigue 23 (6) (2001) 549–560.

[35] A.Y. Saber, G.K. Venayagamoorthy, Resource scheduling under uncertainty in a smart grid with renewables and plug-in vehicles, IEEE Syst. J. 6 (1) (2011) 103–109.

[36] H. Pandžić, I. Kuzle, T. Capuder, Virtual power plant mid-term dispatch optimization, Appl. Energy 101 (2013) 134–141.

[37] S.M. Nosratabadi, R.-A. Hooshmand, E. Gholipour, A comprehensive review on microgrid and virtual power plant concepts employed for distributed energy resources scheduling in power systems, Renew. Sustain. Energy Rev. 67 (2017) 341–363.

[38] R. Kehlhofer, F. Hannemann, B. Rukes, F. Stirnimann, Combined-cycle gas & steam turbine power plants, Pennwell Books, 2009.

[39] Thermoflow, GT Pro 24.0, Thermoflow Inc, 2014.

[40] Modelon, Thermal Power Library, https://www.modelon.com/library/thermal-power-library/, 2015.

[41] Dassault Systemes, https://www.3ds.com/products-services/catia/products/dymola/, 2016.

[42] Modelica Association, https://www.modelica.org/, 2019.

[43] R.M. Montañés, S.Ó. GarDarsdóttir, F. Normann, F. Johnsson, L.O. Nord, Demonstrating load-change transient performance of a commercial-scale natural gas combined cycle power plant with post-combustion CO_2 capture, Int. J. Greenhouse Gas Control 63 (2017) 158–174.

[44] L. Ljung, System identification: theory for the user, Prentice-hall, 1987.

[45] S. Timoshenko, J.N. Goodier, Theory of Elasticity, McGraw-Hill book Company., 1951.

[46] J. Schijve, Fatigue of structures and materials in the 20th century and the state of the art, Int. J. Fatigue 25 (8) (2003) 679–702.

[47] M. Matsuishi, T. Endo, Fatigue of metals subjected to varying stress, Japan Soc. Mech. Eng., Fukuoka, Japan 68 (2) (1968) 37–40.

[48] S.D. Downing, D.F. Socie, Simple rainflow counting algorithms, Int. J. Fatigue 4 (1) (1982) 31–40.

[49] R. Sunder, S. Seetharam, T. Bhaskaran, Cycle counting for fatigue crack growth analysis, Int. J. Fatigue 6 (3) (1984) 147–156.

[50] G. Marsh, C. Wignall, P.R. Thies, N. Barltrop, A. Incecik, V. Venugopal, L. Johanning, Review and application of rainflow residue processing techniques for accurate fatigue damage estimation, Int. J. Fatigue 82 (2016) 757–765.

[51] M. Miner, Cumulative damage in fatigue, J. Appl. Mech. 12 (1945) A159–A164.

[52] A. Fatemi, L. Yang, Cumulative fatigue damage and life prediction theories: a survey of the state of the art for homogeneous materials, Int. J. Fatigue 20 (1) (1998) 9–34.

[53] D.F. Socie, Multiaxial fatigue damage models, J. Eng. Mater. Technol.

[54] B.-R. You, S.-B. Lee, A critical review on multiaxial fatigue assessments of metals, Int. J. Fatigue 18 (4) (1996) 235–244.

[55] S. Lucia, T. Finkler, S. Engell, Multi-stage nonlinear model predictive control applied to a semi-batch polymerization reactor under uncertainty, J. Process Control 23 (9) (2013) 1306–1319.

[56] D. Krishnamoorthy, B. Foss, S. Skogestad, Real-time optimization under uncertainty applied to a gas lifted well network, Processes 4 (4) (2016) 52.

[57] D. Krishnamoorthy, B. Foss, S. Skogestad, A distributed algorithm for scenario-based model predictive control using primal decomposition, IFAC-PapersOnLine 51 (18) (2018) 351–356.

[58] M. Thombre, Z. Mdoe, J. Jäschke, Data-driven robust optimal operation of thermal energy storage in industrial clusters, Processes 8 (2) (2020) 194.

[59] D. Kraft, A software package for sequential quadratic programming, Forschungsbericht- Deutsche Forschungs- und Versuchsanstalt fur Luft- und Raumfahrt.

[60] D. Kraft, Algorithm 733: Tomp–fortran modules for optimal control calculations, ACM Trans. Math. Software (TOMS) 20 (3) (1994) 262–281.

[61] Steven G. Johnson, The NLopt nonlinear-optimization package, http://github.com/stevengj/nlopt.

[62] S. Spigarelli, E. Cerri, P. Bianchi, E. Evangelista, Interpretation of creep behaviour of a 9Cr–Mo–Nb–V–N (T91) steel using threshold stress concept, Mater. Sci. Technol. 15 (12) (1999) 1433–1440.

Publication V

Flexible thermal power plants integrated with CO_2 capture systems can balance the intermittent power generation of renewable energy sources with low-carbon electricity. Among these power systems, natural gas combined cycles will play a fundamental role because of their faster operation and higher efficiency. Optimisation-based control strategies can enhance the flexible power dispatch of these systems and improve their performance during transient operation. This work proposes a model predictive control (MPC) strategy to stabilise these power plants with post-combustion CO_2 capture based on temperature swing chemical absorption and provide offset-free reference tracking. A delta-input formulation with disturbance modelling is proposed, as it provides more efficient computation with offset-free control. Data-based models were developed to replicate the performance of the actual power and capture plants. Prediction of nonlinear behaviour was accomplished by creating a network of local linear models, which allowed the formulation of the dynamic optimisation program in the MPC strategy as a convex quadratic programming problem. A case study demonstrated the effectiveness of the proposed MPC to balance drastic changes on power demand and keep specified capture ratios. Furthermore, the reduced deviations achieved in the reboiler temperature suggest that the nominal value of this parameter could be increased to improve the desorption process without risks of reaching temperatures where the solvent would degradate.

Model predictive control for combined cycles integrated with CO$_2$ capture plants

Jairo Rúa [a,*], Magne Hillestad [b], Lars O. Nord [a]

[a] *Department of Energy and Process Engineering, Norwegian University of Science and Technology, Norway*
[b] *Department of Chemical Engineering, Norwegian University of Science and Technology, Norway*

ABSTRACT

Flexible thermal power plants integrated with CO$_2$ capture systems can balance the intermittent power generation of renewable energy sources with low-carbon electricity. Among these power systems, natural gas combined cycles will play a fundamental role because of their faster operation and higher efficiency. Optimisation-based control strategies can enhance the flexible power dispatch of these systems and improve their performance during transient operation. This work proposes a model predictive control (MPC) strategy to stabilise these power plants with post-combustion CO$_2$ capture based on temperature swing chemical absorption and provide offset-free reference tracking. A delta-input formulation with disturbance modelling is proposed, as it provides more efficient computation with offset-free control. Data-based models were developed to replicate the performance of the actual power and capture plants. Prediction of nonlinear behaviour was accomplished by creating a network of local linear models, which allowed the formulation of the dynamic optimisation program in the MPC strategy as a convex quadratic programming problem. A case study demonstrated the effectiveness of the proposed MPC to balance drastic changes on power demand and keep specified capture ratios. Furthermore, the reduced deviations achieved in the reboiler temperature suggest that the nominal value of this parameter could be increased to improve the desorption process without risks of reaching temperatures where the solvent would degradate.

1. Introduction

Climate change mitigation requires a profound reduction of greenhouse gas emissions (IPCC, 2014; 2018). By sector, power generation is the main contributor to global CO$_2$ emissions because of its reliance on fossil fuels (IEA, 2019). Deployment of intermittent renewable energy sources, mainly wind and solar, has concentrated most of the efforts to decarbonise this sector (IEA, 2019). However, a broader portfolio of technologies is necessary to meet the increasing power demand whilst ensuring a safe, efficient and sustainable electric market. In this context, the integration of flexible carbon capture and storage (CCS) with thermal power plants is expected to play a fundamental role in the reduction of the CO$_2$ emissions associated with the power sector (IPCC, 2005; 2014).

Thermal power plants, especially natural gas combined cycles (NGCC), are recognised as a viable technology to accommodate the intermittent power generation from renewable energy sources and balance the electric grid (Kondziella and Bruckner, 2016; Eser et al., 2017; González-Salazar et al., 2017). Flexible CCS may enhance this dispatchable nature of flexible thermal power plants by providing low carbon electricity in a cost effective manner (Montañés et al., 2016; Heuberger et al., 2016; 2017a; 2017b). Post-combustion CO$_2$ capture (PCC) based on liquid-absorbents is arguably the most mature CCS technology, with two commercial-scale capture facilities integrated with coal power plants in operation (Bui et al., 2018). Nevertheless, the deployment of this technology in power markets dominated by intermittent renewable energy sources requires the demonstration that integration of CCS and thermal power plants does not inhibit flexible and efficient power generation, and stable CO$_2$ capture.

The dominant dynamics that govern the transient operation of thermal power plants, CO$_2$ capture plants and systems integrated by both technologies were extensively analysed by Rúa et al. (2020b). Two different dynamic behaviour define transient operation of these technologies. Thermal power plants operate in short time-scales and are limited by the large heat capacitance of the steam generator, whereas post-combustion CO$_2$ cap-

* Corresponding author.
E-mail addresses: jairo.r.pazos@ntnu.no (J. Rúa), lars.nord@ntnu.no (L.O. Nord).

Nomenclature

Latin Symbols

$\tilde{\tilde{A}}$	State estimation
$\widetilde{A}$	Delta-input state matrix
A	State matrix
$A(q^{-1})$	Polynomial ARX model
A_a	Augmented state matrix
a	Coefficients simplified models
$\widetilde{B}$	Delta-input input matrix
B	Input matrix
$B(q^{-1})$	Polynomial ARX model
B_a	Augmented input matrix
B_d	Disturbance input matrix
b	Coefficients simplified models
$\widetilde{C}$	Delta-input output matrix
C	Output matrix
c	Centre validity function
C_a	Augmented output matrix
C_d	Disturbance output matrix
Δu	Delta-input control vector
δu	Delta-input control action
d	Disturbance vector
F	MIMO delta-input penalty vector
f	Delta-input penalty vector
G	MIMO delta-input inequality matrix
g	Delta-input inequality matrix
H	Delta-input matrix output equation
I	Identity matrix
J	Objective function
K	Observer gain matrix
K_f	Kalman filter
M	number local ARX models
N	Time horizon
P	MIMO delta-input inequality vector
p	Delta-input inequality vector
Q	Weight matrix
q^{-1}	Backwards shift operator
Q_p	Process noise covariance
R	Penalty vector
R^2	Coefficient of determination
R_m	Measurement noise covariance
t	Time (s)
u	Manipulated variable
w	Width validity function
$\widetilde{x}$	Delta-input state vector
x	State vector
x_a	Augmented input state vector
y	Predicted variable, output vector
Z	Estimator covariance matrix

Greek Symbols

Γ	Delta-input weight matrix
γ	Local operating point
λ	Weights objective function
Φ	MIMO delta-input weight matrix
Ψ	Unit lower triangular matrix
ξ	Local validity function
σ^2	Covariance
ε	Stochastic error

Subscripts

0	Initial conditions
d	Disturbance

n_u	Order ARX input
n_y	Order ARX output
pow	Power
ramp	Ramping rate
ref	Reference trajectory
u	Inputs
x	States

Superscripts

-	Previous estimation
low	Lower bound
up	Upper bound

ture plants are characterised by slow responses and long time-scales owing to the large volumes of stored solvent, the impact of large vessels on residence time, and the transport delay introduced by some equipment. This different transient behaviour does not limit power generation since variable steam extraction from the intermediate and low pressure cross-over of the steam turbine does not significantly affect the steam cycle of the power plant, albeit it has an impact on process variables of the CO_2 capture plant (Rúa et al., 2020b). Thus, control strategies must consider the different dynamic nature of thermal power plants and post-combustion CO_2 capture plants to adequately stabilise the process variable of each plant within their operation time-scales.

Control of traditional thermal power plants refers to matching the power generation to the demand and the stabilisation of the steam cycle. Natural gas combined cycles utilise the gas turbine to control power generation owing to their fast dynamics (Kehlhofer et al., 2009). Coal and biomass power plants must adapt the fuel and air injected in the boiler and throttle the superheated and reheated steam flow at the inlet of the steam turbine (Alobaid et al., 2017). Power generation control in coal and biomass power plants is hence dominated by the heat capacitance of the boiler. Therefore, the fast transient operation of gas turbines and their capability to adapt the power output within seconds make NGCCs more suitable for flexible operation and grid balance than coal and biomass power plants (Hentschel et al., 2016; Eser et al., 2017). Furthermore, NGCCs can under- and over-shoot the power generated by the gas turbine to compensate the slower transient of the steam cycle, enhancing the flexibility that this type of power plants provide to the grid (Rúa et al., 2020a; Rúa and Nord, 2020).

Steam cycle control includes the regulation of the fluid inventory in the steam drums, deaerators, condensers, and storage vessels; pressure control of the low-, medium- and high-pressure sections of the steam cycle; and temperature limitation of the superheated and reheated steam to avoid damaging the pipe system and the steam turbine. Inventory control refers to the stabilisation of the mass flows so the steady-state mass balances for each of the components and the overall power plant are satisfied (Aske and Skogestad, 2009). Proportional-integral (PI) controllers are normally used for control of water levels since the main objective of this control layer is to stabilise power plant operation, although three-element controllers where the drum level, feedwater flow and live-steam flow are embedded in a PID (proportional-integral-derivative) cascade controller are traditionally implemented in thermal power plants (Mansour et al., 2003; Kehlhofer et al., 2009). These controllers adjust the feedwater mass flow by changing the speed of the pumps or the opening of the control valves, depending on the type and design of the power plant. Model predictive control (MPC) strategies lead to further improvements in the inventory control of traditional power plants because of the dynamic optimisation carried out to determine the most suitable control action (Lu and Hogg, 1997; Prasad et al., 2000).

Pressure control is achieved by adjusting the feedwater mass flow rate and by valve throttling, specially in the lower-pressure sections of NGCCs where the pressure in the drum and deaerator may be controlled (Casella and Pretolani, 2006; Montañés et al., 2017c). In the high-pressure section of the steam cycle, strategies such partial arc and sliding pressure control lead to better part-load performance (Kehlhofer et al., 2009; Jonshagen and Genrup, 2010). Partial arc control regulates the steam admittance into the steam turbine with several valves in the stator of the first stage. In contrast, these valves are close to fully-open during sliding pressure operation to allow the variation of the high pressure and keep almost constant volumetric flow in the turbine, which results in higher part-load isentropic efficiency (Jonshagen and Genrup, 2010). If the high pressure of the steam cycle is not allowed to fluctuate, optimisation-based strategies lead to improved control of this pressure as they reduce the deviation from its set-point (Lu and Hogg, 1997; Prasad et al., 1998; 2000; Peng et al., 2009).

The temperature in the hot sections of the steam cycle, i.e. the outlet of the supeheater and reheater, must be controlled to avoid damaging the materials. Spray cooling is hence necessary to inject pressurised water in the steam flow and reduce its temperature. The opening of the attemperator valves regulating the flow of pressurised water may be defined by PID controllers (Alobaid et al., 2008; Kehlhofer et al., 2009; Montañés et al., 2017c; Garðarsdóttir et al., 2017), adaptative controllers (Matsumura et al., 1998), or optimisation-based controllers (Peng et al., 2009; Prasad et al., 1998, 2000; Rúa et al., 2020a; Rúa and Nord, 2020). Among the different alternatives to regulate the maximum temperature in the steam cycle, model predictive control shows the minimum offset from the set-point and the fastest stabilisation time (Rúa et al., 2020a; Rúa and Nord, 2020).

In contrast to thermal power plants, control of post-combustion CO_2 capture plants is not a mature field and most of the available knowledge comes from dynamic studies and test campaigns in pilot plants. Basic control of PCC plants reduces to stabilise liquid levels in sumps of absorber and stripper columns, reboiler and condenser; regulate the temperature of lean solvent and condenser; adapt the pressure of the reboiler and CO_2 product, and maintain a constant solvent composition (Panahi and Skogestad, 2011; Schach et al., 2013; Flø et al., 2015; 2016; Walters et al., 2016; Montañés et al., 2017a; 2018; Wu et al., 2020). Temperature control is achieved by heat exchangers where the mass flow rate of cooling water is the manipulated variable, whereas inventory control requires several pumps to stabilise liquid levels in different equipment, although valves may also be used. Throttling regulates the pressure of product of CO_2 and the mass flow rate of make-up solvent, or water, needed for a constant composition. Control of all these process variables may lead to over-constrained systems, and some might be left uncontrolled. For instance, the level in the reboiler is controlled and the sump level in the stripper varies freely in the Brindisi pilot plant (Flø et al., 2016), whereas the opposite inventory control approach is implemented at Technology Centre Mongstad (TCM) (Montañés et al., 2017a; 2018).

This basic control strategy aims at stabilising the main process variables and ensuring safe operation of PCC plants. Therefore, PID controllers are normally implemented. This control layer is similar among different pilot plants and dynamic process models (see e.g. the reviews by Salvinder et al. (2019) and Wu et al. (2020)). The main difference in control strategies and performance of PCC plants lies on the pairings and methods used to control performance indicators, i.e. capture rate or CO_2 product, liquid solvent to gas (L/G) ratios, energy performance ratios, and reboiler performance, where the latter may refer to outlet solvent temperature, outlet lean loading or heat duty. The majority of pairings between controlled and manipulated variables originate from insights obtained during process dynamic simulations, albeit relative gain

array (RGA) analyses and self-optimisation procedures have been proposed (Panahi and Skogestad, 2011; 2012; Schach et al., 2013; Nittaya et al., 2014; Sahraei and Ricardez-Sandoval, 2014; Luu et al., 2015; Manaf et al., 2016; Gaspar et al., 2016). Different control design strategies may lead to distinct pairings with various performance, but none of the design methods have proved systematically superior.

Traditional PID controllers are able to reject disturbances and track references of CO_2 capture rates by modifying the mass flow rate of lean/rich solvent at the inlet/outlet of the absorber column (Lawal et al., 2010; Nittaya et al., 2014; Garðarsdóttir et al., 2015; Luu et al., 2015; Manaf et al., 2016; Gaspar et al., 2016; Montañés et al., 2017a), or the steam flow in the reboiler, i.e. the heat duty (Panahi and Skogestad, 2011; Nittaya et al., 2014; Montañés et al., 2017a). Similarly, PIDs can achieve close to contant reboiler temperature (Lawal et al., 2010; Panahi and Skogestad, 2011; 2012; Nittaya et al., 2014; Walters et al., 2016; Montañés et al., 2017a; 2018), L/G ratios (Garðarsdóttir et al., 2015; Montañés et al., 2017a; 2018), lean solvent loading (Garðarsdóttir et al., 2015; Gaspar et al., 2016) or energy performance indicators (Luu et al., 2015; Manaf et al., 2016) by manipulating the mass flow rate of solvent or the reboiler heat duty. These studies demonstrate PID controllers can stabilise PCC plants subjected to large disturbances within reasonable periods of time, albeit the lack of agreement on the most adequate pairing for key process variables.

Nevertheless, PID controllers may not be able to stabilise process variables within desirable bounds and can require excessively long settling times if the tuning is not adequate or the disturbance too drastic (Luu et al., 2015). Model predictive control can address these challenges by computing the control input through a dynamic optimisation problem where constraints in the controlled and manipulated variables ensure that process parameters remain within acceptable limits. MPC also originates less oscillations of smaller amplitude than PIDs for a given disturbance (Arce et al., 2012; Sahraei and Ricardez-Sandoval, 2014; Luu et al., 2015; Zhang et al., 2016; He et al., 2018; Li et al., 2018; Wu et al., 2018a; 2019a). This behaviour is due to the optimisation of predicted trajectories over a time horizon, which leads to shorter settling times and tighter control of PCC plants. Hauger et al. (2019) demonstrated the tight control achieved by MPC strategies in different tests performed in two pilot facilities (Tiller and TCM).

Furthermore, economic criteria such as market prices or energy cost may be included in MPC formulations to reduce the penalty of CCS systems while keeping PCC plants stable (Arce et al., 2012; Decardi-Nelson et al., 2018). This eases the integration of scheduling and control strategies since the outputs of the scheduling process may modify, in addition to the set-points of the controlled variables, tuning parameters in the optimisation problem included in the MPC (He et al., 2016).

Whilst there are several studies analysing control strategies for these different technologies operating independently, there are relative few studies considering the control of thermal power plants integrated with post-combustion CO_2 capture plants (Lawal et al., 2012; Mechleri et al., 2017; Garðarsdóttir et al., 2017; Montañés et al., 2017c; Marx-Schubach and Schmitz, 2019; Wu et al., 2019b; 2019c). Decentralised PID controllers can stabilise these integrated systems within their different time-scales, where the dominant dynamics of each plant dictate the settling time. However, the integration of CO_2 capture plants increases the settling time of process variables (e.g. steam pressure) in coal and natural gas thermal power plants because of the long stabilisation periods of CO_2 capture systems (Lawal et al., 2012; Garðarsdóttir et al., 2017; Montañés et al., 2017c; Mechleri et al., 2017). Similarly to control strategies in individual PCC plants, pairing of controlled and manipulated variables affects notably the performance of these decentralised controllers, as it influences the amplitude of fluctua-

tion and settling time of different process variables in both plants (Garðarsdóttir et al., 2017; Montañés et al., 2017c; Mechleri et al., 2017). Moreover, PID controllers can also regulate the start-up of integrated systems and achieve desirable CO_2 capture rates and power generation (Marx-Schubach and Schmitz, 2019).

Model predictive control can improve the control of thermal power plants integrated with CO_2 capture systems and reduce the settling time of key performance variables (Wu et al., 2019b; 2019c). MPC also enables the definition of different operation modes, which allows prioritising power generation, grid balancing or CO_2 capture according to market conditions and current regulations (Wu et al., 2019b; 2019c). However, power generation from coal-fired power plants is still limited by the heat capacitance of the steam generator, and MPC strategies can only enhance their flexible operation by reducing the steam extraction from the CO_2 capture plant, which leads to momentarily decreases of carbon capture (Wu et al., 2019b; 2019c). Natural gas combined cycles regulate their power generation through the gas turbine, and do not need to modify the steam extraction from the capture plant to balance the grid. Therefore, application of MPC strategies to NGCCs integrated with PCC plants can further enhance the flexible operation of both systems while taking advantage of the fast transient operation of NGCCs to balance power generation and demand.

This work demonstrates the application of model predictive control strategies to full-scale natural gas combined cycles integrated with post-combustion CO_2 capture plants with the objective of minimising the deviation of key process variables from their set-points. Section 2 describes the dynamic, full-scale NGCC-PCC model and the simplified models used in the MPC strategy, while Section 3 discusses how to achieve offset-free MPC with these simplified models and details its mathematical formulation. Section 4 demonstrates the fast control achieved by the proposed MPC strategy through a case study where the integrated system needs to balance a decrease in power demand. Final remarks and conclusions are included in Section 5.

2. Modelling

This section includes the different models developed to demonstrate the application of model predictive control strategies to natural gas combined cycles integrated with capture plants. Section 2.1 describes the high-fidelity model used to replicate the behaviour of the NGCC-PCC system, whereas Section 2.2 presents the simplified models included in the dynamic optimisation problem to predict the future behaviour of the actual system.

2.1. Dynamic modelling of a NGCC-PCC system

Natural gas combined cycles are expected to balance the intermittent power generation associated with renewable energy sources because of their fast and flexible operation. Moreover, triple-pressure NGCCs with reheating are the most efficient and less polluting fossil-fuelled thermal power plants (Kehlhofer et al., 2009; Alobaid et al., 2017). This study considers a full-scale 615 MWe NGCC with this configuration. The design was carried out with GT PRO (Thermoflow, 2014) because it provides detailed descriptions of the geometry of the equipment, off-design performance, and operation maps of pumps and gas turbines. This data was implemented in a high-fidelity dynamic model developed in Modelica (Modelica Association, 2019; Dassault Systemes, 2016) with the specialized TPL library (Modelon, 2015), which is based on conservation equations, detailed heat transfer and pressure drop correlations, and maps of performance for the turbomachinery components.

This thermal power plant was integrated with a full-scale 30 wt% MEA-based post-combustion capture process, as this is the

most mature CCS technology available. System integration occurred between the intermediate- and low-pressure steam turbines of the NGCC and the reboiler of the PCC plant, where steam extracted from the steam cycle provides the energy to regenerate the solvent in the capture plant. The design of the low-pressure section of the steam turbine was adapted to nominal operating conditions, i.e. steam is extracted to achieve a 90% capture rate at 100% gas turbine load (Jordal et al., 2012; Rezazadeh et al., 2015). Furthermore, the design of the PCC plant considered the nominal CO_2 capture rate, the exhaust gas CO_2 concentration and conditions (i.e. flow rate, temperature, pressure), the allowable pressure drops in the absorber and stripper columns, column flooding limits and a reasonable balance between capital and operational costs (Jordal et al., 2012; Dutta et al., 2017). Because of the size of the NGCC and the amount of flue gas generated, these requirements were met with a parallel configuration with two absorber columns and one stripper (Montañés et al., 2017c; Dutta et al., 2017). A detailed modelling description and thorough validation results of these dynamic models can be found in the work by Montañés et al. (2017c). Fig. 1 represents the layout of the NGCC-PCC system.

These plants exhibit different dynamic behaviour. Load changes in the gas turbine lead to immediate variations in the exhaust gas conditions. However, these changes affect progressively the steam cycle. Thus, the heat capacitance of the HRSG dominates the transient performance of the NGCC. For thermal power plants of this type and size, step changes in the exhaust gas conditions show dominant dynamics of approximately 10 min, with stabilisation times of 20–25 min (Hentschel et al., 2016; Montañés et al., 2017c). PCC plants have slower transient performance because of the long residence time of the solvent, the transport delay introduced by heat exchangers, and the large amount of solvent stored in vessels and liquid hold-ups (Rúa et al., 2020b). Similarly, step changes in the exhaust gas conditions show that the dominant dynamics of PCC plants of this size occur in approximately 60 min with stabilisation times of several hours (Lawal et al., 2010; 2012; Flø et al., 2015; 2016; Garðarsdóttir et al., 2015; Montañés et al., 2017c; 2017b).

2.2. System Identification

The computational cost of simulating the high-fidelity dynamic model of the NGCC-PCC system described in Section 2.1 inhibits its utilisation in optimisation-based control strategies. Therefore, simplified models that replicate the behaviour of specific thermodynamic variables (e.g. reboiler temperature, capture rate, mechanical power generation) are required to predict the performance of the integrated system in the model predictive control strategy proposed in this work.

System identification refers to the development of data-based dynamic models (Ljung, 1987), and was utilised to develop autoregressive models with exogenous variables (ARX) that predict the dynamic behaviour of variables of interest. Eq. (1) represents the general structure of an ARX model:

$$A(q^{-1}) y(t) = B(q^{-1}) u(t) + \varepsilon(t) \tag{1}$$

where y is the predicted and controlled variable, u is the manipulated variable associated with it, A and B are polynomials in the backwards shift operator q^{-1} of order n_y and n_u, respectively, and $\varepsilon \in \mathcal{N}(0, \sigma^2)$.

$$A(q^{-1}) = 1 + a_1 q^{-1} + a_2 q^{-2} + \cdots + a_{n_y} q^{-n_y}$$

$$B(q^{-1}) = b_1 q^{-1} + b_2 q^{-2} + \cdots + b_{n_u} q^{-n_u}$$

Table 1 summarises the set of input-output pairs, i.e. the controlled variable and its associated manipulated variable, considered in this work to control the operation of the NGCC-PCC system. These input-output pairs present nonlinear behaviour and
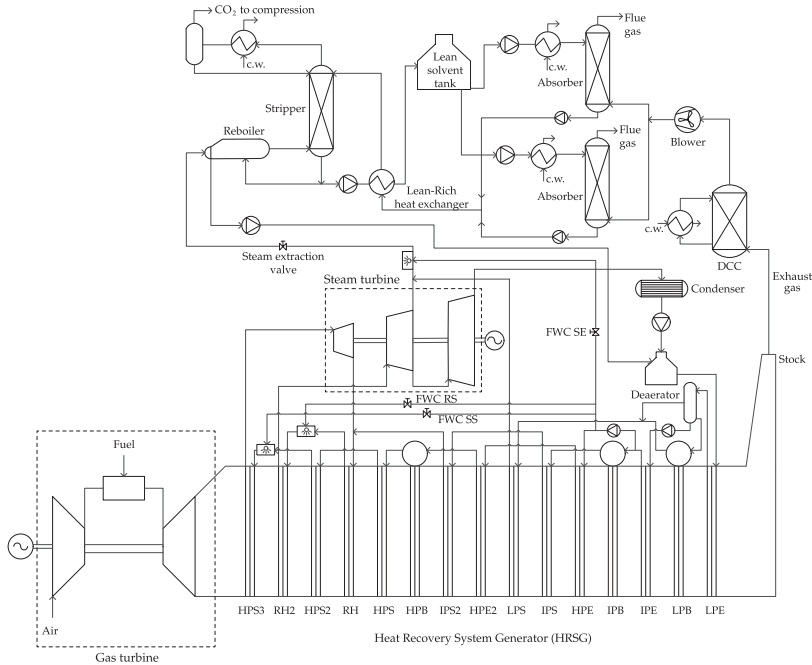
Fig. 1. Process diagram of the natural gas combined cycle integrated with the post-combustion capture plant. The nomenclature is as follows. E: Economiser, B: Boiler, S: Superheater, R: Reheater P: Pressure, L: Low, I: Intermediate, H: High, FWC: Feed-water cooling, RS: Reheated steam, SS: Superheated steam, SE: steam extraction, DCC: Direct contact cooler, c.w.: cooling water.

single ARX models cannot predict them accurately in broad operation ranges because of their linearity. Local model networks of linear ARX models can overcome this limitation (Johansen and Foss, 1993; Wu et al., 2018b; Jung et al., 2020). This modelling approach relies on the development of several linear ARX models at different operation points for each input-output pair. The overall prediction of a local model network is the result of interpolating the individual predictions of the local ARX models according to current operation point (Johansen and Foss, 1993). Thus, local models neighbouring this operation condition contribute more to the overall prediction than locals models of regimes far from the operation point. The output of a local model network is:

$$y(t) = \sum_{i=1}^{M} y_i(t) \; \xi_i(\gamma) \tag{2}$$

where M is the number of local models for each input-output pair, $y_i(t)$ represents the outputs of the local ARX models, ξ is the local validity function that weights the contribution of each local ARX model, and γ is the parameter defining the current operating point. This is equivalent to first interpolating the parameters (a, b) of the local ARX models using the local validity function ξ and then computing the output of the overall ARX model with these parameters.

This work considered a Gaussian validity function because it satisfies a necessary condition to achieve arbitrarily good predictions with local model networks (Johansen and Foss, 1993):

$$\xi_i(\gamma) = \frac{\exp\left(-\frac{1}{2}[(\gamma - c_i)/w_i]^2\right)}{\sum_{j=1}^{M} \exp\left(-\frac{1}{2}\left[(\gamma - c_j)/w_j\right]^2\right)} \tag{3}$$

where c_i and w_i are, respectively, the centres and widths of the local Gaussian interpolation functions. Table A.4 includes the number

of local models for each input-output pair, the parameters of each local ARX model, and the variables defining their validity functions.

Data to generate these models was obtained from excitation of the high-fidelity model described in Section 2.1 at different operation conditions. Therefore, each set of data was used to generate a single local ARX model for every input-output pair. Random gaussian signals (RGS) were superimposed on the controllers of the NGCC-PCC system in closed-loop since this approach enhances the identification of ARX models (Gevers and Ljung, 1986; Forssell and Ljung, 1999; Gevers, 2005; Gevers et al., 2006; Mišković et al., 2008). In addition, an unique validation set of data covering the entire operation range of the NGCC-PCC system was generated following the same approach.

Table 1 summarises the prediction accuracy of the local model network for each input-output pair measured by the coefficient of determination R^2. The low R^2 of the simplified models for the superheating and reheating temperature originate from the nature of the validation data. The RGS signals superimposed on the controllers to generate the identification data fluctuated faster than the dominant dynamics of the steam cycle, which lead to drastic and fast changes in the controlled and manipulated variables of the NGCC. This created a challenging set of data that allowed testing whether the local model network could predict large and frequent fluctuations. In contrast, the PCC data does not show this behaviour because of the slower dominant dynamics of the capture plant and its buffering effect, mainly through solvent vessels and liquid hold-ups (Rúa et al., 2020b). This transient performance results in smoother and slower variations easier to predict that lead to higher R^2 values. Fig. B.4 illustrates this different behaviour between the NGCC and PCC plants for a small set of the validation data, and how the ARX models of the NGCC adequately predict the trajectory of the output variables despite the lower R^2 values.

Table 1
Input-output pairs with model order and coefficient of determination.

Plant	Input-output pair		Order		Nominal		R^2[%]
	Controlled variable (y)	Manipulated variable (u)	n_y	n_u	n_y	n_u	
NGCC	Power generation	Gas turbine load					99.95
	Superheated steam temperature	Opening attemperator valve 1	2	2	592.7 °C	0.02655	69.59
	Reheated steam temperature	Opening attemperator valve 2	2	2	592.5 °C	0.07882	74.37
PCC	Capture rate	Mass flow lean solvent	1	1	90 %	614	98.40
	Reboiler temperature	Opening steam extraction valve	1	1	119.22 °C	0.69	99.09

In contrast to the other simplified models, the power generation of the NGCC was predicted using an unique polynomial over the entire set of operating conditions. A simple representation for this variable is possible owing to the linear relationship between the power generation of the NGCC and the load of the gas turbine over a broad operating region. The structure of this model is:

$$y(t) = a + b\,u(t) \qquad (4)$$

ARX models are suitable for system identification procedures because the computation of their coefficients becomes a simple least-square problem or a convex optimisation, whereas other structures may involve more complex, possibly non-convex, identification problems (Huusom et al., 2010). However, for analysis purposes, state-space forms of ARX models are preferred. The realisation in observable form of the ARX model in Eq. (1) is:

$$x_{k+1} = A x_k + B u_k \qquad (5a)$$

$$y_k = C x_k \qquad (5b)$$

with

$$A = \begin{bmatrix} -a_1 & 1 & 0 & \cdots & 0 \\ -a_2 & 0 & 1 & \cdots & 0 \\ \vdots & \vdots & \vdots & \ddots & \vdots \\ -a_{n_y-1} & 0 & 0 & \cdots & 1 \\ -a_{n_y} & 0 & 0 & \cdots & 0 \end{bmatrix} \quad B = \begin{bmatrix} 0 \\ \vdots \\ b_1 \\ \vdots \\ b_{n_u} \end{bmatrix} \quad C = [1\,0\cdots 0]$$

where B has $n_y - n_u$ zeros, and $x \in \mathbb{R}^{n_y}$, $u, y \in \mathbb{R}$, $A \in \mathbb{R}^{n_y \times n_y}$, $B \in \mathbb{R}^{n_y \times 1}$, and $C \in \mathbb{R}^{1 \times n_y}$. This realisation is valid when the ARX model leads to proper rational transfer functions, i.e. $n_y \geq n_u$. The stochastic error term in Eq. (1) is not included because of the deterministic data used during system identification.

3. Model predictive control

Control strategies based on MPC formulations require the development of different models and optimisation problems to ensure optimal computation of control inputs, offset-free tracking of controlled variables and adequate estimation of states. Fig. 2 shows a diagram of the MPC strategy proposed in this work. The high-fidelity dynamic model of the NGCC-PCC system described in Section 2.1 replicates the behaviour of a real power plant with post-combustion CO_2 capture. Measurements from this model allow the estimation of the states in the system. This estimator uses a Kalman filter to update the state estimations and correct possible mismatches between the predictions of the responses by the simplified models and the measurements from the dynamic simulation of the NGCC-PCC plant. These estimates define the current state, i.e. the initial conditions, from where the dynamic optimisation problem in the MPC strategy starts to compute the optimal sequence of control inputs. The first element of this sequence is the control action imposed in the actual system. This process is repeated periodically, with a frequency dictated by the sampling time, to stabilise the operation of the NGCC integrated with the
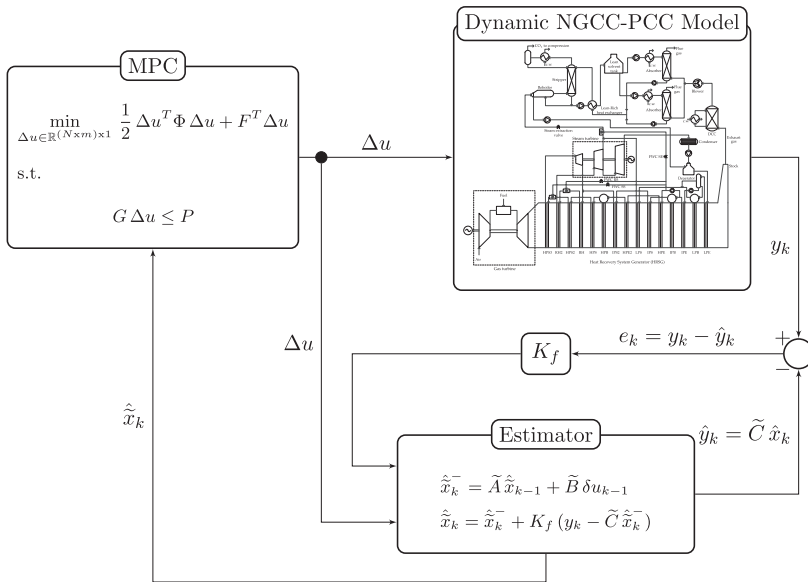

Fig. 2. Diagram of the proposed MPC strategy with a Kalman filter. Expressions within the diagram are developed throughout Section 3, while the dynamic model of the NGCC-PCC system is described in Section 2.1.

PCC plant. This MPC strategy includes all simplified models in a single controller as shown in Fig. 2.

This section describes different models and formulations of the MPC strategy, and details how they are combined in the integrated control structure represented in Fig. 2. Section 3.1 discusses reference tracking and offset-free MPC, and describes the formulation of this optimisation problem, whereas Section 3.2 builds up on this formulation and defines a simpler dynamic optimisation problem, called delta-input formulation, that only depends on the manipulated variables. Section 3.3 describes the estimator that predicts the states on the actual NGCC-PCC systems and presents an algorithm to solve the MPC control problem.

3.1. Reference tracking and offset-free MPC

Reference tracking is one of the main applications of model predictive control. This control strategy minimises the difference between outputs of a system and reference trajectories by computing control inputs through dynamic optimisation problems and implementing the first element of the calculated control sequence. The general formulation of linear MPC problems for reference tracking is:

$$\min_{x,u} \sum_{k=0}^{N-1} \frac{1}{2} \| Q (y_k - y_{\text{ref}}) \| + \| R (u_k - u_{k-1}) \| \tag{6a}$$

s.t.

$$x_{k+1} = A x_k + B u_k \tag{6b}$$

$$y_k = C x_k \tag{6c}$$

$$y^{\text{low}} \leq y_k \leq y^{\text{up}} \tag{6d}$$

$$u^{\text{low}} \leq u_k \leq u^{\text{up}} \tag{6e}$$

where $\| \cdot \|$ represents the two-norm that leads to a quadratic programming (QP) optimisation problem. Eq. (6b) and (6c) ensure that the state-space realisation of the identified ARX models is satisfied. Eqs. (6d) and (6e) limit the minimum and maximum values of the controlled and manipulated variables, respectively. The objective function in Eq. (6a) minimises the difference between controlled variables and their references y_{ref} and imposes a penalty in excessive utilisation of control inputs.

Nevertheless, reference tracking formulations of MPC strategies as in Eq. (6) can lead to offsets in the controlled variables due to unmeasured disturbances and plant-model mismatches. To overcome this limitation and ensure zero offset, models representing actual systems can be augmented with a disturbance model, which acts as an integrator driving the tracking error to zero. This allows finding the control inputs that minimise both the effect of the disturbance on the controlled variables and differences between model and system (Pannocchia and Rawlings, 2003; Borrelli and Morari, 2007; Pannocchia, 2015; Rawlings et al., 2017). The state-space model in Eq. (5) becomes:

$$x_{a,k+1} = A_a x_{a,k} + B_a u_k \tag{7a}$$

$$y_k = C_a x_{a,k} \tag{7b}$$

where vectors and matrices are:

$$\begin{bmatrix} x_{k+1} \\ d_{k+1} \end{bmatrix} = \begin{bmatrix} A & B_d \\ 0 & I \end{bmatrix} \begin{bmatrix} x_k \\ d_k \end{bmatrix} + \begin{bmatrix} B \\ 0 \end{bmatrix} u_k$$

$$y_k = \begin{bmatrix} C & C_d \end{bmatrix} \begin{bmatrix} x_k \\ d_k \end{bmatrix}$$

This augmented model achieves offset-free tracking if the system is stabilisable, the pair (A, C) is observable, the number of disturbances n_d:

$$n_d = p = 1$$

and the following condition holds (Pannocchia and Rawlings, 2003; Borrelli and Morari, 2007; Pannocchia, 2015; Rawlings et al., 2017):

$$\text{rank} \begin{bmatrix} A - I & B_d \\ C & C_d \end{bmatrix} = n_y + n_d$$

Since the disturbance matrices $B_d \in \mathbb{R}^{n_y \times n_d}$ and $C_d \in \mathbb{R}^{1 \times n_d}$ can be chosen freely, the last condition holds if (A, C) is observable. In this work, the state-space realisation of the identified ARX models was expressed in observable form, and hence the pair (A, C) is always observable (Chen, 2013). Therefore, offset-free tracking reduces to the adequate selection of disturbance matrices B_d and C_d.

The MPC formulation in Eq. (6) for the system augmented with a disturbance model becomes:

$$\min_{x,u} \sum_{k=0}^{N-1} \frac{1}{2} \| Q (y_k - y_{\text{ref}}) \| + \| R (u_k - u_{k-1}) \| \tag{8a}$$

s.t.

$$x_{a,k+1} = A_a x_{a,k} + B_a u_k \tag{8b}$$

$$y_k = C_a x_{a,k} \tag{8c}$$

$$y^{\text{low}} \leq y_k \leq y^{\text{up}} \tag{8d}$$

$$u^{\text{low}} \leq u_k \leq u^{\text{up}} \tag{8e}$$

3.2. Delta-input formulation

Delta-input formulations of the MPC described in Eq. (8) are more suitable for reference tracking problems, as they penalise directly the rate of change of the manipulated variables (Borrelli and Morari, 2007). Furthermore, it reduces the number of optimisation variables and the computational cost of the dynamic optimisation. Section 3.2.1 describes the delta-input formulation of the MPC problem in Eq. (8), whereas Section 3.2.2 discusses how several state-space models can be merged into a common MPC problem.

3.2.1. Delta-input formulation for SISO systems

Define the delta-input control action that determines the rate of change of a manipulated variable:

$$\delta u_k := u_k - u_{k-1} \tag{9}$$

and augment the state-space equation in Eq. (7) with this new state and control input:

$$\begin{bmatrix} x_{a,k+1} \\ u_k \end{bmatrix} = \begin{bmatrix} A_a & B_a \\ 0 & I \end{bmatrix} \begin{bmatrix} x_{a,k} \\ u_{k-1} \end{bmatrix} + \begin{bmatrix} B_a \\ I \end{bmatrix} \delta u_k \tag{10a}$$

$$y_k = \begin{bmatrix} C_a & 0 \end{bmatrix} \begin{bmatrix} x_{a,k} \\ u_{k-1} \end{bmatrix} \tag{10b}$$

which can be written:

$$\tilde{x}_{k+1} = \tilde{A} \tilde{x}_k + \tilde{B} \delta u_k$$
$$y_k = \tilde{C} \tilde{x}_k$$

Define the vectors of controlled and manipulated variables over a time horizon N:

$$\delta u = [\delta u_0 \ \delta u_1 \ \ldots \ \delta u_{N-1}]^T$$

$$y = [y_1 \ y_2 \ \ldots \ y_N]^T$$

and eliminate the states in Eq. (10). The output equation, over the time horizon N, becomes:

$$y = H\delta u + A_0 \tilde{x}_0 \tag{11}$$

where

$$H = \begin{bmatrix} H_1 & 0 & \cdots & \cdots & 0 \\ H_2 & H_1 & 0 & \cdots & 0 \\ \vdots & \ddots & \ddots & \ddots & \vdots \\ \vdots & & H_2 & H_1 & 0 \\ H_N & \cdots & \cdots & H_2 & H_1 \end{bmatrix} \quad A_0 = \begin{bmatrix} \tilde{C}\tilde{A} \\ \tilde{C}\tilde{A}^2 \\ \tilde{C}\tilde{A}^3 \\ \vdots \\ \tilde{C}\tilde{A}^N \end{bmatrix}$$

with

$$H_i = \tilde{C}\tilde{A}^{i-1}\tilde{B} \qquad i \in \{1, 2, \ldots, N\}$$

$$\tilde{x}_0 = \tilde{x}[0]$$

With this reduced output equation, Eq. (11), and the definition of the delta control input in Eq. (9), the inequality constraints in the standard MPC formulation, Eq. (8d) and Eq. (8e), can be written as:

$$\begin{bmatrix} -H \\ H \\ -\Psi \\ \Psi \end{bmatrix} \delta u \leq \begin{bmatrix} -(y^{\text{low}} - A_0 \tilde{x}_0) \\ y^{\text{up}} - A_0 \tilde{x}_0 \\ -(u^{\text{low}} - u_{-1}) \\ u^{\text{up}} - u_{-1} \end{bmatrix} \tag{12}$$

where u_{-1} was the control action in the previous sampling time, and Ψ is an unit lower triangular matrix:

$$\Psi = \begin{bmatrix} 1 & 0 & \cdots & \cdots & 0 \\ 1 & 1 & \ddots & & \vdots \\ \vdots & \ddots & \ddots & \ddots & \vdots \\ \vdots & & \ddots & 1 & 0 \\ 1 & \cdots & \cdots & 1 & 1 \end{bmatrix}$$

Following the same approach, the objective function Eq. (8a) becomes:

$$\begin{aligned} J &= \frac{1}{2}(\|Q(y - y_{\text{ref}})\| + \|R\delta u\|) \\ &= \frac{1}{2}(\|Q(H\delta u + A_0 \tilde{x}_0 - y_{\text{ref}})\| + \|R\delta u\|) \\ &= \frac{1}{2}\Big[\delta u^T (H^T Q H + R)\delta u \\ &\quad + 2(A_0 \tilde{x}_0 - y_{\text{ref}})QH\delta u \\ &\quad + (A_0 \tilde{x}_0 - y_{\text{ref}})^T Q(A_0 \tilde{x}_0 - y_{\text{ref}})\Big] \end{aligned} \tag{13}$$

where the last term may be dropped since is constant.

Therefore, the MPC strategy can be expressed as the QP problem:

$$\min_{\delta u \in \mathbb{R}^N} \frac{1}{2}\delta u^T \Gamma \delta u + f^T \delta u \tag{14a}$$

s.t.

$$g\delta u \leq p \tag{14b}$$

with the matrix and vector in Eq. (14b) defined in Eq. (12), and:

$$\Gamma = H^T Q H + R$$
$$f = (A_0 \tilde{x}_0 - y_{\text{ref}})QH$$

The development of the MPC delta-input formulation for the polynomial model in Eq. (4) follows the same approach and is summarized in Appendix C.

3.2.2. Delta-input formulation for MIMO systems

Systems generally require the control of several process variables. Thus, the delta-input formulation of the MPC problem in Eq. (14) is expanded to consider multi-input multi-output (MIMO) systems. Consider m single-input single-output (SISO) models with manipulated variables defined as delta-input control actions and grouped in a vector as:

$$\Delta u := [\delta u_1 \ \delta u_2 \ \ldots \ \delta u_m]^T \tag{15}$$

where each component is a sequence of control actions over a time horizon N for a given manipulated variable:

$$\delta u_j = [\delta u_{j,1} \ \ldots \ \delta u_{j,N}]^T \quad j \in \{1, \ldots, m\}$$

The MPC delta-input formulation can be extended as:

$$\min_{\Delta u \in \mathbb{R}^{(Nxm)x1}} \frac{1}{2}\Delta u^T \Phi \Delta u + F^T \Delta u \tag{16a}$$

s.t.

$$G\Delta u \leq P \tag{16b}$$

where

$$\Phi = \begin{bmatrix} \Gamma_1 & 0 & \cdots & 0 \\ 0 & \Gamma_2 & \ddots & \vdots \\ \vdots & \ddots & \ddots & 0 \\ 0 & \cdots & 0 & \Gamma_m \end{bmatrix} \quad F = \begin{bmatrix} f_1 \\ f_2 \\ \vdots \\ f_m \end{bmatrix}$$

$$G = \begin{bmatrix} g_1 & 0 & \cdots & 0 \\ 0 & g_2 & \ddots & \vdots \\ \vdots & \ddots & \ddots & 0 \\ 0 & \cdots & 0 & g_m \end{bmatrix} \quad P = \begin{bmatrix} p_1 \\ p_2 \\ \vdots \\ p_m \end{bmatrix}$$

3.3. Estimator

States and disturbances need to be estimated from the measurements of the actual system at each sampling time to obtain the current state of the NGCC-PCC plant. The estimator, or observer, computes the augmented state at each discrete time k as a combination of the current, or a priori, state prediction and a correction based on the measured output y_k:

$$\hat{\tilde{x}}_k = \tilde{A}\hat{\tilde{x}}_{k-1} + \tilde{B}\delta u_{k-1} + K(y_k - \tilde{C}(\tilde{A}\hat{\tilde{x}}_{k-1} + \tilde{B}\delta u_{k-1})) \tag{17}$$

where $\hat{\cdot}$ indicates estimated variables, and $K \in \mathbb{R}^{(n_y+n_d+1)x1}$ is the observer gain:

$$K := \begin{bmatrix} K_x \\ K_d \\ K_u \end{bmatrix}$$

in which K_x, K_d, K_u are the observer gains for the states, disturbances and control input, respectively. This observer gain K is chosen so the observer is stable, i.e. the eigenvalues of the system $(\tilde{A} - K\tilde{C}\tilde{A})$ lie inside the unit circle.

Pole placement routines compute observer gain matrices that fix the eigenvalues of a matrix pair in specific coordinates and make the estimator stable (see, e.g. Pannocchia, 2015). However, this work considers a Kalman filter as observer gain matrix (Kalman, 1960). Calculation of the Kalman filter matrix gain is a two-step process. First, the a priori state $\hat{\tilde{x}}_{k-1}^-$ and covariance matrix Z_k^- are computed from previous estimations:

$$\hat{\tilde{x}}_k^- = \tilde{A}\hat{\tilde{x}}_{k-1} + \tilde{B}\delta u_{k-1} \tag{18a}$$

$$Z_k^- = \tilde{A}Z_{k-1}\tilde{A}^T + Q_p \tag{18b}$$

Algorithm 1 MPC for NGCC-PCC systems

Require: coefficients (a, b) in Table~A.4, B_{d}, C_{d}, Q_p, R_m, Q, R, y_{ref}, y^{low}, y^{up}, u^{low}, u^{up}, GT$_{\mathrm{ramp}}$, Ψ, N

Require: $\tilde{\hat{x}}_{k-1}$, Δu_{k-1}, y_k, $\dot{m}_{\mathrm{exhaust}}$, Z_{k-1}
  Compute: interpolated coefficients (a, b) with Eqs.~2, 3
  Compute: $\tilde{A}$, $\tilde{B}$, $\tilde{C}$ in Eq.~10
  Compute: H, A_0 in Eq.~11
  Compute: $\tilde{\hat{x}}_k^-$, Z_k in Eq.~18
  Set: $\tilde{x}_0 := \tilde{\hat{x}}_k$
  Compute: g, p in Eq.~12
  Compute: Γ, f in Eq.~14a
  Compute: G, P, Φ, F in Eq.~16
  Solve:

$$\min_{\Delta u \in \mathbb{R}^{(N \times m) \times 1}} \frac{1}{2} \Delta u^T \Phi \, \Delta u + F^T \Delta u$$

  s.t.

$$G \Delta u \leq P$$

  return Δu_k, $\tilde{\hat{x}}_k$, P_k

with Q_p representing the covariance of the process noise $w \in \mathcal{N}(0, Q_p)$. Then, these a priori estimates are updated based on current measurements:

$$K_f = \frac{Z_k^- \tilde{C}^T}{\tilde{C} Z_k^- \tilde{C}^T + R_m} \tag{18c}$$

$$\tilde{\hat{x}}_k = \tilde{\hat{x}}_k^- + K_f \left(y_k - \tilde{C} \tilde{\hat{x}}_k^- \right) \tag{18d}$$

$$Z_k = (I - K_f \tilde{C}) Z_k^- \tag{18e}$$

where R_m is the covariance associated to the measurement noise $v \in \mathcal{N}(0, R_m)$, and K_f is the Kalman filter used to estimate the current state $\tilde{\hat{x}}_k$ and the covariance matrix Z_k that will be used at the next sampling time.

Algorithm 1 summarises the sequence of computations needed to implement the MPC strategy at each sampling time. The first require condition refers to the parameters, matrices and vectors provided off-line, whilst the second require condition indicates the parameters that are updated every sampling time. The mass flow rate of exhaust gas $\dot{m}_{\mathrm{exhaust}}$ belongs to this second group as it is the parameter needed to interpolate the coefficients of the local ARX models for the capture ratio and reboiler steam temperature (see Table A.4). Moreover, note that the first element of each input control sequence must be selected from Δu_k.

4. Dynamic operation of NGCC-PCC integrated systems

A case study where the NGCC-PCC system needs to reduce its power generation to balance the grid demonstrates the effectiveness of the proposed MPC strategy to respond to fast changes in power demand and stabilise the operation of the integrated plants. The dominant dynamics of the NGCC and PCC described in Section 2.1 occur within 10 and 60 min, respectively. Thus, the MPC strategy considered a sampling time of 30 s in order to capture the transient behaviour in the shortest time-scale, i.e. the dynamic operation of the NGCC. A time horizon $N = 20$ was hence selected to consider the entire period of dominant dynamics in the NGCC. Table 2 includes the bounds for the controlled and manipulated variables considered during the dynamic simulations. Table 3 summarises the matrices and vectors to create the augmented models, the estimator based on the Kalman filter, and the weights in the objective function for each input-output pair. These

Table 2
Lower and upper bounds of the controlled and manipulated variables.

Variable	Lower	Upper
Power [MW]	450	615
Gas turbine load [%]	60	100
Superheating temperature [°C]	587.7	597.7
Attemperator valve 1 [-]	0.01	1
Reheating temperature [°C]	587.5	597.5
Attemperator valve 2 [-]	0.01	1
Capture ratio [-]	0.85	0.95
Mass flow lean solvent [kg/s]	300	800
Reboiler temperature [°C]	115.22	120.22
Steam extraction valve [-]	0.01	1

Table 3
Matrices and vectors defining the disturbance (B_{d}, C_{d}) and noise (Q_p, R_m) models; and weights for controlled variables (λ_Q) and penalties in movement of manipulated variables (λ_R).

Variable	B_{d}	C_{d}	Q_p	R_m	λ_Q	λ_R
Power	-	-	-	-	1	1
Superheating temperature	$\begin{bmatrix} 0 \\ 0 \\ 0.01 \end{bmatrix}$	0	$I_{4 \times 4}$	0.01	10	0.01
Reheating temperature	$\begin{bmatrix} 0 \\ 0 \\ 0.01 \end{bmatrix}$	0	$I_{4 \times 4}$	0.01	10	0.01
Capture ratio	$\begin{bmatrix} 0.1 \\ 0.1 \end{bmatrix}$	0	$I_{3 \times 3}$	0.1	50000	0.001
Reboiler temperature	$\begin{bmatrix} 0.01 \\ 0.01 \end{bmatrix}$	0	$I_{3 \times 3}$	0.1	100	10

weights aimed at compensating the different orders of magnitude between controlled and manipulated variables and at prioritising the tracking of the process variables, albeit their tuning was outside of the scope of this work.

A step change in the power demand drives the transient operation of the power plant, which adapts the gas turbine load to adjust the net power output. Similarly, the change in exhaust gas conditions disturbs the operation of the capture plant. Fig. 3 shows key process variables in the NGCC-PCC system during dynamic operation and demonstrates the effectiveness of the proposed MPC strategy to achieve optimal offset-free control.

Process variables from the NGCC reach their set-point faster because of the shorter dominant dynamics of the power plant compared to the capture system. Net power generation is the fastest variable to meet its target owing to the fast dynamics of the gas turbine, which controls the overall power output of the NGCC and compensates the slow dynamics of the steam cycle. Consequently, power demand and supply are balanced within the dominant dynamics of the NGCC. Temperature control in the superheating and reheating sections of the HRSG requires more time. Heat capacitance in the HRSG slows down the transient performance of the steam cycle compared to the change in gas turbine load. The attemperator valves need to compensate and anticipate these variations in the operating conditions for a longer period of time. Nevertheless, the proposed MPC strategy limited the offset and drove both temperatures to their set-point.

Dynamics in the PCC plant are notably slower than in any type of thermal power plant (Rúa et al., 2020a). However, Fig. 3 illustrates how the MPC strategy controlled the capture ratio almost simultaneously to the temperature in the steam cycle of the NGCC. This behaviour originates from the use of optimisation-based control strategies. MPC considers the dynamic operation of the capture plant and computes optimal control actions that achieved better and faster offset free in key process variables. Fig. 3 also il-
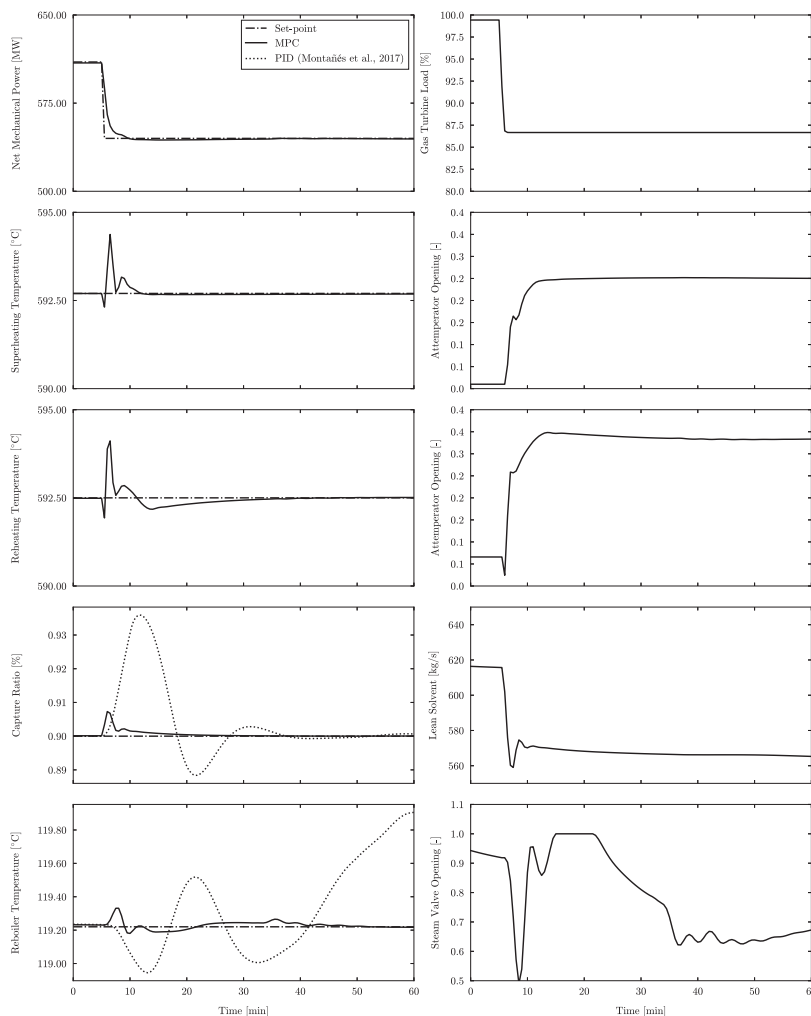
Fig. 3. Dynamic behaviour of process variables from the NGCC-PCC system with the proposed MPC strategy during a power demand reduction of 70 MW.

lustrates how traditional PID controllers require more time and lead to larger offsets than MPC, albeit offset-free control is also achieved because of their integral action (Montañés et al., 2017c).

In contrast, the reboiler temperature needed more time to reach its set-point. Control actions in the mass flow rate of lean solvent to stabilise the capture ratio modify the operation of the desorber, which also affects the lean loading of the solvent at the outlet of this column and the temperature in the reboiler. These process changes are characterised by slow dynamics because of the interaction between the absorber and stripper columns, large volumes of solvent and delays from piping and heat exchangers (Rúa et al., 2020b). Therefore, the MPC needs to adapt the steam extraction from the NGCC to anticipate the interaction between both absorption and desorption sections and compensate these operation changes. This leads to the saturation of the steam extraction valve in the first 20 min of transient performance of the CO_2 capture plant, which results from the combined effect of changing loading in the solvent, the MPC strategy trying to anticipate the dynamic behaviour of the reboiler temperature and the slow dynamics of

the desorption section of the PCC plant. The steam cycle and capture stabilise completely during this time and reduce hence the variations in steam availability and fluctuation in the rich loading of the solvent. These steadier conditions ease the control of the reboiler temperature and allow a more stable and prolonged movements of the steam extraction valve after this stabilisation period.

Despite the saturation of the steam extraction valve, the proposed MPC strategy obtained smaller offsets than $0.15°C$ and achieved offset free in an hour, which is better performance than using PID controllers (Montañés et al., 2017c). This reduced offset achieved by the MPC strategy during drastic changes of load is specially important in the reboiler temperature, as it could allow increasing its set-point, and hence the stripping efficiency, without reaching temperatures that lead to solvent degradation during the regeneration process.

Tuning of the MPC was not the main objective of this study. Improved performance might be achieved with adequate weight values in the objective function, λ_Q and λ_R, disturbance matrices and vectors (Pannocchia, 2003), B_d and C_d, and noise models for

the Kalman estimator, Q_p and R_m. However, the different orders of magnitude among controlled and manipulated variables suppose a challenge to balance the values of these different tuning parameters.

5. Conclusions

Flexible thermal power plants integrated with post-combustion capture systems will play a fundamental role balancing the intermittent power generation from renewable energy sources with low-carbon electricity. The deployment of this technology requires, however, the demonstration that this type of power systems can provide fast changes of power output whilst capturing most of the produced CO_2. Optimisation-based control strategies can enhance the dynamic operation of these integrated systems and contribute to more efficient and stable power systems. Among the different available technologies to produce flexible, low-carbon power, natural gas combined cycles offer the fastest and most efficient performance.

This work presents a linear model predictive control strategy applied to a modern NGCC integrated with a PCC plant. This method achieves offset-free control by augmenting the linear model with a disturbance model that removes any deviation from the set-point. Furthermore, the proposed MPC strategy is formulated in delta-input form, since this form is easier to implement and more computationally efficient due to the reduced amount of optimisation variables. Linear, data-based models were developed and implemented in the MPC strategy because of the excessive computational cost of the high-fidelity dynamic models. System identification allowed the development of several data-based, local ARX models that were combined in a local model network capable of predicting nonlinear behaviour with a set of linear models. This approach permitted the formulation of the dynamic optimisation

program in the MPC strategy as a convex quadratic programming (QP) problem that leads to global optimal solutions.

A case study where a NGCC integrated with a PCC plant needs to balance a step change in power demand demonstrated the effectiveness of the proposed MPC strategy. The key process variables controlled by the MPC presented offset-free in shorter periods of time than those observed with traditional PID controllers. Moreover, the deviations from the set-point during transient operation were smaller. This dynamic behaviour with reduced offsets allows the approximation of nominal values of these parameters to their limits, which could potentially lead to improved performance, e.g. reboiler temperature closer to the degradation limit of the solvent. Linear MPC also presents fast convergence time because of its convexity and favourable numerical properties. Thus, better dynamic operation could be achieved by reducing the sampling time and increasing the predicting horizon. Adequate selection of weights in the objective function, disturbance matrices and vectors, and noise models in the estimator could also lead to improvements in the dynamic performance of the NGCC-PCC system. This topic was not analysed in this study, but it is considered as an interesting direction for future research.

Declaration of Competing Interest

The authors declare that they have no known competing financial interests or personal relationships that could have appeared to influence the work reported in this paper.

Appendix A

Table A.4 summarises the coefficients of the local ARX models identified in Section 2.2. The combination of these parameters with a Gaussian validity function leads to the overall parameters that compose the local model network at each sampling time.

Table A.4
Coefficients of the simplified local ARX models composing the local model networks.

Controlled variable	γ	Local model	Centre	Parameters	
				a	b
Net power generation	-	-	-	90	5.25
Supeheated steam temperature	Gas turbine load	1	100	-1.21, 0.21	-23.06, 23.15
		2	95	-1.50, 0.50	-21.34, 21.46
		3	90	-1.29, 0.29	-24.03, 24.00
		4	85	-1.32, 0.32	-22.74, 22.90
		5	80	-1.34, 0.34	-22.22, 22.34
Reheated steam temperature	Gas turbine load	1	100	-1.06, 0.06	-14.58, 15.02
		2	95	-1.20, 0.20	-15.96, 16.09
		3	90	-1.17, 0.17	-15.10, 15.53
		4	85	-1.19, 0.19	-14.40, 15.08
		5	80	-1.21, 0.21	-14.37, 15.04
Capture ratio	Mass flow exhaust gas	1	436.5	-0.931	7.925e-5
		2	429	-0.938	7.543e-5
		3	412	-0.949	6.093e-5
		4	395	-0.978	2.156e-5
		5	379	-0.972	3.073e-5
Reboiler steam temperature	Mass flow exhaust gas	1	436.5	-0.992	0.166
		2	429	-0.981	0.225
		3	412	-0.997	0.219
		4	395	-0.993	0.089
		5	379	-0.996	0.110

(a) Validation of the NGCC simplified models.

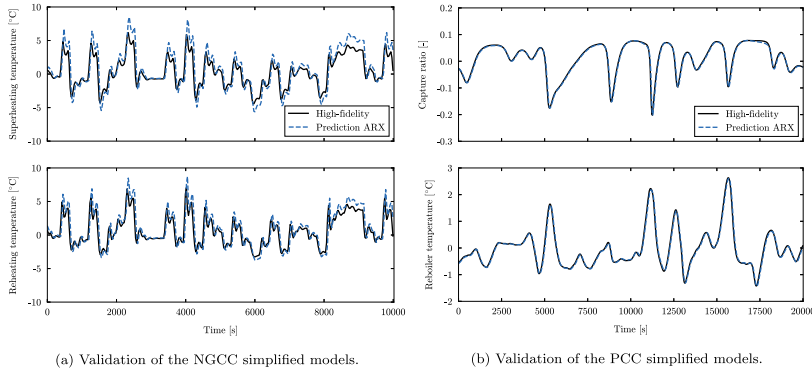(b) Validation of the PCC simplified models.

Fig. B.4. Validation results of the simplified models described in Section 2.2. These results only include a small set of the validation data to ease the visibility, whereas the R^2 values on Table 1 considered the entire set.

Appendix B

Fig. B.4 illustrates a small set of the validation results comparing the predicting capability of the LMN of simplified ARX models and the output of the dynamic high-fidelity model.

Appendix C

Consider the control input action defined in Eq. (9) and substitute it in the simplified polynomial model in Eq. (4):

$$y_k = a + b\left(\delta u_k + u_{k-1}\right) \tag{C.1}$$

If the same sequences of outputs and control inputs over a time horizon N as in Section 3.1 are considered, this polynomial model can be expressed:

$$y = aI + b\Psi\,\delta u + bIu_{-1} \tag{C.2}$$

where I is the identity matrix and Ψ was defined in Section 3.1. Inserting this vector equation and the delta-input definition on the inequality constraints of the standard MPC formulation:

$$g_{pow}\,\delta u \le f_{pow} \tag{C.3}$$

where

$$g_{pow} = \begin{bmatrix} -b\Psi \\ b\Psi \\ -\Psi \\ \Psi \\ -I \\ I \end{bmatrix} \quad f_{pow} = \begin{bmatrix} -(y^{low} - aI - bIu_{k-1}) \\ y^{up} - aI - bIu_{k-1} \\ -(u^{low} - u_{k-1}) \\ u^{up} - u_{k-1} \\ GT_{ramp} \\ GT_{ramp} \end{bmatrix}$$

and GT_{ramp} limits the maximum ramping rate of the gas turbine. This work considers a 15%/min ramp rate, as indicated by most gas turbine manufacturers.

Similarly, the objective function becomes:

$$\begin{aligned} J_{pow} &= \frac{1}{2}\left(\|Q(y - y_{ref})\| + \|R\delta u\|\right) \\ &= \frac{1}{2}\left(\|Q(aI + b\Psi\delta u + bIu_{-1} - y_{ref})\| + \|R\delta u\|\right) \\ &= \frac{1}{2}\Big[\delta u^T\left(b^T\Psi^T Q\Psi b + R\right)\delta u \\ &\quad + 2(aI + bIu_{-1} - y_{ref})^T Q\Psi b\delta u \\ &\quad + (aI + bIu_{-1} - y_{ref})^T Q\left(aI + bIu_{-1} - y_{ref}\right)\Big] \end{aligned} \tag{C.4}$$

These inequality constraints and objective function, Eqs. (C.3) and (C.4) respectively, define the MPC delta-input formulation in Eq. (14) for the polynomial model in Eq. (4). Thus, it may be easily combined with state-space models in the MIMO formulations described in Section 3.2.2.

CRediT authorship contribution statement

Jairo Rúa: Conceptualization, Methodology, Software, Validation, Formal analysis, Investigation, Visualization, Writing - original draft. **Magne Hillestad:** Writing - review & editing, Supervision. **Lars O. Nord:** Resources, Writing - review & editing, Supervision, Funding acquisition.

References

Alobaid, F., Mertens, N., Starkloff, R., Lanz, T., Heinze, C., Epple, B., 2017. Progress in dynamic simulation of thermal power plants. Progress in Energy and Combustion Science 59, 79–162.

Alobaid, F., Postler, R., Ströhle, J., Epple, B., Kim, H.-G., 2008. Modeling and investigation start-up procedures of a combined cycle power plant. Applied Energy 85 (12), 1173–1189.

Arce, A., Mac Dowell, N., Shah, N., Vega, L., 2012. Flexible operation of solvent regeneration systems for CO_2 capture processes using advanced control techniques: Towards operational cost minimisation. International Journal of Greenhouse Gas Control 11, 236–250.

Aske, E.M.B., Skogestad, S., 2009. Consistent inventory control. Industrial & Engineering Chemistry Research 48 (24), 10892–10902.

Borrelli, F., Morari, M., 2007. Offset free model predictive control. In: 2007 46th IEEE Conference on Decision and Control. IEEE, pp. 1245–1250.

Bui, M., Adjiman, C.S., Bardow, A., Anthony, E.J., Boston, A., Brown, S., Fennell, P.S., Fuss, S., Galindo, A., Hackett, L.A., et al., 2018. Carbon capture and storage (CCS): the way forward. Energy & Environmental Science 11 (5), 1062–1176.

Casella, F., Pretolani, F., 2006. Fast start-up of a combined-cycle power plant: a simulation study with modelica. In: Modelica Conference, 4, pp. 3–10.

Chen, B., 2013. Linear Systems Theory and Design.

Dassault Systemes, 2016. https://www.3ds.com/products-services/catia/products/dymola/.

Decardi-Nelson, B., Liu, S., Liu, J., 2018. Improving flexibility and energy efficiency of post-combustion CO_2 capture plants using economic model predictive control. Processes 6 (9), 135.

Dutta, R., Nord, L.O., Bolland, O., 2017. Selection and design of post-combustion CO_2 capture process for 600 MW natural gas fueled thermal power plant based on operability. Energy 121, 643–656.

Eser, P., Chokani, N., Abhari, R., 2017. Operational and financial performance of fossil fuel power plants within a high renewable energy mix. Journal of the Global Power and Propulsion Society 1, 16–27.

Flø, N.E., Knuutila, H., Kvamsdal, H.M., Hillestad, M., 2015. Dynamic model validation of the post-combustion CO_2 absorption process. International Journal of Greenhouse Gas Control 41, 127–141.

Flø, N.E., Kvamsdal, H.M., Hillestad, M., 2016. Dynamic simulation of post-combustion CO_2 capture for flexible operation of the brindisi pilot plant. International Journal of Greenhouse Gas Control 48, 204–215.

Forssell, U., Ljung, L., 1999. Closed-loop identification revisited. Automatica 35 (7), 1215–1241.

Garðarsdóttir, S.Ó., Montañés, R.M., Normann, F., Nord, L.O., Johnsson, F., 2017. Effects of CO_2-absorption control strategies on the dynamic performance of a supercritical pulverized-coal-fired power plant. Industrial & Engineering Chemistry Research 56 (15), 4415–4430.

Garðarsdóttir, S.Ó., Normann, F., Andersson, K., Prölß, K., Emilsdóttir, S., Johnsson, F., 2015. Post-combustion CO$_2$ capture applied to a state-of-the-art coal–fired power plant the influence of dynamic process conditions. International Journal of Greenhouse Gas Control 33, 51–62.

Gaspar, J., Ricardez-Sandoval, L., Jørgensen, J.B., Fosbøl, P.L., 2016. Controllability and flexibility analysis of CO$_2$ post-combustion capture using piperazine and mea. International Journal of Greenhouse Gas Control 51, 276–289.

Gevers, M., 2005. Identification for control: From the early achievements to the revival of experiment design. European Journal of control 11, 1–18.

Gevers, M., Ljung, L., 1986. Optimal experiment designs with respect to the intended model application. Automatica 22 (5), 543–554.

Gevers, M., Mišković, L., Bonvin, D., Karimi, A., 2006. Identification of multi-input systems: variance analysis and input design issues. Automatica 42 (4), 559–572.

González-Salazar, M.A., Kirsten, T., Prchlik, L., 2017. Review of the operational flexibility and emissions of gas-and coal-fired power plants in a future with growing renewables. Renewable and Sustainable Energy Reviews 82, 1497–1513.

Hauger, S.O., Flø, N.E., Kvamsdal, H., Gjertsen, F., Mejdell, T., Hillestad, M., 2019. Demonstration of non-linear model predictive control of post-combustion CO$_2$ capture processes. Computers & Chemical Engineering 123, 184–195.

He, X., Wang, Y., Bhattacharyya, D., Lima, F.V., Turton, R., 2018. Dynamic modeling and advanced control of post-combustion CO$_2$ capture plants. Chemical Engineering Research and Design 131, 430–439.

He, Z., Sahraei, M.H., Ricardez-Sandoval, L.A., 2016. Flexible operation and simultaneous scheduling and control of a CO$_2$ capture plant using model predictive control. International Journal of Greenhouse Gas Control 48, 300–311.

Hentschel, J., Spliethoff, H., et al., 2016. A parametric approach for the valuation of power plant flexibility options. Energy Reports 2, 40–47.

Heuberger, C.F., Rubin, E.S., Staffell, I., Shah, N., Mac Dowell, N., 2017. Power capacity expansion planning considering endogenous technology cost learning. Applied Energy 204, 831–845.

Heuberger, C.F., Staffell, I., Shah, N., Mac Dowell, N., 2016. Quantifying the value of CCS for the future electricity system. Energy & Environmental Science 9 (8), 2497–2510.

Heuberger, C.F., Staffell, I., Shah, N., Mac Dowell, N., 2017. A systems approach to quantifying the value of power generation and energy storage technologies in future electricity networks. Computers & Chemical Engineering 107, 247–256.

Huusom, J.K., Poulsen, N.K., Jørgensen, S.B., Jørgensen, J.B., 2010. Tuning of methods for offset free mpc based on arx model representations. In: Proceedings of the 2010 American Control Conference. IEEE, pp. 2355–2360.

IEA, 2019. World Energy Outlook 2019. https://www.iea.org/reports/world-energy-outlook-2019.

IPCC, 2005. IPCC Special Report on Carbon Dioxide Capture and Storage. Prepared by Working Group III of the Intergovernmental Panel on Climate Change [Metz, B., O. Davidson, H. C. de Coninck, M. Loos, and L. A. Meyer (eds.)]. Cambridge University Press, Cambridge, United Kingdom and New York, NY, USA.

IPCC, 2014. Climate Change 2014: Synthesis Report. Contribution of Working Groups I, II and III to the Fifth Assessment Report of the Intergovernmental Panel on Climate Change [Core Writing Team, R.K. Pachauri and L.A. Meyer (eds.)], IPCC, Geneva, Switzerland.

IPCC, 2018. Summary for Policymakers. In: Global warming of 1.5°C. An IPCC Special Report on the impacts of global warming of 1.5°C above pre-industrial levels and related global greenhouse gas emission pathways, in the context of strengthening the global response to the threat of climate change, sustainable development, and efforts to eradicate poverty. [V. Masson-Delmotte, P. Zhai, H. O. Prtner, D. Roberts, J. Skea, P. R. Shukla, A. Pirani, W. Moufouma-Okia, C. Pan, R. Pidcock, S. Connors, J. B. R. Matthews, Y. Chen, X. Zhou, M. I. Gomis, E. Lonnoy, T. Maycock, M. Tignor, T. Waterfield (eds.)]. World Meteorological Organization, Geneva, Switzerland.

Johansen, T.A., Foss, B., 1993. Constructing NARMAX models using ARMAX models. International Journal of Control 58 (5), 1125–1153.

Jonshagen, K., Genrup, M., 2010. Improved load control for a steam cycle combined heat and power plant. Energy 35 (4), 1694–1700.

Jordal, K., Ystad, P.A.M., Anantharaman, R., Chikukwa, A., Bolland, O., 2012. Design–point and part-load considerations for natural gas combined cycle plants with post combustion capture. International Journal of Greenhouse Gas Control 11, 271–282.

Jung, H., Im, D., Heo, S., Kim, B., Lee, J.H., 2020. Dynamic Analysis and Linear Model Predictive Control for Operational Flexibility of Post-Combustion CO$_2$ Capture Processes. Computers & Chemical Engineering 106968.

Kalman, R.E., 1960. A new approach to linear filtering and prediction problems. Journal of Basic Engineering 35–45.

Kehlhofer, R., Hannemann, F., Rukes, B., Stirnimann, F., 2009. Combined-Cycle Gas & Steam Turbine Power Plants. Pennwell Books.

Kondziella, H., Bruckner, T., 2016. Flexibility requirements of renewable energy based electricity systems–A review of research results and methodologies. Renewable and Sustainable Energy Reviews 53, 10–22.

Lawal, A., Wang, M., Stephenson, P., Koumpouras, G., Yeung, H., 2010. Dynamic modelling and analysis of post-combustion CO$_2$ chemical absorption process for coal-fired power plants. Fuel 89 (10), 2791–2801.

Lawal, A., Wang, M., Stephenson, P., Obi, O., 2012. Demonstrating full-scale post–combustion CO$_2$ capture for coal-fired power plants through dynamic modelling and simulation. Fuel 101, 115–128.

Li, Z., Ding, Z., Wang, M., Oko, E., 2018. Model-free adaptive control for mea-based post-combustion carbon capture processes. Fuel 224, 637–643.

Ljung, L., 1987. System identification: theory for the user. Prentice-hall.

Lu, S., Hogg, B., 1997. Predictive co-ordinated control for power-plant steam pressure and power output. Control Engineering Practice 5 (1), 79–84.

Luu, M.T., Manaf, N.A., Abbas, A., 2015. Dynamic modelling and control strategies for flexible operation of amine-based post-combustion CO$_2$ capture systems. International Journal of Greenhouse Gas Control 39, 377–389.

Manaf, N.A., Cousins, A., Feron, P., Abbas, A., 2016. Dynamic modelling, identification and preliminary control analysis of an amine-based post-combustion CO$_2$ capture pilot plant. Journal of Cleaner Production 113, 635–653.

Mansour, F., Abdul Aziz, A., Abdel-Ghany, S., El-Shaer, H., 2003. Combined cycle dynamics. Proceedings of the Institution of Mechanical Engineers, Part A: Journal of Power and Energy 217 (3), 247–258.

Marx-Schubach, T., Schmitz, G., 2019. Modeling and simulation of the start-up process of coal fired power plants with post-combustion CO$_2$ capture. International Journal of Greenhouse Gas Control 57, 44–57.

Matsumura, S., Ogata, K., Fujii, S., Shioya, H., 1998. Adaptive control for the steam temperature of thermal power plants. In: Proceedings of the 1998 IEEE International Conference on Control Applications (Cat. No. 98CH36104), 2. IEEE, pp. 1105–1109.

Mechleri, E., Lawal, A., Ramos, A., Davison, J., Mac Dowell, N., 2017. Process control strategies for flexible operation of post-combustion CO$_2$ capture plants. International Journal of Greenhouse Gas Control 57, 14–25.

Mišković, L., Karimi, A., Bonvin, D., Gevers, M., 2008. Closed-loop identification of multivariable systems: With or without excitation of all references? Automatica 44 (8), 2048–2056.

Modelica Association, 2019. https://www.modelica.org/.

Modelon, 2015. Thermal Power Library. https://www.modelon.com/library/thermal-power-library/.

Montañés, R.M., Flø, N.E., Nord, L.O., 2017. Dynamic process model validation and control of the amine plant at CO$_2$ technology centre mongstad. Energies 10 (10), 1527.

Montañés, R.M., Flø, N.E., Nord, L.O., 2017. Dynamic process model validation and control of the amine plant at CO$_2$ Technology Centre Mongstad. Energies 10 (10), 1527.

Montañés, R.M., Flø, N.E., Nord, L.O., 2018. Experimental results of transient testing at the amine plant at technology centre mongstad: Open-loop responses and performance of decentralized control structures for load changes. International Journal of Greenhouse Gas Control 73, 42–59.

Montañés, R.M., Garðarsdóttir, S.Ó., Normann, F., Johnsson, F., Nord, L.O., 2017. Demonstrating load-change transient performance of a commercial-scale natural gas combined cycle power plant with post-combustion CO$_2$ capture. International Journal of Greenhouse Gas Control 63, 158–174.

Montañés, R.M., Korpås, M., Nord, L.O., Jaehnert, S., 2016. Identifying operational requirements for flexible CCS power plant in future energy systems. Energy Procedia 86, 22–31.

Nittaya, T., Douglas, P.L., Croiset, E., Ricardez-Sandoval, L.A., 2014. Dynamic modelling and control of mea absorption processes for CO$_2$ capture from power plants. Fuel 116, 672–691.

Panahi, M., Skogestad, S., 2011. Economically efficient operation of CO$_2$ capturing process part i: Self-optimizing procedure for selecting the best controlled variables. Chemical Engineering and Processing: Process Intensification 50 (3), 247–253.

Panahi, M., Skogestad, S., 2012. Economically efficient operation of CO$_2$ capturing process. part ii. design of control layer. Chemical Engineering and Processing: Process Intensification 52, 112–124.

Pannocchia, G., 2003. Robust disturbance modeling for model predictive control with application to multivariable ill-conditioned processes. Journal of Process Control 13 (8), 693–701.

Pannocchia, G., 2015. Offset-free tracking mpc: A tutorial review and comparison of different formulations. In: 2015 European control conference (ECC). IEEE, pp. 527–532.

Pannocchia, G., Rawlings, J.B., 2003. Disturbance models for offset-free model-predictive control. AIChE journal 49 (2), 426–437.

Peng, H., Wu, J., Inoussa, G., Deng, Q., Nakano, K., 2009. Nonlinear system modeling and predictive control using the rbf nets-based quasi-linear arx model. Control Engineering Practice 17 (1), 59–66.

Prasad, G., Irwin, G., Swidenbank, E., Hogg, B., 2000. Plant-wide predictive control for a thermal power plant based on a physical plant model. IEE Proceedings–Control Theory and Applications 147 (5), 523–537.

Prasad, G., Swidenbank, E., Hogg, B., 1998. A local model networks based multivariable long-range predictive control strategy for thermal power plants. Automatica 34 (10), 1185–1204.

Rawlings, J.B., Mayne, D.Q., Diehl, M., 2017. Model predictive control: theory, computation, and design, 2. Nob Hill Publishing Madison, WI.

Rezazadeh, F., Gale, W.F., Hughes, K.J., Pourkashanian, M., 2015. Performance viability of a natural gas fired combined cycle power plant integrated with post-combustion CO$_2$ capture at part-load and temporary non-capture operations. International Journal of Greenhouse Gas Control 39, 397–406.

Rúa, J., Agromayor, R., Hillestad, M., Nord, L.O., 2020a. Optimal dynamic operation of natural gas combined cycles accounting for stresses in thick-walled components. Appl. Ther. Eng. 114858.

Rúa, J., Bui, M., Nord, L.O., Mac Dowell, N., 2020b. Does CCS reduce power generation flexibility? A dynamic study of combined cycles with post-combustion CO$_2$ capture. International Journal of Greenhouse Gas Control 95, 102984.

Rúa, J., Nord, L.O., 2020. Optimal control of flexible natural gas combined cycles with stress monitoring: Linear vs nonlinear model predictive control. Appl. Energy 265 114820.

Sahraei, M.H., Ricardez-Sandoval, L., 2014. Controllability and optimal scheduling of a CO_2 capture plant using model predictive control. International Journal of Greenhouse Gas Control 30, 58–71.

Salvinder, K., Zabiri, H., Taqvi, S.A., Ramasamy, M., Isa, F., Rozali, N., Suleman, H., Maulud, A., Shariff, A., 2019. An overview on control strategies for CO_2 capture using absorption/stripping system. Chemical Engineering Research and Design 147, 319–337.

Schach, M.-O., Schneider, R., Schramm, H., Repke, J.-U., 2013. Control structure design for CO_2-absorption processes with large operating ranges. Energy Technology 1 (4), 233–244.

Thermoflow, 2014. GT Pro 24.0. Thermoflow Inc.

Walters, M.S., Edgar, T.F., Rochelle, G.T., 2016. Regulatory control of amine scrubbing for CO_2 capture from power plants. Industrial & Engineering Chemistry Research 55 (16), 4646–4657.

Wu, X., Shen, J., Li, Y., Wang, M., Lawal, A., Lee, K.Y., 2018. Nonlinear dynamic analysis and control design of a solvent-based post-combustion CO_2 capture process. Computers & Chemical Engineering 115, 397–406.

Wu, X., Shen, J., Li, Y., Wang, M., Lawal, A., Lee, K.Y., 2018. Nonlinear dynamic analysis and control design of a solvent-based post-combustion CO_2 capture process. Computers & Chemical Engineering 115, 397–406.

Wu, X., Shen, J., Li, Y., Wang, M., Lawal, A., Lee, K.Y., 2019. Dynamic behavior investigations and disturbance rejection predictive control of solvent-based post-combustion CO_2 capture process. Fuel 242, 624–637.

Wu, X., Wang, M., Liao, P., Shen, J., Li, Y., 2020. Solvent-based post-combustion CO_2 capture for power plants: A critical review and perspective on dynamic modelling, system identification, process control and flexible operation. Applied Energy 257, 113941.

Wu, X., Wang, M., Shen, J., Li, Y., Lawal, A., Lee, K.Y., 2019. Flexible operation of coal fired power plant integrated with post combustion CO_2 capture using model predictive control. International Journal of Greenhouse Gas Control 82, 138–151.

Wu, X., Wang, M., Shen, J., Li, Y., Lawal, A., Lee, K.Y., 2019. Reinforced coordinated control of coal-fired power plant retrofitted with solvent based CO_2 capture using model predictive controls. Applied Energy 238, 495–515.

Zhang, Q., Turton, R., Bhattacharyya, D., 2016. Development of model and model-predictive control of an mea-based postcombustion CO_2 capture process. Industrial & Engineering Chemistry Research 55 (5), 1292–1308.